

博士論文

**Study on Development of Distributed Water  
Source Heat Pump System Using  
Renewable Energy**

(再生可能エネルギーを利用する水循環・分散型  
ヒートポンプシステムの開発に関する研究)

劉 明哲



# Contents

Contents .....	3
List of figures .....	6
List of tables .....	14
Nomenclature .....	16
Chapter 1: Introduction .....	1
Background .....	2
Current status of renewable energy application for buildings .....	2
Development of renewable energy technologies for sustainable and energy-efficient building .....	6
Research objectives .....	9
Originality of this study .....	10
Thesis structure .....	11
Summary .....	13
Reference .....	14
Chapter 2: Application of heat pump system in building for energy conservation .....	17
2.1 Background .....	18
2.2 Heat Pump Basics .....	18
2.3 Air source heat pump system .....	22
2.4 Geothermal heat pump system .....	26
2.5 Solar assisted heat pump system .....	34
2.6 Summary .....	39
2.7 Reference .....	40
Chapter 3: Fundamentals of distributed water source heat pump system using renewable energy .....	46
3.1 Introduction .....	47
3.2 Concept of distributed water source heat pump system using renewable energy .....	48
3.3 Development of distributed water source heat pump system .....	51
3.3.1 Construction of water loop system .....	51

3.3.2	Development of sky source heat pump	63
3.3.3	Overview of double-helical ground heat exchanger	73
3.3.4	Development of water source heat pump for floor heating	77
3.3.5	Development of water source heat pump for air conditioning	82
3.3.6	Development of water source heat pump for domestic hot water supply	86
3.4	Summary	90
3.5	Reference	91
Chapter 4: Experimental performance analysis of the distributed heat pump system using renewable energy		93
4.1	Introduction of test building and control method	94
4.2	Measurement items and measuring equipment	104
4.3	Evaluation method	110
4.4	Winter experimental results and analysis	112
4.4.1	Winter field testing on a sunny day	113
4.4.2	Winter field testing on a cloudy day	120
4.4.3	Winter field testing results for the whole month	128
4.4.4	Summary of winter field testing	133
4.5	Summer experimental results and analysis	133
4.5.1	Operation status analysis of water source heat pump for air conditioning	134
4.5.2	Operation status analysis of sky source heat pump for cooling	134
4.5.3	Operation status analysis of water source heat pump for domestic hot water supply	135
4.5.4	Summary of summer field testing	141
4.6	Interim period experimental results and analysis	143
4.6.1	Operation status analysis of water source heat pump for air conditioning	143
	Summary of interim period field testing	145
4.7	Summary	146
4.8	Reference	148
Chapter 5: Pressure and temperature analysis of piping system based on CFD		150
5.1	Introduction	151
5.2	Fundamentals of computational fluid mechanics	152

5.3	Previous study of gauge pressure and pressure drop analysis in piping system based on CFD method .....	161
5.3.1	Simulation objectives and method .....	161
5.3.2	Results and discussions .....	164
5.4	Pressure drop and temperature analysis in piping system based on CFD method ..	168
5.4.1	Simulation objectives and method .....	168
5.4.2	Results and discussions .....	175
5.5	Summary.....	177
5.6	Reference .....	179
Chapter 6:	Modeling of distributed heat pump system using renewable energy with Modelica	181
6.1	Introduction and objectives.....	182
6.2	Review of methods and tools for modeling and simulation of HVAC system .....	182
6.3	Fundamentals of Modelica and its application in HVAC and building field .....	186
6.4	Modeling description of distributed water source heat pump system using renewable energy	189
6.4.1	Modeling objectives and method.....	189
6.4.2	Simulation and validation.....	207
6.5	Summary.....	221
6.6	Reference .....	223
Chapter 7:	Conclusions and future work .....	227
7.1	Conclusions .....	227
7.2	Recommendations for future work .....	231
Publications	.....	233
Acknowledgement	.....	236

# List of figures

## Chapter 1

FIGURE 1. 1 WORLD TOTAL FINAL ENERGY CONSUMPTION (TFC) BY SECTOR FROM 1990 TO 2017[9].....	2
FIGURE 1. 2 WORLD TOTAL PRIMARY ENERGY SUPPLY (TPES) BY THE SOURCE FROM 1990 TO 2017[9].....	3
FIGURE 1. 3 WORLD HEAT GENERATION FROM RENEWABLES AND WASTE BY SOURCE FROM 1990 TO 2017[9].....	4
FIGURE 1. 4 CHANGES IN FINAL ENERGY CONSUMPTION AND REAL GDP OF JAPAN FROM THE 1970s[16].....	5
FIGURE 1. 5 CHANGES IN ENERGY CONSUMPTION PER HOUSEHOLD AND ENERGY CONSUMPTION BY APPLICATION IN JAPAN[17].....	5
FIGURE 1. 6 WORLD RENEWABLE HEAT CONSUMPTION FROM (2007-2024)[9].....	7
FIGURE 1. 7 HEATING TECHNOLOGY SALES IN THE SUSTAINABLE DEVELOPMENT SCENARIO (2010-2030)[9].....	8
FIGURE 1.8 GROWTH IN RENEWABLE ENERGY CONSUMPTION FOR HEAT (2013-2024)[9].....	8
FIGURE 1. 9 A SCHEMATIC DRAWING OF THE THERMAL PART OF THE BUILDING ENERGY SYSTEM.[24].....	9
FIGURE 1. 10 INTEGRATED SYSTEM OF THE PHOTOVOLTAIC SYSTEM AND GEOTHERMAL HEAT PUMP FOR RESIDENTIAL BUILDINGS.[23].....	9

## Chapter 2

FIGURE 2. 1 OPERATING PRINCIPLES OF HEAT ENGINES AND HEAT PUMPS [1].....	19
FIGURE 2. 2 FOUR-STAGE REFRIGERANT CYCLE.....	21
FIGURE 2. 3 SIMPLE VAPOR COMPRESSION CYCLE WITH PRESSURE AND ENTHALPY VALUES FOR R134A.....	21
FIGURE 2. 4 PRESSURE-ENTHALPY DIAGRAM, SHOWING THE VAPOR COMPRESSION CYCLE.....	21
FIGURE 2. 5 DIAGRAM OF A TYPICAL ASHP SYSTEM [3].....	22
FIGURE 2. 6 SCHEMATIC DIAGRAMS OF A NOVEL FROST-FREE AIR SOURCE HEAT PUMP SYSTEM[19].	23
FIGURE 2. 7 SCHEMATIC DIAGRAMS OF THE EXPERIMENTAL ASHP SYSTEM FOR DEFROSTING TEST [5], WHICH CAN HELP OPTIMIZE THE CONTROL STRATEGY AND ENERGY SAVING OF THE AIR SOURCE HEAT PUMP.....	25
FIGURE 2. 8 TYPICAL TEMPERATURE OF THE UNDISTURBED GROUND FOR A NORTHERN HEMISPHERE[25].	27
FIGURE 2. 9 SCHEMATICS OF DIFFERENT GROUND-SOURCE HEAT PUMP SYSTEMS[26].	27
FIGURE 2. 10 CLOSED-LOOP GROUND-COUPLED HEAT PUMP WITH DIFFERENT GROUND HEAT EXCHANGERS.....	28
FIGURE 2. 11 SCHEMATIC OF A DIRECT EXPANSION GEOTHERMAL HEAT PUMP SYSTEM[31].....	30
FIGURE 2. 12 SCHEMATIC OF A DUAL-SOURCE(AIR AND GROUND) HEAT PUMP SYSTEM[15].....	33

FIGURE 2. 13 SCHEMATIC OF A DUAL-SOURCE(SOLAR AND GROUND) SOURCE HEAT PUMP SYSTEM[15].	33
FIGURE 2. 14 SCHEMATIC OF A TYPICAL SOLAR-ASSISTED HEAT PUMP WATER HEATING SYSTEM[39].	35
FIGURE 2. 15 SCHEMATIC OF A DIRECT-EXPANSION SOLA-ASSISTED HEAT PUMP WATER HEATING SYSTEM[40].	35
FIGURE 2. 16 SCHEMATIC OF SOLAR-GROUND SOURCE HEAT PUMP EXPERIMENTAL SYSTEM[41].	35
FIGURE 2. 17 SCHEMATIC OF A SOLAR ASSISTED GROUND SOURCE HEAT PUMP SYSTEM BY DAI ET AL.[49].	37
FIGURE 2. 18 SCHEMATICS OF A DIRECT-EXPANSION SOLAR-ASSISTED HEAT PUMP SYSTEM[54].	38
FIGURE 2. 19 SCHEMATIC OF A DIRECT-EXPANSION SOLAR-ASSISTED HEAT PUMP WATER HEATER[55].	38

### Chapter 3

FIGURE 3. 1 CONCEPT OF DISTRIBUTED WATER SOURCE HEAT PUMP SYSTEM USING RENEWABLE ENERGY	50
FIGURE 3. 2 SYSTEM CONFIGURATION OF THE WATER LOOP AND HEAT PUMPS	50
FIGURE 3. 3 CIRCULATING PUMP SET WITH HEAT PUMP TOGETHER	53
FIGURE 3. 4 SMALL DC WATER PUMP (GRUNDFOS ALPHA2)	53
FIGURE 3. 5 PHOTOS OF EXPERIMENTAL APPARATUS(FRONT)	55
FIGURE 3. 6 PHOTOS OF EXPERIMENTAL APPARATUS(SIDE)	55
FIGURE 3. 7 SCHEMATIC OF EXPERIMENTAL APPARATUS THAT CAN IMPLEMENT DIFFERENT PUMPING SYSTEMS	56
FIGURE 3. 8 THREE DIFFERENT CONFIGURATIONS OF PUMPING SYSTEM: (A) CENTRALIZED PUMPING SYSTEM WITH CONSTANT PRESSURE CONTROL, (B) CENTRALIZED PUMPING SYSTEM WITH CONSTANT TERMINAL FLOW RATE CONTROL, (C) DECENTRALIZED PUMPING SYSTEM	57
FIGURE 3. 9 COMPARISON OF THEORETICAL POWER REQUIREMENT UNDER DIFFERENT SCENARIOS	60
FIGURE 3. 10 THE OUTDOOR PANEL OF SKY SOURCE HEAT PUMP	63
FIGURE 3. 11 COMPRESSOR UNIT OF SKY SOURCE HEAT PUMP	63
FIGURE 3. 12 STRUCTURE AND REFRIGERANT CIRCUIT OF SKY SOURCE HEAT PUMP	64
FIGURE 3. 13 DIMENSIONS OF THE OUTDOOR PANEL	65
FIGURE 3. 14 PART CROSS-SECTION OF THE OUTDOOR PANEL	65
FIGURE 3. 15 SOLAR CELL MODULE OF SKY SOURCE HEAT PUMP	65
FIGURE 3. 16 INSTALLATION STATUS OF THE OUTDOOR PANEL ON THE ROOF OF RE HOUSE	66
FIGURE 3. 17 THE STEAM TRAP USED AS THE DRAINER IN SSHP REFRIGERANT CIRCULATION	67
FIGURE 3. 18 THE STRUCTURE OF THE STEAM TRAP. NUMBER IN THE FIGURE: 1. BODY; 2. INNER COVER; 3. BRIM; 4. GUIDE; 5. SCREEN; 6. SPACER; 7. FLOAT; 8. NAME PLATE; 9. ORIFICE; 10. COPPER PIPE; 11. CAP	67
FIGURE 3. 19 HEAT PUMP UNIT IMPORTED INTO THE CIRCULATING WATER TEMPERATURE CONTROL SYSTEM	69

FIGURE 3. 20 PIPE CONNECTION WITH THE WATER LOOP AND SKY SOURCE HEAT PUMP .....	69
FIGURE 3. 21 SPEED CONTROL OF THE COMPRESSOR UNIT .....	71
FIGURE 3. 22 CONTROL METHOD OF SSHP FOR WATER LOOP TEMPERATURE.....	72
FIGURE 3. 23 THE CALCULATION RESULT OF SOIL TEMPERATURE CHANGE AT A SHALLOW DEPTH[9,11].....	74
FIGURE 3. 24 IMAGE OF THERMAL DIFFUSION LENGTH[11]. .....	75
FIGURE 3. 25 DOUBLE-HELICAL GHX AND CONFIGURATION.....	76
FIGURE 3. 26 INLET/OUTLET CONNECTION PIPING WITH GHX COIL.....	77
FIGURE 3. 27 MANUFACTURE OF DOUBLE-HELICAL GROUND HEAT EXCHANGER .....	77
FIGURE 3. 28 REFRIGERANT CIRCUIT OF PROTOTYPE HEAT PUMP FOR FLOOR HEATING .....	79
FIGURE 3. 29 PERFORMANCE TEST OF A PROTOTYPE HEAT PUMP FOR FLOOR HEATING .....	79
FIGURE 3. 30 RESULTS OF THE PERFORMANCE TEST OF THE PROTOTYPE HEAT PUMP FOR FLOOR HEATING .....	80
FIGURE 3. 31 RE HOUSE FLOOR HEATING PIPE SYSTEM. (FLOOR MORTAR & BEFORE FLOOR TILE FINISHING).....	80
FIGURE 3. 32 WATER SOURCE HEAT PUMP FOR FLOOR HEATING INSTALLED IN RE HOUSE .....	80
FIGURE 3. 33 INFRARED PHOTOGRAPHY OF FLOOR HEATING. (WHEN CIRCULATING HOT WATER IS 28 °C) .....	81
FIGURE 3. 34 CONFIGERATION OF FLOOR HEATING PIPE SYSTEM.....	81
FIGURE 3. 35 INSIDE THE HEAT PUMP FOR AIR CONDITIONING.....	82
FIGURE 3. 36 APPEARANCE OF THE PROTOTYPE WATER SOURCE HEAT PUMP FOR AIR CONDITIONING.....	83
FIGURE 3. 37 INSTALLATION IN THE LOFT OF THE RE HOUSE AND CONNECTED THE DUCT AND BLOWOUT NOZZLE. .....	86
FIGURE 3. 38 THE HEAT PUMP FOR AIR CONDITIONING SET ON THE LOFT AND DUCT .....	86
FIGURE 3. 39 CONFIGURATION OF WATER SOURCE DOMESTIC HOT WATER SUPPLY HEAT PUMP PROTOTYPE .....	87
FIGURE 3. 40 STRUCTURE OF WATER SOURCE HEAT PUMP FOR DOMESTIC HOT WATER SUPPLY PROTOTYPE.....	88
FIGURE 3. 41 PERFORMANCE TEST OF HOT WATER SUPPLY HEAT PUMP IN COLD WEATHER(TEST ROOM). .....	88
FIGURE 3. 42 TOP VIEW OF WATER SOURCE HEAT PUMP FOR DOMESTIC HOT WATER SUPPLY. ....	90
FIGURE 3. 43 THE WATER STORAGE TANK AND HEAT PUMP FOR DOMESTIC HOT WATER SUPPLY.....	90
<b>Chapter 4</b>	
FIGURE 4. 1 PHOTOGRAPHY OF RE HOUSE IN SPRING. ....	95
FIGURE 4. 2 TEST BUILDING OF DEVELOPMENT SYSTEM (RE HOUSE). ....	96
FIGURE 4. 3 SYSTEM CONFIGURATION OF THE HEAT PUMP SYSTEM IN THE RE HOUSE. ....	96
FIGURE 4. 4 RE HOUSE FACILITY PLAN AND ELEVATION. ....	97

FIGURE 4. 5 RE HOUSE DUCT PLAN AND ELEVATION.....	98
FIGURE 4. 6 CONFIGURATION OF RE HOUSE FLOOR HEATING SYSTEM.....	99
FIGURE 4. 7 SPEED CONTROL OF THE COMPRESSOR UNIT.....	101
FIGURE 4. 8 CONTROL METHOD OF SSHP FOR WATER LOOP TEMPERATURE.....	102
FIGURE 4. 9 THE SSHP CONTROL SCHEDULES FOR THE CIRCULATING WATER LOOP TEMPERATURE:.....	103
FIGURE 4. 10 MEASURING POINT FOR CONTROL OF FHHP.....	104
FIGURE 4. 11 MEASUREMENTS OF THE ENERGY CONSUMPTION OF EACH HEAT PUMP UNIT.....	106
FIGURE 4. 12 MEASUREMENTS OF UNDERGROUND TEMPERATURE.....	106
FIGURE 4. 13 FLOW METER FOR MEASURING THE FLOW RATE OF CIRCULATING WATER.....	107
FIGURE 4. 14 SCREENSHOT OF DATA LOGGER OF THE WEATHER STATION.....	107
FIGURE 4. 15 SCREENSHOT OF THE DATA LOGGER FOR MEASURING THE MAIN PARAMETERS FOR SYSTEM.....	108
FIGURE 4. 16 DIMENSIONS AND MEASURING POINTS IN THE HEAT PUMP SYSTEM.....	109
FIGURE 4. 17 WEATHER CONDITIONS ON MARCH 25 <sup>TH</sup> .....	114
FIGURE 4. 18 CHANGES IN SSHP PERFORMANCE OVERTIME ON MARCH 25 <sup>TH</sup> .....	115
FIGURE 4. 19 CHANGES IN THE CIRCULATING WATER TEMPERATURE AT THE SSHP UNIT.....	115
FIGURE 4. 20 CHANGES IN FHHP PERFORMANCE OVERTIME ON MARCH 25 <sup>TH</sup> .....	115
FIGURE 4. 21 CHANGES IN THE CIRCULATING WATER TEMPERATURE AT THE FHHP UNIT.....	116
FIGURE 4. 22 CHANGES IN THE FLOOR HEATING LOOP OF THE FHHP UNIT.....	116
FIGURE 4. 23 CHANGES IN THE FLOOR SURFACE AND INDOOR AIR TEMPERATURE.....	116
FIGURE 4. 24 CHANGES IN THE SSHP OUTDOOR PANEL AND REFRIGERANT CIRCULATION.....	117
FIGURE 4. 25 RELATIONSHIP BETWEEN THE COP OF SSHP AND SOLAR RADIATION.....	117
FIGURE 4. 26 RELATIONSHIP BETWEEN THE COP OF SSHP AND DRY BULB TEMPERATURE.....	117
FIGURE 4. 27 CHANGES IN THE CENTRAL BOREHOLE TEMPERATURE.....	118
FIGURE 4. 28 DIFFERENCE BETWEEN UNDISTURBED UNDERGROUND AND BOREHOLE CENTRAL TEMPERATURE...119	119
FIGURE 4. 29 HEATING OPERATION PERFORMANCE ON 25 MARCH(ON THE RIGHT).....	120
FIGURE 4. 30 WEATHER CONDITIONS ON MARCH 21 <sup>ST</sup> .....	122
FIGURE 4. 31 CHANGES IN SSHP PERFORMANCE OVER TIME.....	122
FIGURE 4. 32 CHANGES IN THE CIRCULATING WATER TEMPERATURE IN THE SSHP.....	122
FIGURE 4. 33 CHANGES IN THE FHHP PERFORMANCE OVER TIME.....	123
FIGURE 4. 34 CHANGES IN THE CIRCULATING WATER TEMPERATURE IN THE FHHP.....	123

FIGURE 4. 35 CHANGES IN THE FLOOR HEATING LOOP OF THE FHHP UNIT.....	123
FIGURE 4. 36 CHANGES IN THE FLOOR AND INDOOR AIR TEMPERATURE.....	124
FIGURE 4. 37 CHANGES IN THE SSHP OUTDOOR PANEL AND REFRIGERANT CIRCULATION. ....	124
FIGURE 4. 38 RELATIONSHIP BETWEEN THE COP OF SSHP AND DRY BULB TEMPERATURE. ....	124
FIGURE 4. 39 RELATIONSHIP BETWEEN THE COP OF SSHP AND SOLAR RADIATION.....	125
FIGURE 4. 40 CHANGES IN THE CENTRAL BOREHOLE TEMPERATURE.....	126
FIGURE 4. 41 DIFFERENCE BETWEEN UNDISTURBED UNDERGROUND AND BOREHOLE CENTRAL TEMPERATURE...126	
FIGURE 4. 42 HEATING OPERATION PERFORMANCE ON 21 MARCH(ON THE LEFT).....	127
FIGURE 4. 43 HEAT OUTPUT, POWER CONSUMPTION, AND POWER GENERATION OVER MARCH. ....	128
FIGURE 4. 44 CHANGES IN CENTRAL BOREHOLE TEMPERATURE FROM 1 <sup>ST</sup> TO 27 <sup>TH</sup> MARCH.....	130
FIGURE 4. 45 DRY BULB TEMPERATURE IN MARCH.....	131
FIGURE 4. 46 SOLAR RADIATION IN MARCH .....	131
FIGURE 4. 47 SSHP PERFORMANCE IN MARCH.....	132
FIGURE 4. 48 FHHP PERFORMANCE IN MARCH .....	132
FIGURE 4. 49 WEATHER CONDITION ON 24 <sup>TH</sup> JULY. ....	136
FIGURE 4. 50 TEMPORAL CHANGE OF ACHP PERFORMANCE ON 24 <sup>TH</sup> JULY.....	136
FIGURE 4. 51 TEMPORAL CHANGE OF ACHP PERFORMANCE ON 24 <sup>TH</sup> JULY.....	137
FIGURE 4. 52 INDOOR TEMPERATURE CHANGE DURING COOLING OPERATION ON 24 <sup>TH</sup> JULY.....	137
FIGURE 4. 53 TEMPORAL CHANGE OF SSHP HEAT DISSIPATION PERFORMANCE DURING THE 24 <sup>TH</sup> NIGHT. ....	137
FIGURE 4. 54 TEMPORAL CHANGE OF SSHP HEAT DISSIPATION PERFORMANCE DURING THE 24 <sup>TH</sup> NIGHT. ....	138
FIGURE 4. 55 TEMPERATURE TRANSITION OF OUTDOOR PANEL DURING HEAT DISSIPATION OPERATION.....	138
FIGURE 4. 56 TEMPORAL CHANGE OF HWHP PERFORMANCE ON 24 <sup>TH</sup> JULY. ....	138
FIGURE 4. 57 WEATHER CONDITION ON 25 <sup>TH</sup> JULY. ....	139
FIGURE 4. 58 TEMPORAL CHANGE OF ACHP PERFORMANCE ON 25 <sup>TH</sup> JULY.....	139
FIGURE 4. 59 INDOOR TEMPERATURE CHANGE DURING COOLING OPERATION ON 25 <sup>TH</sup> JULY.....	139
FIGURE 4. 60 TEMPORAL CHANGE OF HWHP PERFORMANCE ON 25 <sup>TH</sup> JULY. ....	140
FIGURE 4. 61 CHANGES IN CENTRAL BOREHOLE TEMPERATURE FROM 24-25 JULY.....	140
FIGURE 4. 62 UNDISTURBED UNDERGROUND AND CENTRAL BOREHOLE TEMPERATURE FROM 24-25 JULY. ....	140
FIGURE 4. 63 COOLING OPERATION PERFORMANCE ON 24-25 JULY.....	142
FIGURE 4. 64 WEATHER CONDITION ON 13 NOVEMBER.....	144

FIGURE 4. 65 TEMPORAL CHANGE OF ACHP SPACE HEATING PERFORMANCE ON 13 NOVEMBER.....	144
FIGURE 4. 66 TEMPORAL CHANGE OF SSHP HEAT COLLECTION PERFORMANCE ON 13 NOVEMBER. ....	145
FIGURE 4. 67 INDOOR TEMPERATURE CHANGE DURING THE SPACE HEATING OPERATION ON 13 NOVEMBER....	145
<b>Chapter 5</b>	
FIGURE 5. 1 MASS FLOW AT A TINY FLUID ELEMENT. ....	152
FIGURE 5. 2 THE STRESS ACTING ON ALL SURFACES IN THE X-DIRECTION. ....	154
FIGURE 5. 3 HEAT FLUX AT A TINY FLUID ELEMENT.....	156
FIGURE 5. 4 SCHEMATIC OF THE COMPUTATIONAL MODEL SHOWING THE TARGET APPARATUS.....	162
FIGURE 5. 5 SCHEMATICS OF THE COMPUTATIONAL MODEL: (A) COMBINATION OF CONCENTRIC REDUCER AND EQUAL TEE; (B) VIEWS OF THE COMPUTATIONAL GRID (POLYHEDRAL MESH AND PRISM LAYER MESH).....	162
FIGURE 5. 6 PIPE INTERNAL WATER PRESSURE DISTRIBUTION FOR SYSTEM FLOW PATH: (A) CENTRALIZED PUMPING SYSTEM WITH CP CONTROL; (B) DECENTRALIZED PUMPING SYSTEM.....	167
FIGURE 5. 7 SCHEMATICS OF THE RE HOUSE HEAT PUMP SYSTEM. ....	169
FIGURE 5. 8 DETAILED PARAMETERS OF GHX USED IN THE PIPING SYSTEM. ....	169
FIGURE 5. 9 SCHEMATICS OF THE PIPING SYSTEM OF THE RE HOUSE.....	170
FIGURE 5. 10 THREE DIMENSIONAL MODEL OF GHX. ....	170
FIGURE 5. 11 VIEWS OF THE COMPUTATIONAL GRID (POLYHEDRAL MESH AND PRISM LAYER MESH) ON SOME OF THE DOMAIN SURFACES: (A) ELBOW; (B) INLET & OUTLET. ....	171
FIGURE 5. 12 CENTRAL GHX TEMPERATURE DISTRIBUTION AT 6:00 AND 13:00 ON MARCH 25.....	173
FIGURE 5. 13 SCHEMATICS OF THE SYSTEM DIAGRAM TO DEMONSTRATE CASE1.....	174
FIGURE 5. 14 SCHEMATICS OF THE SYSTEM DIAGRAM TO DEMONSTRATE CASE2.....	174
<b>Chapter 6</b>	
FIGURE 6. 1 SIMULATION RESULT OF NEWTONSCOOLING. ....	189
FIGURE 6. 2 SCHEMATICS OF RE HOUSE AND HEAT PUMP SYSTEM. ....	191
FIGURE 6. 3 BUILDING PLAN OF RE HOUSE. ....	192
FIGURE 6. 4 BUILDING ELEVATION OF RE HOUSE.....	192
FIGURE 6. 5 CONFIGURATION OF RE HOUSE FLOOR HEATING SYSTEM.....	193
FIGURE 6. 6 THE MODEL OF HEAT PUMP FOR FLOOR HEATING USED IN MODELING. ....	198
FIGURE 6. 7 FHHP PERFORMANCE DATA AT NOMINAL CONDITION(SOLID GREEN LINE).....	198
FIGURE 6. 8 THERMAL RESISTANCE NETWORK OF FLOOR HEATING SYSTEM MODEL[33].....	199

FIGURE 6. 9 MODELING OF SINGLE CIRCUIT SLAB AS THE FLOOR HEATING SYSTEM[34].	199
FIGURE 6. 10 RESISTANCE-CAPACITANCE NETWORK FOR A SINGLE U-TUBE BOREHOLE CONFIGURATION[37].	201
FIGURE 6. 11 HEAT TRANSFER MODEL BETWEEN CIRCULATING FLUID AND FILLING OF A SINGLE U-TUBE[33].	201
FIGURE 6. 12 MODEL OF SOLAR COLLECTOR FOR ASHRAE STANDARD 93-2010 IN MODELICA[36].	202
FIGURE 6. 13 INDIRECT CONFIGURATION OF SOLAR ASSISTED HEAT PUMP.	203
FIGURE 6. 14 MODEL OF COMBINATION OF RE HOUSE AND HEAT PUMP SYSTEM.	204
FIGURE 6. 15 WEATHER CONDITION ON 21 MARCH.	210
FIGURE 6. 16 INDOOR ENVIRONMENT CHANGES IN THE MULTI-PURPOSE ROOM(EXPERIMENT).	210
FIGURE 6. 17 INDOOR ENVIRONMENT CHANGES IN THE MULTI-PURPOSE ROOM(SIMULATION).	210
FIGURE 6. 18 CHANGES OF FLOOR HEATING SYSTEM IN THE MULTI-PURPOSE ROOM(SIMULATION).	211
FIGURE 6. 19 CHANGES OF FLOOR HEATING SYSTEM IN THE MEASUREMENT ROOM(SIMULATION).	211
FIGURE 6. 20 CHANGES IN THE WATER LOOP SIDE OF FHHP(EXPERIMENT).	211
FIGURE 6. 21 CHANGES IN THE WATER LOOP SIDE OF FHHP(SIMULATION).	212
FIGURE 6. 22 CHANGES IN THE PERFORMANCE OF FHHP(EXPERIMENT).	212
FIGURE 6. 23 CHANGES IN THE PERFORMANCE OF FHHP(SIMULATION).	212
FIGURE 6. 24 WEATHER CONDITION ON 25 MARCH.	214
FIGURE 6. 25 INDOOR ENVIRONMENT CHANGES IN THE MULTI-PURPOSE ROOM(EXPERIMENT).	214
FIGURE 6. 26 INDOOR ENVIRONMENT CHANGES IN THE MULTI-PURPOSE ROOM(SIMULATION).	215
FIGURE 6. 27 CHANGES OF FLOOR HEATING SYSTEM IN THE MULTI-PURPOSE ROOM(SIMULATION).	215
FIGURE 6. 28 CHANGES OF FLOOR HEATING SYSTEM IN THE MEASUREMENT ROOM(SIMULATION).	215
FIGURE 6. 29 CHANGES IN THE WATER LOOP SIDE OF FHHP(EXPERIMENT).	216
FIGURE 6. 30 CHANGES IN THE WATER LOOP SIDE OF FHHP(SIMULATION).	216
FIGURE 6. 31 CHANGES IN THE PERFORMANCE OF FHHP(EXPERIMENT).	216
FIGURE 6. 32 CHANGES IN THE PERFORMANCE OF FHHP(SIMULATION).	217
FIGURE 6. 33 CHANGES IN THE PERFORMANCE OF SSHP(EXPERIMENT).	218
FIGURE 6. 34 CHANGES IN THE PERFORMANCE OF SSHP(SIMULATION).	218
FIGURE 6. 35 CHANGES IN THE WATER LOOP SIDE OF SSHP(EXPERIMENT).	218
FIGURE 6. 36 CHANGES IN THE WATER LOOP SIDE OF SSHP(SIMULATION).	219
FIGURE 6. 37 CHANGES IN THE PERFORMANCE OF SSHP(EXPERIMENT).	220
FIGURE 6. 38 CHANGES IN THE PERFORMANCE OF SSHP(SIMULATION).	220

FIGURE 6. 39 CHANGES IN THE WATER LOOP SIDE OF SSHP(EXPERIMENT).....	220
FIGURE 6. 40 CHANGES IN THE WATER LOOP SIDE OF SSHP(EXPERIMENT).....	221
FIGURE 6. 41 CHANGE OF TEMPERATURE DIFFERENCE BETWEEN SSHP INLET AND OUTLET(SIMULATION).....	221

# List of tables

## Chapter 3

TABLE 3. 1 SPECIFICATION OF MEASURING DEVICES USED IN EXPERIMENTS .....	57
TABLE 3. 2 EXPERIMENTAL CONDITIONS OF FIVE EXPERIMENTAL CASES, UNDER THE SAME FLOW RATE CONDITIONS .....	59
TABLE 3. 3 CALORIMETER TEST RESULTS OF WATER SOURCE HEAT PUMP FOR AIR CONDITIONING. (COOLING).....	84
TABLE 3. 4 CALORIMETER TEST RESULTS OF WATER SOURCE HEAT PUMP FOR AIR CONDITIONING. (HEATING).....	85
TABLE 3. 5 OPERATING PERFORMANCE TEST RESULTS UNDER COLD CONDITIONS (TEST ROOM DATA).....	89

## Chapter 4

TABLE 4. 1 MAIN PARAMETER OF EACH HEAT PUMP IN THE SYSTEM.....	105
TABLE 4. 2 COP OF EACH HEAT PUMP AND THE WHOLE SYSTEM IN MARCH .....	120
TABLE 4. 3 COP OF EACH HEAT PUMP AND THE WHOLE SYSTEM IN MARCH .....	127
TABLE 4. 4 COP VALUES FOR THE DIFFERENT HEAT PUMPS AND FOR THE OVERALL SYSTEM.....	128
TABLE 4. 5 RESULTS OF THE PERFORMANCE TEST OF THE WHOLE SYSTEM IN SUMMER. (24 <sup>TH</sup> -25 <sup>TH</sup> JULY).....	142
TABLE 4. 6 RESULTS OF THE PERFORMANCE TEST OF THE WHOLE SYSTEM IN SUMMER. (25 <sup>TH</sup> -26 <sup>TH</sup> JULY).....	142

## Chapter 5

TABLE 5. 1 SUMMARY OF BOUNDARY AND INITIAL CONDITIONS. ....	163
TABLE 5. 2 COMPARISON OF GAUGE PRESSURE BETWEEN CFD AND EXPERIMENT (DISCREPANCY OF CFD MODEL AGAINST EXPERIMENTAL RESULTS IS GIVEN IN PARENTHESES).....	164
TABLE 5. 3 COMPARISON OF PRESSURE LOSS BETWEEN CFD AND EXPERIMENT [KPA] (DISCREPANCY GIVEN IN PARENTHESES).....	166
TABLE 5. 4 SUMMARY OF SIMULATION CONDITIONS.....	173
TABLE 5. 5 COMPARISON OF GAUGE PRESSURE BETWEEN CFD AND EXPERIMENT [KPA] (DISCREPANCY GIVEN IN PARENTHESES).....	176
TABLE 5. 6 COMPARISON OF PRESSURE LOSS BETWEEN CFD AND EXPERIMENT [KPA] (DISCREPANCY GIVEN IN PARENTHESES).....	176
TABLE 5. 7 COMPARISON OF TEMPERATURE BETWEEN CFD AND EXPERIMENT [°C] (DISCREPANCY GIVEN IN PARENTHESES).....	177

## Chapter 6

TABLE 6. 1 CONFIGURATION AND MATERIALS OF RE HOUSE .....	194
TABLE 6. 2 PARAMETERS OF RE HOUSE SETTING. ....	205
TABLE 6. 3 PARAMETERS OF THE FLOOR HEATING SYSTEM. ....	206
TABLE 6. 4 PARAMETERS OF THE GHX .....	206
TABLE 6. 5 PHYSICAL PROPERTY VALUES USED FOR GHX MODELING.....	207
TABLE 6. 6 PARAMETERS OF SSHP, INCLUDING OUTDOOR PANEL AND PERFORMANCE OF HEAT PUMP. ....	207
TABLE 6. 7 CASE SETTING FOR VERIFICATION OF THE SYSTEM MODEL. ....	208

# Nomenclature

$A$ : The upper limit of the measuring range

$f$ : Pressure loss per unit length (kPa/m)

$g$ : Gravitational acceleration (m/s<sup>2</sup>)

$H$ : Total head loss through system (m)

$k$ : Turbulent kinetic energy (m<sup>2</sup>/s<sup>2</sup>)

$k_s$ : Equivalent sand-grain roughness height (m)

$L$ : Total length of the piping system (m)

$\Delta p$ : Pressure loss of entire hydronic system (kPa)

$P_{pi}$ : Pump inlet pressure (kPa)

$P_{po}$ : Pump outlet pressure (kPa)

$P_t$ : Theoretical power requirement of pump (W)

$\Delta P_{b1}$ : Total pressure loss of entire hydronic system for pump in branch pipe 1 (kPa)

$\Delta P_{b2}$ : Total pressure loss of entire hydronic system for pump in branch pipe 2 (kPa)

$\Delta P_m$ : Total pressure loss of entire hydronic system for main pump (kPa)

$R$ : Virtual resistance (kPa)

$\Delta R_{b1}$ : Virtual resistance in branch pipe 1 (kPa)

$\Delta R_{b2}$ : Virtual resistance in branch pipe 2 (kPa)

$\Delta R_{b1-b2}$ : Virtual resistance between branch pipes 1 and 2 (kPa)

$\Delta R_m$ : Virtual resistance in main return pipe (kPa)

$\dot{V}$ : Volumetric flow rate (L/min)

$\dot{V}_{b1}$ : Volumetric flow rate in branch pipe 1 (L/min)

$\dot{V}_{b2}$ : Volumetric flow rate in branch pipe 2 (L/min)

$\dot{V}_m$ : Volumetric flow rate in main pipe (L/min)

## Subscripts

$ac$ : air conditioning

$b_j$ : Branch Pipe 1

$b_2$ : Branch Pipe 2

$b_{1,2}$ : Between Branches 1 and 2

$eg$ : extraction from ground

$fh$ : floor heating

$fit$ : Pipe fittings

$hw$ : hot water

$in$ : inlet

$m$ : Main pipe

$out$ : outlet

$str$ : Straight pipe

$sys$ : system

$w$ : water

$wl$ : water loop

### **Greek letters**

$\gamma$ : Accuracy grade (%)

$\varepsilon$ : Turbulent dissipation rate ( $m^2/s^3$ )

$\mu$ : Dynamic viscosity of the fluid ( $Pa \cdot s$  or  $kg/m \cdot s$ )

$\nu$ : Kinematic viscosity of the fluid ( $m^2/s$ )

$\rho$ : Fluid density ( $kg/m^3$ )

$\tau$ : Shear stress (Pa)

### **abbreviations**

AHP: air conditioning heat pump

CFD: computational fluid dynamics

COP: coefficient of performance

Cu: copper

EER: energy efficiency ratio

FHHP: floor heating heat pump

GHX: ground heat exchanger

HP: heat pump

HVAC: heating, ventilation and air conditioning

HWHP: hot water heat pump

NREL: national renewable energy laboratory

PCM: phase change material

PE: polyethylene

PID: proportional–integral–derivative

PV: photovoltaic

PVC: polyvinyl Chloride

SSHP: sky source heat pump

# **Chapter 1: Introduction**

## Background

### *Current status of renewable energy application for buildings*

The energy input for building operations is mainly composed of fossil fuel-based energy carriers. It, therefore, accounts for a large proportion of global greenhouse gas emissions (~30% of the total worldwide emissions)[1–3]. Although the exact quantity varies by country and region, energy use in buildings is thought to constitute 35–40% of global energy usage[4–7]. Driven by developing countries' increasing demand for more energy, extensive use of energy-consuming equipment, and the rapid growth of global building construction area, the energy demand of buildings and buildings continues to grow[8]. Thus, to decrease the energy demand and its related emissions, significant effort has been focused on boosting renewable energies and improvement of energy efficiency in building operations such as heating and cooling.

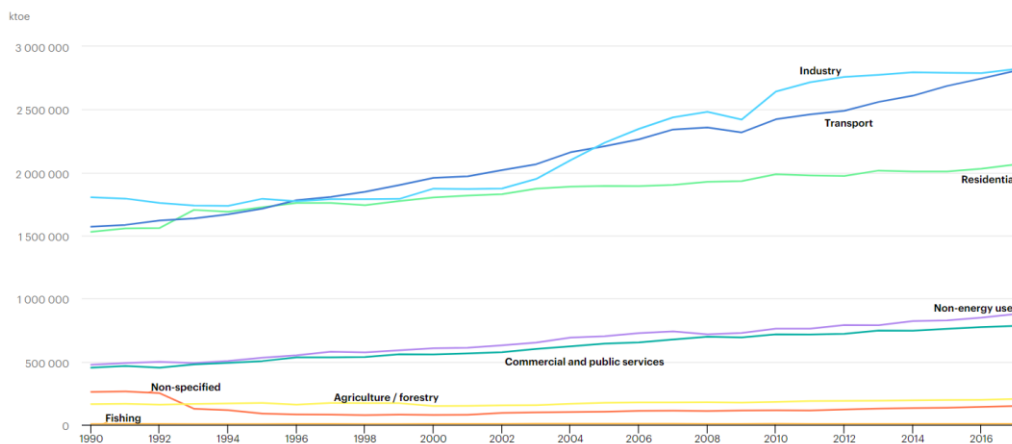


Figure 1. 1 World total final energy consumption (TFC) by sector from 1990 to 2017[9]

However, the growth of floor area and population exceeds the improvement of energy efficiency, leading to strong growth in energy consumption in significant construction industries. Still, the growth of the floor area under current conditions continues to be out of line with increasing global energy demand[10]. As shown in Figure 1. 1, for the world total final consumption by sector from 1990 to 2017, various reasons such as extreme weather result in the increasing energy demand for heating and cooling in almost every country, the energy consumption of the construction industry

represented by residential has increased by as much as 30%. According to the latest research report of International Energy Agency (IEA), due to the widespread use of traditional inefficient energy supply technologies such as coal, the lack of effective policies and insufficient investment in the development of sustainable energy application in the building sector, the energy and building industry has great potential and needs to be developed[11,12].

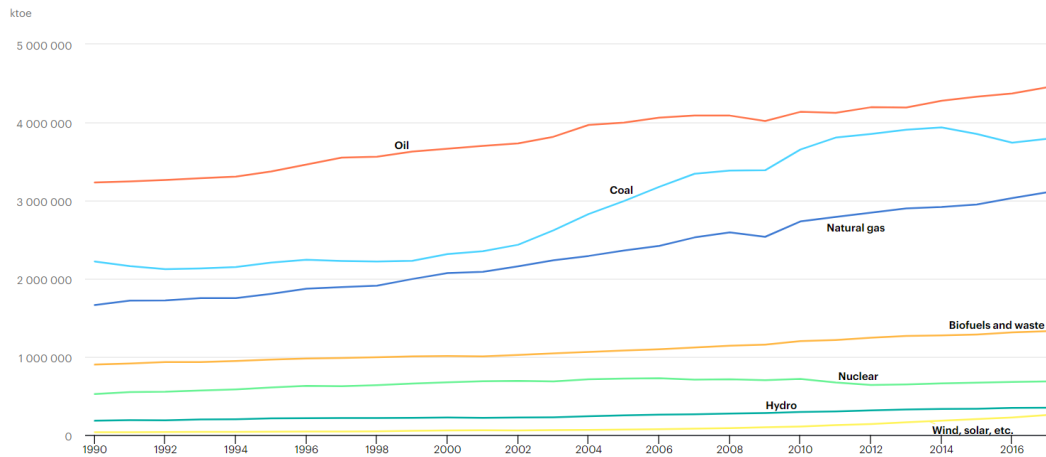


Figure 1. 2 World total primary energy supply (TPES) by the source from 1990 to 2017[9]

Figure 1. 2 shows the world total primary energy supply (TPES) by the source from 1990 to 2017, which will be statistical analysis by IEA every year. Based on this result from 1990 to 2017, it indicates that if we focus on the world's overall energy supply, we can see that traditional fossil energy represented by oil, coal, and natural gas still occupies a significant position in the supply chain. It is worth noting that the use of biofuels and waste heat has gradually increased in recent years. However, although renewable energy sources such as wind and solar are also growing, their share of the overall energy supply is still meager[13]. Therefore, the energy and emissions savings potential remain untapped, mainly because of the continued use of less efficient technologies. A drastic shift towards clean energy technologies such as heat pumps and solar thermal heating is needed to achieve sustainable development goals.

Heat accounts for 50% of global final energy consumption in 2018 and is the largest end-use of energy, accounting for 40% of global carbon dioxide (CO<sub>2</sub>) emissions. Approximately 46% of the total heat generated is consumed in buildings for heating spaces and water. Especially in modern society, heating and cooling are the main components of building aggregate energy demand[14,15]. In recent years, due to the ever-changing extreme weather, the building's energy demand for heating

and cooling has increased. However, due to the limited introduction of renewable energy, the use of fossil fuel-based heating equipment has been used. Also, the growing demand for cooling is affecting power generation and distribution capabilities, especially during peak demand periods and extremely high-temperature events. As shown in Figure 1. 3, which indicates the year-to-year trend of heat from renewable energy and waste, the heat from geothermal and solar thermal energy is not used on a large scale, and these parts are very suitable heat sources for the heating of buildings[15]. Through reasonable heat pumps and energy storage technologies, a stable and efficient operation can be guaranteed for building heating purposes. The scorching weather makes a must for people to keep air conditioning for cooling use; this phenomenon is especially noticeable in tropical regions. Through soil heat storage, the cross-peak ice thermal storage application, it can help alleviate the electricity demand of air-conditioning cooling during peak hours.

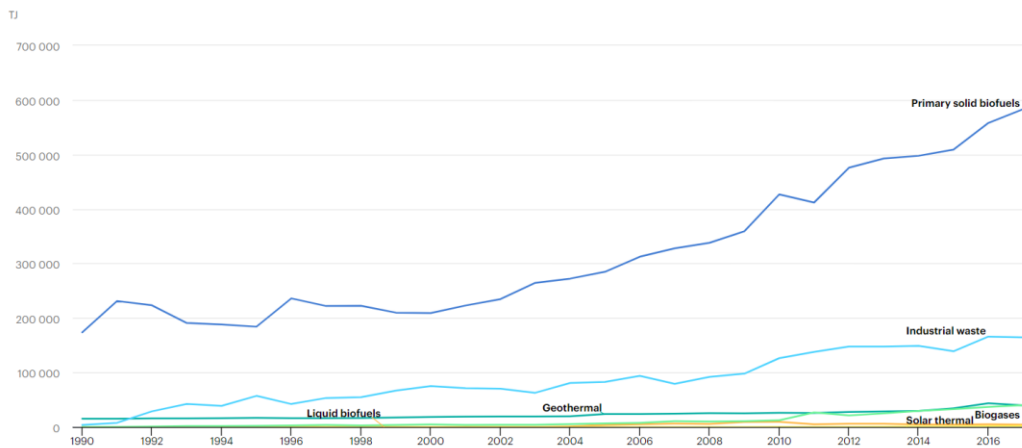


Figure 1. 3 World heat generation from renewables and waste by source from 1990 to 2017[9]

As shown in Figure 1. 4, due to two oil shocks in the 1970s, energy conservation progressed mainly in the manufacturing industry, and the development of energy-saving technologies also flourished in Japan. While crude oil prices remained low throughout the 1990s, energy consumption increased mainly in the household sector and business sector. After the mid-2000s, the cost of crude oil rose again, and the final energy consumption peaked in 2005, showing a downward trend. From fiscal 2011 onward, the number has decreased further due to increased awareness of power-saving since the Great East Japan Earthquake. In 2017, the final energy consumption increased for the first time in seven years, as real GDP increased from 2016, and heating demand increased due to the severe winter compared to the previous year[16].

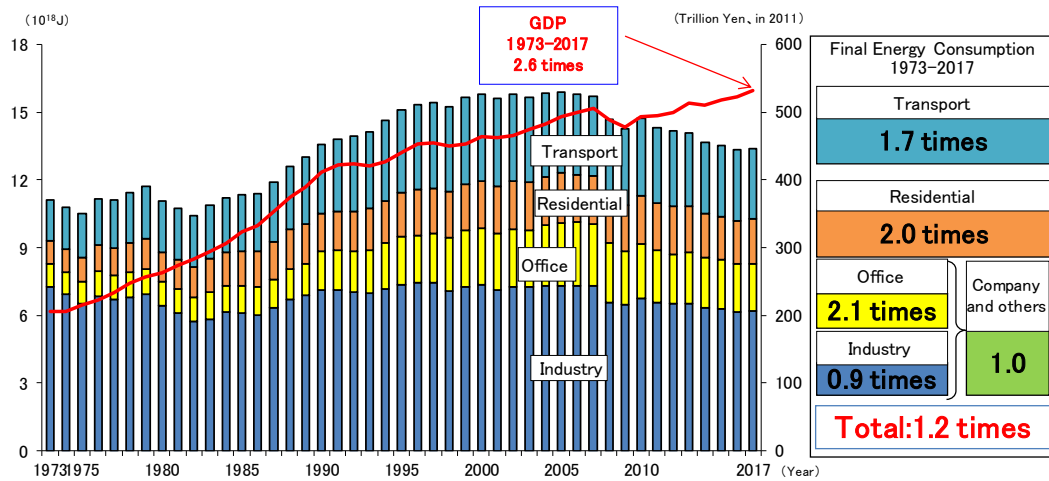


Figure 1. 4 Changes in final energy consumption and real GDP of Japan from the 1970s[16]

Figure 1. 5 shows the changes in energy consumption per household and energy consumption by application in Japan. The household energy consumption can be divided into five methods: cooling, heating, domestic hot water supply, cooking, power, and lighting (use of home appliances). The share in 1965 was in the order of hot water supply, heating, power/lighting, etc., and then air conditioning, but due to the spread, upsizing, and diversification of household appliances and changes in lifestyles, the share for power/lighting has increased.

Besides, due to the popularization of air conditioners, cooling applications have increased, while the demands for heating, cooling, and hot water supply have been relatively reduced. As a result, the market share for power and lighting, etc. in fiscal 2016 was in the order of hot water supply, heating, air conditioning, and air conditioning[17].

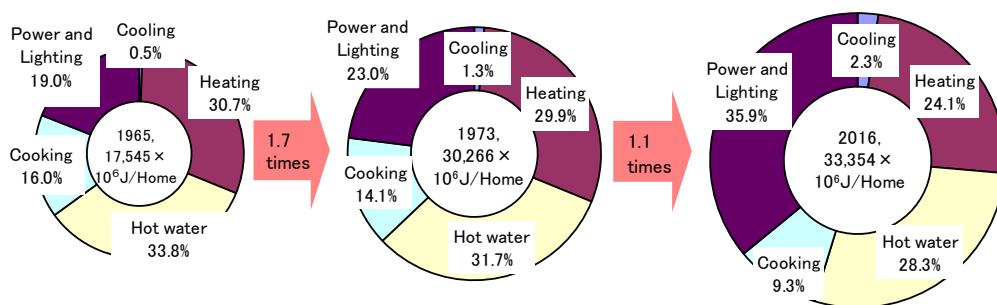


Figure 1. 5 Changes in energy consumption per household and energy consumption by application in Japan[17]

Overall, the building sector accounts for a large portion of total energy-related CO<sub>2</sub> emissions, mainly due to emissions from the power generation of buildings used for cooling and heating and lighting. In recent years, the construction area has increased, and the demand for energy services has, therefore, continued to grow; the electricity consumption has also increased. With the acceleration of urbanization and the impact of extreme weather, the increasing demand for air conditioning and other equipment has put pressure on the power system.

Because of the utilization of heat pumps in buildings and industries, the increase in energy conversion efficiency keeps the power demand for other end uses (such as lighting and cooling) relatively stable, resulting in improved power supply worldwide. Therefore, integrating more renewable energy into the energy system will become the key to solving energy problems.

### *Development of renewable energy technologies for sustainable and energy-efficient building*

As mentioned in the previous section, appropriate energy measures are also essential for energy supply stability and security issues, and the reduction of greenhouse gas emissions. It is expected that the significant use of renewable energy will be the key to solving these problems. Generally, the use of renewable energy imagines the creation of electricity, such as solar power generation and wind power generation. Still, renewable energy for heat utilization, such as solar heat and geothermal heat, has an enormous endowment; renewable energy for heating and cooling purpose is also essential as power generation. However, modern renewable energy such as solar energy, geothermal energy, etc. (biomass energy excluding traditional uses) only met 10% of global thermal demand in 2018[11,12].

As shown in Figure 1. 6, bioenergy accounts for a large portion of the total renewable energy heat consumption, while solar thermal is only a small part. To achieve higher penetration of renewable energy and improve energy efficiency, especially in the building sector, to increase the use of renewable energy in the field of heating, and to improve energy efficiency in buildings and industries have become very important. This same goal as sustainable development can be achieved by increasing solar heat and geothermal utilization in building energy systems in the modern city energy supply system.

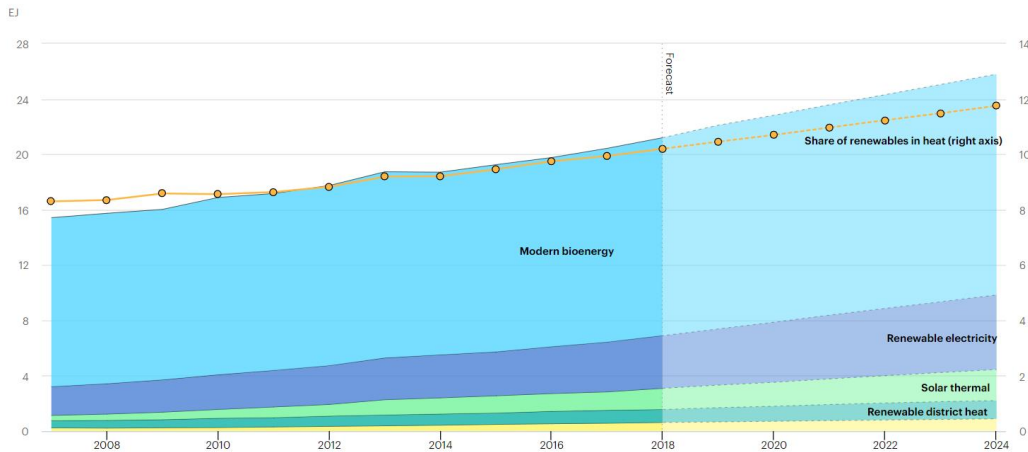


Figure 1. 6 World renewable heat consumption from (2007-2024)[9]

Figure 1. 7 shows the heating technology sales in the Sustainable Development Scenario by IEA from 2010 to 2030. Since 2010, sales of heat pumps and renewable heating equipment (such as solar water heating systems) have continued to grow by about 5% each year. However, fossil fuel-based equipment still accounts for more than half of sales, while traditional electric heating equipment with lower efficiency has increased by another 30%. In order to achieve the goal of renewable development, the share of heat pumps and renewable heating must continue to grow globally.

Heat pumps can still only meet less than 3% of global heating demand in buildings. But at the same time, the installed solar thermal capacity has increased substantially, almost equivalent to the installed solar photovoltaic capacity. Many countries use solar energy as part of their heating measures for sustainable heating of buildings. The field of application is also constantly expanding to change the industrial and regional energy infrastructure. However, on a global scale, solar thermal technology only met 2.1% of space and water heat demand in 2018. For the growth in renewable energy consumption for space heating purposes (Figure 1.8), we can know that although the application of renewable heat such as geothermal energy in the construction field remains at a low level, this takes up a large part of the energy consumption of the building [18,19].

The energy supply of buildings mainly depends on fossil fuels, which account for 25% of global greenhouse gas emissions. The source of energy is a factor that cannot be ignored at the beginning stage of energy system design[20,21]. Heat pumps are attracting attention as an essential technology to solve this problem, and renewable energy sources such as solar and geothermal heat that have less impact on the environment can be used as heat sources for buildings using heat pumps[22–25].

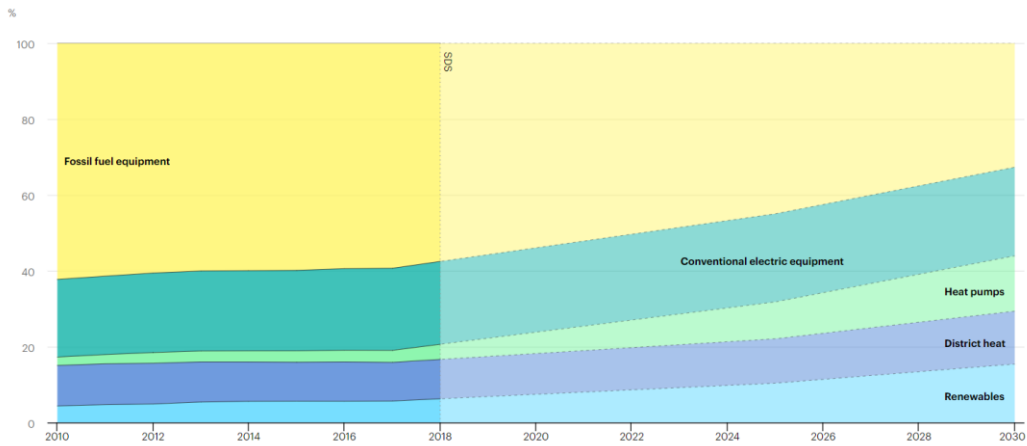


Figure 1. 7 Heating technology sales in the Sustainable Development Scenario (2010-2030)[9]



Figure 1.8 Growth in renewable energy consumption for heat (2013-2024)[9]

Correctly, the utilization and integration of solar and geothermal heat play an essential role in the improvement of the efficiency and stability of building energy systems. Photovoltaic panels (Figure 1. 9) and systems that use solar panels and geothermal heat exchangers to introduce solar energy and geothermal energy into building utilization have received more and more attention this year. However, as described above, many traditional heat pump systems only used one type of renewable energy sources such as geothermal heat or air heat to meet the demand for heating and cooling in buildings[26–30]. Although such a single source heat pump system has contributed to the reduction of the energy consumption of the building, each renewable energy source such as solar heat and geothermal heat has advantages and disadvantages according to its characteristics. For example, since solar heat is intermittent and uncertain, it is difficult to use it alone as a stable heat source,

geothermal heat has a steady output, but the available amount is limited.

Through the complementary use of different renewable energy sources, the development of a stable and efficient renewable energy supply system can solve the current and future building energy problems (example is shown in Figure 1. 10). Such technologies and attempts will play an essential role in the improvement of future urban energy systems and the achievement of the smart and flexible city (the introduction of renewable energy, low-temperature heating, and electric-heating).

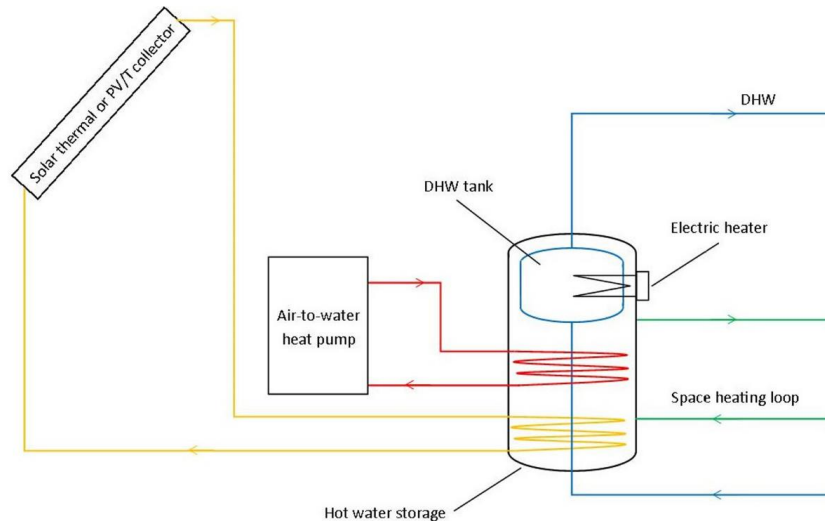


Figure 1. 9 A schematic drawing of the thermal part of the building energy system.[24]



Figure 1. 10 Integrated system of the photovoltaic system and geothermal heat pump for residential buildings.[23]

## Research objectives

As mentioned before, conventional renewable energy heat utilization systems have problems in efficiency and introduction cost and are currently not widely used in comparison with the actual amount. It is crucial to improve the performance of the renewable energy heat utilization system and reduce the introduction cost.

Therefore, in this research, we plan to develop a new distributed heat pump system that can utilize various types of renewable energy. By this kind of structure, we can add a variety of renewable energy into the system through the water circulation loop. It is possible to take these renewable energy sources as heat sources for heat pumps, which can effectively provide cooling, heating, and domestic hot water supply at the required temperature in buildings.

Specifically, the objectives of this research can be concluded as follows:

- (1) the development and improvement of the prototype of each component such as water loop, sky source heat pump, water source heat pump for different purposes, and the whole system;
- (2) the performance evaluation of each heat pump machine and the overall operating performance of the whole system by field testing under different conditions, including winter, summer, and intermediate period;
- (3) Validation and accuracy evaluation of pressure drop and temperature analysis in the piping system based on CFD method by comparing with experimental data;
- (4) the development of system modeling suitable for this novel system based on the Modelica language. This modeling makes it possible to evaluate the performance of the system, optimize the operation, and redevelop the system under different operating conditions, control methods, and locations.

## Originality of this study

- (1) As the originality of this study, a novel distributed water-source heat pump system that can utilize multiple kinds of renewable energy was proposed based on daily cycle operation at a residential scale.
- (2) Then, the heating and cooling operation performance were first evaluated under different conditions based on field testing using a residential scale test building.
- (3) Besides, a CFD method for predicting pressure loss and temperature in the piping system including ground heat exchanger was implemented, and the accuracy was assessed.
- (4) Moreover, this study first developed a Modelica based modeling for this distributed heat pump system for further improvement and optimization, the validity, and accuracy were evaluated by comparing with experimental data.

# Thesis structure

The flow chart below demonstrated the structure of this thesis. This thesis is briefly divided into six sections: introduction; application of heat pump system in building for energy conservation; fundamentals of distributed water source heat pump system using renewable energy; evaluation of the performance of the heat pump system; validation of pressure and temperature prediction in the piping system based on CFD; and Modeling and simulation of distributed water source heat pump system using renewable energy with Modelica. This thesis is divided into seven chapters.

The Chapter1 introduction describes the research background and the purpose of this thesis.

To have a better understanding of the concept and design of this system, we review the related research of different heat pump systems in Chapter2, analyze the existing problems, and explain how the heat pump system proposed in this study solves these problems.

Next, In the Chapter3, we demonstrate the principle and concept of this system in detail. After that, the development of each component that constitutes this system will be described, including the water loop system, each heat pump, and geothermal heat exchanger.

Then, we detailed demonstrate the field testing and experimental performance analysis of the proposed heat pump system in Chapter4. Here, we conduct field testing in winter, summer, and interim period. Based on the experimental results, the heating and cooling performance of this system were tested and evaluated detailedly. The results under different conditions were also collected for modeling and simulation in the next chapter.

In Chapter5, we firstly review a previous study of pressure drop analysis in the piping system based on the CFD method. Then, we discuss and validate the accuracy of the prediction of pressure loss and temperature in the piping system of the RE house based on the CFD method.

Then, in Chapter6, we work on modeling and simulation of the distributed heat pump system based on Modelica language. We firstly review the methods and tools for building energy system modeling and introduce the principle of Modelica language. Then, based on the experiment, we conduct the modeling of the proposed heat pump system and validate its validity and accuracy by comparing it with experimental data.

Finally, Chapter7 summarizes all the critical points in this thesis and describes future subjects about this research.

<b>Chapter 1 Introduction</b>		
<ul style="list-style-type: none"> <li>▪ Background</li> <li>▪ Research objectives</li> </ul>		
↓		
<b>Chapter 2 Application of heat pump system in building for energy conservation</b>		
<ul style="list-style-type: none"> <li>▪ Air source heat pump system</li> <li>▪ Geothermal heat pump system</li> <li>▪ Solar assisted heat pump system</li> </ul>		
↓		
<b>Chapter 3 Fundamentals of distributed water source heat pump system using renewable energy</b>		
<ul style="list-style-type: none"> <li>▪ Concept and development of distributed water source heat pump system</li> <li>▪ Construction of water loop including initial cost and pumping system</li> <li>▪ Development of sky source heat pump, water source heat pump for floor heating, air conditioning and domestic hot water supply</li> <li>▪ Overview of double helical ground heat exchanger</li> </ul>		
↓		
<b>Chapter 4 Experimental performance analysis of distributed heat pump system using renewable energy</b>		
<ul style="list-style-type: none"> <li>▪ Winter experiment and performance analysis of sky source heat pump, floor heating heat pump and whole system on sunny/cloudy day, and one month.</li> </ul>	<ul style="list-style-type: none"> <li>▪ Summer experiment and performance analysis of sky source heat pump, air conditioning and domestic hot water heat pump and whole system in July.</li> </ul>	<ul style="list-style-type: none"> <li>▪ Interim experiment and performance analysis of sky source heat pump, air conditioning and domestic hot water heat pump in November.</li> </ul>
↓		
<b>Chapter 5 Pressure and temperature analysis of piping system based on CFD</b>		
<ul style="list-style-type: none"> <li>▪ Previous study of pressure drop analysis in piping system based on CFD method</li> <li>▪ Pressure drop and temperature analysis in piping system of RE house based on CFD method</li> <li>▪ Validation and discussion of pressure loss and temperature based on experimental results</li> </ul>		
↓		
<b>Chapter 6 Modeling of distributed heat pump system using renewable energy with Modelica</b>		
<ul style="list-style-type: none"> <li>▪ Review of methods and tools for modeling and simulation of building energy system</li> <li>▪ Fundamentals of Modelica and its application in HVAC and building field</li> <li>▪ Modeling description of distributed water source heat pump system using renewable energy</li> <li>▪ Simulation of winter operation and validation based on experimental data</li> </ul>		
↓		
<b>Chapter 7 Conclusions and future works</b>		
<ul style="list-style-type: none"> <li>▪ Conclusions</li> <li>▪ Recommendations for future work</li> </ul>		

## Summary

This chapter demonstrates the research background, research objectives, originality of this research, and the overall structure of this thesis. In a modern city where energy is becoming more precious, the use of renewable energy and the vitality and transformation of energy systems has become an inevitable trend of the future energy system. In this context, this study proposed a heat pump system designed to utilize multiple renewable energy sources, providing an idea and possibility for the next generation building or district energy or heat supply systems. Our purpose is to verify the feasibility and performance of this system through field testing and to build a suitable system model, which can optimize the system composition and control strategy for further explore the performance under different conditions. This thesis reports the detailed system development process and field testing based verification, as well as the modeling of the heat pump system.

---

## Reference

- [1] Tang R, Wang S, Shan K, Cheung H. Optimal control strategy of central air-conditioning systems of buildings at morning start period for enhanced energy efficiency and peak demand limiting. *Energy* 2018;151:771–81. doi:10.1016/j.energy.2018.03.032.
- [2] Ma X, Gao DC, Liang D. Improved Control Strategy of Variable Speed Pumps in Complex Chilled Water Systems Involving Plate Heat Exchangers. *Procedia Eng* 2017;205:2800–6. doi:10.1016/j.proeng.2017.09.889.
- [3] Ma J, Wang Y, Feng X. Simultaneous optimization of pump and cooler networks in a cooling water system. *Appl Therm Eng* 2017;125:377–85. doi:10.1016/j.applthermaleng.2017.07.026.
- [4] Shankar VKA, Umashankar S, Paramasivam S, Norbert H. Real time simulation of Variable Speed Parallel Pumping system. *Energy Procedia* 2017;142:2102–8. doi:10.1016/j.egypro.2017.12.612.
- [5] Bonvin G, Demasse S, Le Pape C, Maïzi N, Mazauric V, Samperio A. A convex mathematical program for pump scheduling in a class of branched water networks. *Appl Energy* 2017;185:1702–11. doi:10.1016/j.apenergy.2015.12.090.
- [6] Zhu X, Wang F, Niu D, Zhao L. Integrated modeling and operation optimization of circulating cooling water system based on superstructure. *Appl Therm Eng* 2017;127:1382–90. doi:10.1016/j.applthermaleng.2017.08.119.
- [7] Torregrossa D, Hansen J, Hernández-Sancho F, Cornelissen A, Schutz G, Leopold U. A data-driven methodology to support pump performance analysis and energy efficiency optimization in Waste Water Treatment Plants. *Appl Energy* 2017;208:1430–40. doi:10.1016/j.apenergy.2017.09.012.
- [8] IEA. Energy efficiency indicators highlights (2019 edition). 2017. doi:10.1787/9789264268692-en.
- [9] IEA. Data and Statistics. IEA 2020. doi:10.1016/b978-0-12-374970-3.00001-9.
- [10] IEA. Global Alliance for Buildings and Construction, International Energy Agency and the United Nations Environment Programme (2019): 2019 global status report for buildings and construction: Towards a zero-emission, efficient and resilient buildings and const. 2019.
- [11] IEA. Renewables 2019. Paris: 2019.

- 
- [12] IEA. Tracking Buildings. Paris: 2020.
- [13] IEA. The Future of Cooling in China. 2019. doi:10.1787/fd5f242d-en.
- [14] Thibaut Abergel, Delmastro C, Janoska P, Lane K, Prag A. Perspectives for the Clean Energy Transition. 2019.
- [15] IEA. Energy Efficiency 2019. 2019.
- [16] 経済産業省資源エネルギー庁. 平成30年度エネルギーに関する年次報告 (エネルギー白書2019) . 2019.
- [17] 経済産業省資源エネルギー庁. 平成30年度エネルギーに関する年次報告 (エネルギー白書2018) . 2018.
- [18] IEA. Introduction to System Integration of Renewables. Paris: 2020.
- [19] IEA. Status of Power System Transformation 2018. 2018. doi:10.1787/9789264302006-en.
- [20] Zhang L, Liu X, Wei H, Zhang X. Experimental study and analysis of heat and mass transfer ability of counter-flow packing tower and liquid desiccant dehumidification system. Energy Build 2018;158:150–61. doi:10.1016/j.enbuild.2017.10.016.
- [21] Liu C, Wu Y, Zhu Y, Li D, Ma L. Experimental investigation of optical and thermal performance of a PCM-glazed unit for building applications. Energy Build 2018;158:794–800. doi:10.1016/j.enbuild.2017.10.069.
- [22] Cao X, Dai X, Liu J. Building energy-consumption status worldwide and the state-of-the-art technologies for zero-energy buildings during the past decade. Energy Build 2016;128:198–213. doi:10.1016/j.enbuild.2016.06.089.
- [23] Franco A, Fantozzi F. Experimental analysis of a self consumption strategy for residential building: The integration of PV system and geothermal heat pump. Renew Energy 2016;86:1075–85. doi:10.1016/j.renene.2015.09.030.
- [24] Good C, Andresen I, Hestnes AG. Solar energy for net zero energy buildings - A comparison between solar thermal, PV and photovoltaic-thermal (PV/T) systems. Sol Energy 2015;122:986–96. doi:10.1016/j.solener.2015.10.013.
- [25] Li ZS, Zhang GQ, Li DM, Zhou J, Li LJ, Li LX. Application and development of solar energy in building industry and its prospects in China. Energy Policy 2007;35:4121–7. doi:10.1016/j.enpol.2007.02.006.
- [26] Poppi S, Sommerfeldt N, Bales C, Madani H, Lundqvist P. Techno-economic review of solar

- heat pump systems for residential heating applications. *Renew Sustain Energy Rev* 2018;81:22–32. doi:10.1016/j.rser.2017.07.041.
- [27] Sebarchievici C, Sarbu I. Performance of an experimental ground-coupled heat pump system for heating, cooling and domestic hot-water operation. *Renew Energy* 2015;76:148–59. doi:10.1016/j.renene.2014.11.020.
- [28] Wang F, Wang Z, Zheng Y, Lin Z, Hao P, Huan C, et al. Performance investigation of a novel frost-free air-source heat pump water heater combined with energy storage and dehumidification. *Appl Energy* 2015;139:212–9. doi:10.1016/j.apenergy.2014.11.018.
- [29] Fiorentini M, Cooper P, Ma Z. Development and optimization of an innovative HVAC system with integrated PVT and PCM thermal storage for a net-zero energy retrofitted house. *Energy Build* 2015;94:21–32. doi:10.1016/j.enbuild.2015.02.018.
- [30] Benli H. Energetic performance analysis of a ground-source heat pump system with latent heat storage for a greenhouse heating. *Energy Convers Manag* 2011;52:581–9. doi:10.1016/j.enconman.2010.07.033.

# **Chapter 2: Application of heat pump system in building for energy conservation**

## 2.1 Background

With the electrification of heat in buildings (through electric heaters and heat pumps) and the increasing share of renewable energy in power generation, renewable energy has become the largest source of renewable heat absorption in buildings in the past decade. New technology solutions such as hybrid heat pumps can help improve the overall energy efficiency of heating equipment, ensuring performance even under extreme conditions. High-performance deep energy renovation of air source, geothermal, and hybrid heat pumps play a crucial role in achieving those energy savings and emissions reduction.

In this chapter, we will briefly introduce the principle of heat pump, and review the application and research of heat pump technology in the construction field in recent years.

## 2.2 Heat Pump Basics

Generally speaking, a heat pump, also known as refrigerator, is an efficient heating device based on the second law of thermodynamics, which can transfer energy from low-temperature source to high-temperature source. The sum of the energy it can provide to the high temperature is greater than the energy required for its operation. The extra heat is obtained from the lower temperature source under the action of its operation.

The heat pump uses a low-boiling liquid to decompress through a throttle valve and then evaporates. It absorbs heat from a lower temperature source, and then compresses the steam through a compressor to increase the temperature. After passing through the condenser, it releases the absorbed heat and liquefies, then returns to the throttle. Such cyclic work can continuously transfer heat from a place with a lower temperature to a place with a higher temperature.

### *Principles*

The law of conservation of energy tells us that when work and heat are exchanged, there is no net gain or energy loss. However, the amount of heat energy that can be converted into work is limited.

When heat flows from hot to cold, a certain amount of energy may be converted into work and

extracted. The first law of thermodynamics and the second law of thermodynamics control the working principle of the heat pump. In particular, unlike heat engines (Figure 2. 1), heat pumps operate in reverse circulation. The purpose of the heat engine is to generate work ( $W$ ) from the heat source ( $Q_2$ ), and the purpose of the heat pump is to raise the heat from the low temperature heat source ( $Q_1$ ) to the high temperature radiator ( $Q_2$ ). It must be said that the heat pump can be used as a heating device or a refrigerator to reverse the refrigerant flow. In order to obey the first law of thermodynamics, the heat engine must emit a certain amount of heat ( $Q_1$ ) to the radiator, and the heat pump must accept  $W$ . Obviously,  $T_2$  temperature is higher than  $T_1$  (Figure 2. 1).

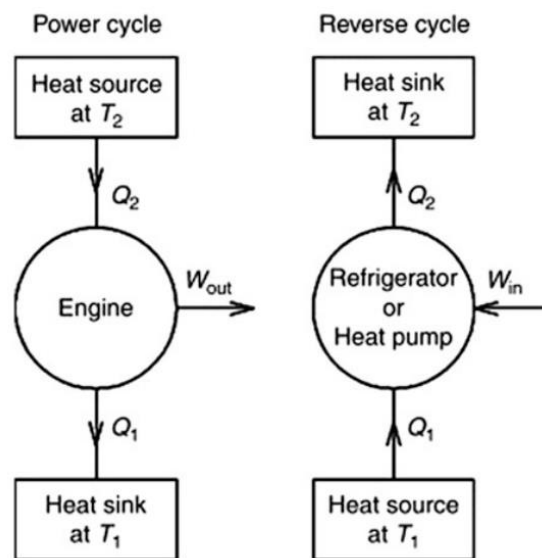


Figure 2. 1 Operating principles of heat engines and heat pumps [1]

For heat pump systems, two efficiency indicators can be formulated according to Figure 2. 1 to evaluate heating or cooling performance. They are the coefficient of performance (COP, mainly used for heating operation) and energy efficiency ratio (EER, mainly used for cooling operation). The higher the COP or EER, the lower the operating cost. COP usually exceeds 1, because COP does not just convert work to heat (if the efficiency is 100%, COP is 1), but pumps additional heat from the heat source to where it is needed. For a complete system, the COP calculation should include the energy consumption of all power-consuming auxiliary equipment. COP is highly dependent on operating conditions, especially the absolute temperature and the relative temperature between the sink and the system, and is usually plotted or averaged for the expected conditions.

Using the characters shown in Figure 2. 1, the COP and EER can be calculated as follows:

$$COP = \frac{Q_2}{|W|} = \frac{Q_2}{Q_2 - |Q_1|} \quad (2.1)$$

$$EER = \frac{Q_1}{|W|} = \frac{Q_1}{Q_2 - |Q_1|} = \left| \frac{Q_2}{W} \right| - 1 \quad (2.2)$$

$$\frac{Q_1}{T_1} - \frac{Q_2}{T_2} = \frac{Q_1}{T_1} - \frac{Q_1}{T_2} - \frac{W}{T_2} = 0 \quad (2.3)$$

Considering that the temperature of  $T_2$  is higher than  $T_1$ ,  $W$  must be large enough to offset the algebraic sum of the first and second terms in Equation 2.3. Therefore, the performance of the heat pump is affected by the temperature levels of the heat source and heat sink. Fixing the heat transferred or discharged from the building, the closer the temperature of the heat sink and source, the less work is required. Theoretically, according to climatic conditions and building energy consumption requirements, if these temperatures are closer during the cooling period than the heating season, the EER value can be higher than the COP value.

### ***Practice***

For a real heat pump, based on the physical characteristics of energy transfer, the heat pump uses renewable energy in combination with power input to generate useful energy through the refrigeration cycle. As shown in Figure 2. 2, the refrigeration cycle usually includes four stages. The refrigeration cycle is divided into four stages: 1) The first step is that the refrigerant enters the compressor in gas form and overheats after the compressor is present. 2) The second stage is the superheated gas exhaust heat through the condenser. The condenser takes away the heat and condenses the gas into a liquid. 3) In the next stage, the liquid refrigerant flows through the expansion valve, forming a mixture of liquid and gas at low pressure and low temperature. 4) Then, the cold air mixture is entirely evaporated by the evaporator in the final stage, and then returned to the compressor to start the cycle again.

Figure 2. 3 shows a simple vapor compression cycle with pressure and enthalpy values for refrigerant R134a. The cooling effect is the heat transferred to the working fluid during evaporation, i.e., the enthalpy change between the fluid entering the evaporator and the steam leaving the evaporator. A simple vapor compression cycle is shown on the P–h diagram in Figure 2. 4. The refrigerant evaporation process or evaporation is a constant pressure process, so a horizontal line

represents it in the figure. In the compression process, the energy used to compress the vapor is converted into heat, which makes its temperature and enthalpy are increased. So at the end of the compression process, the vapor is in the superheated state. Before starting to condense, the vapor must be cooled. As shown in the figure, the final compression temperature is almost always higher than the condensation temperature so that some heat will be discharged at a temperature higher than the condensation temperature. The actual condensation process is represented by the horizontal part of the saturation curve.

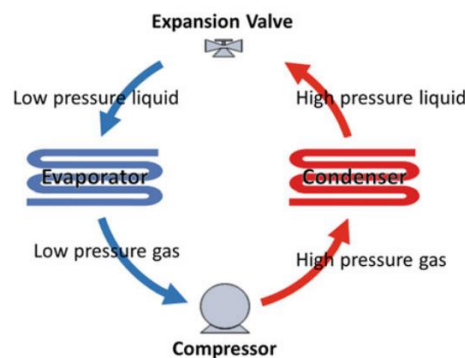


Figure 2. 2 Four-stage refrigerant cycle

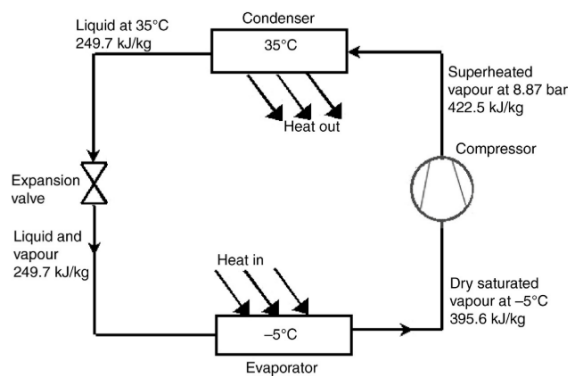


Figure 2. 3 Simple vapor compression cycle with pressure and enthalpy values for R134a.

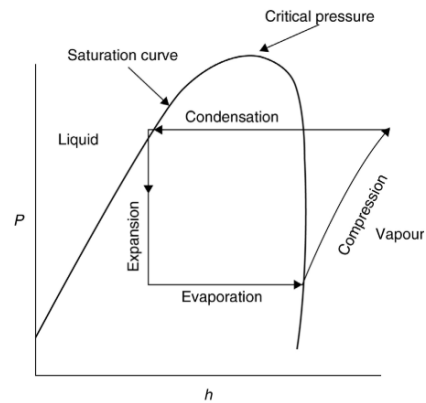


Figure 2. 4 Pressure–enthalpy diagram, showing the vapor compression cycle.

The heat pump converts heat from natural renewable energy or heat from natural renewable energy into useful energy for heating or cooling to ensure the quality of the indoor climate. The renewable natural energy sources used for heat pumps can be air heat energy, geothermal energy, water heat energy, or unnaturally treated waste heat. Next, we will analyze several heat pump systems that are widely used in buildings.

## 2.3 Air source heat pump system

Air source heat pumps are the most popular systems in sustainable building and industrial applications. The system absorbs heat from the outside of the building to provide domestic water and space heating. In a hot climate, reversible external heat dissipation operation can provide indoor space cooling. As shown in Figure 2. 5, the essential components used in refrigeration systems are compressors, expansion valves(capillary tube in this case), heat exchangers as evaporator and condenser(refrigerant-air heat exchangers in this case) and blowers. The air source heat pump absorbs heat from the outside cold air to heat the water. Heat can be used for space heating or domestic hot water supply in cold climates. The heat pump can run in reverse. Therefore, it can also produce chilled water for space cooling and discharge heat to the outside in a hot climate. Air source heat pumps can be devices that integrate advanced programmable logic controllers and sensors to provide a constant indoor temperature solution for summer cooling and winter heating.

However, the gas source has some disadvantages. Outdoor temperature changes can significantly affect capacity and efficiency. Especially the low outdoor temperature will lead to poor performance and bring other problems of icing on the outdoor coil. Although defrosting can be accomplished by using a reversing valve to deliver hot air to the outdoor coil temporarily, this may suddenly cool the hot water supply and cause an undesirable operating condition[2].

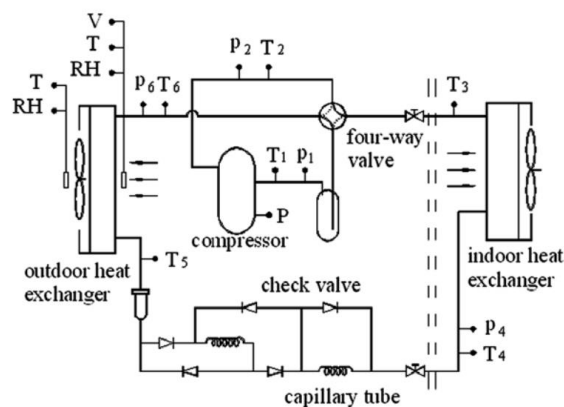


Figure 2. 5 Diagram of a typical ASHP system [3]

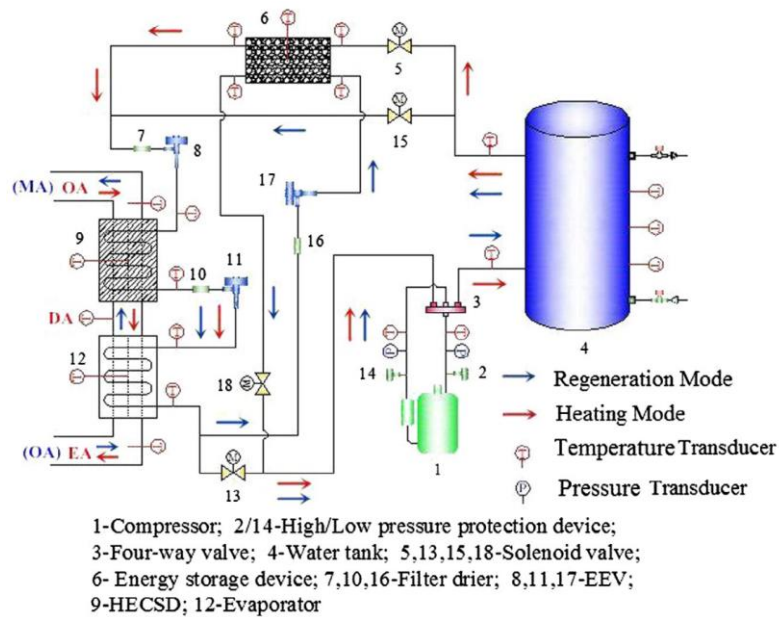


Figure 2. 6 Schematic diagrams of a novel frost-free air source heat pump system[19].

Previous studies have discussed techniques for improving the performance of air source heat pumps and solutions for defrosting [3–19]. Figure 2. 6 shows a novel air source heat pump water heater system developed by Wang et al.[19]. This system does not require the operation of initial frost during operation. An additional heat exchanger coated with solid desiccant and energy storage device was installed in this system. When the air source heat pump water heater/chiller (ASHPWHC) operates at a lower ambient temperature in winter, frosting on the surface of the air-side heat exchanger will cause the performance of the heat exchanger to decrease or even shut down. Yao et al.[20] used the developed frosting and heat exchanger model to evaluate the operating characteristics of the air-side heat exchanger during frosting in the ASHPWHC. Besides, the effect of frosting on the operating performance of the ASHPWHC was also evaluated. Based on the simulation, the optimization of the structural layout of the finned tubes used in the air-side heat exchanger and measures to improve defrosting control were discussed. Byun et al. studied the feasibility of the hot gas bypass method to prevent the formation and spread of frost in the air source heat pump based on the experiment, and compared the performance of this method with the conventional air source heat pump system. Without defrosting equipment such as heaters. The results show that the hot gas bypass method can be used to delay the formation and growth of frost at outdoor coils. In the case of bypass refrigerant flow rate of 0.2 kg/min (accounting for 20% of the entire system refrigerant flow rate), it shows the best performance and obtains an increase in

COP[21]. Shen et al. proposed the design of an air source heat pump with dual drying mode. The operating mode changes between single-stage and cascade cycles to meet the heating requirements at different ambient temperatures. The prototype of this dual-mode heat pump was developed using R22 and R134a as refrigerants. An experiment was conducted to verify the feasibility and characteristics of the heat pump. The supply air temperature, heating capacity, and electrical power in both operating modes will increase as the ambient temperature increases. The difference in energy consumption between the two ways also increases with the ambient temperature, but the difference in supply air temperature will decrease[22]. Wang et al.[23] proposed a new type of jet structure on the blades of a rotary compressor to avoid severe degradation of the air source heat pump at low ambient temperatures. Based on the validated numerical model, the thermodynamic performance of the air source heat pump of the new gas jet rotary compressor was studied. The results show that the injection structure can improve the heating capacity and COP of the air source heat pump by 23.1–28.2% and 4.5–8.1%, respectively, compared with the air source heat pump of the conventional single-stage rotary compressor. Wang et al. proposed a study on a new frost-free ASHP system that combines dehumidification and thermal energy storage functions and works with refrigerant R134a and R407C as R22 alternatives. The simulation results show that at the end of the working time, the compressor discharge pressure of R134a is 29% and 32% lower than the discharge pressure of R22 and R407C. Besides, at a given ambient temperature of 10 °C and relative humidity of 85%, the average COP of R134a is higher than the average COP of R22 and R407C[24]. Wang et al. proposed a new injection structure for the blades of rotary compressors to overcome the shortcomings of traditional injection structures in air source heat pumps[23]. Based on the validated numerical model, the thermodynamic performance of the air source heat pump with a new gas jet rotary compressor was studied. The simulation results show that the proposed injection structure can increase the heat capacity and COP of the air source heat pump by 23.1–28.2% and 4.5–8.1%, respectively, compared with the air source heat pump of the conventional single-stage rotary compressor. In order to save energy of air source heat pump unit, Song et al. proposed an experimental method. The optimal temperature setting of the defrosting operation of the air source heat pump unit with a three-circuit outdoor coil was experimentally studied[8]. Based on the experiment, it is concluded that the defrost termination temperature of this study is suitable at 20–25 °C, about 22 °C. This method has contributed to the optimization of the control strategy and energy saving of the air source heat pump

unit. Tang et al. introduced a new technology for preventing frost and blocking air source heat pumps (ASHP) that reduce thermal discomfort. It uses an auxiliary electric heater (AEH) on the pipeline before (B-AEH) and after (A-AEH) the outdoor evaporator to prevent the formation of frost or prevent the accumulation of frost on the outdoor heat exchanger[7]. This makes it possible to supply hot air to the internal space without interruption. In this study, the orthogonal experimental design (OED) was used to evaluate the performance of an air source heat pump (ASHP) with different AEH powers under a range of frost conditions. The optimal parameter combination that affects ASHP performance is determined, and the most important parameters are determined. Song et al. reported a detailed description of the specially constructed air source heat pump experimental device, as shown in Figure 2. 7. Experiments were carried out to discuss the influence of the downward flow of melted frost on the outdoor coil on the defrosting performance during the reverse cycle defrosting process were given[5]. Li et al. introduced the energy characteristics of the air source heat pump (ASHP) based on the concepts of "cold exergy " and "heat exergy." The quantitative analysis followed by the theoretical analysis shows that in ASHP, the refrigerant cycle divides the compressor power input into "cold exergy" and "heat exergy." The "cold exergy" enters the indoor air, and the "heat exergy" is discharged into the surrounding environment. The analysis also shows that, of the total exergy input, the compressor requires the largest exergy input, and the refrigerant cycle has the highest exergy consumption. Therefore, it is important to improve compressor performance to

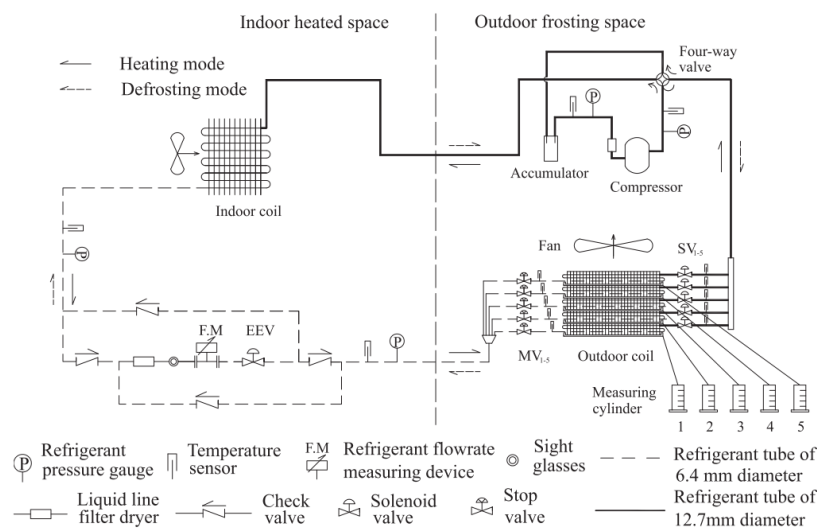


Figure 2. 7 Schematic diagrams of the experimental ASHP system for defrosting test [5], which can help optimize the control strategy and energy saving of the air source heat pump.

reduce power consumption and unnecessary exergy consumption[18]. Kelly et al. [13] used the monitored data and simulations to evaluate the performance of the renovated residence using air source heat pump (ASHP), developed and calibrated the ASHP equipment model, and integrated it into the dynamic simulation tool of the entire building. The comparison between the prediction of the entire building model and the field test data shows that the model provides a suitable test platform for energy performance evaluation. Annual simulations show that compared to an equivalent condensing gas boiler system, the carbon produced by ASHP is reduced by 12%, but the operating cost is about 10% higher. Heo et al. studied and measured the heating performance of the air source heat pump, which used a novel flash tank and super cooler (FTSC) cycle and double expansion supercooler (DESC) cycle steam injection technology. The performance of these cycles was compared with the performance of the flash tank (FT) and subcooler (SC) cycles. Compared with the SC cycle, the average heating capacity of FT, FTSC, and DESC cycles increased by 14.4%, 6.0%, and 3.8%, respectively, but a similar average COP was obtained[14]. Byun et al. [21] studied the feasibility of the hot gas bypass method through experiments, and compared the performance of the method with a common 1.12 kW capacity air source heat pump system, which does not have defrost equipment such as resistance heaters. The results show that the hot gas bypass method can be used to delay the formation and growth of frost at outdoor coils. In the case of bypass refrigerant flow rate of 0.2 kg/min (accounting for 20% of the entire system refrigerant flow rate), it shows the best performance. During 210 minutes of heat pump operation, the hot gas bypass method increased COP and heat capacity by 8.5% and 5.7%, respectively, relative to the normal system.

Based on a review of previous literature, it is not difficult to find that the air source heat pump is the most widely used because of its simple installation and low cost. However, because of its reduced efficiency due to frosting problems in cold conditions, its most significant disadvantage, and studies aimed at improving the performance of air source heat pumps, almost all focus on defrosting. Therefore, eliminating degradation caused by frosting is the key to improving efficiency.

## **2.4 Geothermal heat pump system**

A ground source heat pump is a heating and cooling system that transfers heat to or from the ground. It uses the earth as a heat source (in winter) or a radiator (in summer) all the time. This design

utilizes moderate ground temperatures to increase efficiency and reduce operating costs of heating and cooling systems. It can be used in conjunction with solar heating to form a more efficient geothermal system. The ground source heat pump is a promising technology. The ground source heat pump can be introduced into various buildings such as offices, schools, single houses, or apartment buildings. Among different types of heat pumps, in terms of performance, ground source heat pumps are the most competitive and therefore have recently been extensively studied. Compared with the most widely distributed air source heat pump, it has a more stable temperature during the day and throughout the year. Also, if GSHP is appropriately designed, the risk of performance degradation due to frosting of the evaporator during the heating season can be reduced to almost zero.

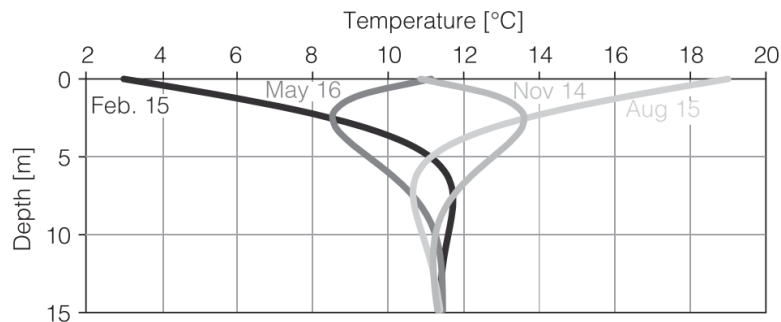


Figure 2. 8 Typical temperature of the undisturbed ground for a northern hemisphere[25].

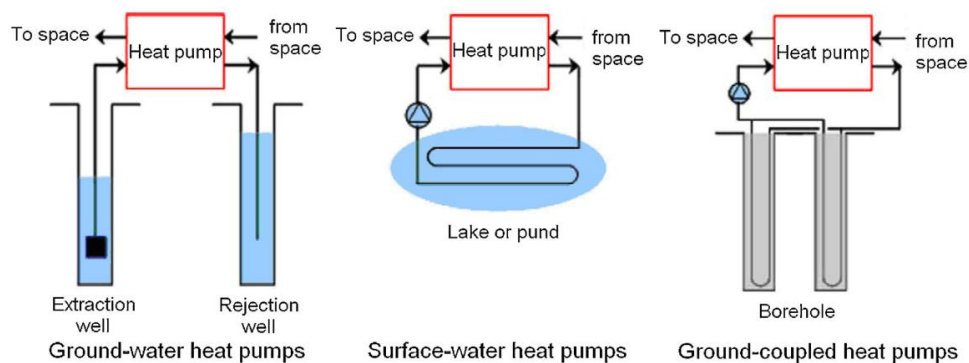


Figure 2. 9 Schematics of different ground-source heat pump systems[26].

According to (IEA Heat Pump Center 2010), as shown in Figure 2. 9, ground source heat pumps can be classified as:

- 1) Groundwater heat pump: underground (aquifer) water is used as a heat source and sink.

- 2) Surface water heat pump: surface water (sea, lakes, etc.) is used as a heat source and sink.
- 3) Ground-coupled heat pump: the ground is used as a heat source and heat sink, and the heat is extracted/dissipated through a vertical or horizontal ground heat exchanger.

Here we focus only on the first type (ground-coupled heat pump system) because it can potentially be installed anywhere and does not require any water source. As shown in Figure 2. 8, for the soil temperature, it is warmer than winter, cooler in summer, and much more stable throughout the year, so it provides better energy for heat pumps than air. This improvement in performance is especially true in extreme climatic conditions where heating or cooling needs are highest. The performance of a geothermal pump is about 20–30% higher than that of an equivalent air source heat pump.

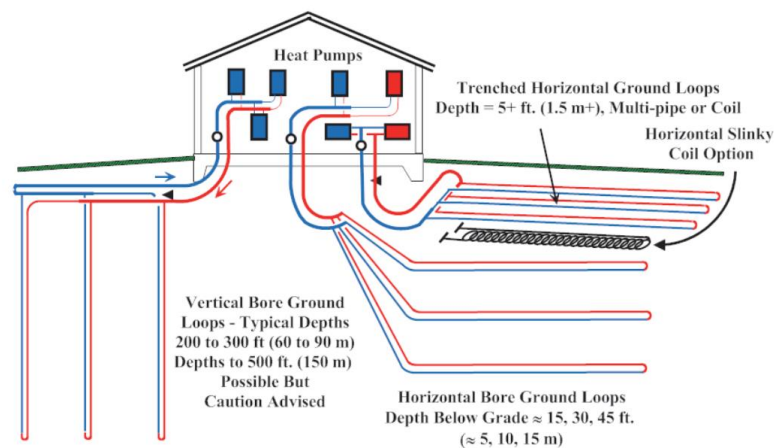


Figure 2. 10 Closed-loop ground-coupled heat pump with different ground heat exchangers.

The ground heat exchanger can be divided into horizontal and vertical according to its physical expansion, and they also determine the depth of heat exchange. Figure 2. 10 shows a variety of different types of ground heat exchangers, including vertical bore, trenched horizontal, horizontal slinky, and horizontal bore types. Although the names are sometimes different, the types are basically the same. Generally, the vertical ground heat exchanger is more efficient. Because more substantial depth grounds have better thermal characteristics, they require less land area and less pumping energy. Therefore, they are more suitable for large systems. However, compared to drilling, the installation cost of the horizontal ground heat exchanger is usually lower, and the risk is less during construction.

The vertical ground heat exchanger consists of vertical boreholes with a typical length ranging from

45 to 150m and a diameter of 10–15 cm. Each borehole is equipped with concentric, U-tube, or double U-tube thermoplastic tubes, spiral with a diameter of 2-4 cm and backfilled with grouting material to enhance heat transfer, usually made of sand and bentonite. The characteristic of the horizontal ground heat exchanger is that placed at a shallow depth, generally between 1-3 m. The horizontal ground heat exchanger can be divided into three types: 1) horizontal, 2) vertical oriented, and 3) architectural integration. Some examples of horizontal directions are zigzag, harp, double wire, capillary, and ground-to-air heat exchangers. Grooves, cages and baskets/spirals are examples of vertical types. Compared with the air source heat pump, the ground heat pump system does not need to defrost, and because the source temperature is more stable, the mechanical stress and thermal stress of the heat pump compressor are smaller. Therefore, the reliability is higher, and the service life of the ground-coupled heat pump is expected to reach 20-25 years[25].

Because the defrosting operation is not required in a ground heat pump system, most of the research on the improvement of ground source heat pumps is to develop advanced operation strategies that can help to ensure the long-term performance of the system. Besides, the development of high-performance geothermal heat exchangers, how to reduce unbalanced soil temperature changes caused by excessive heat extraction, and integration with other types of heat pump systems is also prevalent for researchers. Therefore, here we will review some typical studies in recent years.

Deng et al. proposed the actual energy performance of a mid-deep geothermal heat pump system (MD-GHP) with a temperature of about 70–90 °C and at a depth of nearly 2–3 km underground. The system uses vertical concentric tubes as ground heat exchangers (GHE) to extract heat from mid-depth geothermal energy for space heating purposes in the building. The energy performance of the MD-GHP system and the heat transfer performance of GHE are analyzed based on the short-term and annual field test. The results show that the average temperature of the ground effluent can reach 33.0 °C, which significantly improves the performance of the entire system. The COP of the heat pump reaches 5.43, and the COP<sub>hs</sub> of the heat source reaches 4.58. Therefore, the energy-saving performance of MD-GHP is significantly improved compared with the air source heat pump system, conventional ground source heat pump system, and gas boiler[27]. Esen et al. [28] established a slinky (spiral ring of flexible plastic tubes) type ground heat exchanger (GHE) for solar-assisted ground source heat pump systems. Artificial neural network (ANN) and adaptive neuro-fuzzy inference system (ANFIS) were used in the modeling based on the data obtained from

experiments. On the horizontal tight-fitting GHE, the system performance coefficient (COP<sub>sys</sub>) and heat pump performance coefficient (COP<sub>hp</sub>) are calculated as 2.88 and 3.55 respectively, while in the vertical state, COP<sub>sys</sub> and COP<sub>hp</sub> are calculated as 2.34 and 2.91 respectively. The results also show that ANFIS is more suitable than ANN in predicting the performance of solar ground source heat pump systems. Sivasakthivel et al. proposed a method to optimize the operating parameters of the ground source heat pump system, which will operate in heating and cooling modes. The condenser inlet temperature, the condenser outlet temperature, the dry fraction at the evaporator inlet, and the evaporator outlet temperature are regarded as the influencing parameters of the heat pump. By using the Taguchi method to use L9 (34) orthogonal arrays to make three-level changes to the above parameters, the optimization of these parameters for heating or cooling mode only can be achieved. Higher concepts are used to improve COP. Also, a computer program in FORTRAN has been developed for calculations, and the results under optimal conditions have been analyzed using signal-to-noise ratio and analysis of variance methods[29]. Sebarchievici et al. developed an energy operation optimization device for the ground-coupled heat pump (GCHP) system. This device involves inserting a buffer tank between the heat pump unit and the fan coil unit and using a variable speed circulating pump for quantitative adjustment to achieve user power supply[30]. Then, through experimental measurements, they tested the performance of the GCHP system in different

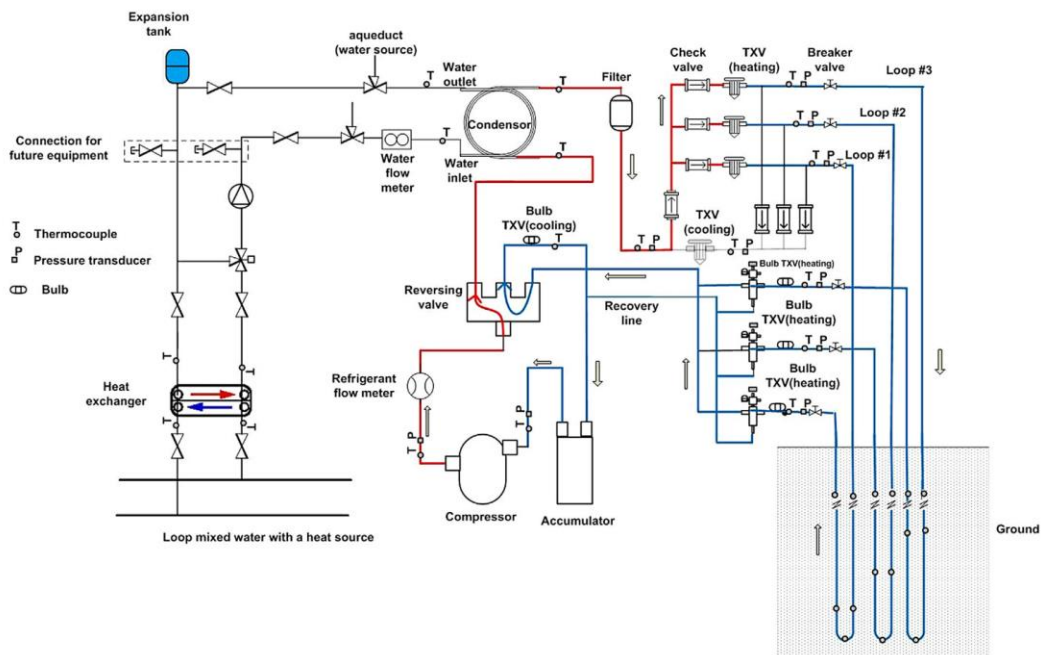


Figure 2. 11 Schematic of a direct expansion geothermal heat pump system[31].

operating modes. By using the classic adjustment and optimization adjustment of the GCHP system, the main performance parameters (energy efficiency and CO<sub>2</sub> emissions) for one month of operation can be obtained, and these performances are compared and analyzed. Two simulation models of thermal energy consumption in heating, cooling, and domestic hot water operation were developed in TRNSYS. Fannou et al. [31] conducted an experimental analysis of the direct expansion (DX) geothermal heat pump (GHP), which consists of three geothermal wells with a depth of 30 m, which use R22 as the refrigerant. During the one-month test activity in early spring, the tests conducted helped highlight the pressure drop and the relatively high overheating phenomenon, thereby revealing the uneven flow distribution in the geothermal evaporator. It also introduces the influence of some factors that affect the performance of the DX system (condenser cooling water inlet temperature, condensation temperature, the pressure drop in the evaporator, and thermal characteristics of soil and cement slurry). Renewable energy and intelligent control are interrelated and interrelated. Without intelligent control, it may not be possible to realize the full benefits of renewable energy technologies, especially ground source heat pump technology[32]. Mokhtar et al. proposed an intelligent multi-agent building management system (MAS BMS) designed to solve this problem to solve the problem of low control efficiency and poor performance of GSHP implemented by GSHP. Intelligence is provided by ARTMAP, which is an artificial neural network that provides incremental learning based on how humans handle memory. The simulation results show that the proposed intelligent MAS BMS can effectively utilize GSHP by analyzing, predicting, and coordinating other energy resources. The proposed method performs better than GSHP's existing control strategies. Guo et al. conducted a technical and economic comparison between the direct expansion ground source heat pump system (DX-GSHP) and the secondary loop ground source heat pump system (SL-GCHP)[33]. Through a demonstration building experiment, the average cooling performance coefficient of the DX-GSHP system is 6.03, and the average cooling performance coefficient of the SL-GCHP system is determined to be 5.64. they found that in the cooling mode, the efficiency of DX-GSHP is 23.8% higher than that of SL-GCHP. For the initial investment of these two systems, based on the annual cost and present value, DX-GSHP is more economical than SL-GCHP. Besides, the DX-GSHP can ensure the minimum refrigerant speed for refrigerant oil return, which can effectively solve the oil return problem. Benli designed[34] a ground source heat pump heating system with a latent heat storage tank and studied its thermal

energy storage performance. The heating system is mainly composed of a ground heat exchanger, a heat pump, a cylindrical latent heat storage tank, a measuring unit, and a 30 square meter model glass greenhouse heating space. Through experiments, it is found that the thermal coefficients of the performance of the ground source heat pump and the entire system are in the range of 2.3–3.8 and 2–3.5, respectively. Although using this heating system can save a lot of money, it may require a lot of investment in equipment and facilities. Pulat et al. [35] evaluated the performance of horizontal ground source heat pump (GSHP) by considering various system parameters of winter weather conditions in Bursa, Turkey. The soil thermal conductivity estimation was extended and discussed, and the preliminary numerical temperature distribution around the ground heat exchanger pipeline was obtained. By testing space heating under laboratory conditions, the effect of outdoor temperature on system capacity and COP relative to outdoor air and average soil temperature was discussed. In the economic analysis, comparing the GSHP system with conventional heating methods, the results show that the GSHP system is more cost-effective than all other conventional heating systems. Similarly, Tarnawski et al. conducted simulation and analysis of a ground-source heat pump system equipped with a horizontal ground heat exchanger in heating and cooling mode for a typical house in Sapporo. Despite the high electricity cost, the ground source heat pump system is more conducive to space heating than oil furnaces and resistance systems. In addition, compared to resistance heating or air source heat pumps, heat pump technology provides relatively low ground environmental thermal degradation, lower heating and cooling costs, and higher operating efficiency. The use of cooling mode can bring more benefits; for example, a shorter return on investment and higher human comfort in summer[36]. Nam et al. [37] established a numerical model that combines a heat transfer model with groundwater flow and a heat exchanger model with an accurate shape. In addition, a soil property estimation method based on ground survey is proposed. Under the experimental conditions started in 2004, the experimental results and numerical analysis were compared based on the above model. The analysis results are in good agreement with the experimental results. The proposed model is used to predict the heat exchange rate of actual office buildings in Japan. Nagano et al. developed a novel design and performance prediction tool for a ground source heat pump (GSHP) system[38]. They verified the temperature calculated by the development tool by comparing it with the experiment and achieved an acceptable accuracy of the development tools. Lazzarin studied two arrangements of dual-source heat pump systems: an air-

source heat pump combined with a solar collector(shown in Figure 2. 12); and a ground-source heat pump connected to a solar collector(shown in Figure 2. 13)[15]. They found that when the solar system is used in series with other heat sources, and when placed in series, a higher COP can be obtained. Based on previous research directions and focus, it can be found that the balance of soil temperature is the key to ensuring the long-term and efficient operation of the ground source heat pump system. Therefore, many researchers optimized the operation mode and tried to introduce

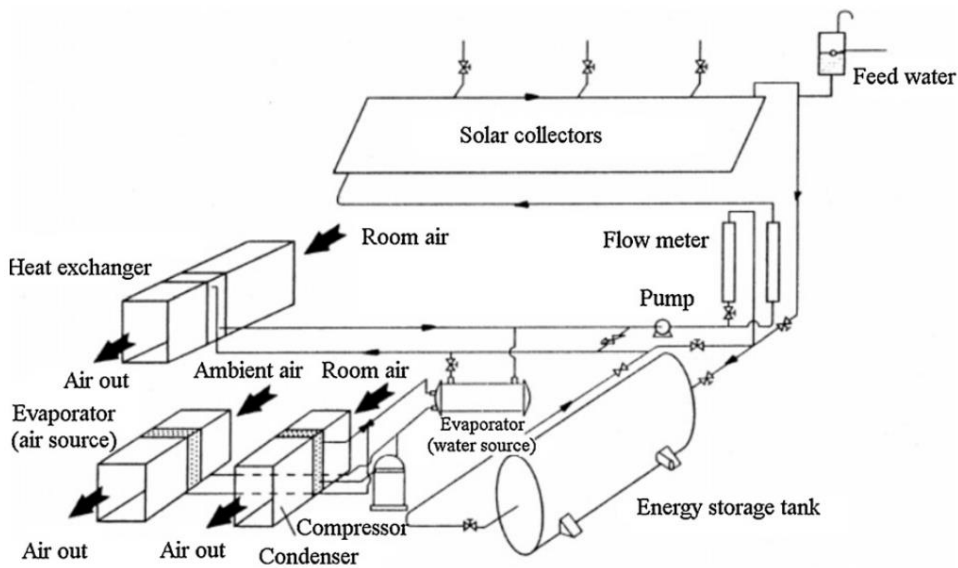


Figure 2. 12 Schematic of a dual-source(air and ground) heat pump system[15].

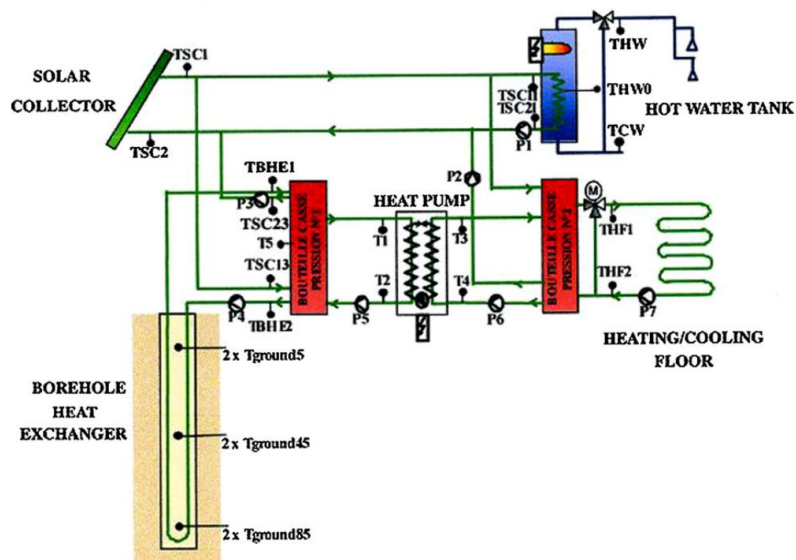


Figure 2. 13 Schematic of a dual-source(solar and ground) source heat pump system[15].

other renewable energy to develop composite systems. The development of a suitable compound energy heat pump system is also one of the critical points of this study. We use solar energy, geothermal energy, and air as the heat source of the system because this can make up for the shortcomings of different renewable energy sources and ensure the overall high-efficiency operation of the system.

## 2.5 Solar assisted heat pump system

As mentioned in the previous section, the solar-assisted ground source heat pump (SAGSHP) system also uses a solar collector to improve the performance of the whole heat pump system, which is somehow connected to the heat pump evaporator. The connection method may be through a water tank, or the solar heat collector panel can directly be used as an evaporator or condenser of the heat pump, which is the so-called direct expansion type. The working principle of using solar heat to increase the temperature of the evaporator is to reduce the ratio of  $Q_1/T_1$  by increasing  $T_1$ , thereby reducing the workload of the heat pump. Another important mode of operation is ground temperature and heat recovery. The process of recovery of the heat or temperature of the soil is designed to heat the soil by using solar energy when the ground source heat pump is turned off.

The circulation pump is a critical component of the SAGSHP system with a water tank and is responsible for pushing the fluid through the solar collector and ground heat exchanger. Circulation pumps must overcome pressure drops in pipes, ground heat exchangers, solar collector panels, and heat exchangers. Typically, there are two pumps in solar collector panels and ground heat exchangers separately, mainly due to specific pressure requirements and enabling multiple operating modes. If it is a direct expansion type, the solar collector circuit loop does not need to be equipped with a circulating water pump. The direct expansion solar-assisted heat pump is a series system in which the solar collector is not filled with antifreeze, but is filled with refrigerant circulated by the heat pump.

Because of its excellent performance for heating and wide application in buildings and industries, the solar-assisted heat pump system has been receiving much attention in recent years. Regarding the previous research on solar-assisted heat pump systems[28,39–61], in terms of innovative system design, many studies have focused on the development of high-efficiency solar collector panels and

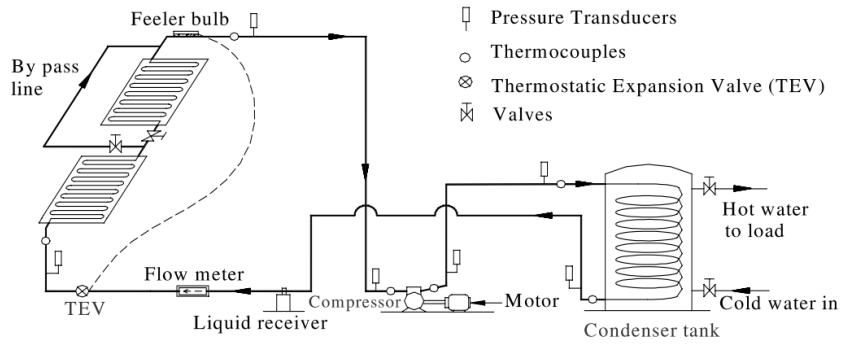


Figure 2. 14 Schematic of a typical solar-assisted heat pump water heating system[39].

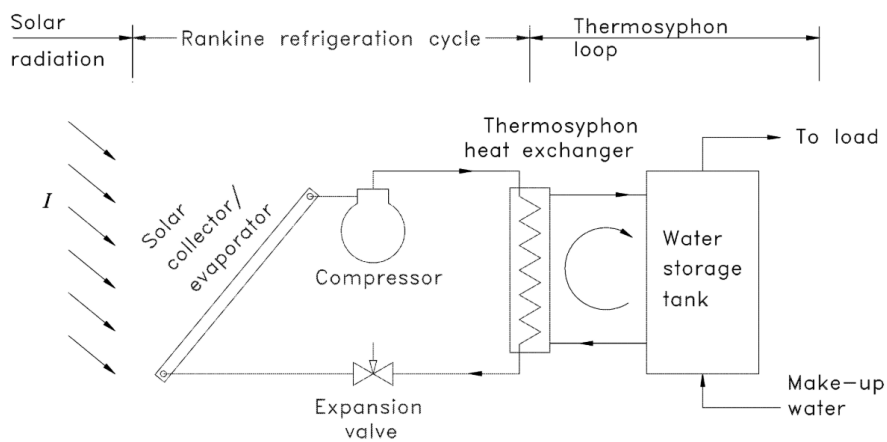


Figure 2. 15 Schematic of a direct-expansion solar-assisted heat pump water heating system[40].

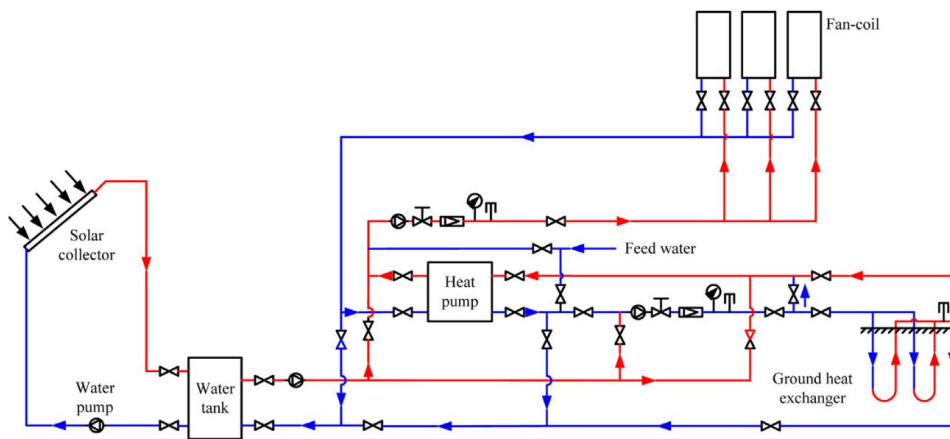


Figure 2. 16 Schematic of solar-ground source heat pump experimental system[41].

even solar collectors that can generate electricity while introducing photovoltaic cells. This kind of solar collector panel is the so-called photovoltaic thermal hybrid solar collector. On the other hand, a reasonable mix of renewable energy and system design are also the focus of the researcher's

attention. For example, the ground source heat pump system coupled with the solar energy heat pump can provide up to power generation, heating, and cooling. Hence, here we will review representative relevant studies in recent years.

Hawladar et al. studied the solar-assisted heat pump water heating system (shown in Figure 2. 14) through experiments and simulations. The system uses an unglazed flat-plate solar collector and uses refrigerant R-134a. It was found that the performance of the system was greatly affected by the collector area, compressor speed, and solar radiation[39]. Chyng et al.[40] studied an integral-type solar assisted heat pump water heater (shown in Figure 2. 15) through simulation. The results found that the total daily COP is about 1.7 to 2.5, depending on the season and weather conditions. Besides, they also studied the online adjustment requirements of the expansion valve through simulation and found that the device does not require online control. Figure 2. 16 shows a solar-ground source heat pump system proposed by Yang et al.[41]. Based on this apparatus, they studied the performance under different dual heat source coupling modes through experiments. As a result, it was found that the solar and ground heat sources were most efficiently operated by the dynamic coupling of the water tank and the plate heat exchanger. Through another simulation result of the system, it is found that the area of the collector and the number of ground heat exchangers have a significant effect on the system efficiency, but the effect of the water tank volume can be ignored.

Kuang et al. [59] studied the direct-expansion solar-assisted heat pump (DX-SAHP) water heating system based on the experiment. The flat solar collector is used as the evaporator. A simulation model was developed to predict the long-term thermal performance of the system roughly, used to obtain the optimal design of the system, and determine the appropriate strategy for system operation control. The effects of various parameters such as sunshine, the ambient temperature on the thermal performance of the DX-SAHP system were studied. The results show that the performance of the system is affected by the sunshine intensity, collector area, compressor speed. Kuang et al. conducted a long-term reliability test of an integrated solar-assisted heat pump water heater. In 5 years, the prototype has been in continuous operation for more than 13,000 hours, with a total operating time of over 20,000 hours. At 57 °C, the measured energy consumption is 0.019 kWh/L of hot water, which is much lower than the backup power consumption of conventional solar water heaters[52]. Ozgener et al.[53] studied the performance characteristics of a solar-assisted ground source heat pump greenhouse heating system (SAGSHPGHS). Ground heat exchanger with a

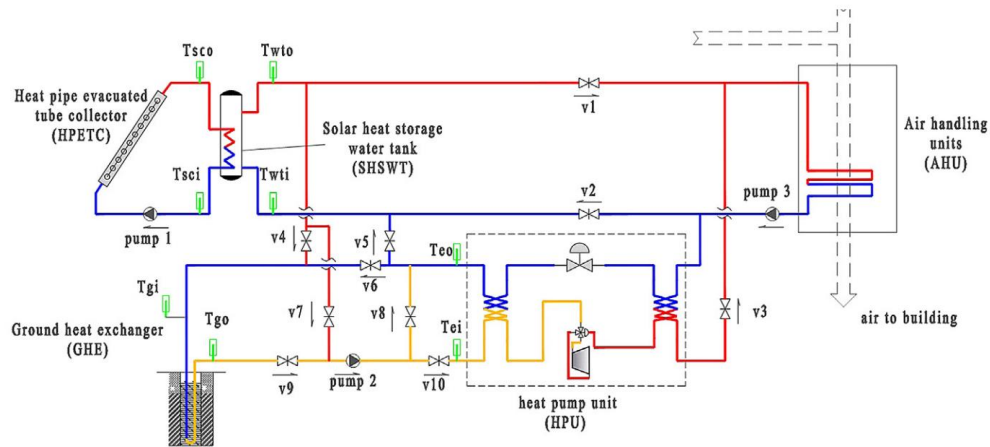


Figure 2. 17 Schematic of a solar assisted ground source heat pump system by Dai et al.[49].

nominal diameter U-tube elbow using exergy analysis. Based on the measurement parameters obtained from the experimental results, the exergy transfer between SAGSHPGHS components and the loss in each part was determined. They determined the efficiency of system components to evaluate their performance and propose the possibility of improvement. Dai et al. [49] conducted an experimental study on the heating performance of a solar-assisted ground source heat pump system (SAGSHPS, as shown in Figure 2. 17). The results of the experiment conducted in January showed that solar energy could be used to accelerate the recovery of soil temperature, but the time to supplement solar energy for the borehole should be optimized according to the water temperature in the solar storage tank. Kuang et al. studied the long-term performance of a direct-expansion solar-assisted heat pump (DX-SAHP) system for home use (shown in Figure 2. 18). Through experiments, they introduced and analyzed the performance of different operating modes in detail, and proved that the system can run stably under different weather conditions for a long time, and has a lower operating cost[54]. Li et al. analyzed the direct-expansion solar-assisted heat pump water heater (DX-SAHPWH); the experimental device is shown in Figure 2. 19. Exergy analysis of each component of the system revealed that the most considerable exergy loss occurred in the compressor, followed by the collector/evaporator, condenser, and expansion valve[55]. Ji et al. studied a novel photovoltaic solar-assisted heat pump (PV-SAHP) system. The performance test was conducted at a specific range of condenser water supply temperature, and the dynamic performance of the PV-SAHP system was analyzed. The results show that the PV-SAHP system has a higher coefficient of performance than the conventional heat pump system. At the same time, photovoltaic efficiency is

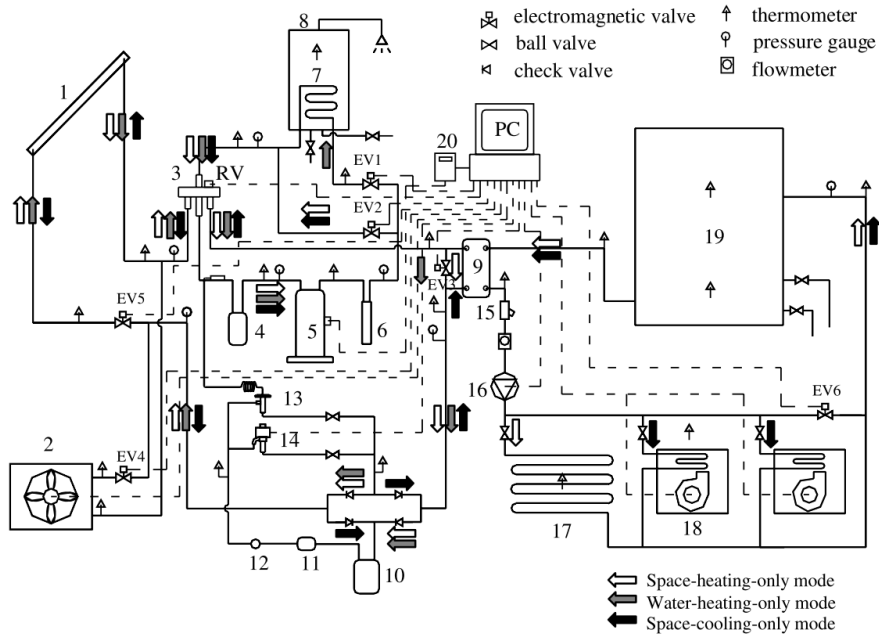


Figure 2. 18 Schematics of a direct-expansion solar-assisted heat pump system[54].

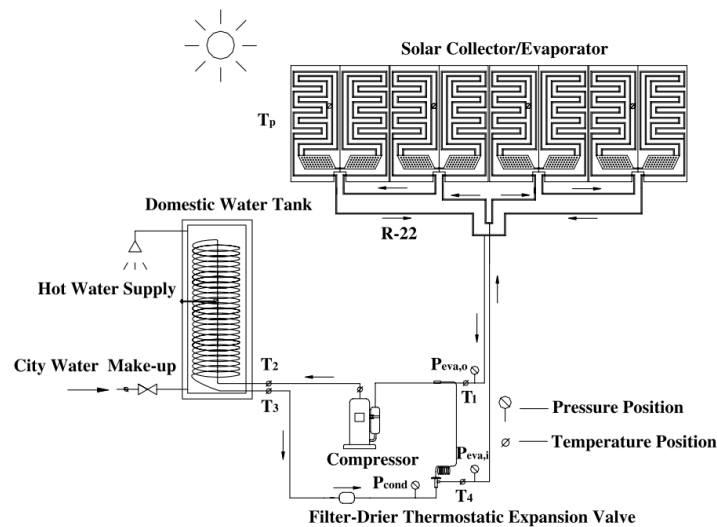


Figure 2. 19 Schematic of a direct-expansion solar-assisted heat pump water heater[55].

also higher. The COP of the heat pump can reach 10.4, with an average value of about 5.4. The average photovoltaic efficiency is about 13.4%. Combining photovoltaic and thermal efficiency, the highest comprehensive coefficient of performance is about 16.1[62]. Wang et al.[63] developed a new type of hybrid solar ground source heat pump system (HSGSHPS), which is composed of GSHPS and solar-assisted GSHPS (SAGSHPS), and developed a simulation model in TRNSYS to predict the multi-year performance of the system. The simulation results show that the proposed

HSGSHPS can solve the problem of ground temperature imbalance every year. According to the coefficient of performance (COP) of SAGSHPS, a control strategy suitable for solar energy collection and storage was found. Before extracting heat from BHE/BTES, injecting thermal energy into the wellbore heat exchanger (BHE) or wellbore thermal energy storage device (BTES) is beneficial to the overall COP of the system. Fiorentini et al. proposed a new type of solar-assisted HVAC system. The HVAC system consists of an air-based photovoltaic heat (PVT) collector integrated with a reverse circulation heat pump and a phase change material (PCM) heat storage unit in the piping system. The system is designed to operate based on the solar radiation during the day and sky radiation during the night in winter and summer, respectively. The PVT collector heats or cools the ambient air, thereby directly providing heating or cooling to the indoor space or PCM storage unit. The heat stored in the PCM can later be used to adjust the area temperature or pre-treat the air entering the air treatment unit[47].

## 2.6 Summary

This chapter reviews several heat pump systems widely used in the building/industries and analyzed their characteristics based on the review of previous research. In the field of building heating and cooling, heat pump technology has significant advantages over traditional heating and cooling systems. For example, renewable energy can be introduced into the building's energy supply system to improve overall operating efficiency and reduce dependence on non-renewable fossil energy. On the other hand, with the proposal and development plan of the fifth generation heat supply network, the realization of low heating temperature and the integration of renewable energy have become the future trend. These trends require the use of systems that can cope with such low-temperature heat sources, and heat pumps are the best choice that can meet the requirements. However, as mentioned above, each renewable energy has its advantages and disadvantages. The energy supply system that relies on a single heat source cannot efficiently and stably meet the heat demand of buildings that may change at any time. The heat pump system will become an optimal solution. Therefore, this research is also from this aspect; the goal is to build a heat pump system that can utilize a variety of renewable energy, can provide a stable and high-efficiency building heat supply.

As far as I know, this technology is still in its infancy in the world. This principle helps to achieve

the fifth generation of district heating, and cooling network is intimately connected, so it is very promising to become a mainstream solution. Therefore, we built an actual system based on this principle and verified and evaluated its performance through experiments. Then, based on the experimental results and physical laws, a model of this system was constructed based on Modelica, and general and advanced control can be achieved based on this model. The development of the scheme can further promote and improve system performance.

## 2.7 Reference

- [1] Chwieduk DA. Solar-assisted heat pumps. *Compr. Renew. Energy*, 2012. doi:10.1016/B978-0-08-087872-0.00321-8.
- [2] Hundy GF, Trott AR, Welch TC. *REFRIGERATION, AIR CONDITIONING AND HEAT PUMPS*. vol. 44. Fifth Edit. 1970.
- [3] Guo XM, Chen YG, Wang WH, Chen CZ. Experimental study on frost growth and dynamic performance of air source heat pump system. *Appl Therm Eng* 2008;28:2267–78. doi:10.1016/j.applthermaleng.2008.01.007.
- [4] Wang F, Wang Z, Zheng Y, Lin Z, Hao P, Huan C, et al. Performance investigation of a novel frost-free air-source heat pump water heater combined with energy storage and dehumidification. *Appl Energy* 2015;139:212–9. doi:10.1016/j.apenergy.2014.11.018.
- [5] Song M, Pan D, Li N, Deng S. An experimental study on the negative effects of downwards flow of the melted frost over a multi-circuit outdoor coil in an air source heat pump during reverse cycle defrosting. *Appl Energy* 2015;138:598–604. doi:10.1016/j.apenergy.2014.09.010.
- [6] Kelly JA, Fu M, Clinch JP. Residential home heating: The potential for air source heat pump technologies as an alternative to solid and liquid fuels. *Energy Policy* 2016;98:431–42. doi:10.1016/j.enpol.2016.09.016.
- [7] Tang J, Gong G, Su H, Wu F, Herman C. Performance evaluation of a novel method of frost prevention and retardation for air source heat pumps using the orthogonal experiment design method. *Appl Energy* 2016;169:696–708. doi:10.1016/j.apenergy.2016.02.042.
- [8] Song M, Gong G, Mao N, Deng S, Wang Z. Experimental investigation on an air source heat pump unit with a three-circuit outdoor coil for its reverse cycle defrosting termination

- temperature. *Appl Energy* 2017;204:1388–98. doi:10.1016/j.apenergy.2017.01.068.
- [9] Zhao M, Gu ZL, Kang WB, Liu X, Zhang LY, Jin LW, et al. Experimental investigation and feasibility analysis on a capillary radiant heating system based on solar and air source heat pump dual heat source. *Appl Energy* 2017;185:2094–105. doi:10.1016/j.apenergy.2016.02.043.
- [10] Su W, Zhang X. Performance analysis of a novel frost-free air-source heat pump with integrated membrane-based liquid desiccant dehumidification and humidification. *Energy Build* 2017;145:293–303. doi:10.1016/j.enbuild.2017.04.024.
- [11] Qu M, Fan Y, Chen J, Li T, Li Z, Li H. Experimental study of a control strategy for a cascade air source heat pump water heater. *Appl Therm Eng* 2017;110:835–43. doi:10.1016/j.applthermaleng.2016.08.176.
- [12] Bertsch SS, Groll EA. Two-stage air-source heat pump for residential heating and cooling applications in northern U.S. climates. *Int J Refrig* 2008;31:1282–92. doi:10.1016/j.ijrefrig.2008.01.006.
- [13] Lohani SP, Schmidt D. Comparison of energy and exergy analysis of fossil plant, ground and air source heat pump building heating system. *Renew Energy* 2010;35:1275–82. doi:10.1016/j.renene.2009.10.002.
- [14] Kelly NJ, Cockroft J. Analysis of retrofit air source heat pump performance: Results from detailed simulations and comparison to field trial data. *Energy Build* 2011;43:239–45. doi:10.1016/j.enbuild.2010.09.018.
- [15] Heo J, Jeong MW, Baek C, Kim Y. Comparison of the heating performance of air-source heat pumps using various types of refrigerant injection. *Int J Refrig* 2011;34:444–53. doi:10.1016/j.ijrefrig.2010.10.003.
- [16] Lazzarin RM. Dual source heat pump systems: Operation and performance. *Energy Build* 2012;52:77–85. doi:10.1016/j.enbuild.2012.05.026.
- [17] Safa AA. Masters thesis 2 2012.
- [18] Ibrahim O, Fardoun F, Younes R, Louahlia-Gualous H. Air source heat pump water heater: Dynamic modeling, optimal energy management and mini-tubes condensers. *Energy* 2014;64:1102–16. doi:10.1016/j.energy.2013.11.017.
- [19] Li R, Ooka R, Shukuya M. Theoretical analysis on ground source heat pump and air source heat pump systems by the concepts of cool and warm exergy. *Energy Build* 2014;75:447–55.

- doi:10.1016/j.enbuild.2014.02.019.
- [20] Yao Y, Jiang Y, Deng S, Ma Z. A study on the performance of the airside heat exchanger under frosting in an air source heat pump water heater/chiller unit. *Int J Heat Mass Transf* 2004;47:3745–56. doi:10.1016/j.ijheatmasstransfer.2004.03.013.
- [21] Byun JS, Lee J, Jeon CD. Frost retardation of an air-source heat pump by the hot gas bypass method. *Int J Refrig* 2008;31:328–34. doi:10.1016/j.ijrefrig.2007.05.006.
- [22] Shen J, Guo T, Tian Y, Xing Z. Design and experimental study of an air source heat pump for drying with dual modes of single stage and cascade cycle. *Appl Therm Eng* 2018;129:280–9. doi:10.1016/j.applthermaleng.2017.10.047.
- [23] Wang B, Liu X, Shi W. Performance improvement of air source heat pump using gas-injected rotary compressor through port on blade. *Int J Refrig* 2017;73:91–8. doi:10.1016/j.ijrefrig.2016.09.017.
- [24] Wang Z, Wang F, Ma Z, Song M. Numerical study on the operating performances of a novel frost-free air-source heat pump unit using three different types of refrigerant. *Appl Therm Eng* 2017;112:248–58. doi:10.1016/j.applthermaleng.2016.10.040.
- [25] Hadorn J-C. *Solar and Heat Pump Systems for Residential Buildings*. Ernst & Sohn; n.d.
- [26] Sarbu I, Sebarchievici C. General review of ground-source heat pump systems for heating and cooling of buildings. *Energy Build* 2014;70:441–54. doi:10.1016/j.enbuild.2013.11.068.
- [27] Deng J, Wei Q, Liang M, He S, Zhang H. Field test on energy performance of medium-depth geothermal heat pump systems (MD-GHPs). *Energy Build* 2019;184:289–99. doi:10.1016/j.enbuild.2018.12.006.
- [28] Esen H, Esen M, Ozsolak O. Modelling and experimental performance analysis of solar-assisted ground source heat pump system. *J Exp Theor Artif Intell* 2017;29:1–17. doi:10.1080/0952813X.2015.1056242.
- [29] Pandey N, Murugesan K, Thomas HR. Optimization of ground heat exchangers for space heating and cooling applications using Taguchi method and utility concept. *Appl Energy* 2017;190:421–38. doi:10.1016/j.apenergy.2016.12.154.
- [30] Sebarchievici C, Sarbu I. Performance of an experimental ground-coupled heat pump system for heating, cooling and domestic hot-water operation. *Renew Energy* 2015;76:148–59. doi:10.1016/j.renene.2014.11.020.

- [31] Fannou JL, Rousseau C, Lamarche L, Stanislaw K. Experimental analysis of a direct expansion geothermal heat pump in heating mode. *Energy Build* 2014;75:290–300.  
doi:10.1016/j.enbuild.2014.02.026.
- [32] Mokhtar M, Stables M, Liu X, Howe J. Intelligent multi-agent system for building heat distribution control with combined gas boilers and ground source heat pump. *Energy Build* 2013;62:615–26. doi:10.1016/j.enbuild.2013.03.045.
- [33] Guo Y, Zhang G, Zhou J, Wu J, Shen W. A techno-economic comparison of a direct expansion ground-source and a secondary loop ground-coupled heat pump system for cooling in a residential building. *Appl Therm Eng* 2012;35:29–39.  
doi:10.1016/j.applthermaleng.2011.09.032.
- [34] Benli H. Energetic performance analysis of a ground-source heat pump system with latent heat storage for a greenhouse heating. *Energy Convers Manag* 2011;52:581–9.  
doi:10.1016/j.enconman.2010.07.033.
- [35] Pulat E, Coskun S, Unlu K, Yamankaradeniz N. Experimental study of horizontal ground source heat pump performance for mild climate in Turkey. *Energy* 2009;34:1284–95.  
doi:10.1016/j.energy.2009.05.001.
- [36] Tarnawski VR, Leong WH, Momose T, Hamada Y. Analysis of ground source heat pumps with horizontal ground heat exchangers for northern Japan. *Renew Energy* 2009;34:127–34.  
doi:10.1016/j.renene.2008.03.026.
- [37] Nam Y, Ooka R, Hwang S. Development of a numerical model to predict heat exchange rates for a ground-source heat pump system. *Energy Build* 2008;40:2133–40.  
doi:10.1016/j.enbuild.2008.06.004.
- [38] Nagano K, Katsura T, Takeda S. Development of a design and performance prediction tool for the ground source heat pump system. *Appl Therm Eng* 2006;26:1578–92.  
doi:10.1016/j.applthermaleng.2005.12.003.
- [39] Hawlader MNA, Chou SK, Ullah MZ. The performance of a solar assisted heat pump water heating system. *Appl Therm Eng* 2001;21:1049–65. doi:10.1016/S1359-4311(00)00105-8.
- [40] Chyng JP, Lee CP, Huang BJ. Performance analysis of a solar-assisted heat pump water heater. *Sol Energy* 2003;74:33–44. doi:10.1016/S0038-092X(03)00110-5.
- [41] Yang W, Zhang H, Liang X. Experimental performance evaluation and parametric study of a

- solar-ground source heat pump system operated in heating modes. *Energy* 2018;149:173–89. doi:10.1016/j.energy.2018.02.043.
- [42] Huang BJ, Chyng JP. Performance characteristics of integral type solar-assisted heat pump. *Sol Energy* 2001;71:403–14. doi:10.1016/S0038-092X(01)00076-7.
- [43] Kuang YH, Sumathy K, Wang RZ. Study on a direct-expansion solar-assisted heat pump water heating system. *Int J Energy Res* 2003;27:531–48. doi:10.1002/er.893.
- [44] Kuang YH, Wang RZ, Yu LQ. Experimental study on solar assisted heat pump system for heat supply. *Energy Convers Manag* 2003;44:1089–98. doi:10.1016/S0196-8904(02)00110-3.
- [45] Huang BJ, Lee JP, Chyng JP. Heat-pipe enhanced solar-assisted heat pump water heater. *Sol Energy* 2005;78:375–81. doi:10.1016/j.solener.2004.08.009.
- [46] Ji J, He H, Chow T, Pei G, He W, Liu K. Distributed dynamic modeling and experimental study of PV evaporator in a PV/T solar-assisted heat pump. *Int J Heat Mass Transf* 2009;52:1365–73. doi:10.1016/j.ijheatmasstransfer.2008.08.017.
- [47] Torío H, Angelotti A, Schmidt D. Exergy analysis of renewable energy-based climatisation systems for buildings: A critical view. *Energy Build* 2009;41:248–71. doi:10.1016/j.enbuild.2008.10.006.
- [48] Rezaie B, Esmailzadeh E, Dincer I. Renewable energy options for buildings: Case studies. *Energy Build* 2011;43:56–65. doi:10.1016/j.enbuild.2010.08.013.
- [49] Shi L, Chew MYL. A review on sustainable design of renewable energy systems. *Renew Sustain Energy Rev* 2012;16:192–207. doi:10.1016/j.rser.2011.07.147.
- [50] Fiorentini M, Cooper P, Ma Z. Development and optimization of an innovative HVAC system with integrated PVT and PCM thermal storage for a net-zero energy retrofitted house. *Energy Build* 2015;94:21–32. doi:10.1016/j.enbuild.2015.02.018.
- [51] Sichilalu SM, Xia X. ScienceDirect Optimal energy control of grid tied PV – diesel – battery hybrid system powering heat pump water heater. *Sol Energy* 2015;115:243–54. doi:10.1016/j.solener.2015.02.028.
- [52] Dai L, Li S, DuanMu L, Li X, Shang Y, Dong M. Experimental performance analysis of a solar assisted ground source heat pump system under different heating operation modes. *Appl Therm Eng* 2015;75:325–33. doi:10.1016/j.applthermaleng.2014.09.061.
- [53] Buker MS, Riffat SB. Solar assisted heat pump systems for low temperature water heating

- applications: A systematic review. *Renew Sustain Energy Rev* 2016;55:399–413.  
doi:10.1016/j.rser.2015.10.157.
- [54] Poppi S, Sommerfeldt N, Bales C, Madani H, Lundqvist P. Techno-economic review of solar heat pump systems for residential heating applications. *Renew Sustain Energy Rev* 2018;81:22–32. doi:10.1016/j.rser.2017.07.041.
- [55] Huang BJ, Lee CP. Long-term performance of solar-assisted heat pump water heater. *Renew Energy* 2004;29:633–9. doi:10.1016/j.renene.2003.07.004.
- [56] Ozgener O, Hepbasli A. Experimental performance analysis of a solar assisted ground-source heat pump greenhouse heating system. *Energy Build* 2005. doi:10.1016/j.enbuild.2004.06.003.
- [57] Kuang YH, Wang RZ. Performance of a multi-functional direct-expansion solar assisted heat pump system. *Sol Energy* 2006;80:795–803. doi:10.1016/j.solener.2005.06.003.
- [58] Li YW, Wang RZ, Wu JY, Xu YX. Experimental performance analysis on a direct-expansion solar-assisted heat pump water heater. *Appl Therm Eng* 2007;27:2858–68.  
doi:10.1016/j.applthermaleng.2006.08.007.
- [59] Ji J, Pei G, Chow T tai, Liu K, He H, Lu J, et al. Experimental study of photovoltaic solar assisted heat pump system. *Sol Energy* 2008;82:43–52. doi:10.1016/j.solener.2007.04.006.
- [60] Wang E, Fung AS, Qi C, Leong WH. Performance prediction of a hybrid solar ground-source heat pump system. *Energy Build* 2012;47:600–11. doi:10.1016/j.enbuild.2011.12.035.

# **Chapter 3: Fundamentals of distributed water source heat pump system using renewable energy**

## 3.1 Introduction

In this chapter, we will introduce the development concept and composition of this system in detail. The critical components in this system include a water loop pipe network and heat pumps for different purposes. Besides, we will also briefly introduce the spiral tube geothermal heat exchanger used in this system, which is designed for shallow (10-15m) geothermal utilization.

As mentioned in the previous chapter, every renewable energy has its advantages and disadvantages. For example, solar radiation is a type of energy that has a property of flow and therefore is almost no restriction in quantity. Still, it has a problem of fluctuation and cannot be utilized effectively at night. On the other hand, geothermal heat is a heat source with a stable temperature, but there is an upper limit to the amount that can be used because of its stock property (a type of stored energy). Terrestrial radiation is an essential heat radiation source of the earth and radiates long wavelengths radiation into outer space day and night, but it becomes evident at night. Air heat, like geothermal heat, is a heat carrier that maintains temperature by the balance between solar and terrestrial radiation and is therefore considered as renewable energy when used by high-performance air source heat pumps. The atmosphere is a simple heat-collecting and heat-dissipating source of the air source heat pump. But there is a problem that the heat-collecting ability of the air source heat pump will decrease when the heating load becomes large in cold weather. Therefore, the heating ability cannot be obtained during the defrosting operation. In the cooling mode, when the outside air temperature rises, the refrigerant condensing pressure increases, and the power consumption increases accordingly, which causes a power shortage during the summer daytime. The air source heat pump can get and dissipate heat with the atmosphere by forced ventilation. However, if the heat exchange is conducted through natural ventilation by wind, it will be a more effective utilization of wind to generate power than running the fan by the power of wind power generation.

In this study, we are aiming to develop a system for a small-scale residential house that can supply such as heating, cooling and domestic hot water. By installing this heat pump system into a test building, we will verify this technology and evaluate its performance through experiments. In addition, this system can be expanded for various applications in the future due to a thermal network in the building, other functions such as refrigeration will be discussed and evaluated in the future.

## 3.2 Concept of distributed water source heat pump system using renewable energy

As described previously, a lot of previous studies focused on only one renewable energy source, such as ground heat or air heat to meet the heating and cooling demand of buildings. Such a single heat pump system has contributed to the reduction of the energy consumption of the building. Still, it is difficult to provide a highly efficient and stable energy supply system in this way. The multi-source, multi-use heat pump system (MMHP system) researched and developed by Ooka and Hino et al. Correspond to the heat pump system that uses all of the geothermal heat, solar heat, and air heat in Japan. In the MMHP system, several renewable energy such as solar radiation, geothermal heat, and air heat, and various heat-use heat pumps for cooling, heating, domestic hot water supply, freezing, etc., are used to construct a thermal network heat through water pipes within the building. A full-scale test building facility for verification of the proposed novel system was built at the Chiba Experiment Station, Institute of Industrial Science, The University of Tokyo. Also, there is room for improvement in each heat pump device such as air conditioning and hot water supply, and the effect and efficiency of the system were not apparent.

Therefore, in this thesis, we carry out the development research of the improved equipment and import it to a full-scale test building for verification, and confirm the system performance based on field testing. As shown in Figure 3. 1, the basic configuration of this system is introduced in detail. This figure is the distributed heat pump system designed to use these multiple kinds of renewable energy complementarily. Renewable energy, such as geothermal heat is utilized through the underground heat exchanger(GHX). A sky source heat pump(SSHP) uses renewable energy from the sky, such as solar radiation and air heat from the atmosphere. A water circulation loop integrates both renewable energy sources from earth and sky. The HVAC system for heating, cooling, and domestic hot water supply purposes are constructed by using several water source heat pumps.

This system is a technology that realizes energy saving of heat supply by aiming to maximize efficiency based on the second law of thermodynamics, based on a heat pump (HP). HP is a technical means that uses power to move heat from a low-temperature source (source) to a high-temperature location (sink). A heat source (heat collection source) and a heat sink(heat demand sink) require a

large heat capacity, and reducing the temperature difference between the two is the key to reducing power and increasing operating efficiency (coefficient of performance, COP). From this point of view, the earth (underground) is optimal as a heat source, and an individually distributed HP that supplies heat at a temperature that is just enough for the heat demand is desirable. Therefore, in the proposed system shown in Figure 3. 2, since each element is connected to a water loop, each component allows mutual heat exchange. As a result, the hot exhaust heat of the water source HP that supplies the cooling demand for space cooling will become the heat source of the water source HP that provides the heating demand such as space heating and domestic hot water supply. On the other hand, the exhaust heat of the water source HP for space cooling can be seen as the heat radiation source of the water source HP that provides the cooling purpose. The heat storage effect of soil adjusts the non-simultaneity of the exhaust heat, and the imbalance of the daily integrated amount can be adjusted by using the ground heat exchanger and collecting and dissipating heat by SSHP. For example, although the soil temperature around the GHX decreases due to the heat collection of heating, it is possible to recover it to the undisturbed soil temperature by collecting heat from solar radiation and air with SSHP. For air conditioning, the exhaust heat of daytime air conditioning raises the soil temperature near GHX, and by lowering it by SSHP through terrestrial radiation and natural ventilation at night. This operation can make soil temperature recover to a natural condition. This system has not only the normal use of geothermal heat but also the use of solar radiation and air heat that takes the ground as a heat storage medium. This operation can also be seen as the concept of a two-stage heat pump system that uses the underground heat as a buffer. In this way, the soil temperature around the ground heat exchanger can be kept close to the natural soil temperature (for example, the temperature of the constant-earth-temperature layer in Tokyo is about 17 °C). Therefore, the water source HP is optimal for both heating and cooling operation and maintain a high-performance simultaneously. In cold regions and warm regions, the temperature of the constant-earth-temperature layer can vary from around 10 °C to around 25 °C. Still, even so, a significant improvement in performance is possible compared to the conventional HP that uses outdoor air as a heat source. The heat pump and circulating pump in this system are distributed and installed to reduce the heat transfer power, and the start and stop of the circulating pump, and the flow rate control are controlled according to the heat pump operation.

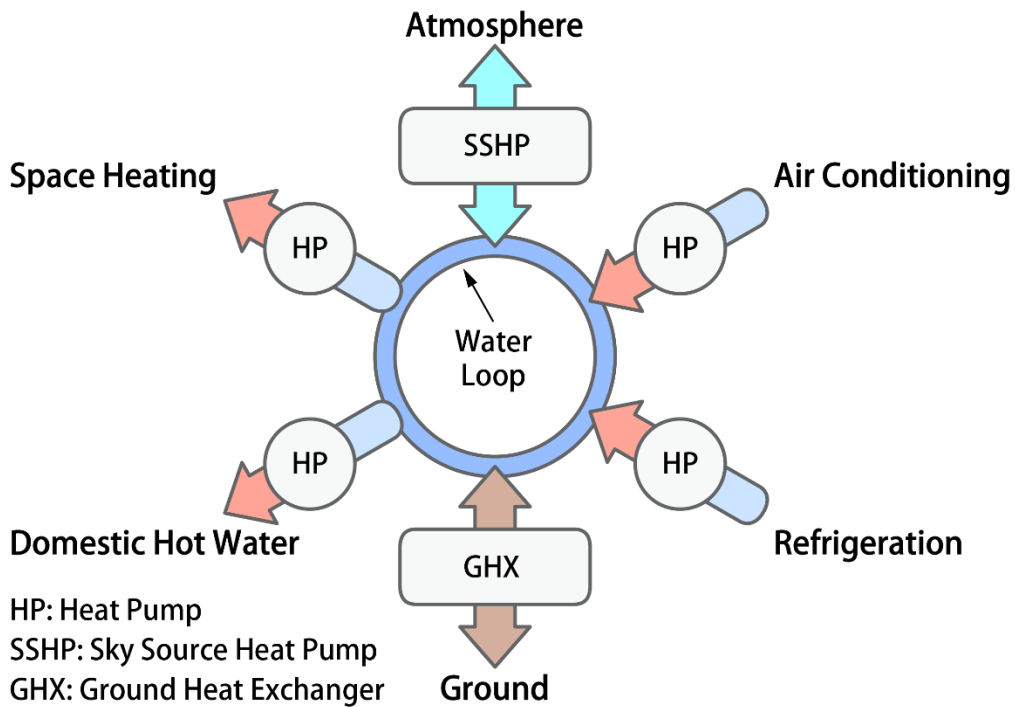


Figure 3. 1 Concept of distributed water source heat pump system using renewable energy

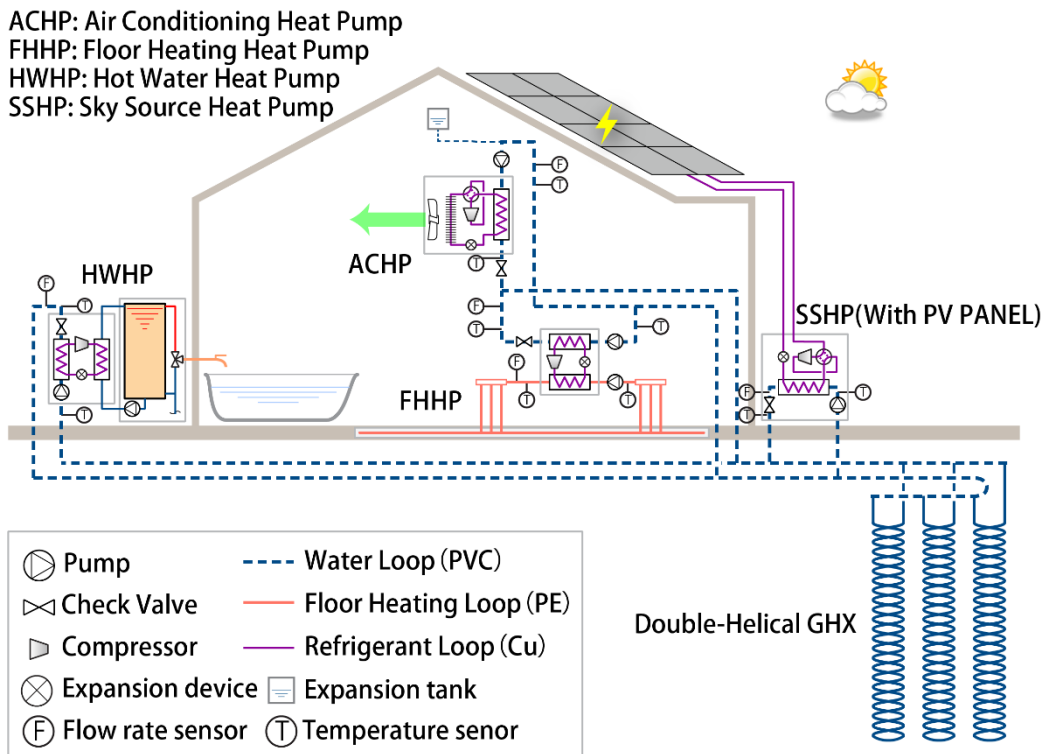


Figure 3. 2 System configuration of the water loop and heat pumps

With this configuration, the following effects can be obtained in the utilization of geothermal heat:

- In the conventional geothermal heat utilization technology, the U-tube type GHX required a large

installation area. This requirement is one of the obstacles to the spread of geothermal heat applications in Japan. In this system, the recovery of the ground temperature is conducted by the daily cycle through the SSHP. Therefore, the distance between the boreholes can decrease, and the laying area of the GHX becomes small. For this reason, the possibility of utilizing geothermal heat will significantly expand even in buildings built on restricted sites in Japan.

- For excavation, a simple construction method using a special screw can be used so that the excavation cost can be reduced compared to the conventional drilling method.
- Due to the soil heat storage, it is possible to expect power load leveling comparable to thermal storage air conditioning. That is, in the summer, the SSHP can help recover the soil temperature by radiative cooling using night-time off-peak power. Therefore, in the daytime, the high COP operation for space cooling of the water source heat pump halves the power consumption during on-peak. In the winter season, since the soil temperature will increase by the daytime heat collection operation of the SSHP, it is possible to improve the performance of the water source heat pump at night.
- This system recovers soil temperature in a daily cycle, so soil heat pollution does not occur. For this reason, it is possible to cope with future applications such as when geothermal heat utilization facilities are adjacent to each other.
- The antifreeze can be eliminated because the temperature of the circulating water in the water loop can be prevented from being too low by the heating operation of the SSHP.

In this system, a water loop network constitutes a thermal network within the building, and the individual distributed water source HP that exchanges heat with this network can supply the necessary heating and cooling. This individually distributed network system can be used for a variety of purposes. It can be expected to offer the advantage of a high potential to expand for various applications[1–16].

## **3.3 Development of distributed water source heat pump system**

### *3.3.1 Construction of water loop system*

In Japan, there are few examples of air conditioning system using a water piping system. The reasons are: 1) the installation cost of the water piping system is expensive. 2) it is difficult to reduce the operating cost due to the energy consumption of the circulating water pump, and 3) the commercialization and popularization of the air source heat pump using the refrigerant piping system directly; and so on.

Concerning reason 3) above, since the amount of refrigerant enclosed is large and it is challenging to avoid leakage of refrigerant when discarded, so we think that it will be necessary to reuse the water piping system in the future regarding the global warming issue. In the case of the water source HP, we can modularize the refrigerant circuit, which means the amount of refrigerant enclosed can be minimized. Also, it can be returned to the facility for thorough recycling and destruction of the refrigerant when discarded. Based on this way, it is possible to solve the problems 1) and 2) related to the water piping system. Regarding the above issue 2), we confirmed the reduction effect of heat transfer power (operation cost) by adopting a distributed pumping configuration through experiments. Regarding the above problem 1), reduction of the installation cost and the operation cost under actual conditions can be verified using the RE house (the test building for verification of this system). In this part, we will introduce the content of the pumping experiment to demonstrate that the decentralized pumping system has the highest energy saving potential and is the most suitable pumping configuration for the distributed heat pump system. In the water loop, the heat transport is based on the distributed pump system. Water is circulated by a dedicated pump installed separately with each heat pump unit. This configuration can reduce the pressure loss caused by the control valve, and the flow rate is controlled by an inverter when necessary. Figure 3. 3 shows the configuration of installing the circulating pump with a heat pump unit together. Figure 3. 4 shows the circulating pump adopted in this system, this kind of water pump (Grundfos ALPHA2) can be used to transport domestic hot water; hence it can be used in the temperature range in this system.



Figure 3. 3 Circulating pump set with heat pump together



Figure 3. 4 Small DC water pump (Grundfos ALPHA2)

### ***Energy saving potential of centralized and decentralized pumping systems***

In order to reduce equipment costs, heat transfer consumption, and improve heat exchange performance, this system has a configuration in which individually distributed equipment (water source heat pump) is connected to a thermal network (water loop). Therefore, there are advantages that the degree of freedom of use and the expandability are high, and the fault of one terminal won't affect the whole system. In addition, the water loop is powered by a distributed pump for each heat pump through interlocking to avoid unnecessary pressure loss; high-efficiency DC pumps are used to reduce the pressure loss due to control valves. In energy distribution systems, thermal energy is

usually transferred by a heat carrier fluid via pumps. Improper design and unreasonable control of pumping systems result in inefficient operation, which accounts for a significant part of electricity consumption in the industry. The need to save energy has been sharpened the focus on improving energy efficiency in pumping systems. The application of a decentralized pumping system with the variable-frequency drive can be considered a technological improvement that has the potential to save energy compared to the conventional centralized pumping system[1,8].

In this study, a reduced-scale hydronic system was built to carry out experiments comparing the performance of centralized and decentralized pumping systems under the same flow rate conditions. Figure 3. 5 shows the experimental system from the front perspective. Figure 3. 6 shows the console in the experimental system, including a computer for collecting/monitoring data, and the control panel for controlling all circulating pumps. Figure 3. 7 shows a schematic and photos of the experimental system. To ensure the consistency of unrelated variables in experiments in which different pumping control strategies were adopted, the experimental apparatus was designed to be switched between different configurations by switching the gate valves installed in the bypass. The experimental system consisted of two branches and a bypass which was connected in parallel with the branches. The size of the entire piping system was  $4.5 \times 2.4$  m (length  $\times$  width, as shown in Figure 3. 7). The entire piping system was made from stainless steel. The main pipe had an inner diameter of 26.58 mm; the branch and bypass pipes had the same inner diameter of 20.22 mm. Water was used as the heat carrier fluid.

Valves  $R_{b1}$  and  $R_{b2}$  were arranged in each branch pipe to model the pressure loss caused by HVAC components such as heat exchangers and fan coil units in real piping systems. Because the actual length of a piping system is typically much longer than that in a reduced-scale experimental setup, valves  $R_{(b1-b2)}$  and  $R_m$  were arranged in the branch pipe 1 and main return pipe respectively, in order to model the pressure loss over a long pipeline. To prevent reverse-flow between the two branch pipes, a check valve was installed in between branch pipes 1 and 2.



Figure 3. 5 Photos of experimental apparatus(front).



Figure 3. 6 Photos of experimental apparatus(side).



gauge pressures and flow rate with high accuracy. As shown in Figure 3. 7, a total of twelve pressure sensors were installed at the inlet and outlet of the main pump, the outlet of two branch pumps, before and after the virtual resistances, and the branch inlet. Three electromagnetic flow meters were installed at each branch pipe and the main pipe. A data logger was used to record the analog output from the pressure and flow rate sensors. The specifications of sensors used are listed in Table 3. 1.

Table 3. 1 Specification of measuring devices used in experiments

Device	Accuracy
Pressure sensor	$\pm 1.0\%$ of the full scale
Flow rate sensors	$\pm 1.6\%$ of the full scale
Data Logger	$\pm 0.05\%$ of reading $\pm 2$ digits

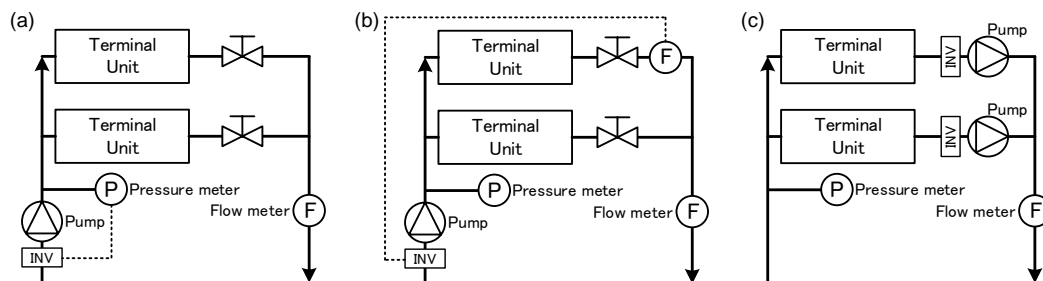


Figure 3. 8 Three different configurations of pumping system: (a) Centralized pumping system with constant pressure control, (b) Centralized pumping system with constant terminal flow rate Control, (c) Decentralized pumping system.

In the experiments, three different variable water volume systems—two different control strategies for the centralized pumping system and the decentralized pumping system—were compared, as shown in Figure 3. 8. Figure 3. 8(a) depicts the centralized pumping system with constant pressure (CP) control, which is typically used for water supply and pressure holding in circulation systems. For this system, the discharge pressure of the pump was maintained at a constant value during operation, regardless of changes in flow rate due to heating or cooling load changes. In general, although adjustment according to changes in the load mainly depends on pump speed regulation and two-way valves, the pump discharge pressure is constant. As a result, the rotation speed of the pump cannot be too significantly reduced; therefore, the energy savings that can be achieved are very limited. Specifically, even if the flow rate decreases, it is necessary to operate the pump to maintain a constant pressure, and thus this unnecessary pump head results in inefficiency. Figure 3.

8(b) depicts the centralized pumping system with constant terminal flow rate (CTF) control. In this control strategy, the rotational speed of the pump was regulated by inverters in accordance with the necessary heating or cooling load. Unlike CP control, it is not necessary to maintain a high pressure at a small flow rate, so the rotational speed of the pump can be reduced as the flow rate decreases, offering improved energy efficiency. Finally, Figure 3. 8(c) depicts the decentralized pumping system. In this configuration, variable speed pumps were installed at each branch pipe; speed can be adjusted according to the load change of each user. The flow rates of all pumps in three control strategies can be controlled by the proportional–integral–derivative controller. There were no balancing or control valves to regulate the flow rate in the branch pipe.

Because the energy use of each pump is affected by its mechanical characteristics, a direct comparison between different types of pumps is not valid. Therefore, to avoid the effects of the different performance characteristics of the pumps and to enable the comparison of the energy savings potential of three different pumping system configurations, the theoretical power requirement of the pump  $P_t$ , was used as the evaluation index. The theoretical power requirement represents the kinetic energy loss in the form of a pressure loss in the pipe. This index is typically used to analyze and calculate the hydraulic performance of pipelines. The theoretical power requirement of the pump depends directly on the flow rate  $V$ ; water density  $\rho$ , total head loss  $H$ , and gravitational acceleration  $g$ , as expressed in Eq.(1). It should be noted that the denominator in Eq.(1) is for the conversion of the flow rate,  $V$ ; in units from L/min to m<sup>3</sup>/s. The denominator in Eq.(2) is for the conversion of pressure units from kPa to m.  $P_{pi}$  and  $P_{po}$  is the pump inlet and outlet pressure, respectively.

Based on the three different configurations mentioned above, the five different cases were established to compare energy use via the theoretical pump power requirement.

$$P_t = \frac{\rho g \dot{V} H}{60 \times 1000} \quad (1)$$

$$H = (P_{po} - P_{pi})/9.8 \quad (2)$$

The five cases described in Table 3. 2 were investigated to compare the performance of decentralized and two typical centralized pumping systems under various flow rate conditions. The branch pipe

closest to the main pump was labeled Branch Pipe 2, and the other was labeled Branch Pipe 1, as shown in Figure 3. 7. Cases 1 and 2 represent a centralized pumping system with CP control and a decentralized pumping system, respectively, at the rated flow rates condition. Cases 3 and 4 represent centralized pumping systems with CP control and CTF control, respectively, at partial flow rates condition(80% of the rated flow). Case 5 represents a decentralized pumping system with the same flow rates as in Cases 3 and 4. In all cases, the flow rate in each branch pipe was assumed to be half of the total flow rate. The two-way electronic valve was only used in the centralized pumping system to regulate the flow rate and control the balance between the branch pipes. The effective length of the virtual resistance in the main return pipe was assumed to be 4.7 m, and between branches 1 and 2 it was assumed to be 15 m. For CP control in Cases 1 and 2, the setting discharge pressure was set to the value at the rated flow rate (rated load condition), which was 21.5 kPa in this experiment.

In the centralized pumping systems, only the main pump was operated, so the two branch pumps were turned off, while in the decentralized pumping systems the circumstance is reversed. At the rated flow rate, the virtual resistances  $\Delta R_{b1(b2)}$ ,  $\Delta R_{b1-b2}$ , and  $\Delta R_m$  were set to 5, 1.5, and 4.5 kPa, respectively. These values were reduced to 3, 1.1, and 3.3 kPa, respectively, when the flow rate was decreased to 80% of the rated flow.

Table 3. 2 Experimental conditions of five experimental cases, under the same flow rate conditions

Case	System configuration	Control strategy	Design flow rate (L/min)			Design virtual resistance (kPa)			
			$\dot{V}_m$	$\dot{V}_{b1}$	$\dot{V}_{b2}$	$\Delta R_{b1}$	$\Delta R_{b2}$	$\Delta R_{b1-b2}$	$\Delta R_m$
1	Centralized	CP control	26	13	13	5	5	1.5	4.5
2	Decentralized	Inverter control	26	13	13	5	5	1.5	4.5
3	Centralized	CP control	21	10.5	10.5	3	3	1.1	3.3
4	Centralized	CTF control	21	10.5	10.5	3	3	1.1	3.3
5	Decentralized	Inverter control	21	10.5	10.5	3	3	1.1	3.3

A comparison of the theoretical power required by the different cases is shown in Figure 3. 9. Under the same flow rate conditions, the theoretical power requirement of the centralized pumping system

is higher than that of the decentralized pumping system due to additional energy for throttling. Compared to the rated flow rate operation, the theoretical power of the centralized pumping system decreased by 19% under constant pressure control at the partial (80%) flow rate. In the decentralized pumping system, the theoretical power decreased by 47% when the flow rate was decreased to 80% of the rated flow rate, which shows that the energy saving effect is more remarkable when system is operating at the partial load than at the rated load. This is of particular interest for buildings with frequent load changes, such as office buildings.

The pumping system is generally designed according to the maximum heat/cold load, but most pumping systems operate at partial load inefficiently for most of the time. In the decentralized pumping system, the flow rate is adjusted by changing the pump speed rather than throttling to cope with load changes, there is no need to input extra energy for throttling and balancing. Therefore, the use of a decentralized pumping system helps to improve the energy efficiency in buildings, which can significantly reduce the overall energy demand and eventually reduce the global environmental impact. In addition, based on the results of this study, this kind of decentralized configuration can also be extended to other fluid delivery systems for efficient energy supply.

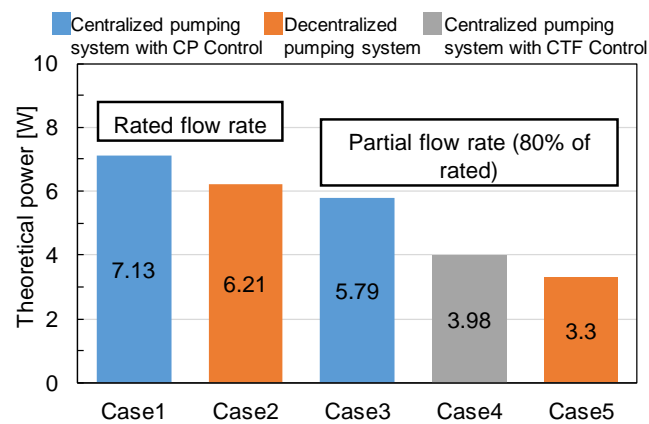


Figure 3. 9 Comparison of theoretical power requirement under different scenarios.

For example, the decentralized configuration can be adopted in the HVAC duct system to achieve variable air volume operation while avoiding energy waste at the damper. Also, the decentralized configuration can be used in cooling water systems to improve the efficiency of a chilled water plant and district heating/cooling system. These applications can help realize the optimal use of energy

resources and optimization of fluid and energy delivery in whole industries, such as the energy industry and the chemical industry.

### ***Reduction of installation costs of water loop***

#### ***No antifreeze***

Usually, the equipment for utilizing geothermal heat uses antifreeze liquid for circulating water of the ground heat exchanger and the water source heat pump. The main reason why antifreeze liquid is needed is that if the geothermal heat is insufficient during the heating operation in winter, the ground temperature and circulating water temperature will drop, and freshwater may cause freezing. Freezing occurs on the waterside of the evaporator of the water source heat pump that supplies heat, such as space heating and domestic hot water supply. As a result, the flow rate of circulating water decreases, and the heat exchanger may be damaged. Even when the heat pump is stopped, a pipe freezing accident due to cold outside air may occur. For these reasons, it is common to use antifreeze for circulating water.

The antifreeze is typically an aqueous solution of ethylene glycol (EG) or propylene glycol (PG). EG is toxic, and there is concern about soil contamination due to leakage. When PG is adopted, the cost will increase, and the energy consumption of the circulating pump will increase due to the high viscosity, and the heat transfer coefficient in the heat exchanger will decrease accordingly. In the geothermal heat utilization system, the amount of antifreeze added into the ground heat exchangers is very large, so the cost of antifreeze and work costs cannot be ignored.

In the developed system, the sky source heat pump (SSHP) is used to collect heat regardless of day or night weather (however, operating efficiency may fluctuate)[10]. Using this method, we have developed a system in which the water loop circulating water is made fresh, and antifreeze is not required. In the test system described later, the tap water was enclosed in the water loop, and the antifreeze control based on the SSHP was developed so that the circulating water temperature will not fall below three degrees. For about two years of field testing(2017-2019), The operation result showed that the freezing accident could be avoided.

#### ***Piping cost reduction***

In the geothermal heat utilization system, it is common to use polyethylene (PE) pipes for the pipes

of the geothermal heat exchanger and the connecting pipes to the water source heat pump. It has been confirmed that PE pipes have long-term (50 years) durability unless exposed to ultraviolet light. However, since PE pipes cannot be connected using an adhesive, they must be melted by heat before joining. Therefore, a particular joint with a built-in heating wire is used, and a dedicated fusion machine is used to control the melting temperature.

On the other hand, since vinyl chloride (PVC) pipes can be connected with an adhesive, so the workability becomes higher. It is also confirmed to have almost the same or better durability as PE pipe. However, PVC is generally not used in geothermal heat utilization systems because it tends to dissolve in glycol antifreeze. As mentioned above, the developed system does not require antifreeze liquid, so there is a possibility that inexpensive PVC piping can be used.

According to previous research, the material cost of PE piping is about five times that of PVC piping. From this, it was judged that the adoption of PVC piping would be indispensable for the diffusion of geothermal heat utilization technology, and the subsequent technological development was advanced. The water loop system of the test building consisted entirely of PVC piping, the main pipe was 40A, the branch pipe was 25A in Japanese standard, and tap water was used as the circulating water for the operation experiment.

### ***Control method***

The circulating water temperature of the water loop of this system is designed to operate not only the heat pump for heating and domestic hot water supply but also the heat pumps for cooling with high efficiency. To maintain a natural soil temperature of  $\pm 5\text{K}$  (corresponding to the annual average temperature, about 12-22 °C in Tokyo) by "natural recovery" by the ground heat exchanger and "artificial recovery" by using sky source heat pump[3–6,13].

Since this temperature range is close to the underground temperature, the underground heat can be used efficiently without being diffused and lost. On the other hand, the water loop can be used as the heat source for heating and domestic hot water supply, and can also be used at a heat sink for cooling and refrigeration. That is, the exhaust heat from the different equipment can be recovered effectively. For the actual operation, the sky source heat pump is turned on and off at the water loop circulating water temperature to keep the circulating water temperature of the water loop close to the natural soil temperature.

### 3.3.2 Development of sky source heat pump

#### **Development of a prototype of the sky source heat pump**

To further improve the economic efficiency and energy saving of this system, based on the sol-air heat pump by Hino et al., we developed and improved the new sky source heat pump[2,3,7,10,14]. We developed a sky-source heat pump (SSHP) that can collect and dissipate heat using solar radiation, air, and longwave radiation. Figure 3. 10 shows the outdoor panel of SSHP, which can work as an evaporator or condenser. Figure 3. 11 shows other parts of the SSHP, mainly including the compressor and refrigerant circuit, as well as the control board. As shown in Figure 3. 12, the SSHP has composed of an outdoor heat collecting and dissipating panel (right side in Figure 3. 12, abbreviated as SS panel) and a refrigerant compressor unit (left side in Figure 3. 12).



Figure 3. 10 The outdoor panel of sky source heat pump.



Figure 3. 11 Compressor unit of sky source heat pump.

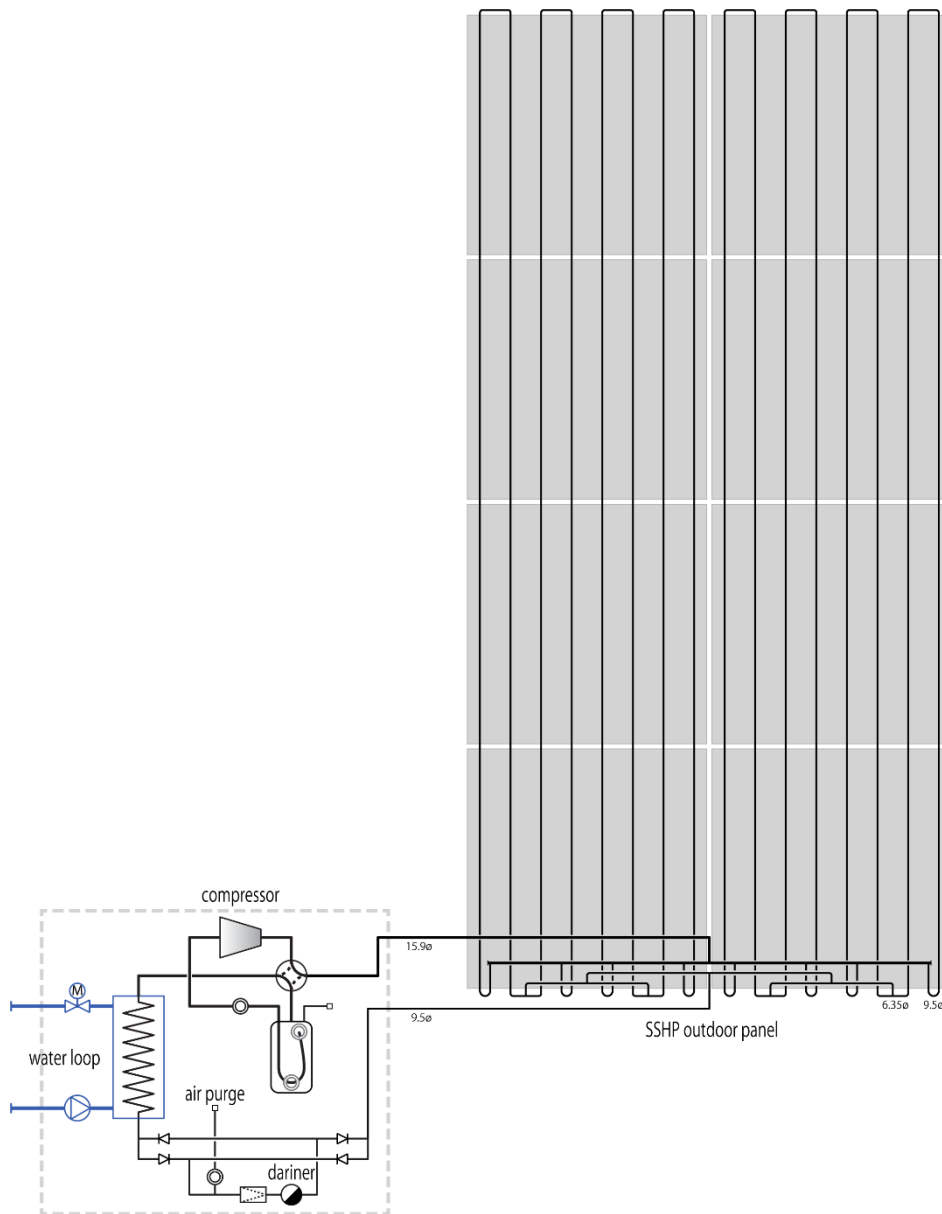


Figure 3. 12 Structure and refrigerant circuit of sky source heat pump

The outdoor panel is constructed by arranging multiple finned tubes, which are formed by extruding aluminum, in parallel. The finned tube has a central refrigerant passage and a plurality of outside air heat exchange fins, and evaporates the liquid refrigerant to absorb heat during the heat collection operation, and condenses the gas refrigerant to release heat during the heat dissipation operation. The fin is installed to facilitate heat exchange with air using natural convection and wind. For example, at the time of heating operation (heat collection), the panel temperature is made lower than the outside air temperature so that that heat can be quickly taken from the air. Similarly, during cooling operation (heat dissipation), the panel temperature is higher than the outside air temperature

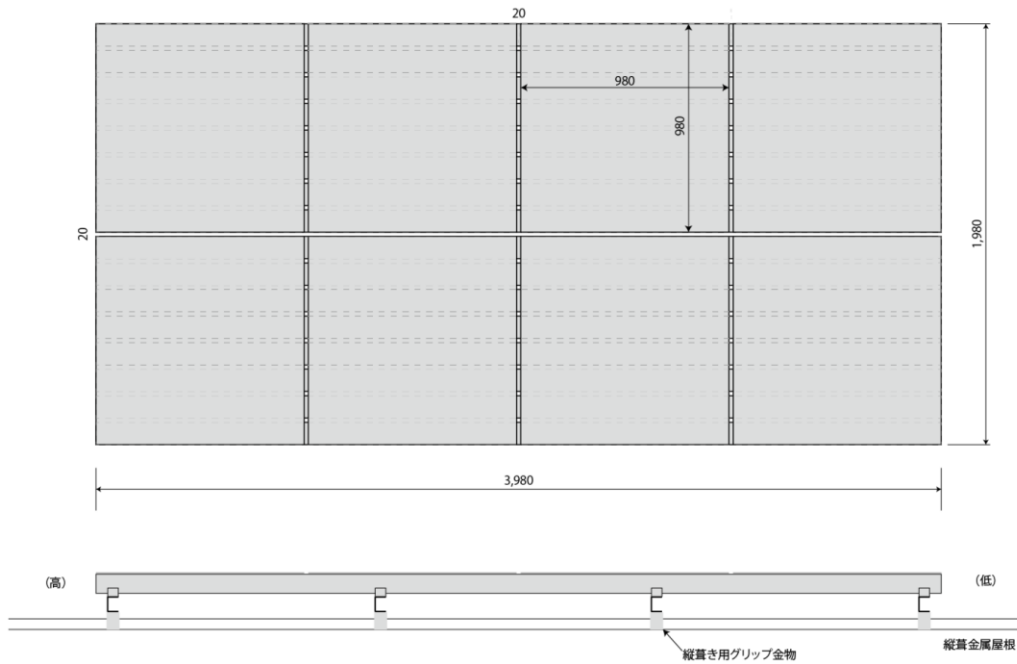


Figure 3.13 Dimensions of the outdoor panel

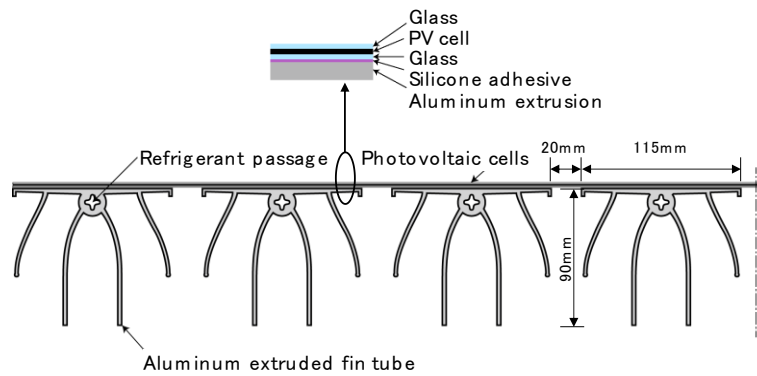


Figure 3.14 Part cross-section of the outdoor panel

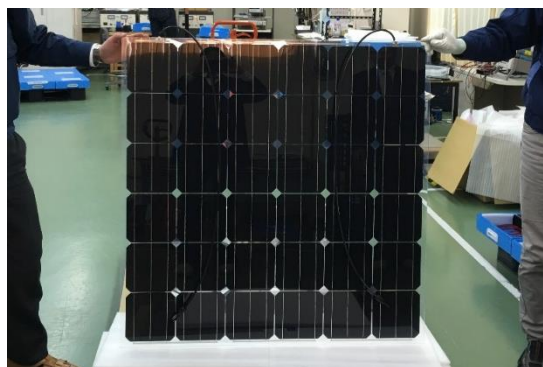


Figure 3.15 Solar cell module of sky source heat pump

so that heat can be efficiently dissipated from the fins to the air. Although the fin is provided based on the above basic design, heat may be lost depending on environmental conditions because sometimes the real operation does not follow the design purpose. For example, in the heating

operation (heat collection), when the solar radiation is sufficient, the panel fin temperature may rise and become higher than the outside air temperature, which means the heat escapes to the surrounding air. Although this will be a heat loss, this is acceptable when considering the prevention of compressor failure due to the excessive rise of the evaporation temperature and total environmental conditions (such as when there is little radiation). We made the panel with fins because the efficient extraction of heat from the air when there is little sunlight is more important than the heat loss.



Figure 3. 16 Installation status of the outdoor panel on the roof of RE house.

Compared with conventional solar heat collectors, it has a simple structure with only a heat collecting panel without a cover glass or heat insulation box, and because it gathers heat by evaporating the refrigerant. The metal corrosion and freezing will not occur. It also condenses the refrigerant to become a radiator at night. The dimensions of the outdoor panel are shown in Figure 3. 13. The heat collection area is about  $8 \text{ m}^2$ , the solar heat collection capacity is about  $6 \text{ kW}$ , and the air heat exchange capacity is about  $5 \text{ kW}$ .

Photovoltaic cells were attached to the upper surface of the outdoor panel (Figure 3. 14). As shown in Figure 3. 15, the photovoltaic cell is a module in which 36 6-inch single-crystal type cells are

connected in series, and thin glass is used on both sides to seal them with an ionomer (IO) (Figure 3. 14). These eight modules were silicon-bonded to the surface of the aluminum extruded fin tube.

Figure 3. 16 shows the outdoor panel installed with photovoltaic cells on the roof.

The compressor is a closed rotary type compressor. Besides, in the sky source heat pump, in the case of the panel work as an evaporator, it is necessary to spread a gas-liquid two-phase flow over the entire surface of the panel, prevent liquid back to the compressor and make oil (lubricating oil) return to the compressor reliably. When the panel works a condenser, it is necessary to discharge the condensed liquid refrigerant from the panel quickly. The commonly used expansion valve



Figure 3. 17 The steam trap used as the drainer in SSHP refrigerant circulation.

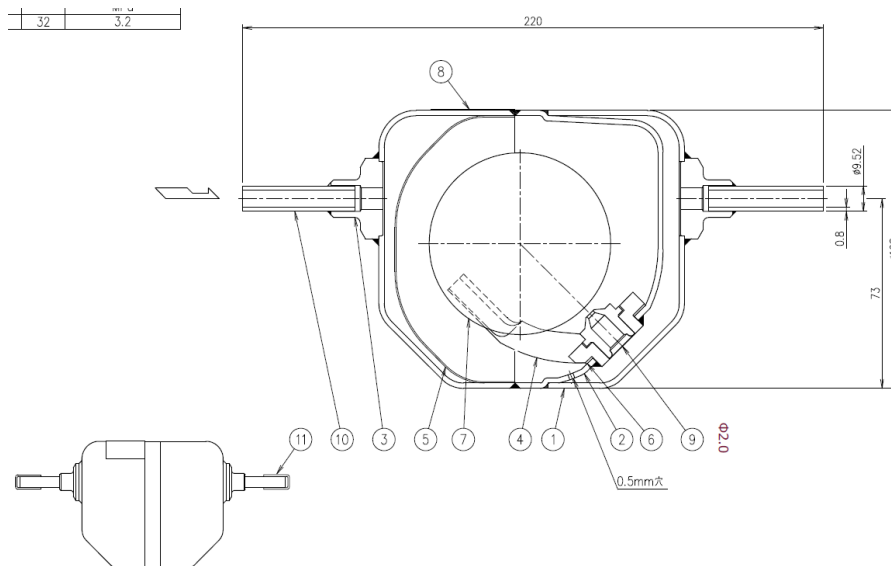


Figure 3. 18 The structure of the steam trap. Number in the figure: 1. body; 2. inner cover; 3. brim; 4. guide; 5. screen; 6. spacer; 7. float; 8. name plate; 9. orifice; 10. copper pipe; 11. cap

method cannot sufficiently perform such a function, and therefore the drainer method is used. The steam trap is used as the drainer (TLV: SS5N-HP-32, appearance is shown in Figure 3.17), it has a maximum operating pressure of 3.2 MPa, and a maximum operating temperature of 425°C. Figure 3.18 shows the detailed structure of the steam trap used as the drainer in this system.

## ***Principle of heating and cooling operation mode***

### ***Heat collection operation***

For the heating and domestic hot water supply in this system, the heat is collected during the daytime when solar heat is sufficient and stored in the ground. Then the heat is supplied by individually distributed water source heat pumps, which outdoor panel work as an evaporator. On a cloudy day or at night, when there is not enough solar radiation, the outdoor panel temperature becomes lower than the outside air temperature, heat is absorbed from the ambient air by natural convection, and heat is exchanged with the sky by long-wavelength radiation. Based on the experiment, it has been confirmed that when the wind speed is low, the temperature drops by about 10 K compared to the outside air, and when the humidity is high, dew condensation occurs and frost forms below freezing, but defrosting is not required.

If there is not sufficient solar radiation, the refrigerant evaporating temperature will rise. When the amount of solar radiation is enough (approximately 1 kW/m<sup>2</sup>), the average panel temperature (almost refrigerant evaporation temperature) may exceed the outside air temperature. However, since the temperature difference between the panel and outside air is small, the heat loss can be ignored. When the amount of solar radiation is low, the temperature at which the refrigerant evaporates falls below the ambient temperature, gathering both solar radiation and air. For this reason, the cover glass and heat insulation box, which are indispensable for ordinary solar water heaters, are not required in this system. This outdoor panel is also advantageous in terms of solar cell power generation efficiency. For example, when the heat pump is turned off, the fins on the back surface act as a radiator to suppress the temperature rise of the solar cell and prevent the power generation efficiency from decreasing. Furthermore, when the heat pump is operating, the solar cells are actively cooled, which increases the power generation efficiency.

### *Heat dissipation operation*

In the heat dissipation operation in this system, the cooling exhaust heat from space cooling during the daytime is stored in the ground, and this heat stored underground is dissipated mainly by the sky source heat pump at night to recover the ground temperature. At this time, the outdoor panel becomes a condenser, and the temperature of the outdoor panel rises accordingly. Then, the long-wavelength radiation is enhanced, and natural convection and wind are utilized to dissipate heat to the ambient air. If there is rainfall, the latent heat of vaporization of water can also be used, and the refrigerant condensing temperature decreases. As a result, the heat dissipation operation efficiency (take COP as a factor) can increase. It can be said that this system is a peak shift system that not only increases the cooling COP to reduce power during the daytime but also uses the power at night to dissipate heat. The solar cells dissipate heat through the fins on the backside during the daytime in summer, so the maximum stays around outside temperature plus 15 K.

For example, when the outside air temperature is 35 °C, the maximum temperature is about 50 °C even in the daytime on a sunny day, which is significantly lower than that of a typical solar cell, so it can help keep the power generation at an adequate level.



Figure 3. 19 Heat pump unit imported into the circulating water temperature control system



Figure 3. 20 Pipe connection with the water loop and sky source heat pump

### ***Compressor and circulating water control***

The compressor unit of the sky source heat pump (SSHP) (left part in Figure 3. 12, Figure 3. 19) is connected to the outdoor panel by the refrigerant circulation loop. During heat collection operation, the gas refrigerant evaporated in the outdoor panel is compressed to heat the circulating water in the water loop. During heat dissipation operation, the condensed liquid refrigerant in the outdoor panel is evaporated to cool the water loop circulating water.

As described above, the tap water is used in the water loop system as the water loop circulating water. For the material of the piping system, the insulated PVC pipe was buried underground in the refrigerant compressor unit, and water loop communication piping (Figure 3. 20), and the geothermal heat from GHX and the heating operation of SSHP were used to prevent freezing occurs in water loop.

In the heat collection operation of SSHP, the refrigerant evaporation temperature rises during fine weather on warm days, and conversely, the refrigerant evaporation temperature decreases during cold nights. The heat collection capacity changes greatly depending on the weather conditions. To avoid drastic changes and obtain a stable output of the compressor, the rotation speed of the compressor was controlled by an inverter.

That is, as shown in Figure 3. 21, when the refrigerant evaporation temperature is above 10 °C, the minimum speed is 30 rpm, and below minus 26 °C, the maximum speed is 90 rpm, and the compressor speed will change linearly.

Besides, we developed a program for operation control of SSHP to keep the circulating water temperature of the water loop near the natural temperature. The control flow is improved based on the feeding back from the experimental result. The latest version is shown in Figure 3. 22.

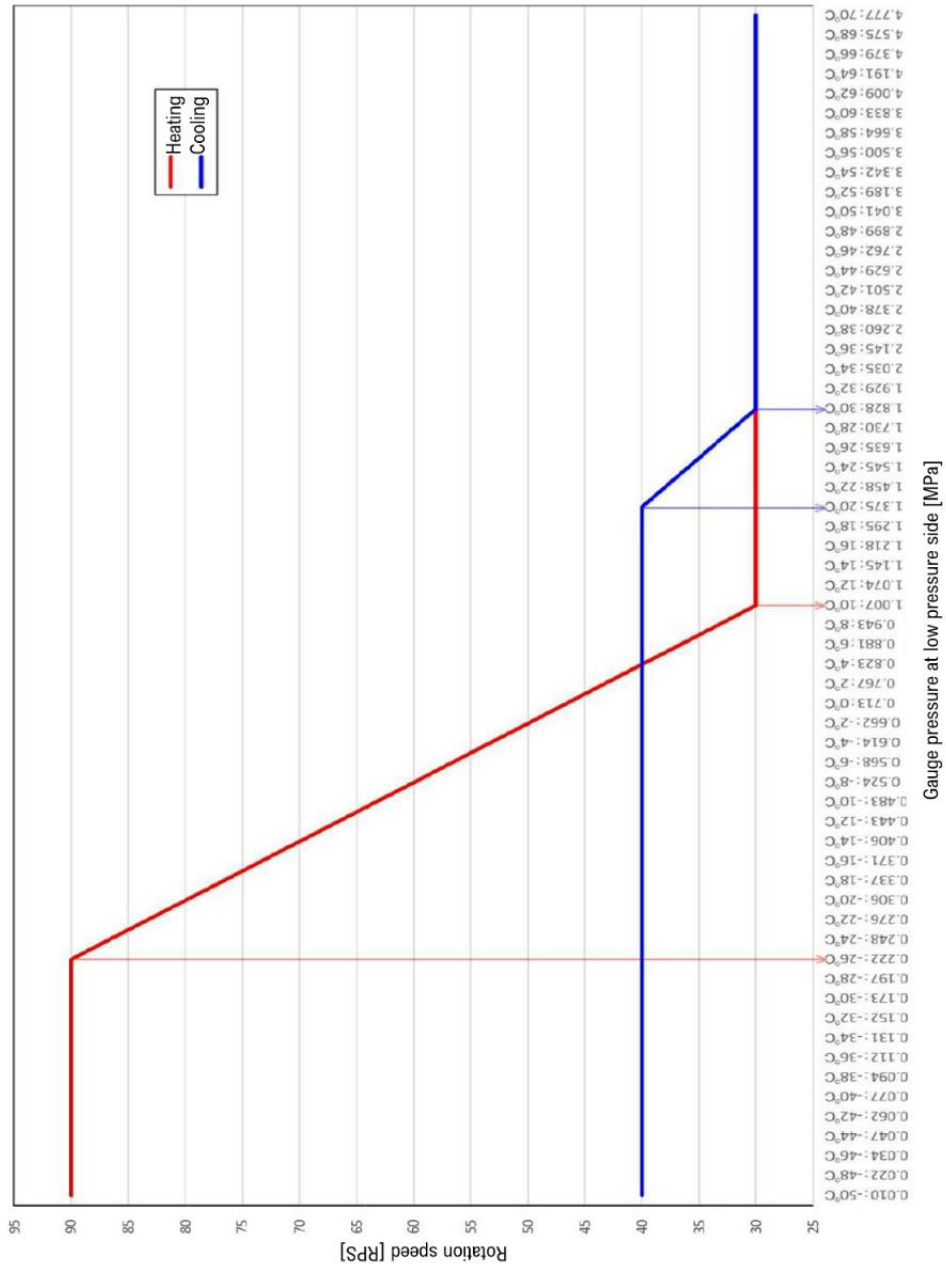


Figure 3. 21 Speed control of the compressor unit



### *3.3.3 Overview of double-helical ground heat exchanger*

#### ***Shallow depth geothermal utilization***

In the use of geothermal heat, it is desirable that the amount of soil heat collected in winter heating be almost equal to the amount of soil heat released in summer cooling to maintain high-efficiency operation over many years. In other words, the use of geothermal heat is an annual heat storage process, and it is necessary to exchange heat with a large amount of soil, which is a heat storage medium. The U-tube ground heat exchanger is usually buried by excavation, and the space between each heat exchanger is about 3 to 5 m. Deeply burying the ground heat exchanger reduces the laying area of the geothermal heat exchanger, but it still requires nearly half of the air conditioning area. The requirement for burying area is one of the reasons why it cannot be covered all the air conditioning load. Furthermore, since hot water is only heat collection from the soil, it is not suitable for underground heat utilization due to the unbalance of heat storage.

Conventional ground heat exchangers generally is a U-tube type that buried up to a depth of about 100 m. Therefore, it takes a long time for excavation and bury, which also causes high installation costs. In addition to the use of such a significant depth, a horizontal spiral loop method of burying at a depth of about 2 m is another solution. However, there is a problem that the required area is still considerable. Therefore, considering the daily operation in this heat pump system, we developed a helical ground heat exchanger that aims to use the shallow depth geothermal heat at a depth of about 15 to 20 m.

As shown in Figure 3. 23, the soil temperature deeper than 10 m is constant temperature throughout the year and is called a constant-earth-temperature layer. While seasonal temperature fluctuations occur in shallower strata. For example, in a level with a depth of 5 m, there is a fluctuation of 3 to 4 K per year. The change in soil temperature at this depth was greater than the hard layer temperature in January and lower than the hard layer temperature in July. In other words, it was more advantageous than the constant-earth-temperature layer for heating heat collection in winter and cooling heat dissipation in summer. It was judged that this critical depth was up to 3 m.

Moreover, the advantage of using geothermal heat at shallow depth is that high-speed excavation is possible by using a dedicated excavator[9,11,13].

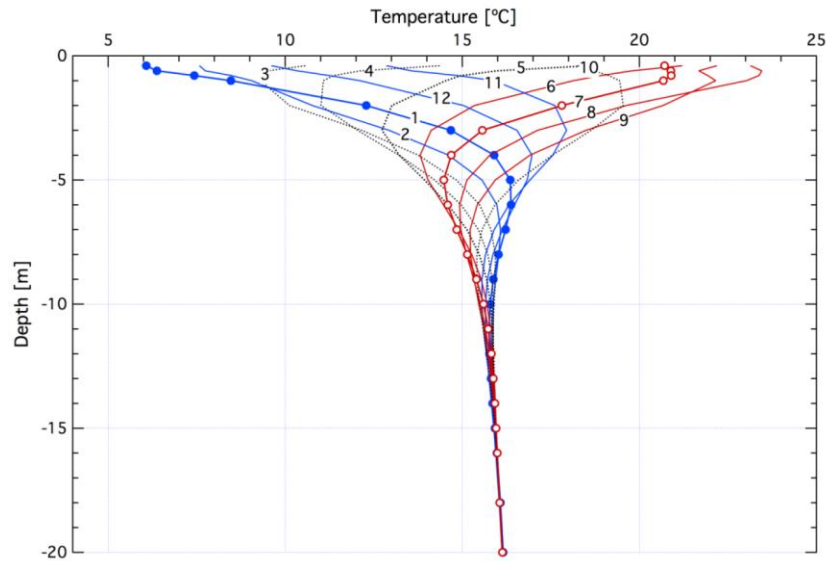


Figure 3. 23 The calculation result of soil temperature change at a shallow depth[9,11].  
(number indicates month)

### ***Principle of double-helical ground heat exchanger***

Helical type ground heat exchangers have been used for a long time[9,11,13], but we point out the problem from the viewpoint of practical use. One of the issues is that since the heat exchange tubes are arranged at a high density, heat exchange capacity for a short time is possible, but it is not suitable for heat exchange for a long time. This is because the soil temperature around the heat exchange tube is saturated. For example, when the helical pitch (tube interval) is small, the temperature of the sandwiched soil will be saturated in a few hours to a few days. Conventional geothermal heat utilization is usually annual cycle heat storage; the temperature influence range (thermal diffusion length) can reach 3 m or more[9,11]. The ideal pitch needs to be 6 m or more, so it is hard to say that it is a proper helical shape utilization.

This system collects and dissipates heat from the sky source heat pump to store heat in a daily cycle. For example, in the winter, heat is collected (stored) during the daytime and used (dissipated) at night time. In the summer, exhaust heat from space cooling is stored in the soil and dissipated at night time by long-wavelength radiation.

The thermal diffusion length of this kind of operation method is less than 20 cm, which means the heat exchangers can be arranged more closely[11]. Figure 3. 24 illustrates the thermal diffusion length by image. Collecting heat or dissipating heat to the soil can be seen to give a temperature

wave to the soil. As the temperature wave diffuses, the distance at which the temperature amplitude decreases to  $1/e$  is defined as the thermal diffusion length  $\mu$ . The thermal diffusion length can be calculated as equation (1)[11]; in this equation,  $k$  is the thermal conductivity,  $\rho$  is the density,  $c_p$  is the specific heat, and  $f$  is the frequency.

$$m = \sqrt{\frac{k}{\rho r c_p f}} \quad (1)$$

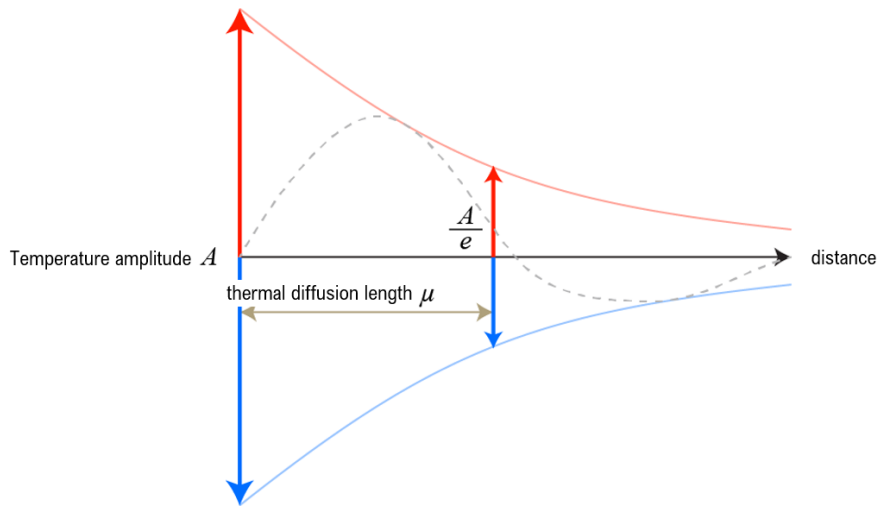


Figure 3. 24 Image of thermal diffusion length[11].

The typical conventional helical shape is a structure in which the connecting pipe (starting pipe) from the bottom of the coil is raised inside the coil, and the manufacturing method is typically the method of winding around the reinforcing bar basket on site. In the improvement in this study, a double-helical shape was formed by folding back at the bottom and winding up (show in Figure 3. 25). This kind of structure made it possible to manufacture long resin pipes without connecting them in the middle part, and because there was no start-up pipe, it was possible to compress compactly and transport easily.

The double helix ground heat exchanger has a unique three-dimensional structure and is accompanied by unsteady heat transfer due to the heat storage effect. The design parameters of the double-helical exchanger were decided based on simulation; the design parameters are shown in Figure 3. 25. Accurate calculation and introduction can be found in the previous study[9,11].

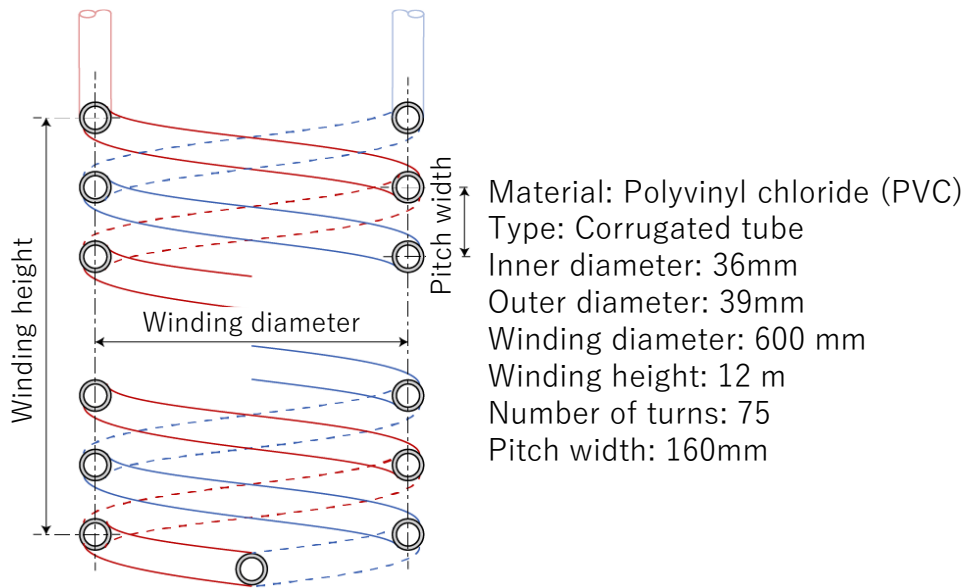


Figure 3. 25 Double-helical GHX and configuration

In the double-spiral structure, circulating water enters from the top and goes down to the bottom, then rises from the bottom and back to the top. Therefore, the temperature of spiral tubes adjacent to each other has a significant difference at the top of helix but a small difference at the bottom. However, the amount of heat exchange with soil between spiral pipes is expected to be almost the same regardless of the top and bottom of the spiral part. In this way, the fact that uniform ground heat exchange can be carried out over the entire spiral part is also an advantage over the conventional ground heat exchanger.

The double-helical ground heat exchanger used this time is made of PVC corrugated pipe with a length of 150 m and an inner diameter of 36 mm, and three tubes are installed at 2 m intervals.

As shown in Figure 3. 26, a straight pipe section is used as a transition for 3m from the ground surface to avoid the influence of the weather. The spiral tube section (heat exchange section) is below 3 m underground, with a borehole length of 15 m and an inner diameter of 0.7 m.

The double-helical structure also has an advantage in manufacturing. As shown in Figure 3. 27, the middle of the PVC corrugated long tube (about 150 m) was set on the winding machine, and it was confirmed that a double-helical tube could be manufactured at a stretch while rotating the whole. Since the coil is likely to come loose if left as it is, we also devised a coil unit (outer diameter 600 mm, length 3.5 m) by covering the outer circumference of the coil with a steel plate (Fig. 2.4.7). Unitization also reduced transportation costs.



Figure 3. 26 Inlet/outlet connection piping with GHX coil



Figure 3. 27 Manufacture of double-helical ground heat exchanger

### *3.3.4 Development of water source heat pump for floor heating*

#### **Overview of water source heat pump for floor heating**

This system uses a water source heat pump that optimizes the equipment configuration and supplying temperature according to the cooling, heating, and domestic hot water supply. Duct air conditioning and floor heating The water source heat pump used drainer (steam trap) for the expansion mechanism instead of the conventional expansion valve. The drainer quickly discharges the liquid refrigerant by the action of the float and blocks the passage of uncondensed vapor to

reduce the necessary pressure, and the correction operation is fast. Compared to the conventional expansion valve, the flow rate control range is more extensive with quicker and more stable operation. It is expected to have high evaporation heat transfer, and high condensation heat transfer with improved condensate discharge performance can be achieved, maintaining a wet condition up to the evaporator outlet during operation. The system is individually distributed and has a thermal network inside the building, so it has excellent expandability.

For air conditioning in the building, not only energy saving but also comfort is essential. Although the floor heating system is highly comfortable because of the radiant heating method, the conventional floor heating system is not energy saving because it usually uses electric heaters and hot water from gas and oil boilers. Therefore, we developed a floor heating heat pump (has a heat output of about 5 kW) for floor heating based on a water source heat pump that can utilize the geothermal heat, which is a stable heat source, to improve the COP by supplying water at a low-temperature zone.

### ***Development of the prototype heat pump for floor heating***

The prototype is developed based on a commercial water source heat pump that can use geothermal heat. The heat exchanger (evaporator and condenser) is changed to a plate-type to improve heat exchange performance, and the expansion valve is replaced with a drainer. Besides, it is a refrigerant circuit with a low-pressure receiver (Figure 3. 28). R32 was used as the refrigerant in the circulation. Regarding the capacity of the plate heat exchanger, the heat transfer area is 1.44 m<sup>2</sup>, and the external dimensions are width 820 mm, depth 300 mm, and height 300 mm.

The operation performance of the prototype (Figure 3. 29) was tested at the manufacturer's test facility. The results are shown in Figure 3. 30. Compared to the base machine for the modification (H6000 in Figure 3. 30, called commercial HP), the COP is about twice higher than the base product. The reason for the improvement in COP is that the evaporator and condenser are replaced with plate heat exchangers to improve the heat exchange capacity. Because of the drainer system, the evaporator keeps the wet condition up to the outlet, and the condenser keeps the refrigerant liquid. The improvement is considered to be the effect of eliminating the retention of liquid refrigerant. The prototype water source heat pump for floor heating was connected to a cross-linked polyethylene pipe (Figure 3. 31 and Figure 3. 32) installed on the floor of the RE house and used for operation

experiments. Figure 3. 33 is a thermal image when circulating hot water at 28 °C. The floor surface temperature was 23.3 °C, and it demonstrates that the floor heating function was fulfilled. Figure 3. 34 shows the detailed configuration of the floor heating system, the material for the floor heating pipe is PEX 20, the piping length of the multi-purpose and measurement room is 200m, 100m, respectively.

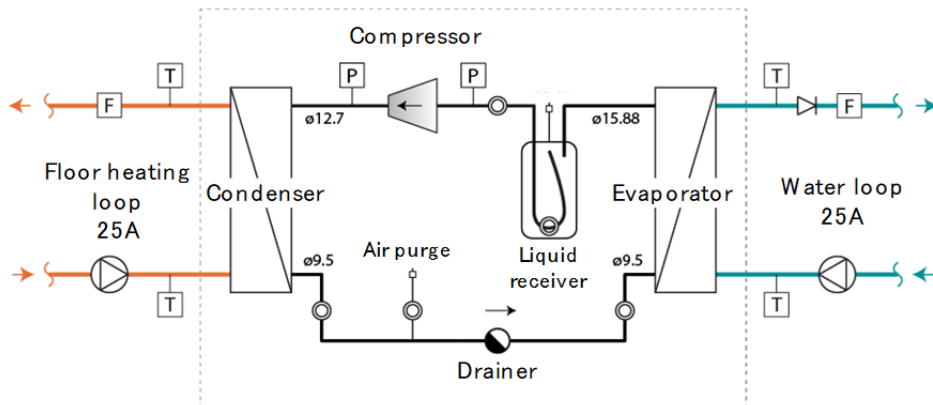


Figure 3. 28 Refrigerant circuit of prototype heat pump for floor heating



Figure 3. 29 Performance test of a prototype heat pump for floor heating

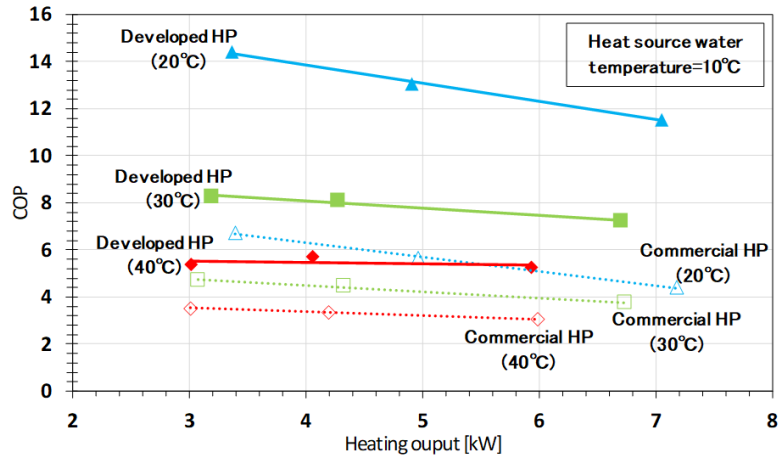


Figure 3. 30 Results of the performance test of the prototype heat pump for floor heating



Figure 3. 31 RE house floor heating pipe system. (floor mortar & before floor tile finishing)



Figure 3. 32 Water source heat pump for floor heating installed in RE house.



Figure 3. 33 Infrared photography of floor heating. (when circulating hot water is 28 °C)

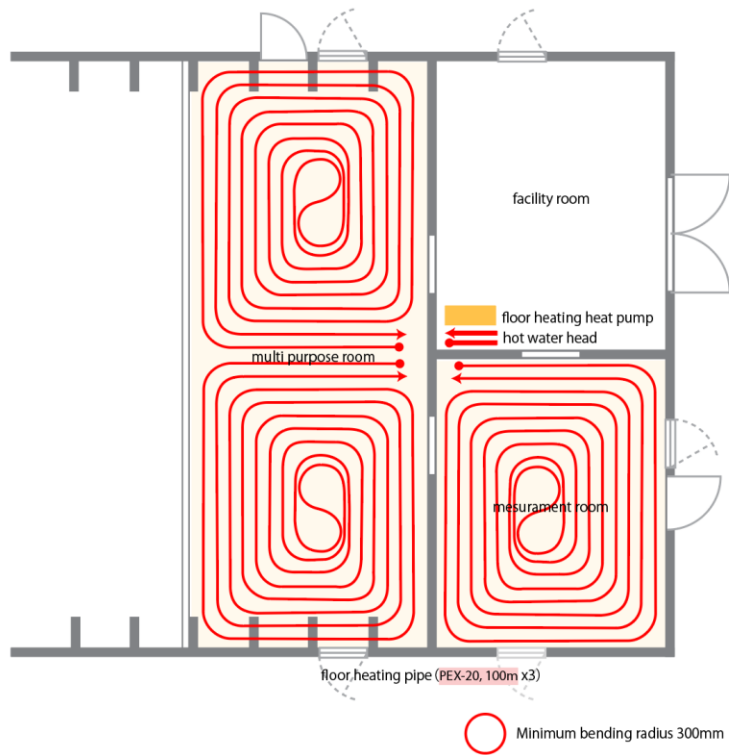


Figure 3. 34 Configuration of floor heating pipe system.

### *3.3.5 Development of water source heat pump for air conditioning*

#### **Overview of water source heat pump for air conditioning**

Besides the requirement of floor heating for a better comfort environment in the room, as the airtight insulation of the building improves, the importance of space cooling increases accordingly. The problem of space cooling in the prior art is that a power peak (power shortage) requirement problem occurs because the power consumption increases as the outside temperature rise, such as in the afternoon in summer. On the other hand, in this heat pump system, we developed a system (peak shift system) that uses soil heat storage to increase the daytime cooling operation COP and shift part of the power consumption to nighttime. The water source heat pump for air conditioning developed was a duct-type air conditioning system(heat output of about 5 kW) throughout the building.

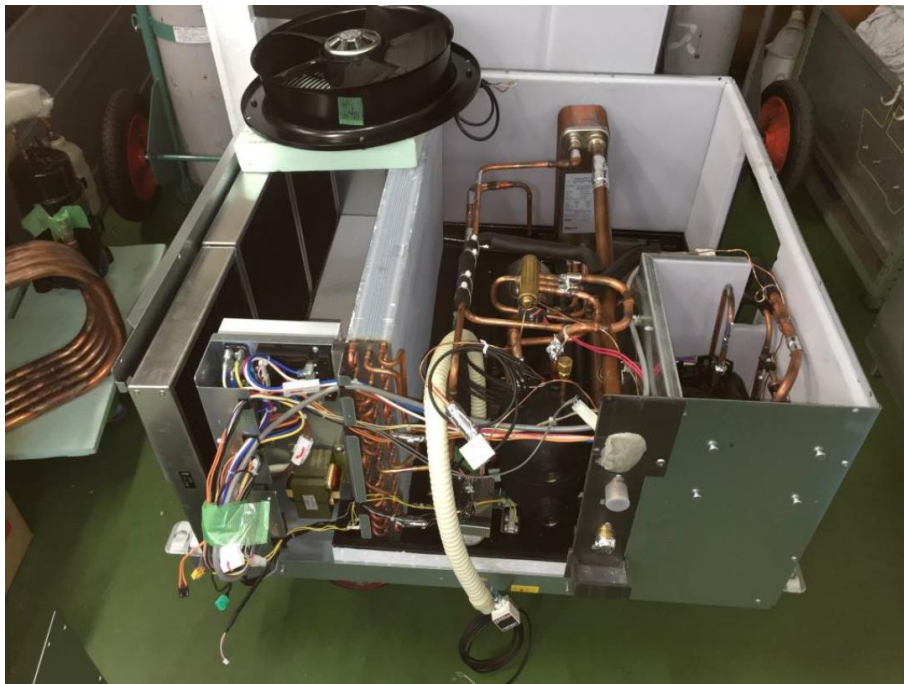


Figure 3. 35 Inside the heat pump for air conditioning

It is known that to maintain the indoor air temperature only by floor heating, it is necessary to keep the floor temperature at a high level, and comfort may reduce accordingly. Here, we made a prototype of a water source heat pump assuming that the floor heating system and space heating

system are used together, that the entire building is air-conditioned with a ventilation duct. With this duct-type water source heat pump for air conditioning, we focused mainly on improving the cooling COP during the daytime in summer.

### ***Development of the prototype heat pump for air conditioning***

The water source heat pump for air conditioning is an improvement of an existing commercial product for buildings. Figure 3. 35 shows the internal structure of the prototype when manufacturing. The water heat exchanger was changed from a double-pipe type to a plate type, the capacity of the plate heat exchanger, the heat transfer area is  $1.44 \text{ m}^2$ . The superheat degree control based electronic expansion valve was changed to a drainer. Besides, the refrigerant R-32 was adopted, and the blower was turned from a sirocco fan to an axial fan. Standard parts in the commercial based product were used for the refrigerant compressor and the air heat exchanger. The external dimensions are width 820 mm, depth 300 mm, and height 300 mm. The facility room and measurement room have a 200 mm wide  $\times$  200 mm long outlet on the ceiling. The appearance of the prototype water source heat pump for air conditioning is shown in Figure 3. 36.



Figure 3. 36 Appearance of the prototype water source heat pump for air conditioning.

The manufacturer's calorimeter tested the performance of the prototype after finished the prototype. The results are shown in Table 3. 3 and Table 3. 4. The heat source water temperature was set at

around 17 °C, which is the same for both the cooling cycle and the heating cycle, assuming the use of underground heat. From Table 3. 3, the COP for the air-conditioning operation was about 15, and we can know that the possibility of reducing the power consumption during the hot summer daytime is considerable.

However, the heating operation COP was about 6. The low operating efficiency means that the low-pressure pressure (gauge pressure) is 0.84 MPa when the outlet water temperature (heat source water) is about 14 °C in heating in Table 3. 4, which is 5.3 °C when converted to the evaporating temperature. The reason is that because there is a problem with the shape of the refrigerant pipe inside the air heat exchanger, and the condensate is hard to flow down, so the refrigerant flow rate to the evaporator was insufficient. Based on the result, this part (air heat exchanger) needs to be improved further.

Table 3. 3 Calorimeter test results of water source heat pump for air conditioning. (cooling)

Space cooling

Operating frequency (rps)	43	
Indoor dry bulb temperature (°C)	26.94	
Indoor wet bulb temperature (°C)	19.08	
Inlet temperature (°C)	16.94	
Outlet temperature (°C)	20.81	
Flow rate of source water (L/min)	20	
Voltage (V)	200.1	
Current (A)	2.18	
Cooling capacity (kW)	5.049	
Energy consumption (kW)	0.332	
COP	15.207	
Pressure at high pressure side (MPaG)	1.42	Pressure sensor
Temperature of high-pressure gas (°C)	37.5	
Temperature before drainer (°C)	21.1	
Temperature after drainer (°C)	15.6	

Pressure at low pressure side (MPaG)	1.14	Evaporating temperature: 14.7°C
Pressure at high pressure side (°C)	21.9	

Table 3. 4 Calorimeter test results of water source heat pump for air conditioning. (heating)

## Space cooling

Operating frequency (rps)	58	
Indoor dry bulb temperature (°C)	20.01	
Indoor wet bulb temperature (°C)	14.04	
Inlet temperature (°C)	17.08	
Outlet temperature (°C)	13.92	
Flow rate of source water (L/min)	20	
Voltage (V)	200.2	
Current (A)	5.38	
Cooling capacity (kW)	5.264	
Energy consumption (kW)	0.856	
COP	6.147	
Pressure at high pressure side (MPaG)	1.88	Pressure sensor
Temperature of high-pressure gas (°C)	71.2	
Temperature before drainer (°C)	31.2	
Temperature after drainer (°C)	6.8	
Pressure at low pressure side (MPaG)	0.84	Evaporating temperature: 5.3°C
Pressure at high pressure side (°C)	18.8	

Figure 3. 37 and Figure 3. 38 show the configuration of the heat pump unit and the ducts. Through the duct, the heat pump for air conditioning delivers treated air to the facility and the measurement room. And the treated air is directly delivered to the multi-purpose room through the outlet.



Figure 3. 37 Installation in the loft of the RE house and connected the duct and blowout nozzle.



Figure 3. 38 The heat pump for air conditioning set on the loft and duct

### *3.3.6 Development of water source heat pump for domestic hot water supply*

#### **Overview of water source heat pump for domestic hot water supply**

The utilization of geothermal heat is not suitable for domestic hot water supply. The reason is that the domestic hot water supply needs to consume heat over the whole year; therefore, there will be

is a shortage of geothermal heat. Here, as mentioned previously, it was confirmed experimentally that the sky source heat pump could collect solar radiation and air heat to compensate for the lack of geothermal heat. Besides, due to the water loop system, the exhaust heat from space cooling during summer can be stored in the soil in the cooling operation for recovery and utilization.

### **Development of the prototype heat pump for domestic hot water supply**

Domestic hot water supply in the building may require a large amount of heat instantaneously, such as filling the bathtub, so the hot water storage type is suitable for this purpose. Although the commercially available EcoCute[16] heat pump is a hot water storage type, it has a problem that performance deteriorates in cold weather because it is a heat pump that uses the air as a heat source. Therefore, we made a prototype of a water source heat pump based on the EcoCute (a hot water storage type and using the CO<sub>2</sub> refrigerant) that can utilize geothermal heat in this way.

As shown in Figure 3. 39, the prototype was developed based on a commercial EcoCute product, but the water/air heat exchanger was changed to a water/water heat exchanger (evaporator in Figure 3. 39). The internal structure is shown in Figure 3. 40. As shown in Figure 3. 41, through the manufacturer's environmental laboratory, the operating data under cold conditions was tested, and the result is shown in Table 3. 5.

Figure 3. 42 shows the top view of the heat pump for domestic hot water supply installed in the system. Figure 3. 43 shows the actual setup of the hot water tank and heat pump. The gray pipe is the connection to the water loop, and the white pipe is the connection to the water tank.

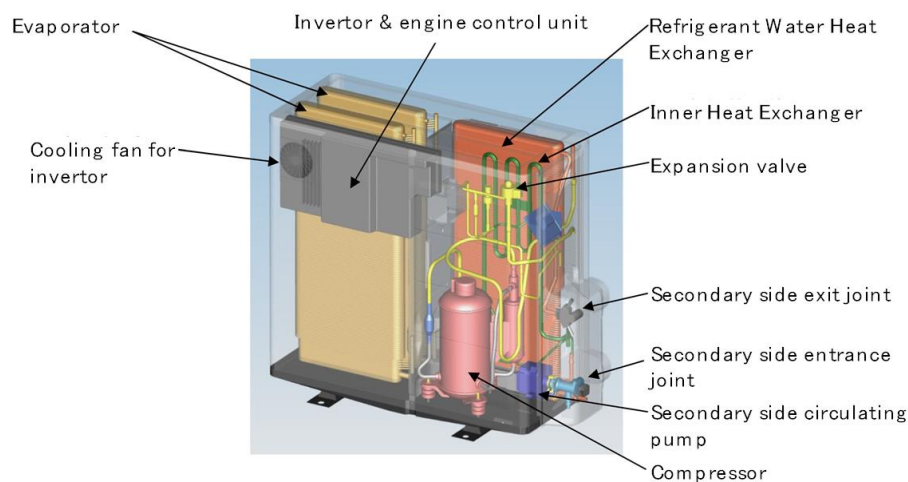


Figure 3. 39 Configuration of water source domestic hot water supply heat pump prototype



Figure 3. 40 Structure of water source heat pump for domestic hot water supply prototype.



Figure 3. 41 Performance test of hot water supply heat pump in cold weather(test room).

Table 3. 5 Operating performance test results under cold conditions (test room data)

Outlet of compressor (°C)	75
Outlet of water/water heat exchanger (°C)	17.4
Expansion valve (°C)	17.2
Inlet of evaporator (°C)	11.6
Outlet of evaporator (°C)	16.2
Inlet of compressor (°C)	16.5
Water supply temperature (°C)	8.95
Water heat temperature (°C)	63.7
Inlet temperature of primary water (°C)	17.0
Outlet temperature of primary water (°C)	13.3
Primary side flow rate (L/min)	16.0
Secondary side flow rate (kg/min)	1.15
Energy consumption (kw)	0.780
Low pressure (MPaG)	4.52
High pressure (MPaG)	9.56
Heat output capacity (kW)	4.38
COP	5.62



Figure 3. 42 Top view of water source heat pump for domestic hot water supply.

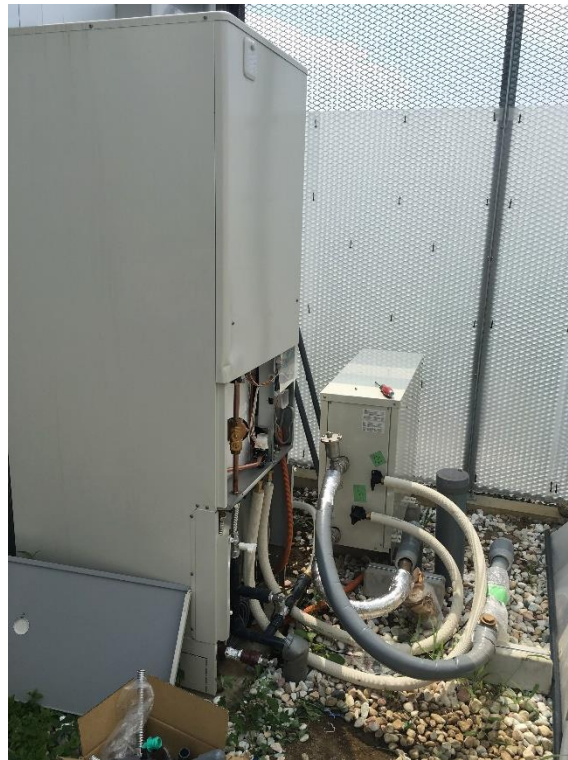


Figure 3. 43 The water storage tank and heat pump for domestic hot water supply.

## 3.4 Summary

In this chapter, we started with the basics and explained the concept and composition of this system. These include the development of sky source heat pumps, floor heating heat pumps, air conditioning

heat pumps and hot water heat pumps. The concept, structure and performance test of each machine are also explained in detail. The development and improvement of each device are to cooperate with the design and operation concept of the system, that is, the integrated use of multiple renewable energy sources, including solar radiation, air heat, and geothermal heat. Also, the soil is used as a heat storage body to achieve peak shaving operation.

In the next chapter, we will introduce experiments which are the field testing, and test each machine and the overall performance of the system through experiments.

## 3.5 Reference

- [1] Liu M, Ooka R, Choi W, Ikeda S. Experimental and numerical investigation of energy saving potential of centralized and decentralized pumping systems. *Appl Energy* 2019;251. doi:10.1016/j.apenergy.2019.113359.
- [2] Hino T, Ooka R, Miura K, Ono K, Yoshida S, Li R, et al. 太陽熱と地中熱を利用する水循環ヒートポンプシステムの開発 (その2) ソルエアヒートポンプの集熱運転特性. 平成24年度空気調和・衛生工学会学術講演会講演論文集, vol. 98, 札幌: 2012, p. 7–10.
- [3] Yoshida S, Ooka R, Hino T. マルチソース・マルチユース・ヒートポンプシステムに関する技術開発: 第3報-太陽空気熱源ヒートポンプの試作機における運転特性の確認と性能検証. *空気調和・衛生工学会 論文集* 2015;40:9–18. doi:https://doi.org/10.18948/shase.40.217\_9.
- [4] Yoshida S, Ooka R, Hino T. マルチソース・マルチユース・ヒートポンプシステムに関する技術開発: 第2報-水熱源空調ヒートポンプの開発と性能検証. *空気調和・衛生工学会 論文集* 2015;40:1–10. doi:https://doi.org/10.18948/shase.40.215\_1.
- [5] Yoshida S, Ooka R, Hino T. マルチソース・マルチユース・ヒートポンプシステムに関する技術開発: 第1報-水熱源瞬間式給湯ヒートポンプの開発と性能検証. *空気調和・衛生工学会 論文集* 2014;39:11–20. doi:https://doi.org/10.18948/shase.39.208\_11.
- [6] Yoshida S, Ooka R, Hino T. マルチソース・マルチユース・ヒートポンプシステムに関する技術開発: 第4報-年間運転性能予測シミュレーションによるシステム構成と運用に関する研究. *空気調和・衛生工学会 論文集* 2015;40:11–20. doi:https://doi.org/10.18948/shase.40.221\_11.

- [7] Hino T, Ooka R. Water-Loop Heat Pump System that Stores Multiple Renewable Energies in the Ground. Proc. EnerSTOCK2018, Adana, Turkey: EnerSTOCK2018; 2018.
- [8] Liu M, Ooka R, Choi W, Ikeda S. Comparison of the energy saving potential between centralized and decentralized pumping systems under various flow conditions. ASHRAE Trans 2017:LB-17-068.
- [9] Hino T, Ooka R, Lim J, Choi W. 中深度の地中熱を利用するヘリカル熱交換器の開発. 平成27年度大会（大阪）学術講演論文集, vol. G-10, 大阪: 2015, p. 16–9.
- [10] Hino T, Ooka R. 多様な再生可能エネルギーを集放熱源とする水ループ式ヒートポンプシステムの構築. 平成29年度大会（高知）学術講演論文集, 高知: 2017, p. 5–8.
- [11] Exchanger DGH. 二重らせん地中熱交換器の開発. 平成27年度大会（鹿児島）学術講演論文集, 鹿児島: 2016, p. 129–32.
- [12] Hino T, Ooka R. 建物熱供給の将来技術を考える. 平成28年度日本建築学会大会, 2016.
- [13] Hino T, Ooka R. 地中熱利用と地中蓄熱を統合するシステムのコンセプト. 日本建築学会大会学術講演梗概集, 2018, p. 1337–8.
- [14] Hino T, Ooka R. 夜間放熱と地中熱を利用する冷房システムの開発. 日本建築学会大会学術講演梗概集 2014.
- [15] Liu M, Toshiyuki H, Ryoza O, Ke W, Wonjun C, Doyun L, et al. 再生可能エネルギーを利用する分散型マルチソース・マルチユース ヒートポンプシステムの開発 試験建屋の構築及び実測による冷暖房性能評価. 日本建築学会環境系論文集 2020;85:361–70.  
doi:<https://doi.org/10.3130/aije.85.361>.
- [16] コロナ. エコキュート製品情報 2016. <https://www.corona.co.jp/eco/>.

# **Chapter 4: Experimental performance analysis of distributed heat pump system using renewable energy**

## 4.1 Introduction of test building and control method

### *Testing building (RE house)*

In this distributed heat pump system, a water loop network constitutes a thermal network within the building, and the individual distributed water source heat pump that can exchange heat with this thermal network to supply the necessary heating and cooling. Such an individually distributed network system can be used for a variety of purposes and can offer the advantage of high flexibility in scale expansion.

To verify the concept of this technology and test the performance of the proposed heat pump system, we constructed a small-scale experimental facility (test building,) assuming a detached house and verified the feasibility of both the essential components and the whole system. Figure 4. 1 and Figure 4. 2 show the appearance of the test building (called RE house, located in the Chiba Experiment Station, Institute of Industrial Science, University of Tokyo) incorporating the proposed distributed heat pump system using multiple kinds of renewable energy[1–10]. As shown in Figure 4. 3, this heat pump system is a research and development targeting a residential system that can offer heating, cooling, and domestic hot water supply while refrigeration is an issue for future development and improvement of this system.

As mentioned in the chapter3, Renewable energy, such as geothermal heat is utilized through the underground heat exchanger(GHX). A sky heat source heat pump(SSHP) uses renewable energy from the sky, such as solar radiation and air heat from the atmosphere. A water circulation loop integrates both renewable energy sources from earth and sky. The HVAC system for heating, cooling, and domestic hot water supply purposes are constructed by using several water source heat pumps. This system is a technology that realizes energy saving of heat supply by aiming to maximize efficiency based on the second law of thermodynamics, based on a heat pump (HP). HP is a technical means that uses power to move heat from a low-temperature source (source) to a high-temperature location (sink). A heat source (heat collection source) and a heat sink(heat demand sink) require a large heat capacity, and reducing the temperature difference between the two is the key to reducing

power and increasing operating efficiency (coefficient of performance, COP). From this point of view, the earth (underground) is optimal as a heat source, and an individually distributed HP that supplies heat at a temperature that is just enough for the heat demand is desirable. Therefore, in the proposed system shown in Figure 4. 3, since each element is connected to a water loop, each component allows mutual heat exchange. As a result, the hot exhaust heat of the water source HP that supplies the cooling demand for space cooling will become the heat source of the water source HP that provides the heating demand such as space heating and domestic hot water supply. On the other hand, the exhaust heat of the water source HP for space cooling can be seen as the heat radiation source of the water source HP that provides the cooling purpose. The heat storage effect of soil adjusts the non-simultaneity of the exhaust heat, and the imbalance of the daily integrated amount can be adjusted by using the ground heat exchanger and collecting and dissipating heat by SSHP.

The floor area of RE house is about 60 m<sup>2</sup>, which is enough for testing the performance of the distributed heat pump system on a practical scale. There is a facility room, a measurement room, and a multipurpose room. Considering the weight of the outdoor panel of the sky source heat pump on the roof, we used the galvalume steel sheet as roof material, and the outer wall is also the galvalume steel sheet. The heat transmission coefficient  $U$  of the outer wall is  $0.40 \text{ W} / (\text{m}^2 \cdot \text{K})$ , and the heat loss coefficient  $Q$  of the test building is  $0.90 \text{ W}/(\text{m}^2 \cdot \text{K})$ . There is a ventilation fan in the multi-purpose room that operation for 24 hours, and the design ventilation rate is 0.6 times/h.



Figure 4. 1 Photography of RE house in spring.



Figure 4. 2 Test building of development system (RE house).

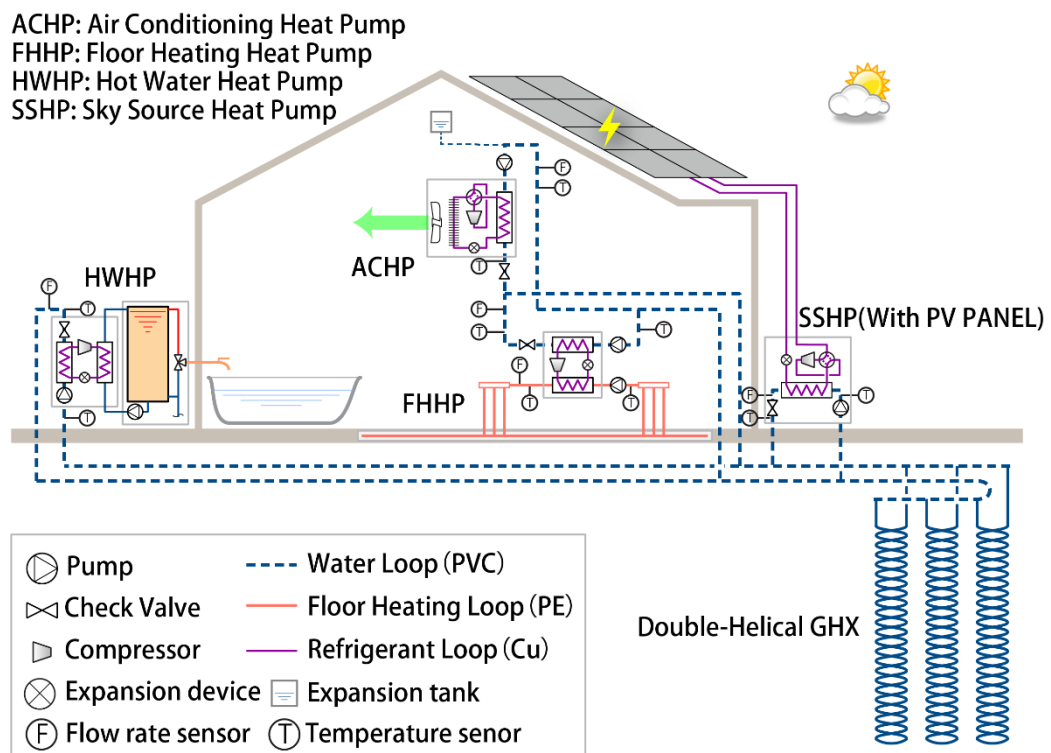
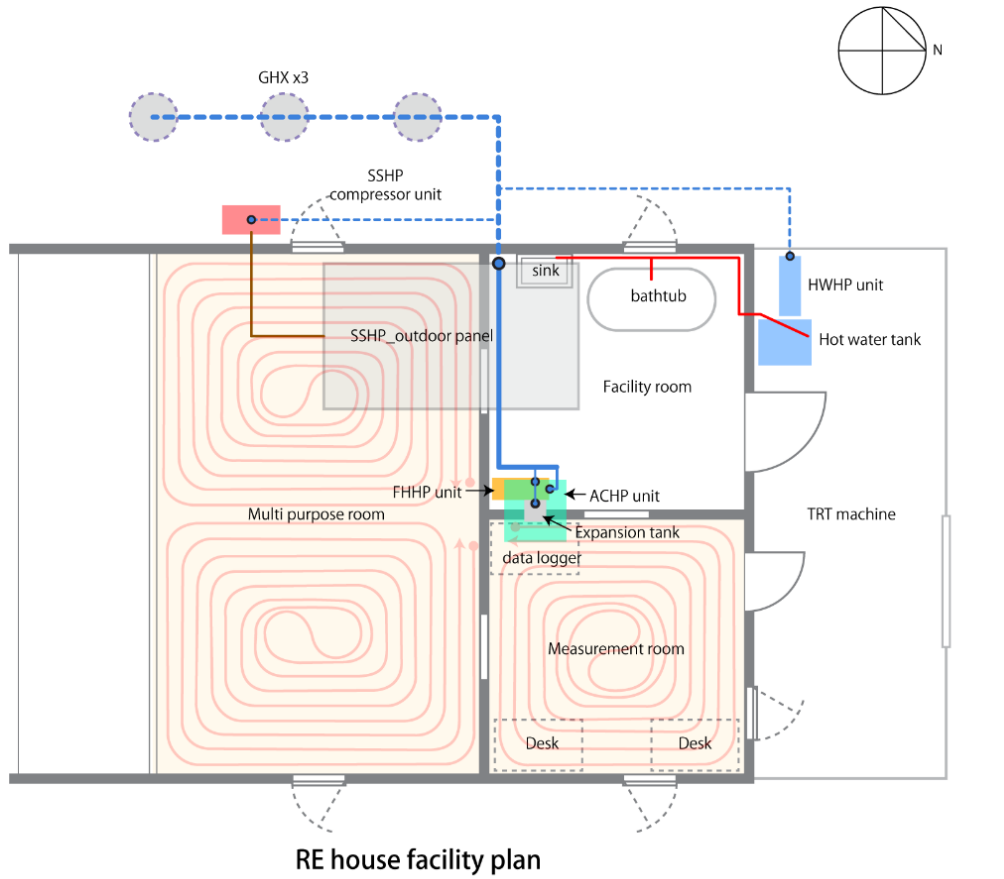
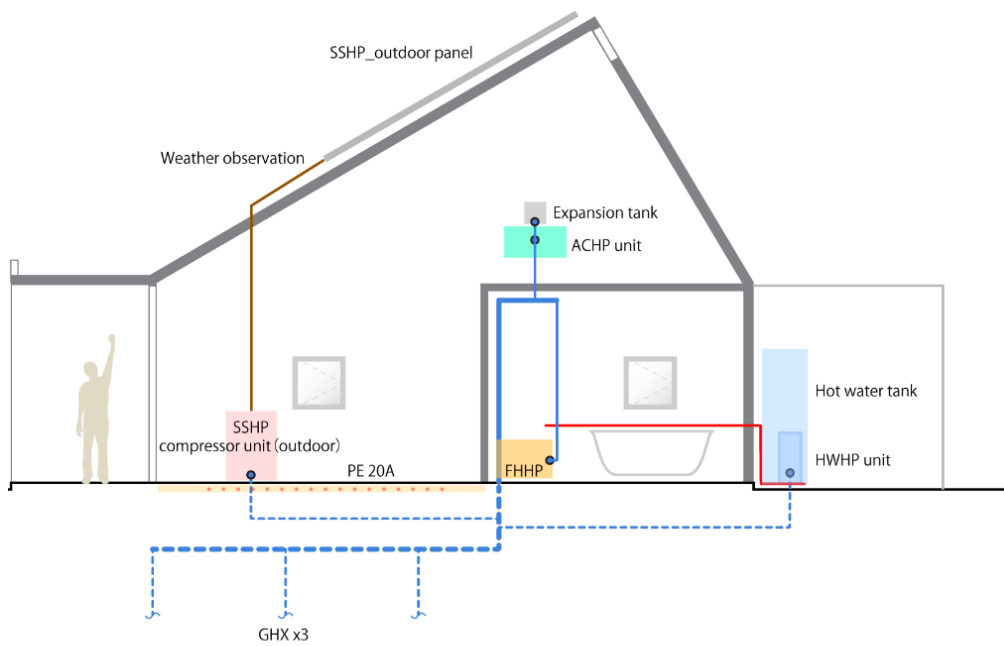


Figure 4. 3 System configuration of the heat pump system in the RE house.



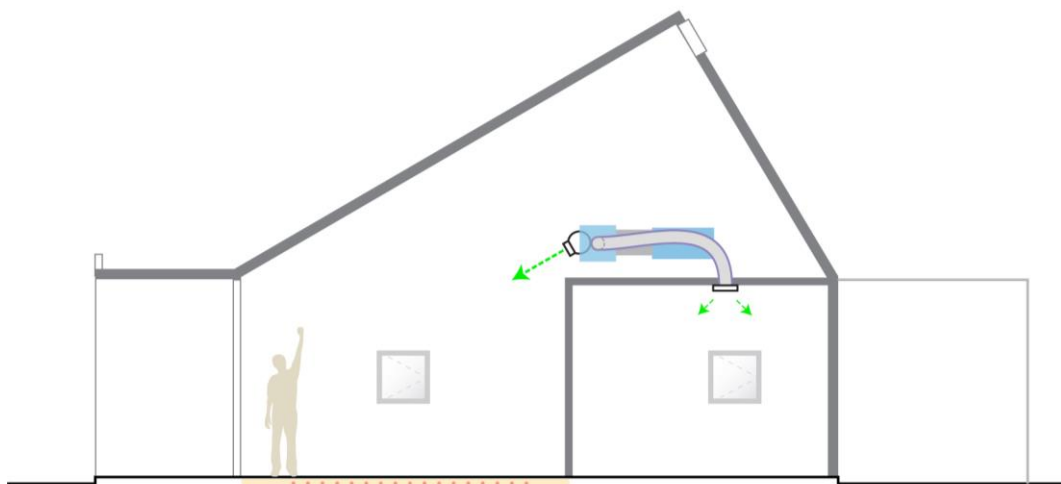
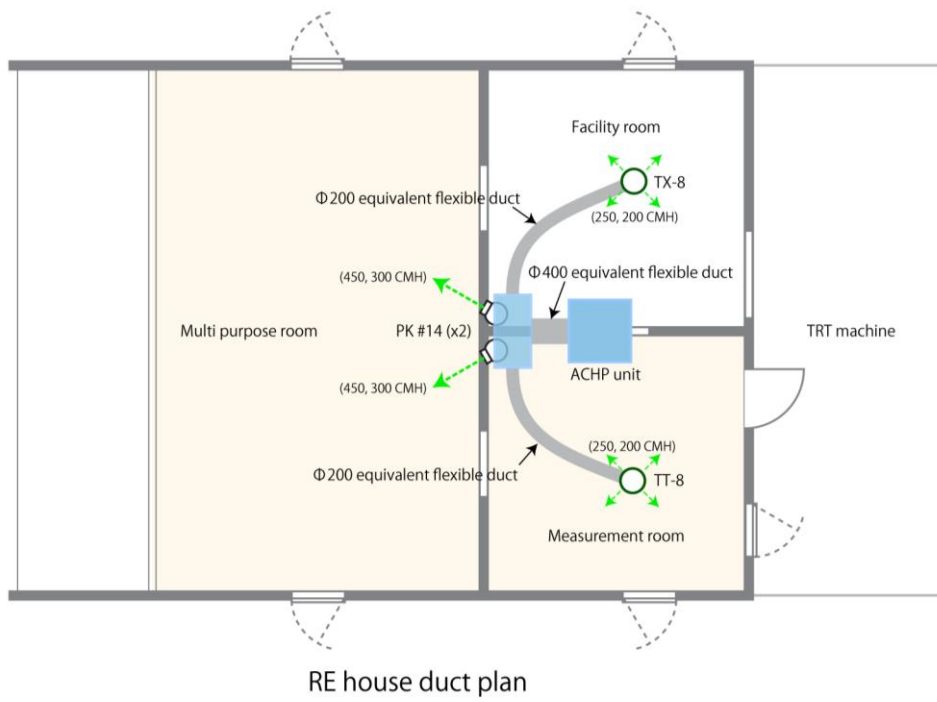
RE house facility plan

- PVC 40A
- - - PVC 40A (underground)
- PVC 25A
- - - PVC 25A (underground)
- PE20A (in slab)
- Refrigerant circulation tube
- Hot water supply pipe

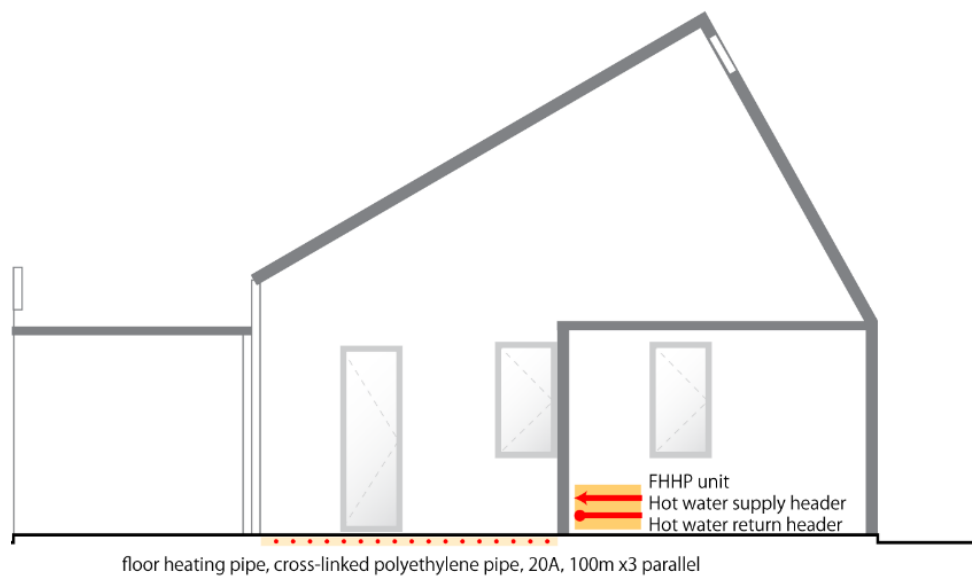
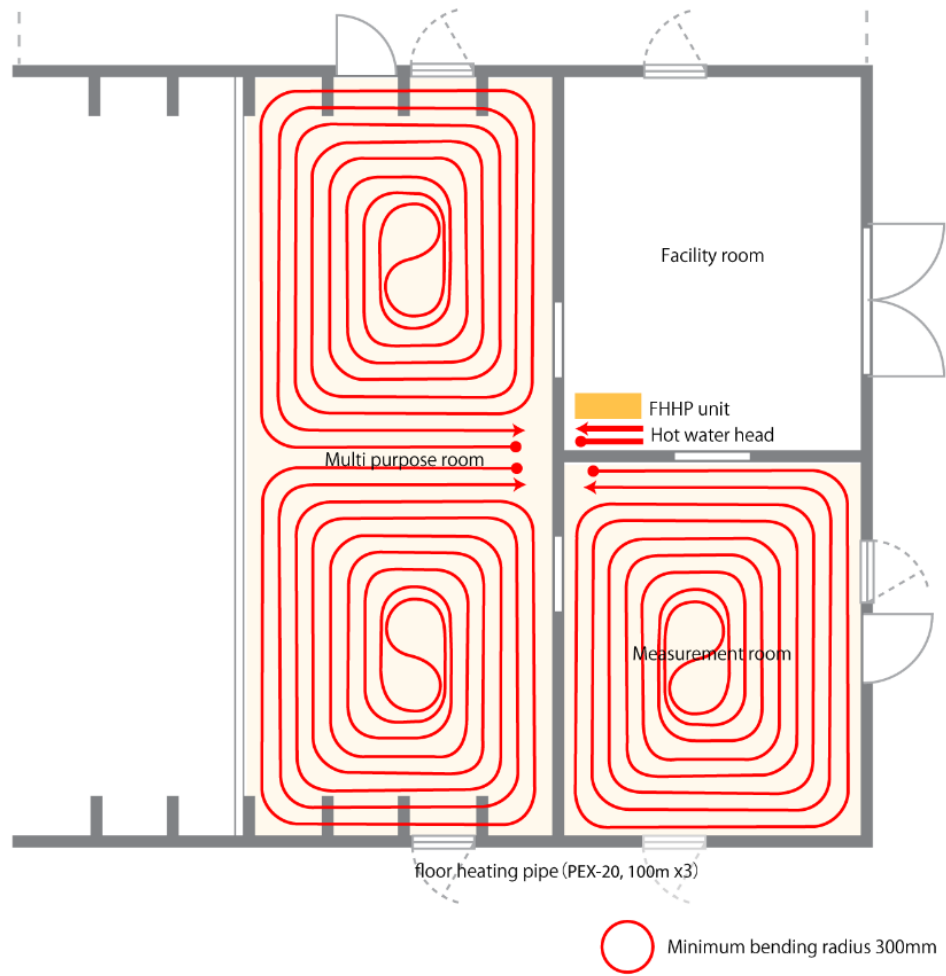


RE house facility elevation

Figure 4. 4 RE house facility plan and elevation.



RE house duct elevation  
Figure 4. 5 RE house duct plan and elevation.



### RE house floor heating system

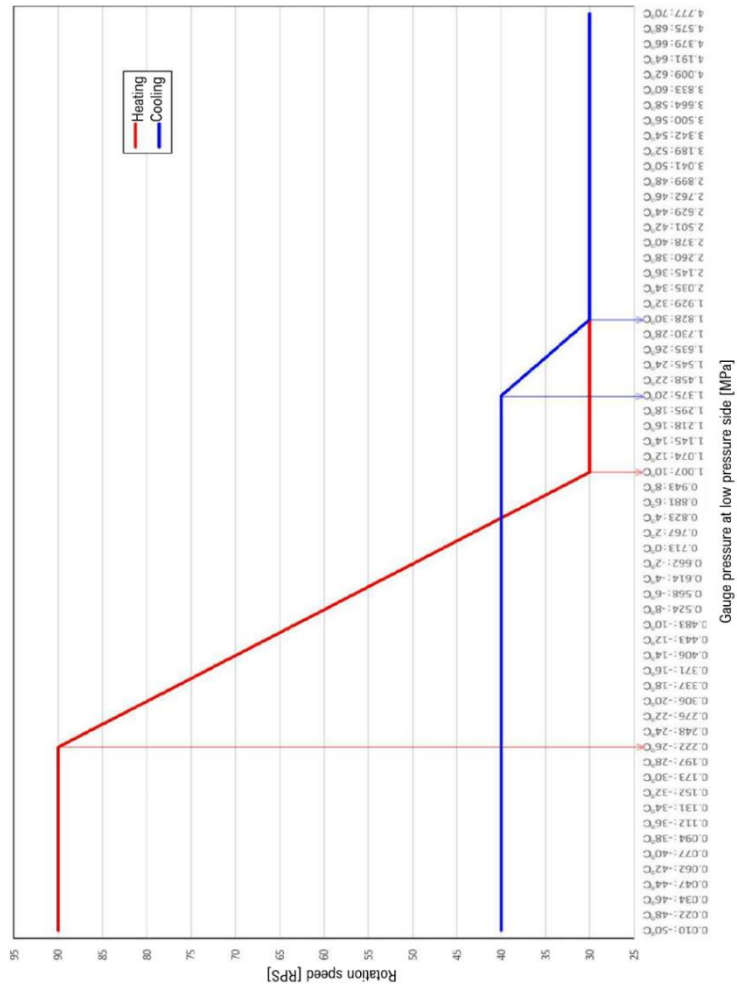
Figure 4. 6 Configuration of RE house floor heating system.

Figure 4. 4 shows the facility plan and elevation of RE house. The whole heat pump system is connected by a water loop, to form a thermal network within the building. The main pipes of the water loop system are PVC 40A (main pipe) and PVC 25A (branch pipe) in Japanese standard. The dotted line indicates the underground pipeline. The pipe of the floor heating system is PEX20. Figure 4. 5 shows the setting of the duct system in the RE house. The treated air is sent to all rooms from the heat pump for air conditioning through the duct with an equivalent diameter of 200 mm. Also, two adjustable blowers are used for the multi-purpose room. Figure 4. 6 shows the configuration of the floor heating system, as mentioned earlier, the multi-purpose and measurement room is installed with a floor heating system except for the facility room.

### ***Control method***

As described in chapter3, we developed a program for operation control of SSHP to keep the circulating water temperature of the water loop near the natural soil temperature. The control flow is improved based on the feeding back from the experimental result. The latest version is shown in Figure 4. 8.

In the heat collection operation of SSHP, the refrigerant evaporation temperature rises during good weather on warm days, and conversely, the refrigerant evaporation temperature decreases during cold nights. The heat collection capacity changes greatly depending on the weather conditions. To avoid drastic changes and obtain a stable output of the compressor, the rotation speed of the compressor was adjusted by an inverter. That is, as shown in Figure 4. 7, when the refrigerant evaporation temperature is above 10 °C, the minimum speed is 30 rpm. Below minus 26 °C, the maximum speed is 90 rpm, and the compressor speed will change linearly.



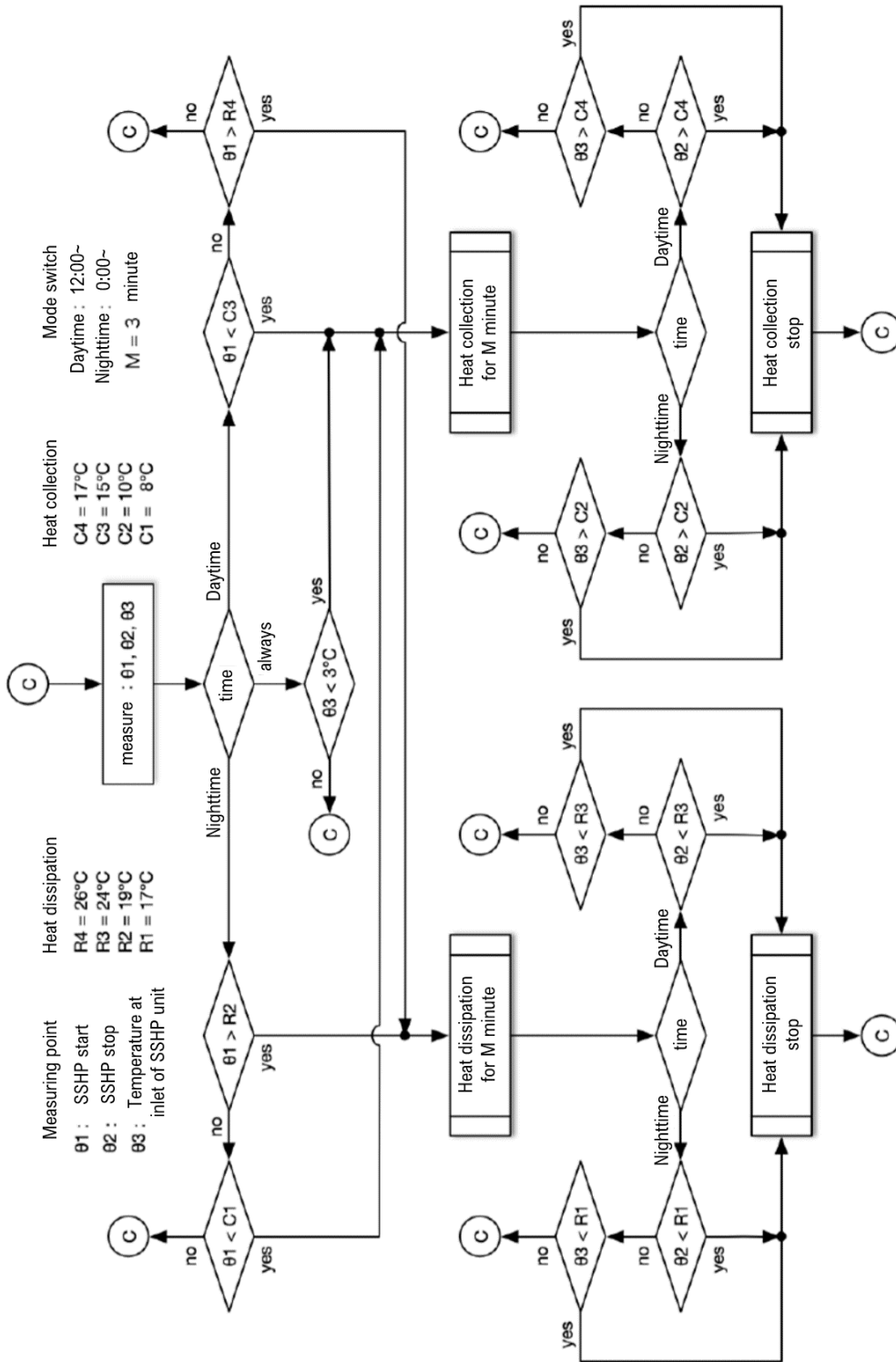


Figure 4. 8 Control method of SSHP for water loop temperature.

During the winter field experiment, the circulating water temperature of the water loop was maintained within a specific temperature range by the SSHP, and this temperature range was based on the underground temperature. The circulating water inlet temperature of the SSHP was set as the reference point. Two different control schedules based on the SSHP turn-on/turn-off time were

adopted, as shown in Figure 4. 8. Based on the above control logic shown in Figure 4. 8, we set the control schedule described as follows. During the period from the 1st to the 9th of March, the heat pump collected heat from the circulating water loop during the daytime (i.e., from 8:00 to 18:00). The SSHP later began heat collection when the inlet circulating water temperature dropped to 15 °C and kept heating the water until it exceeded 17 °C. During the night (i.e., from 18:00 to 8:00 the following day), the SSHP start/stop temperature setting was lowered, and it was set to utilize geothermal heat.

From the 10th to the 31st of March, the daytime period was altered to range from 12:00 to 20:00, to ensure that the SSHP turn-on time coincided with the time at which solar radiation was at its maximum. The nighttime period was also changed, in this case, from 20:00 to 12:00 the next day. Furthermore, the setting of the SSHP and the turn-off temperature were lowered to 10 °C. For the sampling of the temperature of the water loop circulating, we made the SSHP operate at a cycle of 30 min. In one operation cycle of SSHP, where the circulation pump in the SSHP ran every 27 min and stopped after 3 min of operation. Therefore, when the circulating water temperature dropped, the heat collection operation of the SSHP began to heat the circulating water in the water loop regardless of the time, which prevented the freezing of the circulating water.

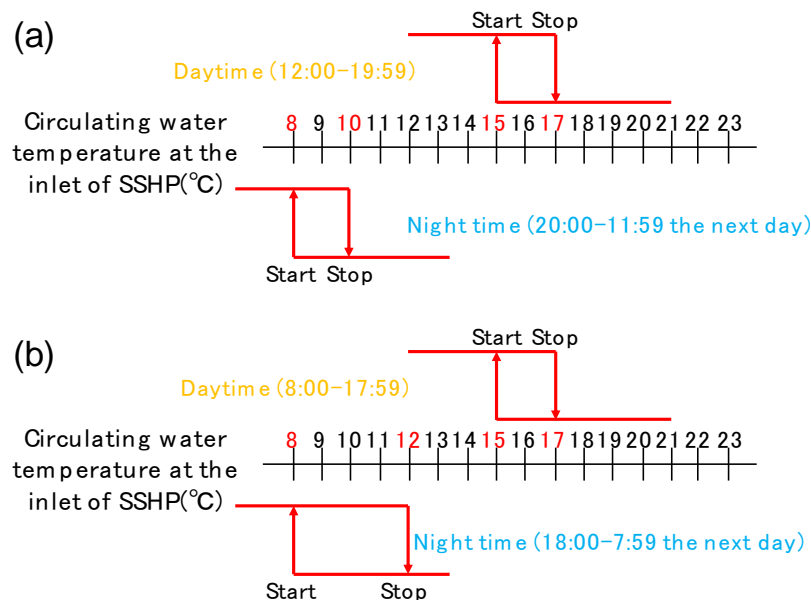


Figure 4. 9 The SSHP control schedules for the circulating water loop temperature:

(a) from the 1st to the 9th of March, and (b) from the 10th to the 31st of March.

For the control schedule of FHHP, the operation control of the FHHP was carried out based on the hot water temperature in the warm water loop, i.e., the underfloor heating pipes. More specifically, when the warm water supply temperature (outlet in the floor heating system in Figure 4. 10) exceeded 27 °C, the FHHP stopped heating. To maintain the room at a suitable temperature, the FHHP turned on once again to heat the water in the warm water loop when the water supply temperature dropped below 22 °C.

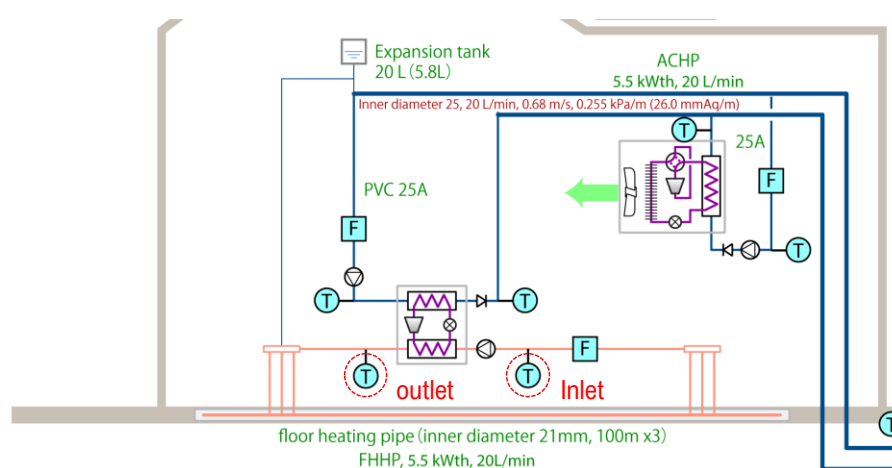


Figure 4. 10 measuring point for control of FHHP

## 4.2 Measurement items and measuring equipment

To calculate and evaluate the performance of each heat pump and the whole system, the following physical quantities were recorded with regular time intervals of 5 s, and the average values were calculated per minute:

- Measurement of the volumetric flow rates of the circulating water in the water loop system at each heat pump (including the hot water side in the floor heating system in the room) using a flowmeter (appearance shown in Figure 4. 13, accuracy:  $\pm 1.6\%$  of full scale);
- Measurement of the inlet and outlet temperatures of the circulating water in the water loop system at each heat pump (including the warm water side of the floor heating system in the room) using platinum resistance bulbs (Pt-100, accuracy:  $\pm (0.15 + 0.002|t|)$  °C);
- Measurement of the inlet (before diversion) and outlet (after confluence) temperatures of the

- circulating water at GHX using platinum resistance bulbs (Pt-100, accuracy:  $\pm (0.15 + 0.002|t|)$  °C);
- (d) Measurement of the outside air temperature and humidity using a weather station equipped with a thermo-hygrometer (temperature measurement accuracy:  $\pm (0.226 - 0.0028t)$  °C);
- (e) Measurement of solar radiation using a weather station set with a pyranometer (accuracy: non-linearity < 1%);
- (f) Measuring the energy consumption of each component using a power monitor (accuracy:  $\pm 2.0\%$  of full-scale  $\pm 1$  digit). The data were recorded and total calculated over the measurement period;
- (g) Measurement and monitoring on a computer of the instantaneous total power consumption of each heat pump compressor and pump unit, in addition to all other parameters.

Besides, the power consumption was recorded at time intervals of 1 min. As shown in Figure 4. 11, the energy consumption of each heat pump unit is measured separately. As the power consumption of the compressor and the circulating water pump of each heat pump were measured together and could not be separated due to the initial installation, the energy consumption of the pumping system is not discussed separately. However, we can calculate an estimate based on the performance curve of the pump because each pump runs at a constant rotation speed. Figure 4. 12 shows the measurement of the soil temperature, mainly including the central borehole temperature, natural underground temperature, and soil temperature under the floor.

Based on the field experiment measurements, we can get the coefficient of performance(COP) for each heat pump and the whole system.

Table 4. 1 Main parameter of each heat pump in the system.

	Maximum heat output (kW)	Remarks
SSHP	6(solar)/5(air)	Facing south; tilt angle: 30 degree
		Refrigerant: R32; Panel area: about 8 m <sup>2</sup>
		Photovoltaic power generation: 1.2 kW
GHX	-	Spiral part depth: 12 m; parallel installation
FHHP	5	Refrigerant: R32; Floor heating area: 47 m <sup>2</sup>
ACHP	5	Refrigerant: R32; Duct covers every room
HWHP	5	Water storage type



Figure 4. 11 Measurements of the energy consumption of each heat pump unit.

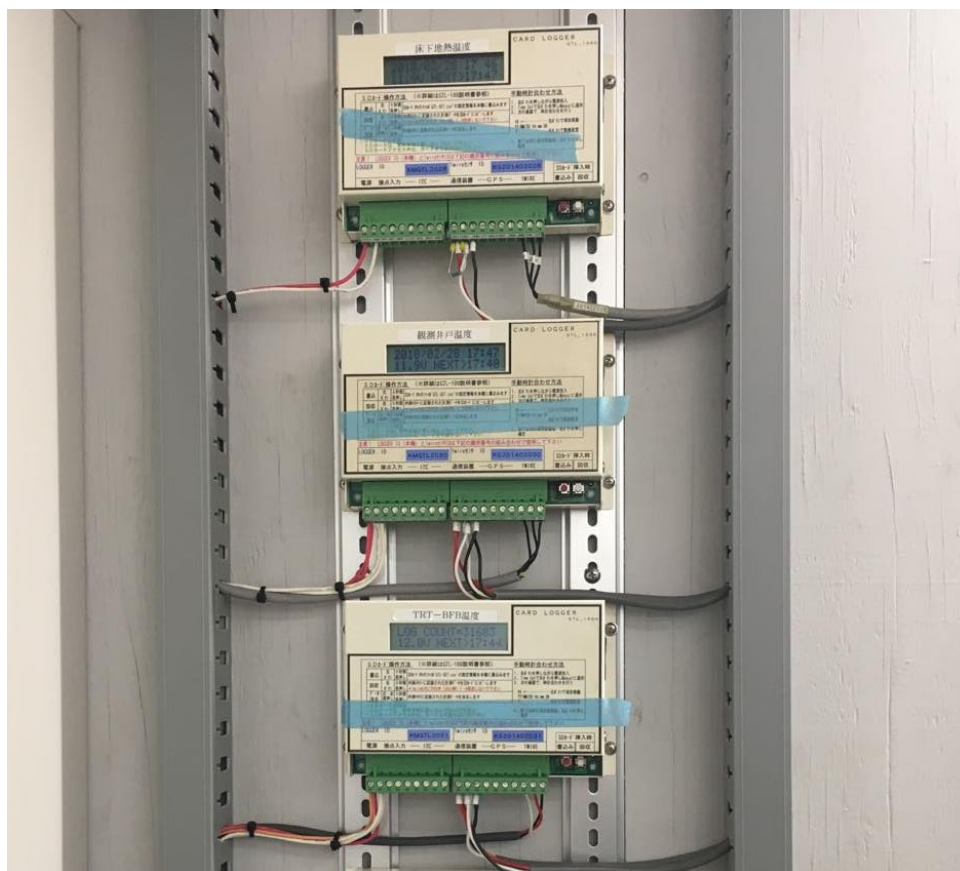


Figure 4. 12 Measurements of underground temperature.



Figure 4. 13 flow meter for measuring the flow rate of circulating water.

<span>オーバービュー</span> <span>MENU</span> <span>収集中</span> <span>233day</span> <span>2020/04/27</span> <span>1:37:17</span>			
Tdb_unit 9.80 °C	Mg4.0 0.000 V	Mg4.0 -3.90 Pct	IshDn -4.42 W/m <sup>2</sup>
RH 75.90 Pct	Mg3.5 1.074 V	Mg3.5 78.27 Pct	IshUp 1.36 W/m <sup>2</sup>
IshDh -0.05 mV	Mg3.0 1.068 V	Mg3.0 77.89 Pct	I IngDn 309.05 W/m <sup>2</sup>
IshUp 0.02 mV	Mg2.5 0.826 V	Mg2.5 62.32 Pct	I IngUp 360.52 W/m <sup>2</sup>
I IngDn -0.77 mV	Mg2.0 0.623 V	Mg2.0 48.96 Pct	Net I -57.26 W/m <sup>2</sup>
I IngUp -0.04 mV	Mg1.0 0.000 V	Mg1.0 -3.90 Pct	
Vw 0.936 m/s	Mg0.5 -0.027 V	Mg0.5 -9.44 Pct	
Wdir 33.76 Deg	Mg0.1 0.000 V	Mg0.1 -3.90 Pct	

Figure 4. 14 Screenshot of data logger of the weather station.

オーバービュー		収集中 35day 6h		2020/04/27 1:38:06									
iUPS	-0.01	fWLS	BURNOUT	tA11A	19.30	pWL3H	39.927	pWL3F	25.075	tWOn2S	13.32	qFLF	-4.85
iDNS	0.00	tWL2S	18.92	tA12A	19.32	pWL4H	36.587	pWL4F	25.050	tWOn1S	13.40		
rDNS	6.99	tWL1S	18.46	pWL3A	13.817	pRC1F	1.294	pRC1S	BURNOUT	tROOM	19.00		
rUPS	-0.07	tRD1S	14.92	pWL4A	7.000	pRC2F	1.298	pRC2S	BURNOUT	Humidity	48.61		
tAOW	9.98	tRC2S	17.00	pWL2A	30.872	fWLF	-0.075	tPGS	11.92	eS	0.000		
tUBS	4.30	pWL1S	BURNOUT	pRC1H	-2.450	tWF3F	18.24	tPLS	10.94	eA	0.000		
tUDS	3.88	pWL2S	BURNOUT	pRC2H	-2.450	tWF4F	19.48	tPFS	11.56	eF	0.000		
tDBS	4.52	pRC1A	BURNOUT	fWLH	0.000	fWFF	-0.025	tPBS	12.46	eH	0.000		
tDDS	4.54	pRC2A	BURNOUT	tWL3H	14.76	tWL2F	18.00	AT0.1m	17.30	iUPS	-1.48		
wPFS	0.75	fWLA	0.025	tWL4H	14.58	tWL1F	18.74	AT0.6m	17.60	iDNS	0.00		
ePVS	1.00	tWL3A	20.12	tWCH	14.24	tFLF	17.48	AT1.1m	17.80	rDNS	2764.23		
tRC1S	16.84	tWL4A	20.40	tWHH	14.08	qFLF	-0.13	AT1.7m	18.05	rUPS	311.52		

Figure 4. 15 Screenshot of the data logger for measuring the main parameters for system.

Besides, as shown in Figure 4. 14 and Figure 4. 15, we can monitor the operating status and weather conditions from the data logger through the computer. The weather data and system operating are measured and recorded separately. Figure 4. 16 shows the distribution of measurement points in the system. The measurement mainly includes the inlet/outlet temperature and flow rate of each heat pump unit. Also, the amount of electricity generated by the photovoltaic cell is also measured. Besides, the capacity of each heat pump and the detailed specifications of the piping system are also clearly marked.



## 4.3 Evaluation method

The measured values for the flow rates, changes in the circulating water temperature, and the electrical power inputs were used to determine the performance of the heat pump system. Although Energy Efficiency Ratio (EER) is usually used to indicate the cooling energy efficiency of the heat pump or chiller, the coefficient of performance (COP) is used to express the performance of each heat pump in this article. The reason is that the principle of EER is totally same as the COP. It is noted that the calculation of method and energy under refrigeration conditions the efficiency ratio is consistent.

In the case of the cycle calculations for the distributed heat pump system, it was assumed that there was no heat loss on the pipe due to enough insulation layer installed, and so for the overall system during the winter experiment, the thermal energy balance can be expressed as follows:

$$Q_{eg} + Q_{sshp} = Q_{fh}$$

Where,  $Q_{eg}$  is the heat extracted from the ground [kW],  $Q_{sshp}$  is the heat transferred into the water loop by the SSHP [kW],  $Q_{fh}$  is the heat for space heating that rejected to the floor heating room [kW]. The heat rejected to the floor heating room,  $Q_{fh}$  is calculated from the following equation:

$$Q_{fh} = \rho \times c_w \times V_{wl} \times (T_{wl,out} - T_{wl,in})/60$$

Where, the  $T_{wl,out}$  and  $T_{wl,in}$  is the temperature of hot water in the floor heating pipe system [ $^{\circ}\text{C}$ ],  $V_{wl}$  are the volumetric flow rates [L/min],  $\rho$  is the density of water [0.999 kg/dm<sup>3</sup>],  $c_w$  is the specific heat capacity of water [4.18 kJ/kg $\cdot^{\circ}\text{C}$ ].

The heat output of the SSHP  $Q_{sshp}$ , which is the heat transferred into the water loop by the SSHP, can be calculated as follows:

$$Q_{sshp} = \rho \times c_w \times V_{sshp} \times (T_{sshp,out} - T_{sshp,in})/60$$

Where, the  $T_{sshp,out}$  and  $T_{sshp,in}$  is the temperature of hot water in the floor heating pipe system [ $^{\circ}\text{C}$ ],

$V_{sshp}$  are the volumetric flow rates [L/min],  $\rho$  is the density of water [0.999 kg/dm<sup>3</sup>],  $c_w$  is the specific heat capacity of water [4.18 kJ/kg·°C].

According to equation (1), the heat extracted from the ground  $Q_{eg}$  can be calculated from the following equation:

$$Q_{eg} = Q_{fh} - Q_{sshp}$$

Thus, for the heat pump system, the COP of the heat pump unit (SSHP :  $COP_{sshp}$ , FHHP :  $COP_{fh}$ ) and for the whole heat pump system ( $COP_{sys}$ ) can be defined as follows:

$$COP_{sshp} = Q_{sshp}/W_{sshp}; \quad COP_{fh} = Q_{fh}/W_{fh}$$

$$COP_{sys,heating} = Q_{fh}/(W_{fh} + W_{sshp})$$

Where,  $W_{fh}$  and  $W_{sshp}$  are the power consumptions of the heat pump unit, which includes the power input to the compressor, the circulation pump, and the automatic control system.

Similarly, for the space cooling and domestic hot water supply operation, the heat out of heat pump for air conditioning  $Q_{ac}$  and domestic hot water supply  $Q_{hw}$ , they can be calculated as follows:

$$Q_{hw} = \rho \times c_w \times V_{hw} \times (T_{hw,out} - T_{hw,in})/60$$

$$Q_{ac} = \rho \times c_w \times V_{ac} \times (T_{ac,out} - T_{ac,in})/60$$

$$COP_{hw} = (Q_{hw} + W_{hw})/W_{hw}$$

$$COP_{ac,cooling} = (Q_{ac} - W_{ac})/W_{ac}; \quad COP_{ac,heating} = (Q_{ac} + W_{ac})/W_{ac}$$

$$COP_{sys,cooling} = (Q_{ac} + Q_{hw} + W_{hw} - W_{ac})/(W_{hw} + W_{ac} + W_{sshp})$$

Where,  $Q_{hw}$  is the heat for domestic hot water supply by the how water heat pump,  $Q_{ac}$  is the heat for space cooling or heating that put to the floor heating room by the air conditioning heat pump,  $V_{hw}$  and  $V_{ac}$  are the volumetric flow rates,  $\rho$  is the density of water,  $c_w$  is the specific heat capacity of water, and  $W_{hw}$  and  $W_{ac}$  are the power consumptions of each heat pump unit, which includes the power input to the compressor, the circulation pump, and the automatic control system.

## 4.4 Winter experimental results and analysis

### *Introduction of the winter experiment*

The winter field testing was conducted from March 1 to March 31, 2018 (continuous operation for one month). By filed testing of the floor heating heat pump (FHHP) and sky source heat pump (SSHP), we verified and evaluated the performance of each component. During the experiment measurement period, SSHP and GHX were used as heat source devices to provide heat for space heating in RE house, and only FHHP operated as a heating device to heat the multi-purpose and measurement room.

Based on the amount of solar radiation and outside dry bulb temperature, the most suitable day for collecting heat (March 25, clear weather, the average dry bulb temperature was 11.3 °C, sunshine duration was 11.5 h); the most unsuitable day (March 21, cloudy day, the average dry bulb temperature was 3.8 °C and the sunshine duration was 0 h) was selected as a representative example to analyze the performance of this system in detail.

Because the SSHP mainly collect heat from solar radiation on a sunny day and from the air on a cloudy day, we made this selection. We will evaluate the heating operation performance of this system by using the coefficient of performance(COP)) as a representative value of the actual measurement results.

### *4.4.1 Winter field testing on a sunny day*

#### **Operation status analysis of sky source heat pump and water source heat pump for floor heating**

Figure 4. 17 to Figure 4. 26 show the experimental results obtained on March 25<sup>th</sup>. Figure 4. 17 shows the weather of March 25<sup>th</sup>. It is evident that 25<sup>th</sup> was a sunny day, there was sufficient solar radiation during the daytime, and the dry bulb temperature was above 10 °C during the daytime. Therefore, it can be expected that SSHP will have excellent performance, and the heat load of the RE house will not be too much.

Between 0:00 and 12:00, and from 15:00 to 24:00, the SSHP stopped, but the GHXs extracted heat from the ground and supplied heat to the FHHP to heat the room. From 12:00 to 15:00, the SSHP gathered heat from both solar radiation and the air. During the operation from 12:00 to 15:00, the SSHP maintained a heat output of ~5.5 kW. From the beginning of the operation, the COP of the SSHP continued to rise with increasing solar radiation and outside dry bulb temperature, giving a maximum COP of ~50 during this period. However, when less solar radiation was available, the COP of the SSHP dropped, and an average COP of 42.9 was obtained for the overall heat collection operation.

As shown in Figure 4. 19, the heat generated by the SSHP was used to heat the ground through the GHXs, which can recover the decrease in the soil temperature due to heat extraction for floor heating. Besides, Figure 4. 20 shows the changes in FHHP performance over time. In this case, the COP remained relatively constant in the stable period from 23:30 to 10:30 the following day. Because of the increase in indoor temperature, the decrease in the temperature of the circulating water in the floor heating loop gradually decreased, and the operation was stopped after reaching the set value around 10:30. The observed fluctuation in the COP every 30 min is due to the temperature change caused by switching on of the SSHP circulation pump, which is set to sample the water temperature. This sampling is to prevent freezing in the water loop system.

Figure 4. 23 shows the change in the indoor temperature of the multi-purpose room and its floor surface. Because there is a wide French window in the room, the indoor temperature increased as the increasing solar radiation during the daytime. At around 3 pm, the indoor temperature became higher than floor temperature, which caused by solar radiation through the window.

Figure 4. 25 and Figure 4. 26 show the relationship between the COP of SSHP, solar radiation, and dry bulb temperature, respectively. As shown in Figure 4. 25, we can know that on a sunny day, the performance of SSHP is correlated with the intensity of sunlight. As the intensity of solar radiation increases, the performance of SSHP increases accordingly. In comparison, in the case of a sunny day, the performance of SSHP is not directly related to the outside temperature. The reason is that the SSHP is a direct expansion heat pump. When the sunlight is sufficient, the SSHP can get enough heat from the sunshine, and does not need to get heat from the air. As can be seen from Figure 4. 24, during this period, the temperature of the panel is higher than the surrounding air temperature, that is, there will be heat loss to the surrounding air at this time.

But the heat loss is acceptable because, during this period, the SSHP achieved an excellent performance in heat collection, though there is heat loss from the panel to ambient air. At the same time, because the evaporation of the refrigerant absorbs heat from the outdoor panel installed with photovoltaic cells on the top. This kind of heat collection makes the temperature of the photovoltaic cell not increase too high to avoid the reduction of power generation efficiency.

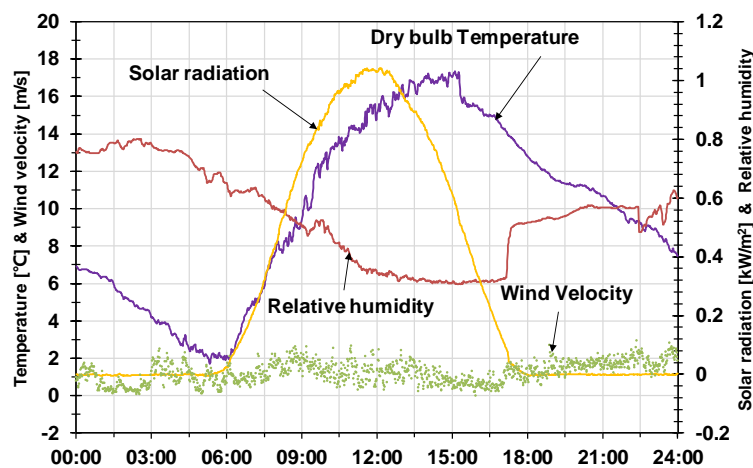


Figure 4. 17 Weather conditions on March 25<sup>th</sup>.

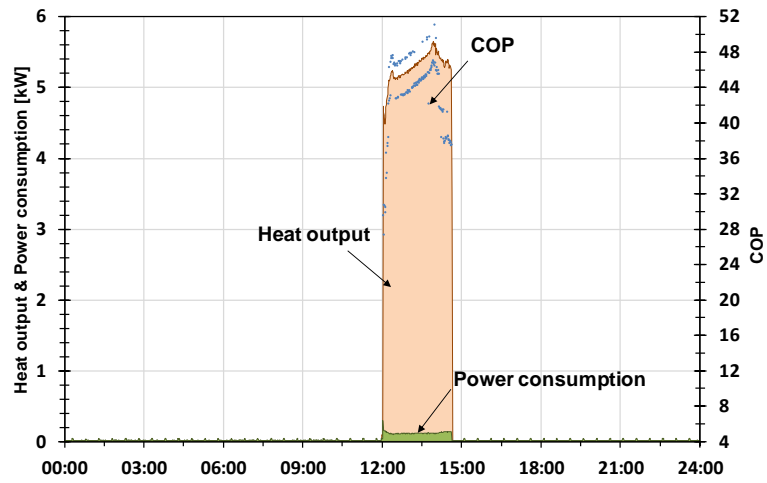


Figure 4. 18 Changes in SSHP performance overtime on March 25<sup>th</sup>.

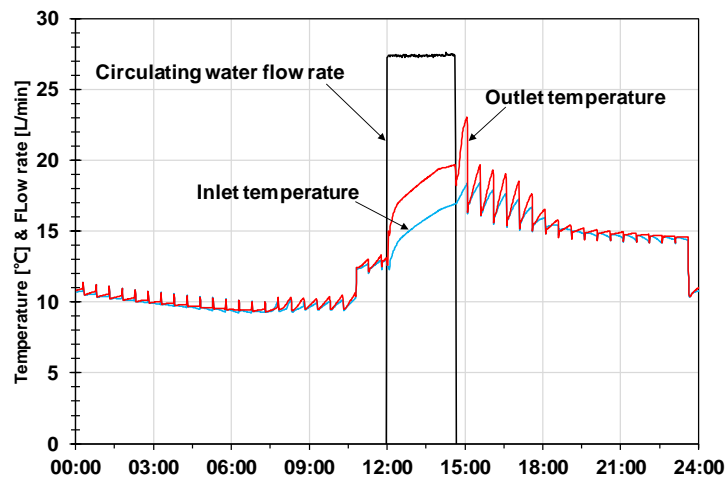


Figure 4. 19 Changes in the circulating water temperature at the SSHP unit.

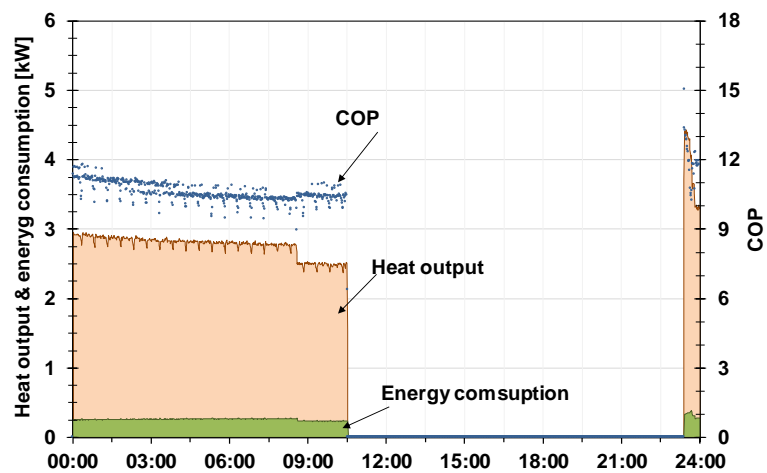


Figure 4. 20 Changes in FHHP performance overtime on March 25<sup>th</sup>.

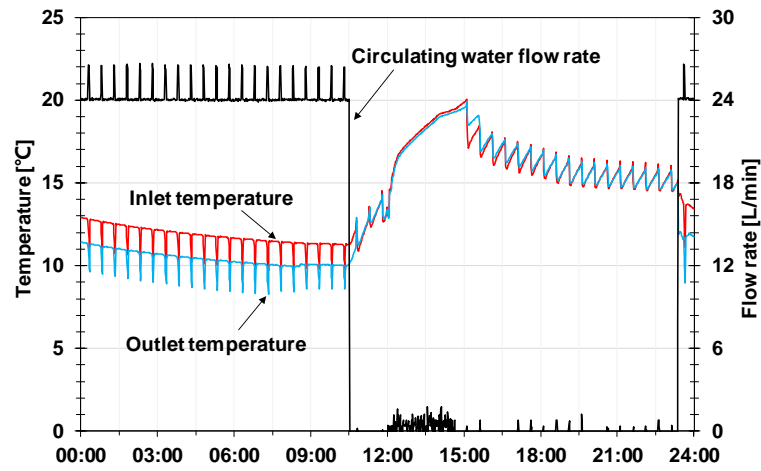


Figure 4. 21 Changes in the circulating water temperature at the FHHP unit.

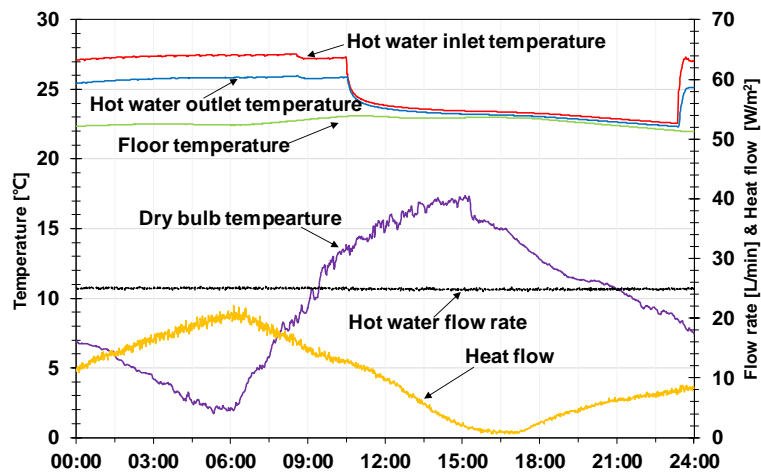


Figure 4. 22 Changes in the floor heating loop of the FHHP unit.

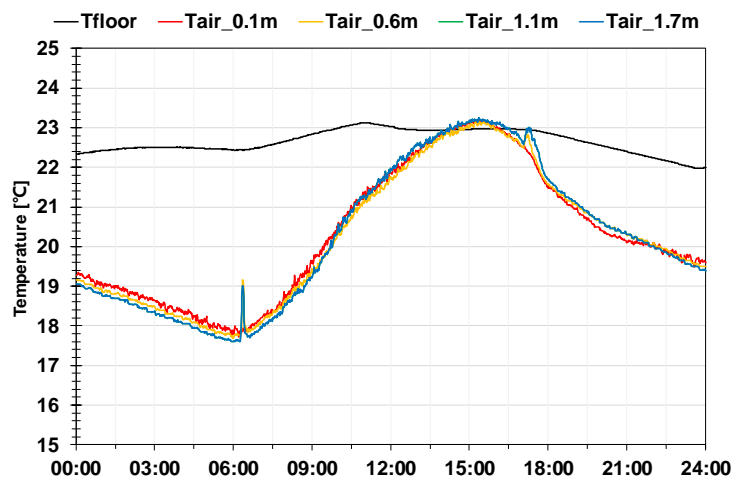


Figure 4. 23 Changes in the floor surface and indoor air temperature.

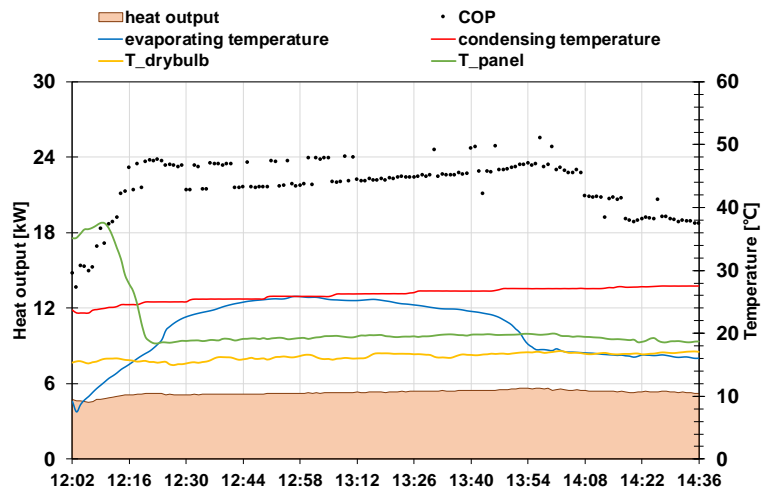


Figure 4. 24 Changes in the SSHP outdoor panel and refrigerant circulation.

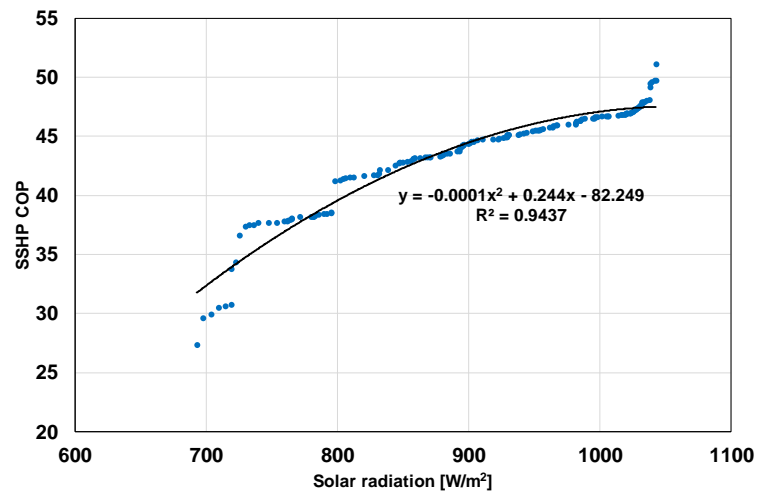


Figure 4. 25 Relationship between the COP of SSHP and solar radiation.

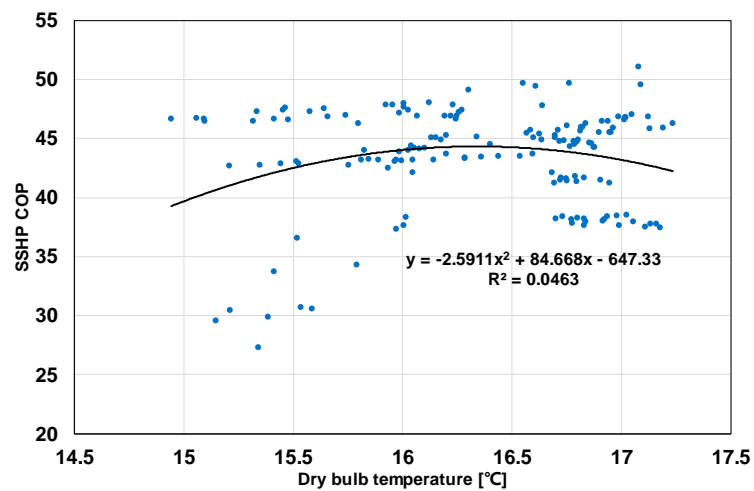


Figure 4. 26 Relationship between the COP of SSHP and dry bulb temperature.

### Operation status analysis of double-helical ground heat exchanger

Figure 4. 27 and Figure 4. 28 show the changes in the central borehole temperature and undisturbed underground temperature. As shown in Figure 4. 27, on 24<sup>th</sup> March, the solid blue line is the central borehole temperature; it is around 11 °C at 10:30 on 24<sup>th</sup> pm when the FHHP stopped. The solid orange line represented the central borehole temperature at 16:00 24<sup>th</sup> when the heating operation of SSHP stopped. Based on the results, we can know that the central borehole temperature recovered from 11 °C to 13.5 °C after a 4-hour SSHP heating operation, which collected heat from solar or air to heat the soil. On 25<sup>th</sup> March, the results represented by the dashed line at 10:30 and green solid line at 15:00. Based on the results, we can know that after a daily cycle operation, the central borehole temperature at 10:30 kept almost the same between 24<sup>th</sup> and 25<sup>th</sup>, with only a small deviation, which was about 0.2 °C. We also got the same result of central borehole temperature after the heating operation of SSHP, which can be seen as the recovery of soil temperature. The value after heating operation of SSHP restored to around 13.5 °C on both 24<sup>th</sup> and 25<sup>th</sup>, which shows the control schedule adopted during this period has an acceptable performance on the soil temperature recovery.

Figure 4. 28 shows the result between the undisturbed underground and borehole central temperature. A dashed line represents the undisturbed underground temperature(also is the natural soil temperature), while the solid line represents the central borehole temperature. The results indicate that the undisturbed underground temperature was higher than the central borehole temperature.

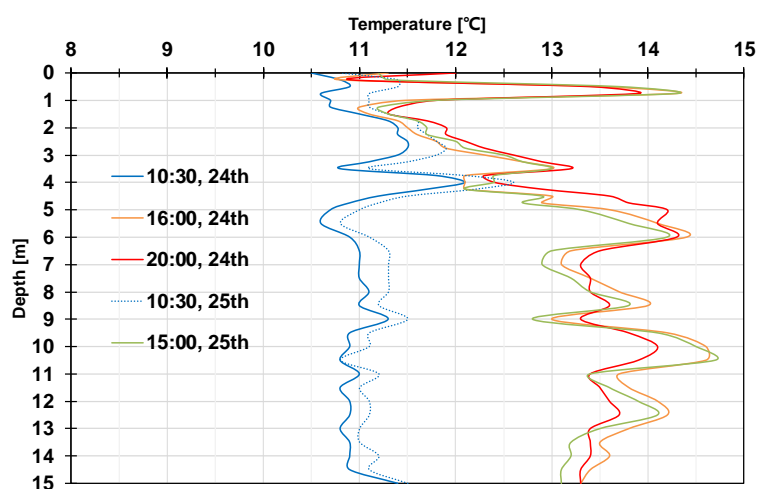


Figure 4. 27 Changes in the central borehole temperature.

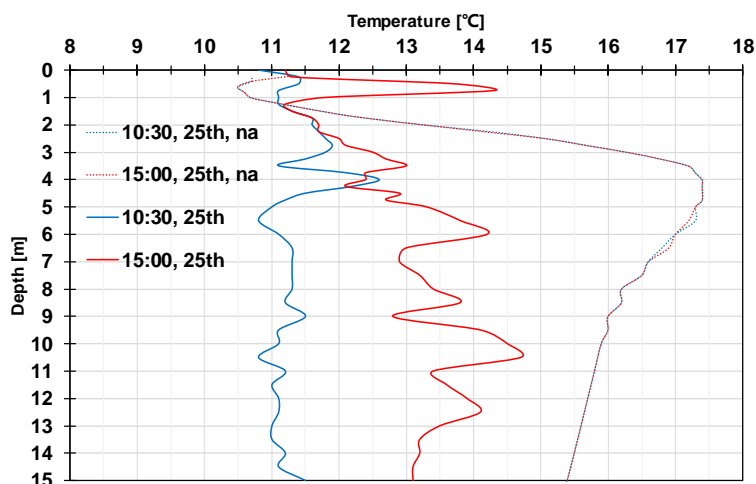


Figure 4. 28 Difference between undisturbed underground and borehole central temperature.

In soil layers less than 1-meter depth, the undisturbed underground temperature was lower than the central borehole temperature due to the influence of winter weather conditions (low air temperature), which means there is no usable geothermal heat at this level. Therefore, we put the spiral part from the 3-meter depth from the ground surface; the soil temperature was higher and stable, which indicates an available geothermal heat can be achieved.

The difference between undisturbed underground and borehole central temperature varied according to the depth, and the maximum temperature difference started from about 3-meter depth, and the minimum value was about 15.5 °C.

### **Summary of system performance on a sunny day**

This section described the field testing on 25<sup>th</sup> March that is a sunny day. Based on the experimental results, we analyzed and evaluated the performance of the SSHP heating operation, and the floor heating system includes the FHHP and floor heating loop.

The results show that the SSHP achieved excellent performance on heat collection with an average COP 23.2, mainly from solar radiation on a sunny day. The performance of FHHP was also tested, and the experimental results showed noticeable improvement compared with a basic commercial product by changing components such as the heat exchanger.

The FHHP can offer a stable and efficient heating output with a COP around 11. The COP of SSHP and FHHP during 25<sup>th</sup> March are shown in Table 4. 2, as marked in grey shading. The heat output, energy consumption, and power generation are shown in Figure 4. 29.

Table 4. 2 COP of each heat pump and the whole system in March

	21 <sup>st</sup> March	25 <sup>th</sup> March	Monthly average
SSHP	7.4	23.2	14.9
FHHP	11.3	11.4	11.6
Whole system	8.2	9.6	8.4

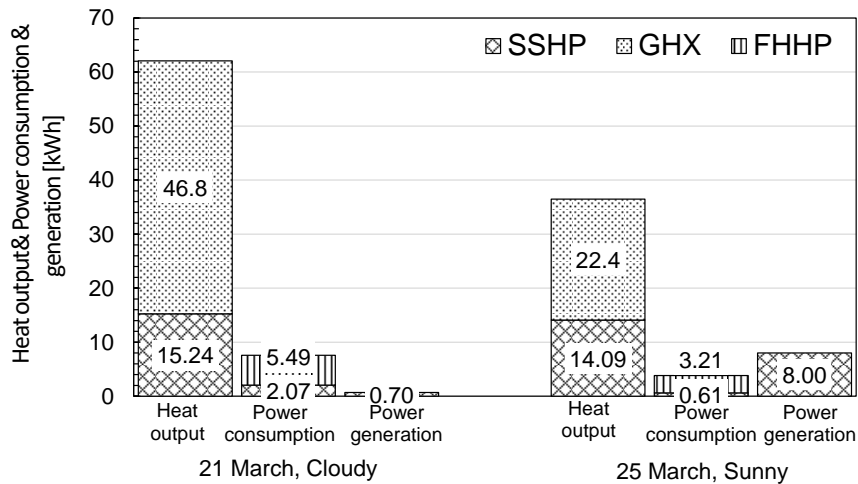


Figure 4. 29 Heating operation performance on 25 March (on the right).

#### 4.4.2 Winter field testing on a cloudy day

##### **Operation status analysis of sky source heat pump and water source heat pump for floor heating**

Figure 4. 30 to Figure 4. 39 show the experimental results obtained on March 21<sup>st</sup>. Figure 4. 30 shows the weather of March 21<sup>st</sup>. It is evident that 25<sup>th</sup> was a sunny day, there was almost no solar radiation due to the cloud, and the dry bulb temperature was also at a low level that was lower than 5 °C all day. Therefore, it can be expected that the performance SSHP will drop due to the weather, and the heat load of the RE house will increase accordingly.

Figure 4. 31 to Figure 4. 33 show the measurement results obtained on the 21<sup>st</sup> of March. From 20:00 to 12:00 the following day, the GHX extracted heat from the ground and supplied heat to the FHHP unit. Between 12:00 and 20:00, the SSHP maintained the temperature of the circulating water between 15–17 °C. This operation caused a fluctuation in circulating water temperature and flow

rate every 30 minutes, which is the same as the schedule.

In addition, the heat load increased because of low outdoor temperature on the 21<sup>st</sup>. Therefore, the FHHP maintained a continuous operation, and the majority of the heat generated by the SSHP was used for floor heating, with no recovery of the soil temperature being achieved by the SSHP. Furthermore, as it was a cloudy day, and both the quantity of solar radiation and the outside temperature was reduced, a lower average COP of 8.3 was obtained for the SSHP.

The result of the FHHP is shown in Figure 4. 33. As mentioned previously, the FHHP maintained a continuous operation due to the high heat load. Although the FHHP can maintain a stable operation with a COP of ~11, fluctuation in the COP due to the temperature rise of the circulating water was observed. As the performance of the FHHP increases as the temperature of the circulating water increases, it appears that there is still room for improvement in the performance by adjusting the operating conditions.

Figure 4. 35 and Figure 4. 36 shows the change in the indoor temperature of the multi-purpose room and its floor surface. Because there is a wide French window in the room, there was a heat loss from the window. Therefore, the indoor temperature didn't increase as described on the 25<sup>th</sup>. As the outside temperature drops, the indoor temperature drops accordingly.

Figure 4. 38 and Figure 4. 39 show the relationship between the COP of SSHP, solar radiation, and dry bulb temperature, respectively. As shown in Figure 4. 38, we can know that on a cloudy day, the performance of SSHP is correlated with the intensity of ambient air temperature. As the intensity of outdoor temperature increases, it is expected that the performance of SSHP increases accordingly due to the same operation as an air source heat pump. However, on the 21<sup>st</sup>, the outside temperature does not change much during SSHP operation, so it can not be seen that its performance has an apparent relationship with the outdoor temperature from this result. Similarly, as shown in Figure 4. 39, there was no evident relationship between the performance of SSHP and solar radiation because the SSHP does not collect heat from solar radiation in this case. Still, based on the result in Figure 4. 37, it indicated that during this period, the evaporating temperature in the panel of the SSHP obviously changed with the change of the outside air temperature. Therefore, it can be inferred that the performance of SSHP is closely related to the outdoor temperature in this case. However, in the results on the 21<sup>st</sup>, because the outdoor temperature range is very narrow, this relationship is not apparent based on the result.

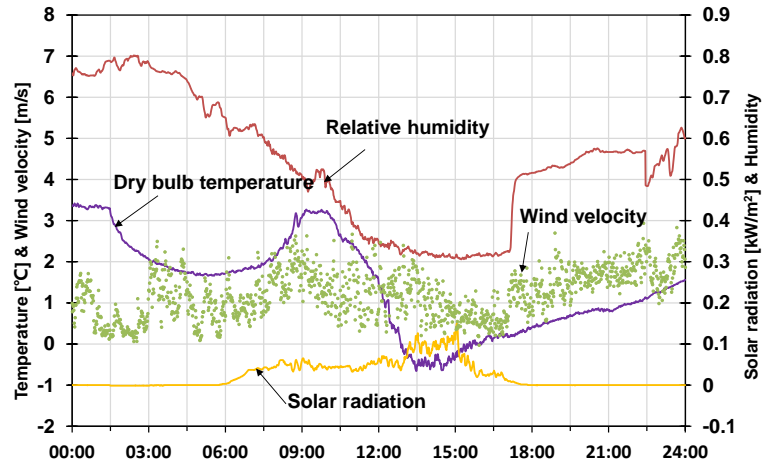


Figure 4.30 Weather conditions on March 21<sup>st</sup>.

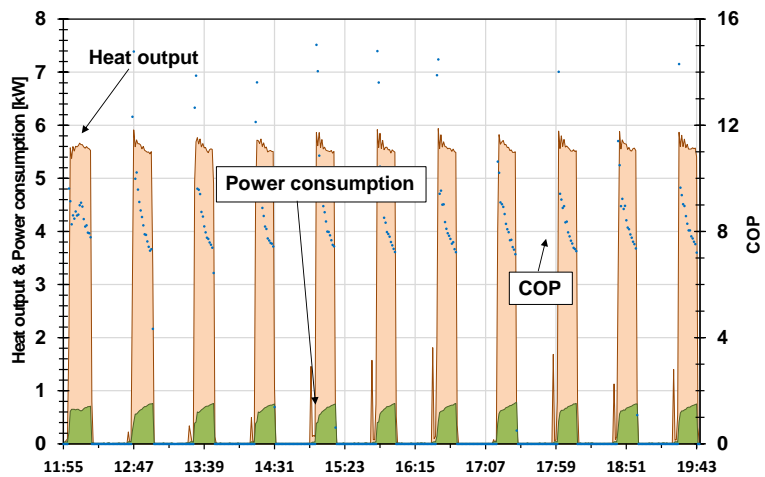


Figure 4.31 Changes in SSHP performance over time.

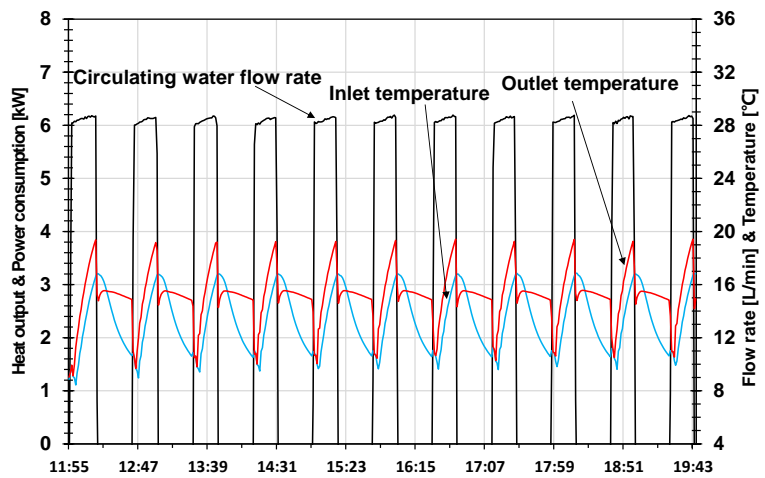


Figure 4.32 Changes in the circulating water temperature in the SSHP.

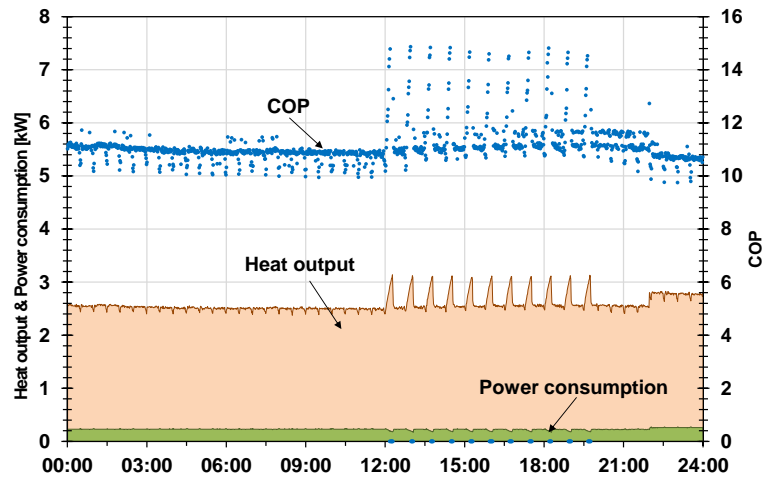


Figure 4. 33 Changes in the FHHP performance over time.

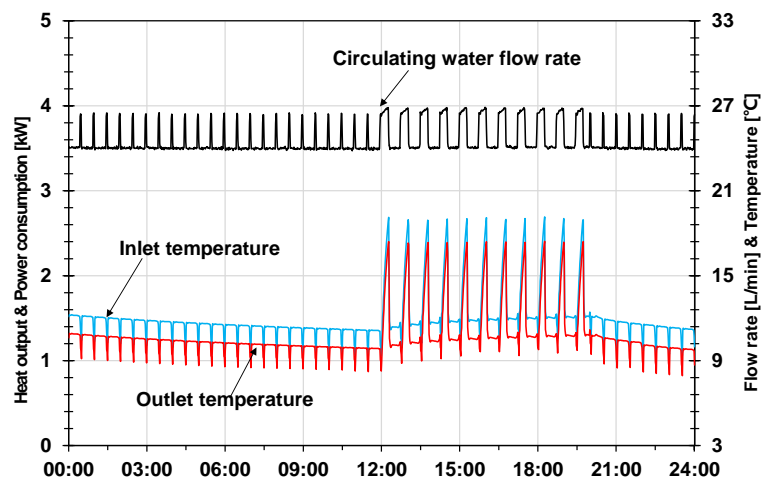


Figure 4. 34 Changes in the circulating water temperature in the FHHP.

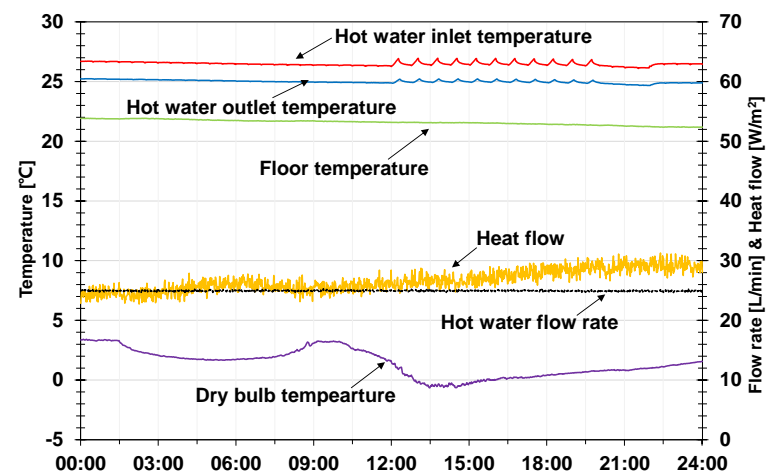


Figure 4. 35 Changes in the floor heating loop of the FHHP unit.

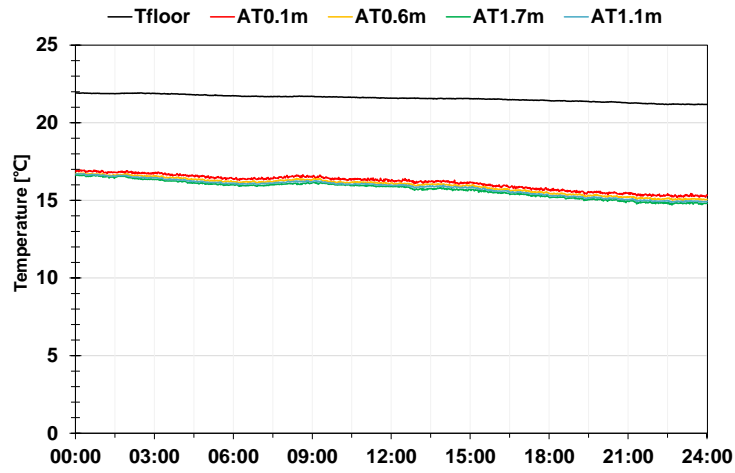


Figure 4. 36 Changes in the floor and indoor air temperature.

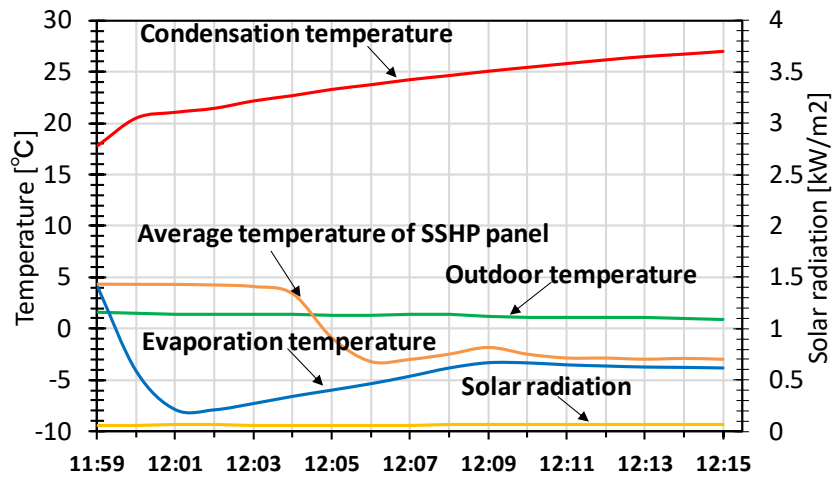


Figure 4. 37 Changes in the SSHP outdoor panel and refrigerant circulation.

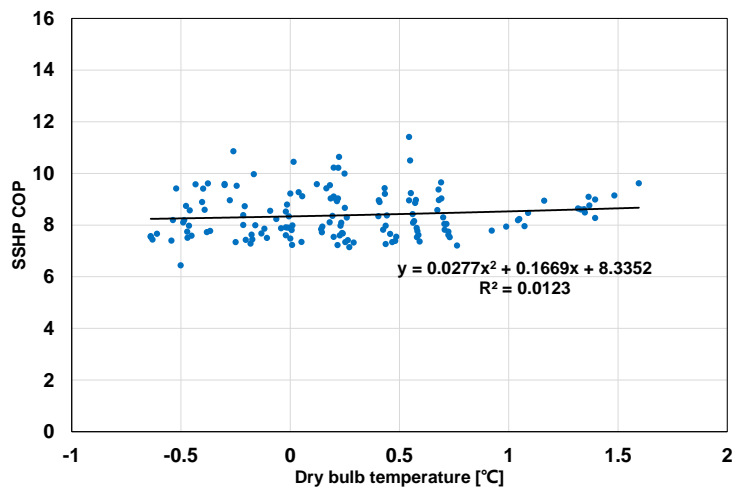


Figure 4. 38 Relationship between the COP of SSHP and dry bulb temperature.

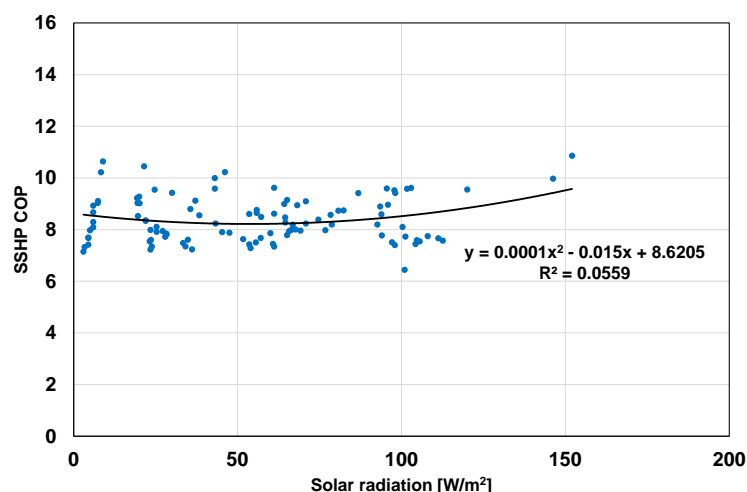


Figure 4. 39 Relationship between the COP of SSHP and solar radiation.

### **Operation status analysis of double-helical ground heat exchanger**

Figure 4. 40 and Figure 4. 41 show the changes in the central borehole temperature and undisturbed underground temperature. As shown in Figure 4. 40, on 20<sup>th</sup> March, the solid blue line is the central borehole temperature; it is around 11.5 °C at 12:00 on 20<sup>th</sup> pm when the FHHP stopped. The solid orange line represented the central borehole temperature at 14:45 when the heating operation of SSHP stopped. Based on the results, we can know that the central borehole temperature recovered from 11 °C to 13.5 °C after a 3-hour SSHP heating operation, which collected heat from solar or air to heat the soil. On 21<sup>st</sup> March, the results represented by the dashed line at 10:30 and green solid line at 19:45. Based on the results, we can know that after a daily cycle operation, the central borehole temperature at 10:30 kept almost the same between 20<sup>th</sup> and 25<sup>th</sup>, with only a small deviation. However, due to the continuous operation of FHHP on the 21<sup>st</sup>, the heating operation of SSHP occurred periodically to recover the soil temperature. Compared with 25<sup>th</sup> and 20<sup>th</sup>, the value after heating operation of SSHP only restored to less than 13 °C on both 21<sup>st</sup>, which shows an insufficient soil temperature recovery.

Figure 4. 41 shows the result between the undisturbed underground and borehole central temperature. A dashed line represents the undisturbed underground temperature (also is the natural soil temperature), while the solid line represents the central borehole temperature. The results indicate that the undisturbed underground temperature was higher than the central borehole temperature.

In soil layers less than 1-meter depth, the undisturbed underground temperature was lower than the

central borehole temperature due to the influence of winter weather conditions (low air temperature), which means there is no usable geothermal heat at this level. Therefore, we put the spiral part from the 3-meter depth from the ground surface; the soil temperature was higher and stable, which indicates an available geothermal heat can be achieved.

The difference between undisturbed underground and borehole central temperature varied according to the depth, and the maximum temperature difference started from about 3-meter depth, and the minimum value was about 15.5 °C. Compared with 25<sup>th</sup>, there was no apparent difference in the distribution of undisturbed underground temperature.

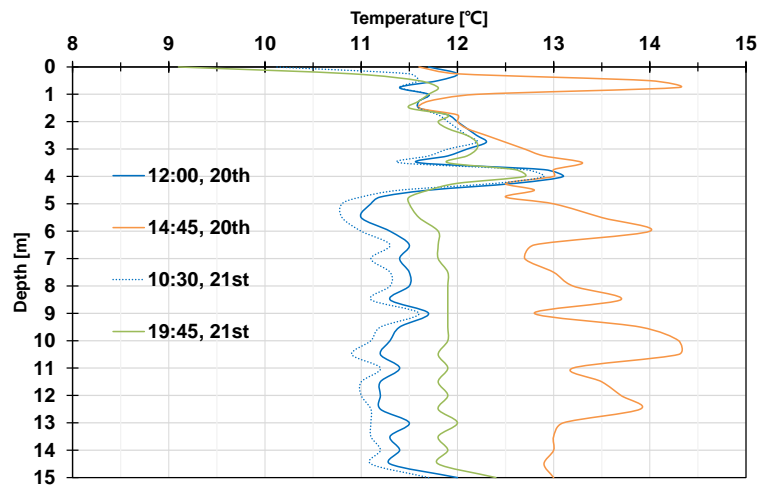


Figure 4. 40 Changes in the central borehole temperature.

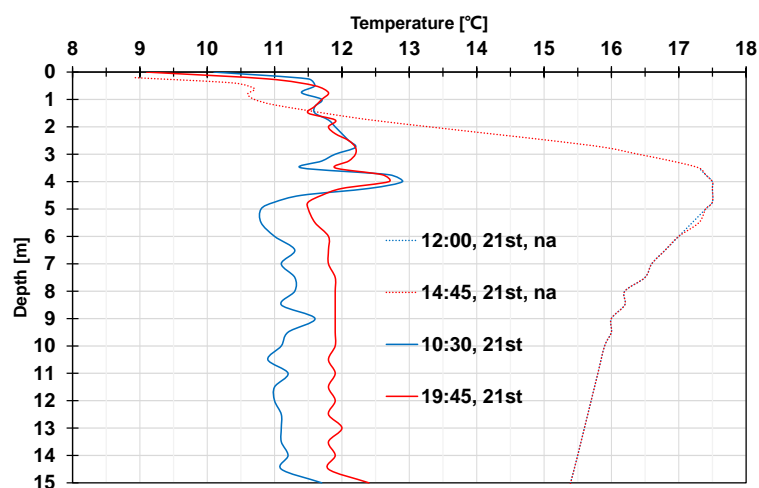


Figure 4. 41 Difference between undisturbed underground and borehole central temperature.

### Summary of system performance on a cloudy day

This section described the field testing on 21<sup>st</sup> March that is a cloudy day. Based on the experimental results, we analyzed and evaluated the performance of the SSHP heating operation, and the floor heating system includes the FHHP and floor heating loop.

The results show that the SSHP achieved a lower heating performance than 25<sup>th</sup> with an average COP 7.4, mainly collecting heat from ambient air on a sunny day. The performance of FHHP was also tested, and the experimental results were almost the same with 25<sup>th</sup> and showed noticeable improvement compared with a basic commercial product by changing components such as the heat exchanger. The FHHP can offer a stable and efficient heating output with a COP around 11. The COP of SSHP and FHHP during 21<sup>st</sup> March are shown in Table 4. 3, as marked in grey shading. The heat output, energy consumption, and power generation are shown in Figure 4. 42.

Table 4. 3 COP of each heat pump and the whole system in March

	21 <sup>st</sup> March	25 <sup>th</sup> March	Monthly average
SSHP	7.4	23.2	14.9
FHHP	11.3	11.4	11.6
Whole system	8.2	9.6	8.4

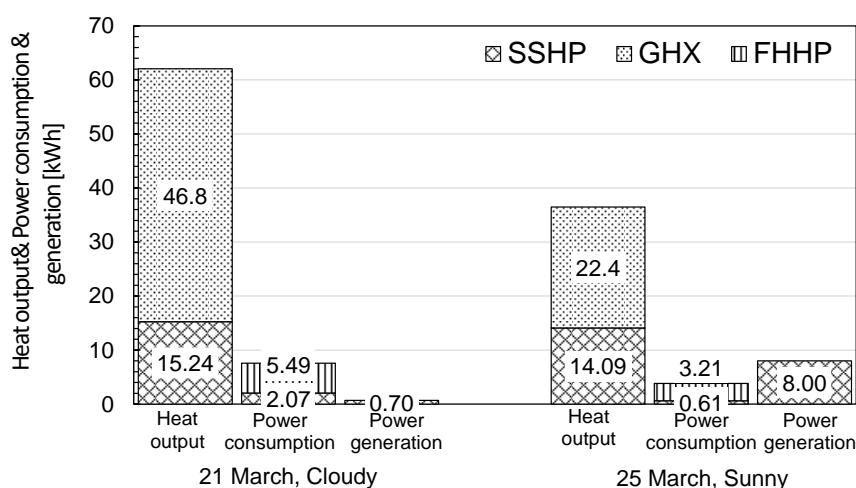


Figure 4. 42 Heating operation performance on 21 March(on the left).

### 4.4.3 Winter field testing results for the whole month

#### Overview of winter field testing for the whole month

The results obtained from the winter field testing over the heating period between the 1<sup>st</sup> and the 31<sup>st</sup> March were evaluated to determine the performance characteristics of the proposed distributed heat pump system. Based on the accumulated value of heat output and power consumption over March, we calculated the average COP of each heat pump and the whole system. Figure 4. 43 shows the heat output, power consumption, and power generation for the two representative days and for the whole experimental period, respectively.

The COP values of the various heat pumps and for the whole system are given in Table 4. 4.

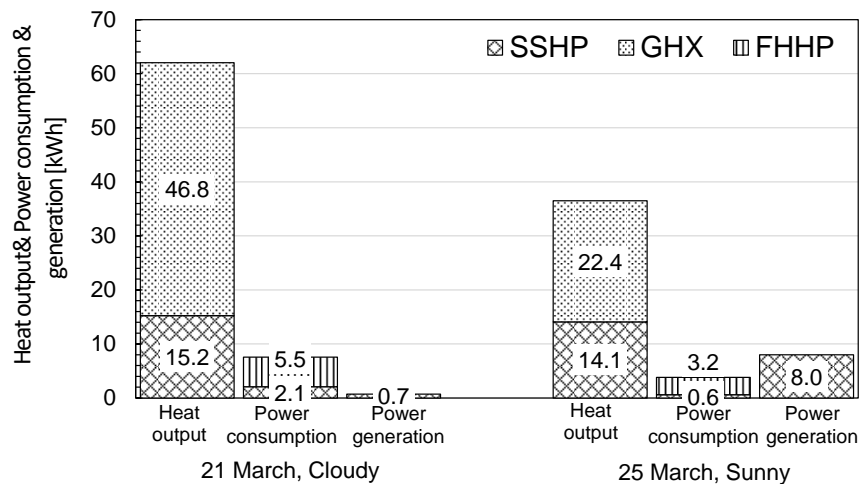


Figure 4. 43 Heat output, power consumption, and power generation over March.

Table 4. 4 COP values for the different heat pumps and for the overall system

		21st March	25th March	1 <sup>st</sup> –31 <sup>st</sup> March
Average for a specific period	SSHP	7.4	23.2	14.9
	FHHP	11.3	11.4	11.6
	Whole system	8.2	9.6	8.4
Average for actual operation	SSHP	8.3	42.9	-

### **Operation status and performance analysis of the whole system**

The heating output of FHHP is the total value of the heat output of SSHP and GHX. The COP of the entire system on the 25<sup>th</sup> was 9.6 per day on average. Besides, the amount of solar power generation was 8.0 kWh, exceeding the daily integrated power consumption of 3.8 kWh. However, due to the decrease in solar radiation and the decrease in outside temperature due to cloudy weather, the COP of the entire system on the 21<sup>st</sup> was 8.2 on average per day, and the amount of power generation was 0.7 kWh, lower than the daily total power consumption of 7.6 kWh.

For the operation result for one month in winter operation, the ratio of SSHP and geothermal heat to the total heat output (for floor heating) was almost the same. This result also indicated that SSHP recovered half of the of heat taken from the ground during the heating period.

In the case of a sunny day (i.e., 25<sup>th</sup> March), the average system COP was 9.6, and the power generation by the photovoltaic cell on the SSHP panel was 8.0 kWh, which exceeded the power consumption of the whole system. However, due to the decreased solar radiation and lower outdoor temperature on a cloudy day (i.e., 21<sup>st</sup> March), the average system COP was 8.2, and the SSHP efficiency also reduced. Moreover, although the heat output of the SSHP was higher than that of geothermal heat on the two representative days, the SSHP and the geothermal heat accounted for similar proportions of the heat output from the overall system when considering the complete winter operation result. Also, the amount of power generated by SSHP was 159.8 kWh, which exceeded the power consumption of the entire system of 151.4 kWh in the whole experiment period.

Figure 4. 44 shows the changes in central borehole temperature from 1<sup>st</sup> to 27<sup>th</sup> March, which is the start and end time of the winter field testing. As shown in this figure, the central borehole temperature below from 3m to 15m in depth was 13 degrees on average, which is about 1 degree lower than the 25<sup>th</sup>. Besides, the natural soil temperature between 3m and 6m in depth decreases about 0.5 degrees, while there was almost no change in the natural soil temperature between 6m and 15m.

Figure 4. 45 and Figure 4. 46 show the dry-bulb temperature and solar radiation in March 2018, respectively. Figure 4. 47 shows the performance changes of SSHP in the winter experiment. The result indicates that the performance of SSHP changes with the weather, the COP can reach about 30-40 on average when there were sufficient solar radiation and high dry-bulb temperature in sunny

day. However, the COP was about 10 on average when it was cloudy in winter.

Due to the stable circulating water temperature, as shown in Figure 4. 48, the operation of FHHP kept stable and efficient during the whole experiment in winter, with an average COP of around 11.

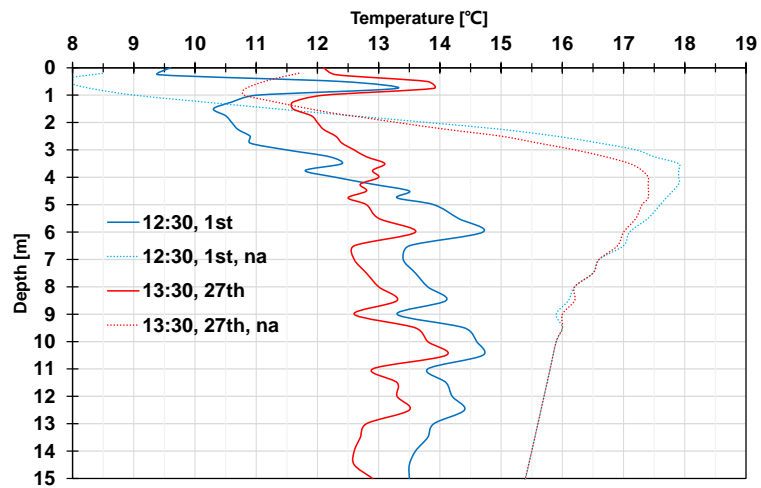


Figure 4. 44 Changes in central borehole temperature from 1<sup>st</sup> to 27<sup>th</sup> March.

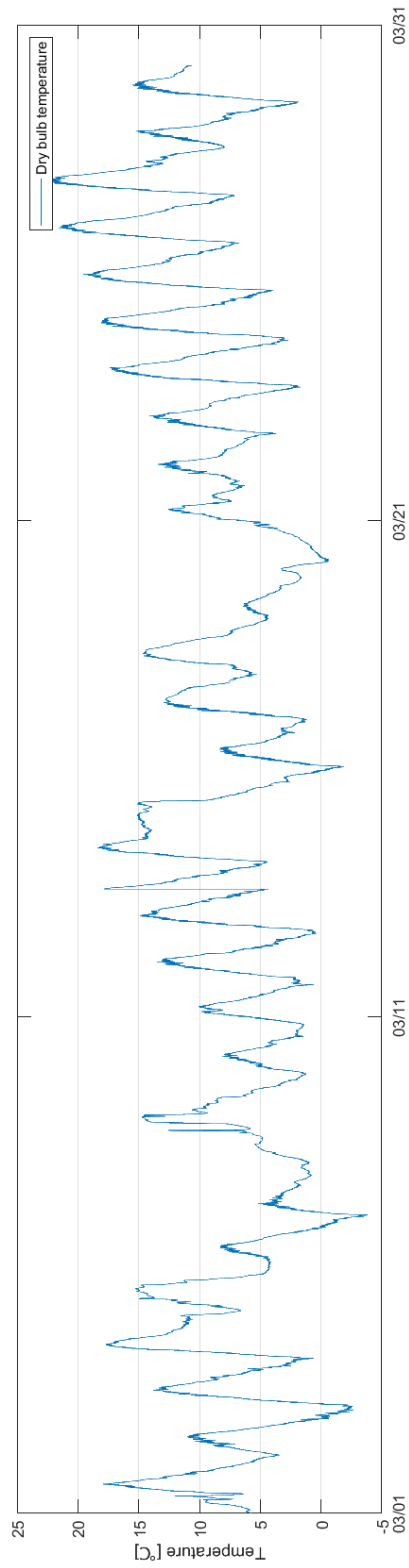


Figure 4. 45 Dry bulb temperature in March

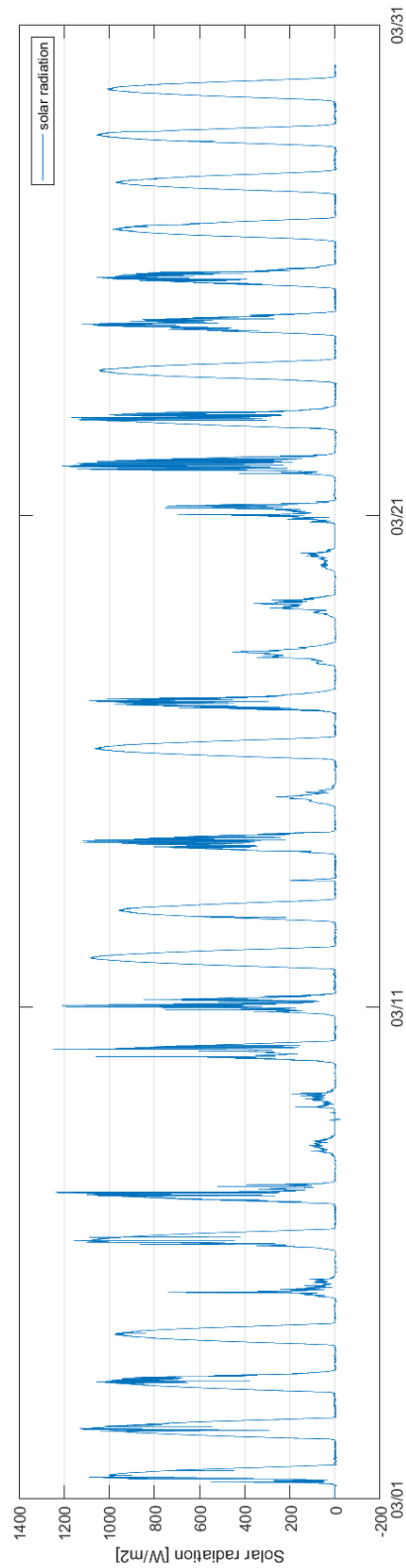


Figure 4. 46 Solar radiation in March

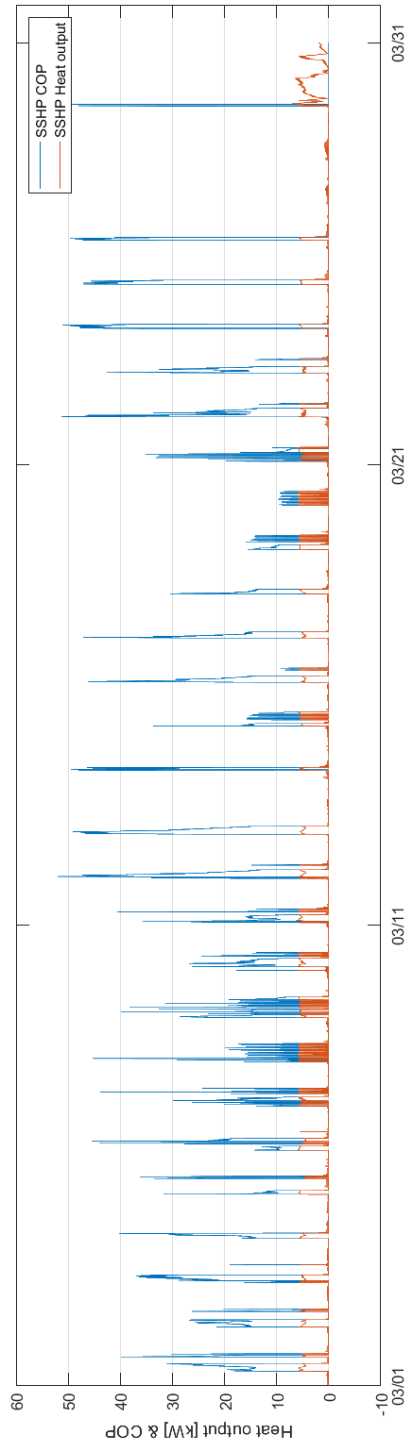


Figure 4. 47 SSHP performance in March

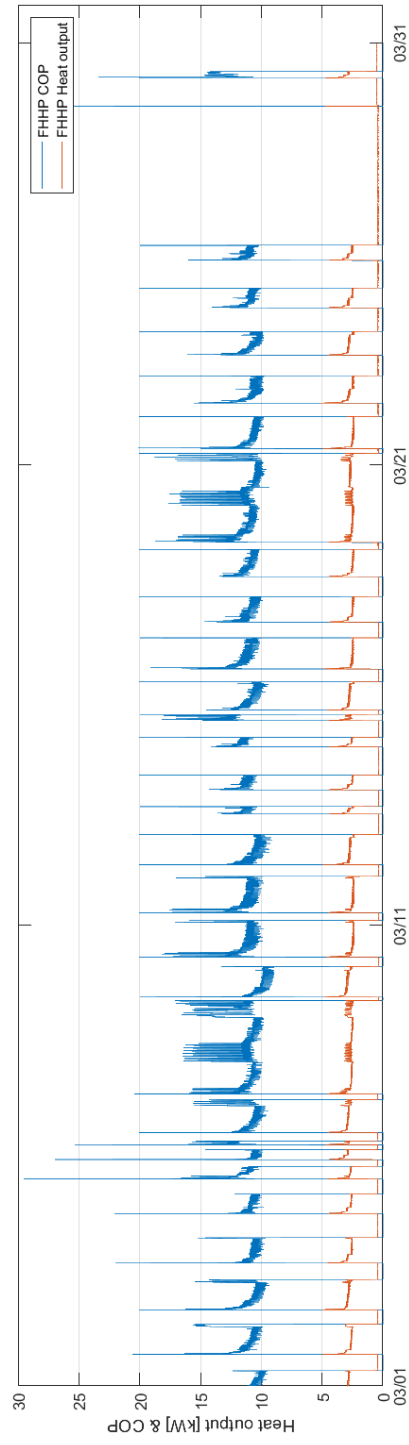


Figure 4. 48 FHHP performance in March

#### *4.4.4 Summary of winter field testing*

To the evaluation of the system performance, a winter field experiment was carried out under different weather conditions in Chiba, Japan. Based on a comparative experimental analysis of the performance of the heat pump system under different weather conditions, several conclusions were reached. Firstly, the custom-made heat pump for floor heating (FHHP) maintained a stable operation with a coefficient of performance (COP) of  $\sim 11.5$  during the heating period. However, the performance of the FHHP increased as the temperature of the circulating water increased, and so it is apparent that there is still room for improving the performance by adjusting the circulating water temperature. In addition, the operation of the sky-source heat pump (SSHP) had a positive effect on the recovery of the soil temperature; however, the performance of the SSHP varied significantly with changes in the quantity of solar radiation and on the outside temperature. The operating schedule of the SSHP should, therefore, be optimized based on the weather conditions to achieve a continuous high-efficiency operation. Finally, since SSHP improves the COP of the overall system, and aids in the recovery of the soil temperature, optimization of the operating method to enhance the performance of the whole system is necessary[1–3,5,6].

## **4.5 Summer experimental results and analysis**

As representative examples of space cooling operation, the space cooling performance of this system will be evaluated based on the measurement results of 24 to 26 July 2018.

Since the cooling load would increase due to the increase in outside temperature and solar radiation in the summer, and it would be necessary to turn on the cooling, the cooling operation started from around noon. The details of the building and equipment are the same as the winter field testing described in the last chapter.

The SSHP and GHX were used as a heat source device, and an air conditioning water source heat pump (ACHP) operated as a cooling device. A hot water heat pump (HWHP) also served to check the performance.

### *4.5.1 Operation status analysis of water source heat pump for air conditioning*

The results of the ACHP cooling operation from 24<sup>th</sup> to 25<sup>th</sup> July (cooling set temperature 27 °C) are shown in Figure 4. 50 to Figure 4. 52. Figure 4. 49 shows the weather condition on 24<sup>th</sup> July, which is a typical summer afternoon. The dry bulb temperature was around 30 °C, and because the testing started from noon with a value of approximately 900 kW/m<sup>2</sup>, so the solar radiation decreased with the time. As shown in Figure 4. 50 and Figure 4. 51, from 12:30 to 17:00, ACHP cools the room, and GHX stores heat in the soil by using the ground as a heat storage body. The COP showed a high COP of about 20 immediately after the ACHP started operating, but then gradually decreased, and became stable after 2.5 hours at about 10. After that, as shown in Figure 4. 52, the room temperature was steady at about 27 °C. From the operation results, it can be seen that the experimental conditions remained flat, and the indoor space was obtained stably. During the cooling operation, the cooling capacity of ACHP was about 6 kW, the power consumption was 0.48 kW, and the average period COP was about 12.5.

Figure 4. 52 shows the changes in indoor air temperature during the ACHP space cooling operation. Since the start of the ACHP operation, the indoor temperature has gradually decreased. After about 2 hours and 30 minutes, the indoor temperature dropped from 33 °C to 27 °C. This temperature meets the indoor comfort temperature standard set by Japan in summer, so this result proves the excellent performance of ACHP, which can meet the indoor temperature requirements under high-efficiency operation.

### *4.5.2 Operation status analysis of sky source heat pump for cooling*

Figure 4. 53, Figure 4. 54, and Figure 4. 55 show the results of the nighttime heat dissipation operation of SSHP. As shown in Figure 4. 53, SSHP started heat dissipation operation from 12:00 am. During the heat dissipation period, the refrigerant condenses in the refrigerant passage of the outdoor panel, the temperature of the panel gradually rises, and heat is radiated to the sky and ambient are by the convection and long-wave radiation.

During this period, the heat dissipation operation of SSHP eliminates the heat accumulated in the

ground due to the space cooling operation of the previous day and recovers the temperature rise in soil. After about 30 minutes, the panel temperature became higher than the outside air temperature by nearly 10 °C. The condensing temperature of the refrigerant was slightly higher than the panel temperature. The high COP of heat dissipation operation immediately after startup is considered to be due to the heat capacity of the panel. During the stable operation period, after 30 minutes, the circulating water cooling amount was maintained at about 4 kW. The maximum heat dissipation operation COP of SSHP reached about six from the start of the operation. Still, the average COP of heat dissipation operation became about five after a stable operation.

As shown in Figure 4. 54 and Figure 4. 55, we found that the refrigerant evaporating temperature fluctuated during the heat dissipation operation of SSHP. Regarding the reason, the refrigerant piping distance from the SSHP outdoor panel to the drainer was too long (about 4 meters). It is conceivable that the liquid and gas refrigerant separated during the process, causing hunting of the refrigerant flow rate due to sudden opening and closing of the drainer, that is, unstable operation occurred. As a result, the heat output of the heat pump oscillated, and the refrigerant circulation amount became insufficient compared to the design value.

The difference between the evaporation temperature and the water loop circulating water outlet temperature became 10 °C at maximum (ideally 2 °C or less). We think that one of the countermeasures against this problem is to adopt an electronic expansion valve capable of PID control instead of a mechanical drainer in the future.

This electronic expansion valve controls the degree of supercooling at the outlet of the condenser, not the conventional control of superheat at the outlet of the evaporator. After conducting a simple prototype experiment, a problem remains regarding the optimization of control variables such as the degree of supercooling, although it is functionally promising. Such an expansion valve has the advantage of better load followability than the mechanical expansion mechanism, and not only enhances the stability of control but also has the advantage of downsizing the refrigerant parts.

### *4.5.3 Operation status analysis of water source heat pump for domestic hot water supply*

Figure 4. 56 shows the operation results of HWHP. From 22:00 to 23:00, the geothermal heat

exchanger takes heat from the ground and supplies heat to the HWHP. This heat extraction contributes to the elimination of the heat stored in the ground. The vibration every 30 minutes was caused by water temperature sampling by SSHP. The heating output during the stable operation was maintained at about 4 kW, and the average period COP was about 3.8.

As explained in the previous chapter, the HWHP got a COP of about 5.5 when we tested the performance of the prototype at the factory. Because of the performance limitations of EcoCute itself, the experimental results obtained in this experiment are within a reasonable range. We think that there may be a performance bonus through the use of instant-heating hot water heat pumps based on the previous study[11–14].

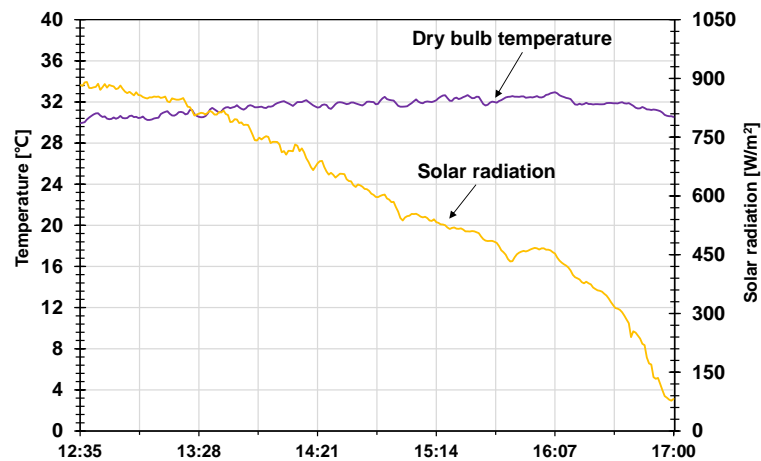


Figure 4. 49 Weather condition on 24<sup>th</sup> July.

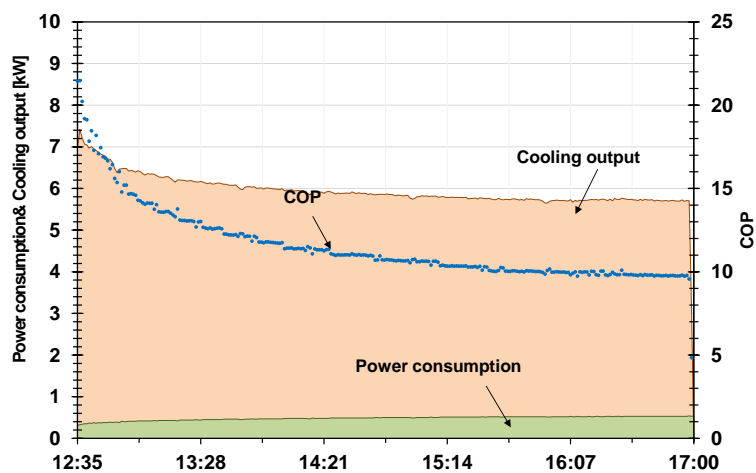


Figure 4. 50 Temporal change of ACHP performance on 24<sup>th</sup> July.

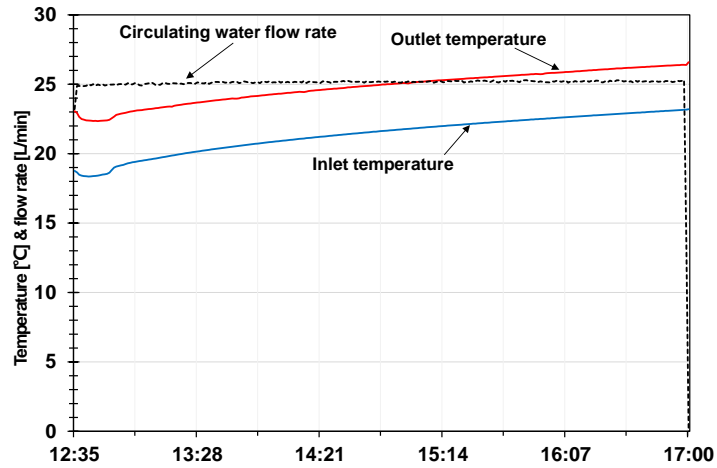


Figure 4. 51 Temporal change of ACHP performance on 24<sup>th</sup> July.

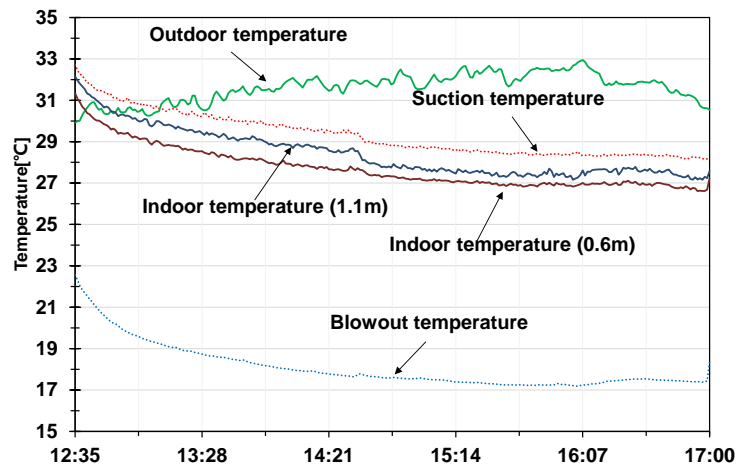


Figure 4. 52 Indoor temperature change during cooling operation on 24<sup>th</sup> July.

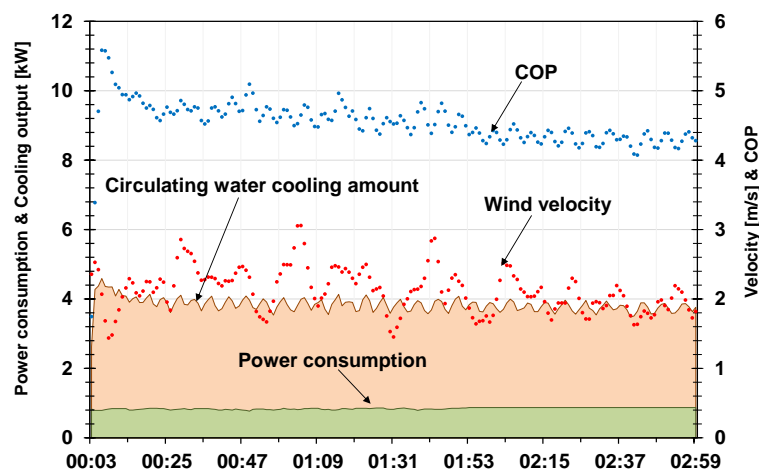


Figure 4. 53 Temporal change of SSHP heat dissipation performance during the 24<sup>th</sup> night.

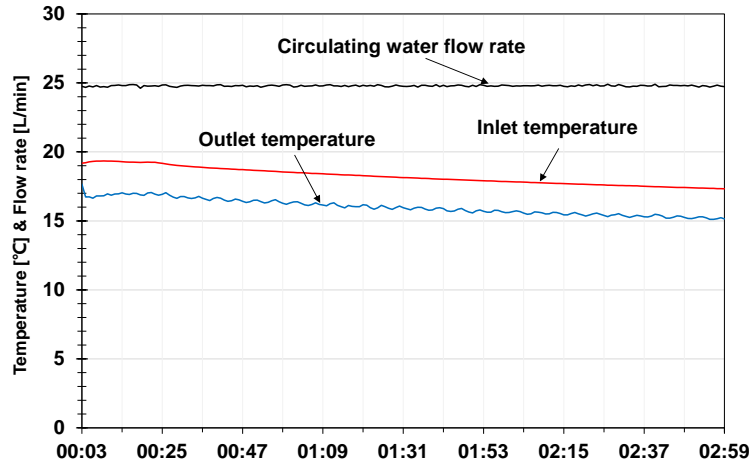


Figure 4. 54 Temporal change of SSHP heat dissipation performance during the 24<sup>th</sup> night.

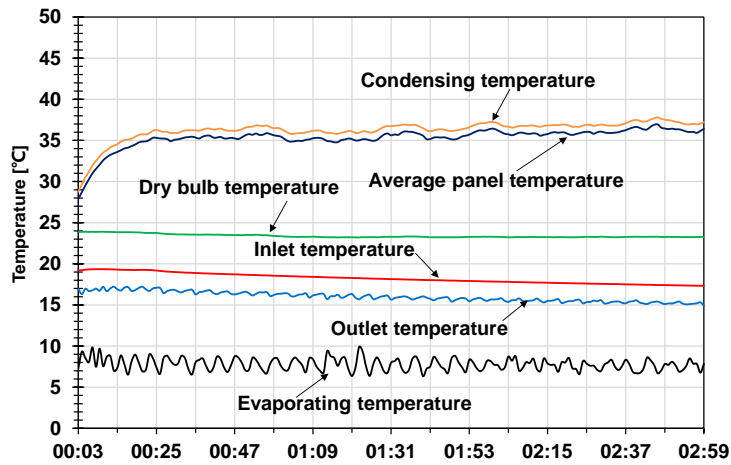


Figure 4. 55 Temperature transition of outdoor panel during heat dissipation operation.

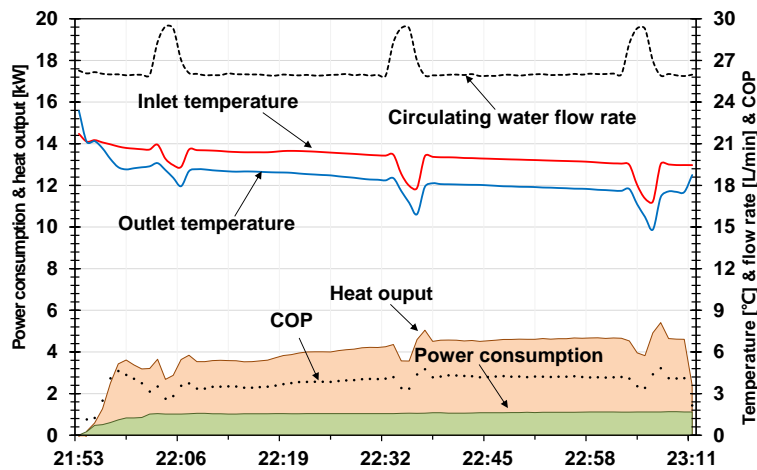


Figure 4. 56 Temporal change of HWHP performance on 24<sup>th</sup> July.

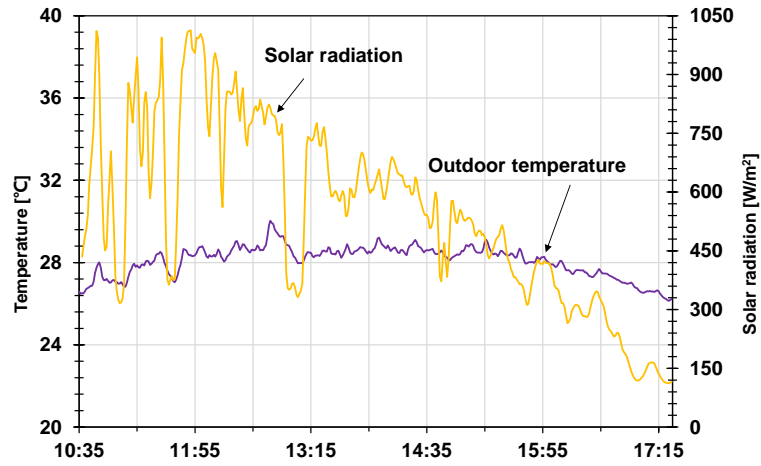


Figure 4. 57 Weather condition on 25<sup>th</sup> July.

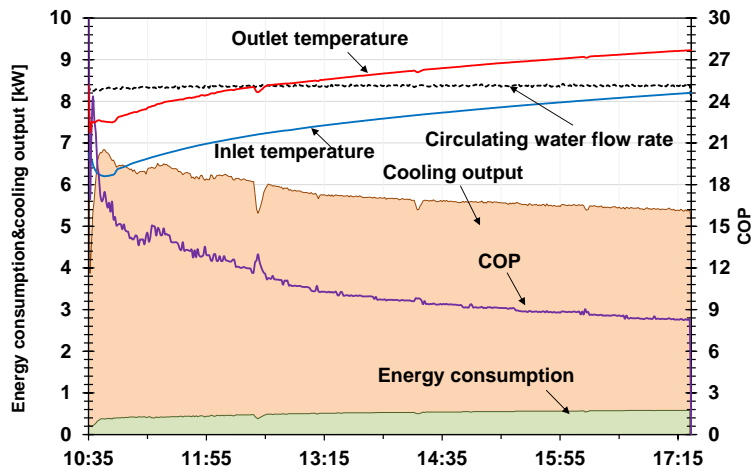


Figure 4. 58 Temporal change of ACHP performance on 25<sup>th</sup> July.

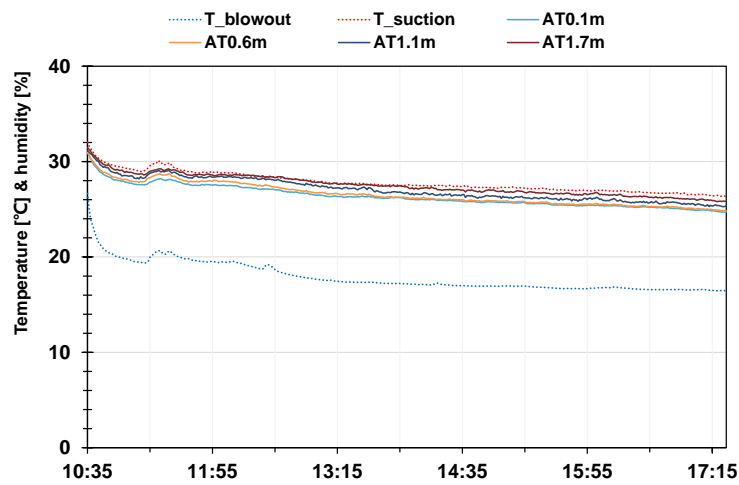


Figure 4. 59 Indoor temperature change during cooling operation on 25<sup>th</sup> July.

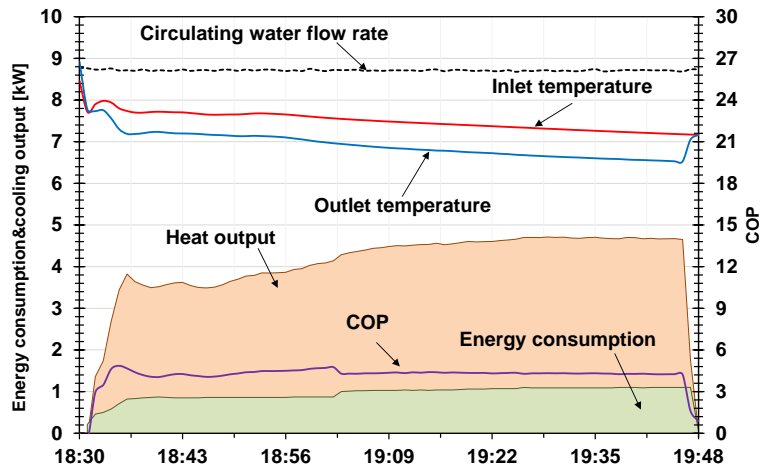


Figure 4. 60 Temporal change of HWHP performance on 25<sup>th</sup> July.

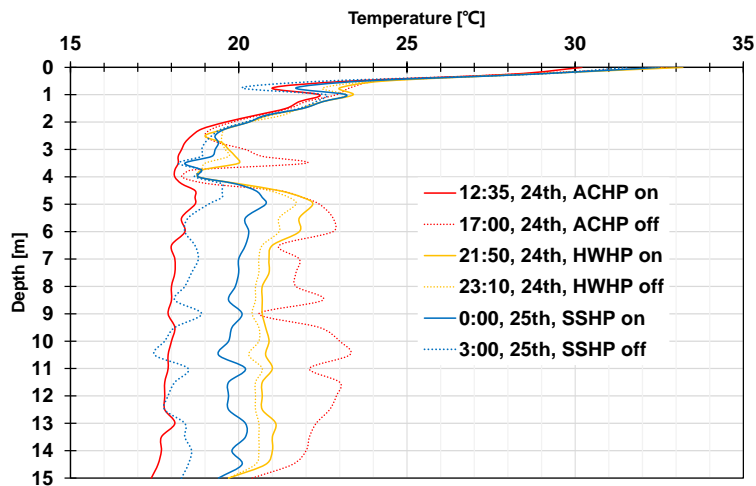


Figure 4. 61 Changes in central borehole temperature from 24-25 July.

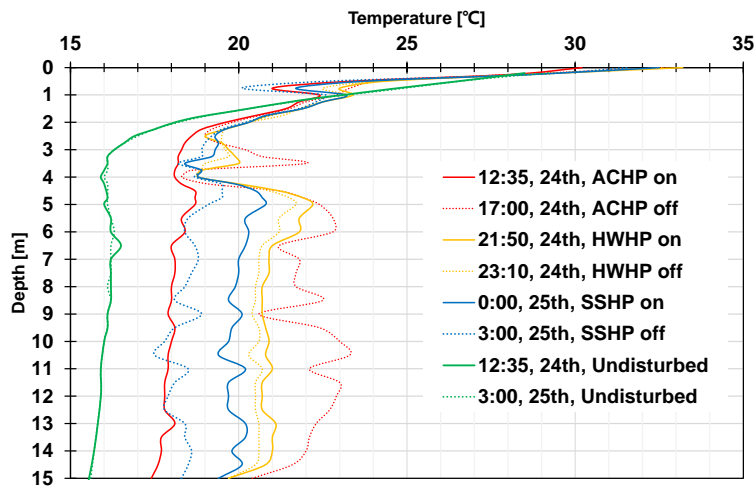


Figure 4. 62 Undisturbed underground and central borehole temperature from 24-25 July.

Figure 4. 57 to Figure 4. 60 show the weather conditions and operation result on the 25 July. During this operation, the SSHP didn't run because of a machine error. The ACHP and HWHP operation condition was the same as the day before, and the weather condition was almost the same. Therefore, as shown in Figure 4. 58 to Figure 4. 60, we can know that the performance of ACHP and HWHP kept the same high performance represented by COP as the 24 July.

For the indoor air temperature results, as shown in Figure 4. 59, the indoor temperature reached a stable value after about 3 hours of operation that meets the standard by Japan. This result indicated that the performance of ACHP maintained the same as 24 July. For the effect of HWHP, there was no apparent difference between the COP on 24 and 25 July. Because the tap water temperature was the same in both typical days, which is the heat source water, so the performance of HWHP didn't change too much.

#### *4.5.4 Summary of summer field testing*

For the evaluation of the entire system in the summer experiment, the performance is evaluated using the same system COP as the winter experiment. In the summer experiment, however, the heating and cooling heat output is the sum of the ACHP and HWHP heat outputs, and the power consumption is the sum of both. Table 4. 5 and Table 4. 6 shows the COP of each device and the COP of the entire system. Figure 4. 63 shows the cooling operation performance on 24–25 July because the operation of SSHP was also included on 24 July. The system COP on 24-25 July was 5.3 based on the integrated value for one day. For the experiment on 25-26 July, the system COP was 9.5 includes only the ACHP and HWHP. However, the heat dissipation operation is essential because it helps recover the soil temperature, which is a promise for long-term and efficient operation. For the performance of SSHP, the average COP was 4.5, which was lower than the winter heat collection operation. For the air conditioning machine, the ACHP achieved excellent performance for space cooling in summer, which got a COP of about 12 on average. For the HWHP, however, the result showed a typical performance result due to the limitation of the basic EcoCute machine.

Table 4. 5 Results of the performance test of the whole system in summer. (24<sup>th</sup> -25<sup>th</sup> July)

	Heat output[kWh]	Energy consumption [kWh]	COP
SSHP	11.3	2.5	4.5
GHX	13.1		
ACHP	26.3	2.1	12.5
HWHP	5	1.3	
System	31.3	5.9	5.3

Table 4. 6 Results of the performance test of the whole system in summer. (25<sup>th</sup> -26<sup>th</sup> July)

	Heat output[kWh]	Energy consumption [kWh]	COP
GHX	35.5		
ACHP	39.5	3.5	11.3
HWHP	5.2	1.2	4.3
System	44.7	4.7	9.5

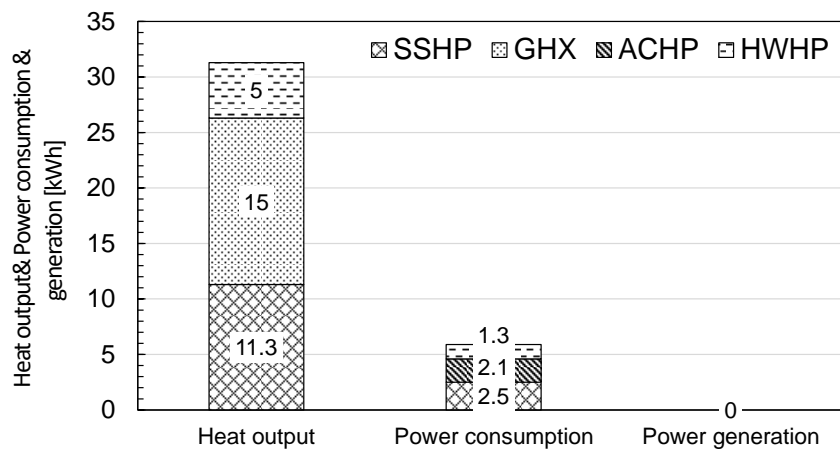


Figure 4. 63 Cooling operation performance on 24–25 July.

## 4.6 Interim period experimental results and analysis

### *4.6.1 Operation status analysis of water source heat pump for air conditioning*

As representative examples of space heating operation, the space cooling performance of this system will be evaluated based on the measurement results of 13 November 2018, which is also the so-called interim period for air conditioning.

Since the cooling load would increase due to the increase in outside temperature and solar radiation in November, and it would be necessary to turn on the space heating. Therefore, the cooling operation started from around the afternoon. The details of the building and equipment are the same as the winter field testing described previously.

During this experiment period, the SSHP and GHX were used as a heat source device, and the air conditioning water source heat pump (ACHP) operated as a space heating device. The floor heating was also turned on at the same time, but we only analyzed the ACHP for evaluation of its space heating performance, and the evaluation of FHHP was already conducted in the winter operation.

Figure 4. 64, Figure 4. 65, Figure 4. 66, and Figure 4. 67 shows the experimental result of the space heating operation on 13 November. As shown in Figure 4. 64, the dry bulb temperature was around 13 °C, which is a typical autumn temperature in Chiba, there was also no enough solar radiation due to the cloud. The temporal change of ACHP space heating performance is shown in Figure 4. 65, within 20 minutes after the machine started running, ACHP achieved a higher COP due to the higher circulating water temperature and lower indoor air temperature. Over time, the performance of ACHP for space heating is gradually stable. In the smooth operation stage, ACHP maintains a heat output of about 4.5KW, and the COP is steady at about 6.5.

Figure 4. 66 shows the temporal change of SSHP heat collection performance on 13 November. Similarly, there was an increase of COP at the starting period of the SSHP operation. Over time, the performance of the SSHP gradually stabilized. During the smooth operation phase, the SSHP maintained a heat output of approximately 5 kW, and the COP stabilized at around 12. Because there is no solar radiation during this period, SSHP mainly draws heat from the surrounding air, which

can be regarded as similar to an air source heat pump.

Figure 4. 67 shows the Indoor temperature change during the space heating operation on 13 November. It can be seen from the figure that the indoor temperature starts at 19 °C, and the ACHP blowing temperature is about 35 °C. As the indoor temperature gradually increases, the blowing temperature of ACHP also increases, because ACHP maintains a stable heat output. At the end of the operation, the indoor temperature reached approximately 25 °C.

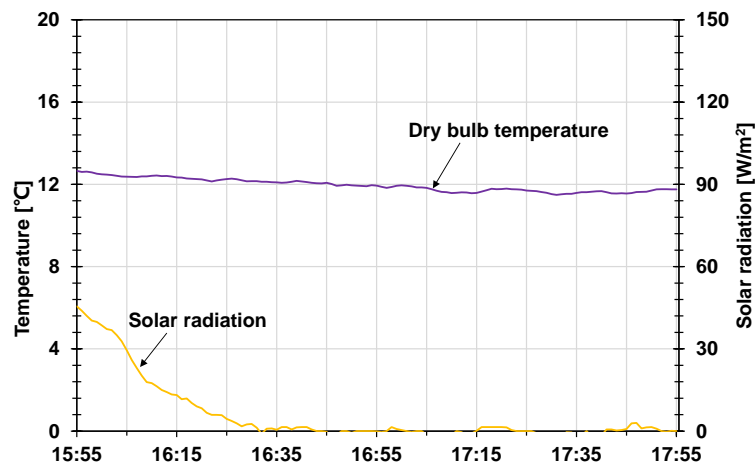


Figure 4. 64 Weather condition on 13 November.

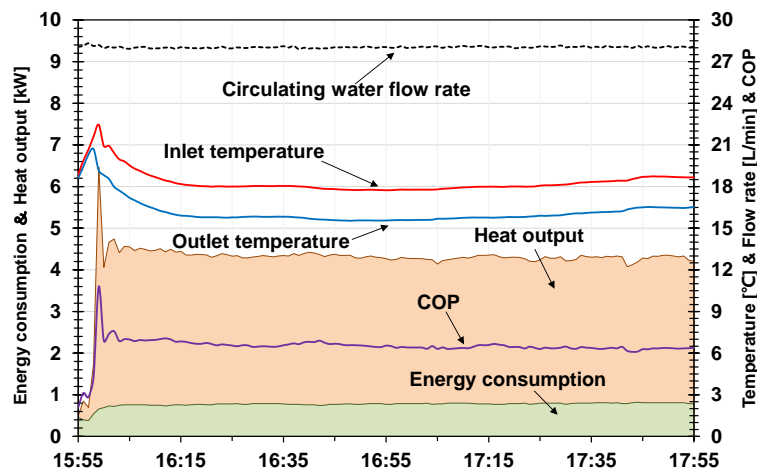


Figure 4. 65 Temporal change of ACHP space heating performance on 13 November.

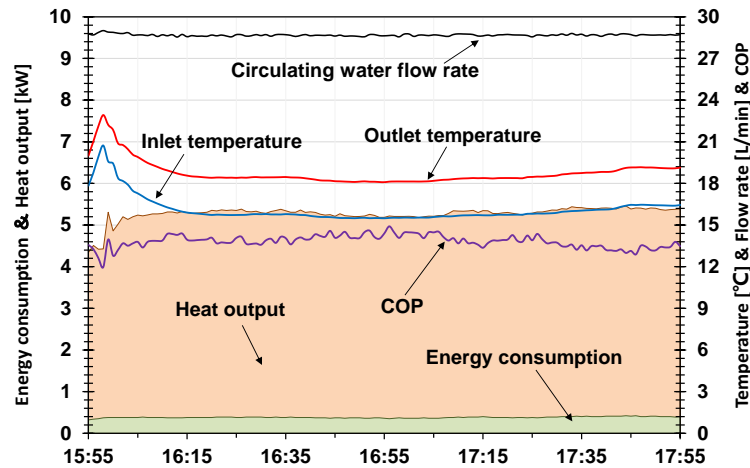


Figure 4. 66 Temporal change of SSHP heat collection performance on 13 November.

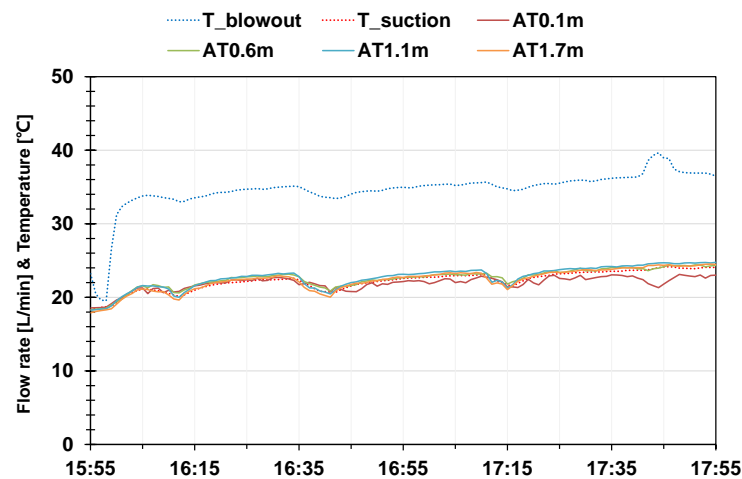


Figure 4. 67 Indoor temperature change during the space heating operation on 13 November.

### *Summary of interim period field testing*

To evaluate the entire system in the middle period, we use the same system COP as the summer/winter experiment to evaluate the performance. For the experiment on November 13, the average COP of the heat collection operation of the SSHP on cloudy days (without solar radiation and an average dry bulb temperature of 12 °C) was 13. This performance was higher than the heat collection operation on cloudy days in winter (21 March with an average dry bulb temperature of 2 °C) in terms of performance of the SSHP Performance. We think that the reason is because of the higher dry bulb temperature in November. For air conditioning operation in the interim period, the ACHP generally performed in terms of heating in the 13 November. The average COP was about

6.5 and lower than the cooling performance in summer. It is inferred that the reason for the low COP of space heating is that the low pressure (gauge) pressure during heating was 0.84 MPa (saturated vapor pressure temperature 5.3 °C). However, the evaporating temperature was expected to be around 12 °C (saturated gauge pressure 1.07 MPa) in the plan(as shown in chapter3). We think that this is because the condensate stayed in the air heat exchanger; it indicated that the amount of refrigerant charged was insufficient. To solve this problem, we charged the additional refrigerant, a COP of 8 for space heating of ACHP or more was obtained as a result in later experiments.

## 4.7 Summary

In order to evaluate the system performance of each heat pump and the entire system for heating or cooling supply, a test building (RE house) was constructed for the field testing of the proposed heat pump system. The heating and cooling operation performance evaluations obtained by the field testing are summarized below.

We have developed a sky heat source heat pump that collects and radiates heat using solar heat, air heat, and nighttime radiation. It was confirmed by the field testing that the performance of the heat collection operation of the sky heat source heat pump greatly changed mainly depending on the amount of solar radiation and the ambient temperature. A COP of about 23.2 was achieved on a clear winter day and a COP of about 7.4 on a cloudy day in winter. Although COP was 4.5 for heat dissipation operation at night in summer, it is considered that there is room for performance improvement by adopting an electronic subcooling degree control expansion valve. The average COP of the heat collection operation was 12 on a cloudy day in the interim period because the outside temperature was higher than that of winter. Besides, it was confirmed by a long-term continuous operation test that the daily cycle operation method combined with GHX and SSHP could help eliminates the temporal disagreement between the cold heat demand and the hot heat demand and the non-equilibrium of the heat quantity. It can expect a stable and efficient long-term system operation based on this system.

However, we found that the refrigerant evaporating temperature repeatedly fluctuated during the heat dissipation operation of SSHP. It is conceivable that the liquid and gas refrigerant separated during the process, causing hunting of the refrigerant flow rate due to sudden opening and closing

of the drainer, that is, unstable operation occurred. As a result, the heat output of the heat pump oscillated, and the refrigerant circulation amount became insufficient compared to the design value. We also have developed water source heat pumps for floor heating and air conditioning. After satisfying the thermal comfort range, a stable COP of about 11 of the floor heating heat pump was obtained during the space heating operation in Chiba for one month in March. In a space cooling experiment conducted on 24-26 July under an average temperature of 26.6 °C and a sunshine duration of 7.2 hours, the COP of the air conditioning heat pump was stable and achieved a value of 12.5. In a space heating experiment conducted on 13 November under an average temperature of 12 °C and no solar radiation, the COP of the air conditioning heat pump achieved a value of 6.5. A prototype water source heat pump for hot water supply was developed based on commercial EcoCtue. The performance of the heat pump for hot water supply was evaluated based on field testing in summer. The result shows an average COP of around 4 due to the limitation of the basic EcoCute machine. Based on the previous studies(an average COP of about 8 for instant hot water supply type), we think it is possible to get a higher COP, such as by using an instant hot water supply heat pump.

## 4.8 Reference

- [1] Liu M, Toshiyuki H, Ryozo O, Ke W, Wonjun C, Doyun L, et al. 再生可能エネルギーを利用する分散型マルチソース・マルチユース ヒートポンプシステムの開発 試験建屋の構築及び実測による冷暖房性能評価. 日本建築学会環境系論文集 2020;85:361–70.  
doi:<https://doi.org/10.3130/aije.85.361>.
- [2] Liu M, Ooka R, Hino T, Wen K, Choi W, Lee D, et al. Experimental performance analysis of a multiple-source and multiple-use heat pump system: Winter field experiment and heating operation performance evaluation. E3S Web Conf 2019;111.  
doi:10.1051/e3sconf/201911101076.
- [3] 劉明哲, 大岡龍三, 日野俊之, 文可, 崔元準, 李度胤, et al. 再生可能エネルギー利用のための水循環・分散型ヒートポンプシステムの開発 その14: 夏期運転試験及び運転性能実測. 平成31年度日本建築学会大会, vol. 8, 2019, p. 109–10. doi:10.2504/kds.8.109\_3.
- [4] Hino T, Ooka R. Water-Loop Heat Pump System that Stores Multiple Renewable Energies in the Ground. Proc. EnerSTOCK2018, Adana, Turkey: EnerSTOCK2018; 2018.
- [5] Liu M, Wen K, Hino T, Lee D, Choi W, Ikeda S, et al. 再生可能エネルギー利用のための水循環・分散型ヒートポンプシステムの開発 (第10報) 冬期運転試験及び実測による暖房運転性能評価. 平成30年度空気調和・衛生工学会大会 (名古屋) 学術講演論文集, 2018, p. 9–12.
- [6] 劉明哲, 大岡龍三, 日野俊之, 文可, 崔元準, 李度胤, et al. 再生可能エネルギー利用のための水循環・分散型ヒートポンプシステムの開発 その9: 冬期運転試験及び暖房運転性能の実測. 平成30年度日本建築学会大会, 2018, p. 1327–8.
- [7] Hino T, Ooka R. 地中熱利用と地中蓄熱を統合するシステムのコンセプト. 日本建築学会大会学術講演梗概集, 2018, p. 1337–8.
- [8] Hino T, Ooka R. 多様な再生可能エネルギーを集放熱源とする水ループ式ヒートポンプシステムの構築. 平成29年度空気調和・衛生工学会大会 (高知) 学術講演論文集, 高知: 2017, p. 5–8.
- [9] Hino T, Ooka R. 建物熱供給の将来技術を考える. 平成28年度日本建築学会大会, 2016.
- [10] Exchanger DGH. 二重らせん地中熱交換器の開発. 平成27年度空気調和・衛生工学会大会 (鹿児島) 学術講演論文集, 鹿児島: 2016, p. 129–32.

- [11] Yoshida S, Ooka R, Hino T. マルチソース・マルチユース・ヒートポンプシステムに関する技術開発：第4報-年間運転性能予測シミュレーションによるシステム構成と運用に関する研究. 空気調和・衛生工学会 論文集 2015;40:11–20.  
doi:[https://doi.org/10.18948/shase.40.221\\_11](https://doi.org/10.18948/shase.40.221_11).
- [12] Yoshida S, Ooka R, Hino T. マルチソース・マルチユース・ヒートポンプシステムに関する技術開発：第2報-水熱源空調ヒートポンプの開発と性能検証. 空気調和・衛生工学会 論文集 2015;40:1–10. doi:[https://doi.org/10.18948/shase.40.215\\_1](https://doi.org/10.18948/shase.40.215_1).
- [13] Yoshida S, Ooka R, Hino T. マルチソース・マルチユース・ヒートポンプシステムに関する技術開発：第3報-太陽空気熱源ヒートポンプの試作機における運転特性の確認と性能検証. 空気調和・衛生工学会 論文集 2015;40:9–18.  
doi:[https://doi.org/10.18948/shase.40.217\\_9](https://doi.org/10.18948/shase.40.217_9).
- [14] Yoshida S, Ooka R, Hino T. マルチソース・マルチユース・ヒートポンプシステムに関する技術開発：第1報-水熱源瞬間式給湯ヒートポンプの開発と性能検証. 空気調和・衛生工学会 論文集 2014;39:11–20. doi:[https://doi.org/10.18948/shase.39.208\\_11](https://doi.org/10.18948/shase.39.208_11).

# **Chapter 5: Pressure and temperature analysis of piping system based on CFD**

## 5.1 Introduction

Heating ventilation and air conditioning (HVAC) systems are generally responsible for a large portion of the total building operation energy use in modern cities[1,2]. By optimizing the efficiency of HVAC systems, the overall energy efficiency of buildings can be improved, and substantial reductions in energy use can be achieved[3,4]. Although easy to overlook, the pumping system has a significant impact on the overall energy efficiency of HVAC systems[5]. An essential criterion for the optimal operation of an energy system is the minimization of the costs of operating a fluid transport system, which related to the pressure loss in the piping system. The energy used by the pumps to transport thermal energy into rooms is responsible for a significant portion of the total HVAC energy use[6,7]. Therefore, it is essential to obtain the pressure loss in the pipeline system correctly in different conditions.

Although experiments are the most effective and reliable method for verifying the performance of a new system or system changes under different conditions, model experiments are not always efficient in terms of the considerable time and resources required to build a hydronic system. Numerical simulations of HVAC applications make it possible to design and test a device without manufacturing it[8]. Computational fluid dynamics (CFD) were initially introduced for industrial applications such as pumps and other mechanical designs, and are now used to study the building environment and energy efficiency issues[9].

Based on the previous studies, we confirmed that predicting the pressure loss in an experimental hydronic facility has acceptable accuracy. Therefore, in this chapter, we use the CFD method to predict the pressure loss in the piping system of the RE house, including the ground heat exchanger(GHX).

## 5.2 Fundamentals of computational fluid mechanics

### Conservation of Mass

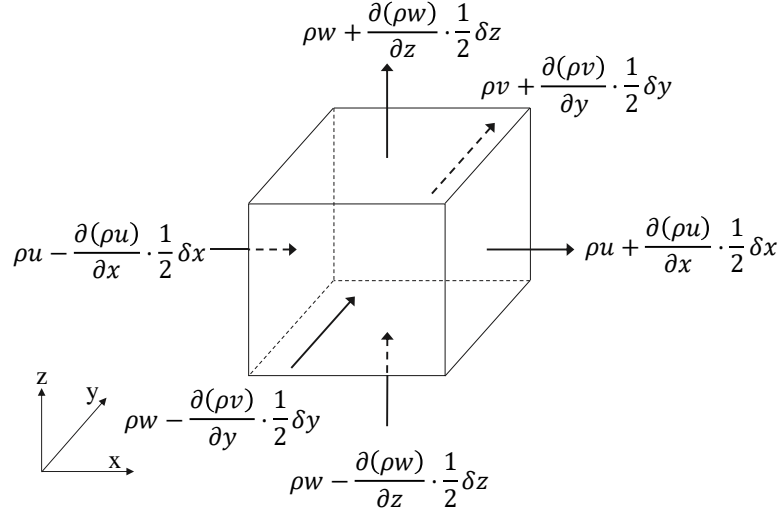


Figure 5. 1 Mass flow at a tiny fluid element.

The mass change rate can be written as follows in consideration of the mass balance of the tiny fluid element.

$$\frac{\partial}{\partial t}(\rho \delta x \delta y \delta z) = \frac{\partial \rho}{\partial t} \delta x \delta y \delta z \quad (1)$$

Consider the mass conservation of a fluid (volume  $\delta V = \delta x \delta y \delta z$ ) in a tiny fluid element whose lengths on each side in the  $x$ ,  $y$ , and  $z$  directions are  $\delta x$ ,  $\delta y$ ,  $\delta z$ . Assuming that it is in the Cartesian coordinate system, the surface of the cube is parallel to the coordinate axes. The conservation of mass within a tiny fluid element indicates that the difference in mass flow in and out of the tiny fluid element is equal to the mass change rate of the tiny fluid element. As shown in Figure 5. 1, the mass flow on the surface of a minute volume can be written as follows.

$$\begin{aligned}
& \left( \rho u - \frac{\partial(\rho u)}{\partial x} \frac{1}{2} \delta x \right) \partial y \partial z - \left( \rho u + \frac{\partial(\rho u)}{\partial x} \frac{1}{2} \delta x \right) \partial y \partial z \\
& + \left( \rho v - \frac{\partial(\rho v)}{\partial x} \frac{1}{2} \delta y \right) \partial x \partial z - \left( \rho v + \frac{\partial(\rho v)}{\partial x} \frac{1}{2} \delta y \right) \partial x \partial z \\
& + \left( \rho w - \frac{\partial(\rho w)}{\partial z} \frac{1}{2} \delta z \right) \partial x \partial y - \left( \rho w + \frac{\partial(\rho w)}{\partial z} \frac{1}{2} \delta z \right) \partial x \partial y
\end{aligned} \tag{2}$$

The following expression (3) can be obtained from equation (1) and (2).

$$\frac{\partial \rho}{\partial t} + \frac{\partial(\rho u)}{\partial x} + \frac{\partial(\rho v)}{\partial y} + \frac{\partial(\rho w)}{\partial z} = 0 \tag{3}$$

Equation (3) is the equation of continuity. It is also called the Euler equations.

For non-compressible fluid: For non-compressible fluid, the density is constant because it does not change. Therefore, when the density is partially differentiated in time and space, it becomes 0.

From this, the equation of continuity for an incompressible fluid is expressed as follows.

$$\frac{\partial(\rho u)}{\partial x} + \frac{\partial(\rho v)}{\partial y} + \frac{\partial(\rho w)}{\partial z} = 0 \tag{4}$$

### ***Conservation of momentum***

The law of conservation of momentum is a physical law in which the sum of momentum in a system is invariant unless an external force is applied to the system. The law of conservation of momentum can be applied to a tiny fluid element, and the formula obtained by this is called the law of conservation of momentum in fluid dynamics. In particular, in the case of the incompressible fluid, it is called the Navier-Stokes equations, which is a critical equation to describe the behavior of the fluid.

Similarly to the case of deriving the continuity equation, we take a tiny fluid element (rectangle or rectangular parallelepiped) in the region and consider the law of conservation of momentum, which leads to the equation of motion.

Consider a fluid particle with length  $\delta x$ ,  $\delta y$ ,  $\delta z$ , and a volume  $\delta V = \delta x \delta y \delta z$ . According to Newton's second law, the temporal change in the momentum of a fluid particle is equal to the sum of the forces acting on it. Fluid forces can be divided into two types: volume forces and surface forces.

Considering the material derivative of the tiny volume element in the fluid to which the target momentum conservation is applied, Newton's second law is expressed by the following equation.

$$dF_i = dm \frac{DU_i}{Dt} = dm \left( \frac{U_i}{\partial t} + U \frac{U_i}{\partial x} + V \frac{U_i}{\partial y} + W \frac{U_i}{\partial z} \right) \quad (5)$$

The stress acting on all surfaces in the x-direction in the fluid element is shown in Figure 5. 2.

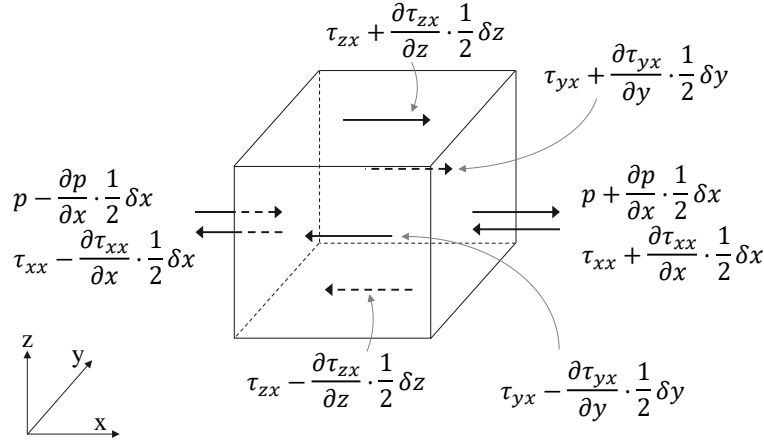


Figure 5. 2 The stress acting on all surfaces in the x-direction.

The stress acting in the x-direction on all surfaces in the fluid element can be expressed by Equation 6 of the momentum balance equation.

$$\begin{aligned} dF_{S_x} &= \left( p - \frac{\partial p}{\partial x} \frac{1}{2} \delta x \right) \delta y \delta z - \left( p + \frac{\partial p}{\partial x} \frac{1}{2} \delta x \right) \delta y \delta z \\ &+ \left( \tau_{xx} + \frac{\partial \tau_{xx}}{\partial x} \frac{1}{2} \delta x \right) \delta y \delta z - \left( \tau_{xx} - \frac{\partial \tau_{xx}}{\partial x} \frac{1}{2} \delta x \right) \delta y \delta z \\ &+ \left( \tau_{yx} + \frac{\partial \tau_{yx}}{\partial y} \frac{1}{2} \delta y \right) \delta x \delta z - \left( \tau_{yx} - \frac{\partial \tau_{yx}}{\partial y} \frac{1}{2} \delta y \right) \delta x \delta z \\ &+ \left( \tau_{zx} + \frac{\partial \tau_{zx}}{\partial z} \frac{1}{2} \delta z \right) \delta x \delta y - \left( \tau_{zx} - \frac{\partial \tau_{zx}}{\partial z} \frac{1}{2} \delta z \right) \delta x \delta y \end{aligned} \quad (6)$$

By calculating Equation 6 of the momentum balance equation, the surface force applied to the fluid element can be described by Equation 7 as follows.

$$dF_{S_x} = \left( -\frac{\partial p}{\partial x} + \frac{\partial \tau_{xx}}{\partial x} + \frac{\partial \tau_{yx}}{\partial y} + \frac{\partial \tau_{zx}}{\partial z} \right) \delta x \delta y \delta z \quad (7)$$

The total volume force  $S_{M_x}$  acting on the unit area of the surface of the tiny fluid element perpendicular to the x-direction per unit time can be represented by the following Expression 8.

$$dF_x = dF_{S_x} + dF_{S_x} = \left( -\frac{\partial p}{\partial x} + \frac{\partial \tau_{xx}}{\partial x} + \frac{\partial \tau_{yx}}{\partial y} + \frac{\partial \tau_{zx}}{\partial z} + S_{M_x} \right) \delta x \delta y \delta z \quad (8)$$

Substituting Equation 8 into Equation 5 using the relational expression of  $dm = \rho \cdot \delta x \delta y \delta z$ , the equation of motion can be written as the following equation.

$$\begin{aligned} \rho \frac{Du}{Dt} &= -\frac{\partial p}{\partial x} + \frac{\partial \tau_{xx}}{\partial x} + \frac{\partial \tau_{yx}}{\partial y} + \frac{\partial \tau_{zx}}{\partial z} + S_{M_x} \\ \rho \frac{Dv}{Dt} &= -\frac{\partial p}{\partial y} + \frac{\partial \tau_{xy}}{\partial x} + \frac{\partial \tau_{yy}}{\partial y} + \frac{\partial \tau_{zy}}{\partial z} + S_{M_y} \\ \rho \frac{Dw}{Dt} &= -\frac{\partial p}{\partial z} + \frac{\partial \tau_{xz}}{\partial x} + \frac{\partial \tau_{yz}}{\partial y} + \frac{\partial \tau_{zz}}{\partial z} + S_{M_z} \end{aligned} \quad (9)$$

### ***Conservation of energy***

The Law of conservation of energy is dealt with in various fields of physics. In particular, the law of conservation of energy in thermodynamics is called the first law of thermodynamics. It is a fundamental law of thermodynamics.

The first law of thermodynamics is recognized as an essential requirement in thermodynamics. It is one of the theorems that should be established in constructing thermodynamic theory. The grounds for establishing the first law are based only on a series of experiments and observations, and in this sense, the first law is a so-called empirical law.

On the other hand, in general mechanics such as Newtonian mechanics and quantum mechanics, the Law of conservation of energy is not always premised.

In the field of fluid mechanics, the energy equation of fluid elements is derived from the first law of thermodynamics and represents the energy conservation of the system. The rate of change of energy content in the tiny fluid element is equal to the sum of the net energy content transferred across the system boundary due to heat transfer and work. Figure 5. 3 shows heat transfer by heat flux.

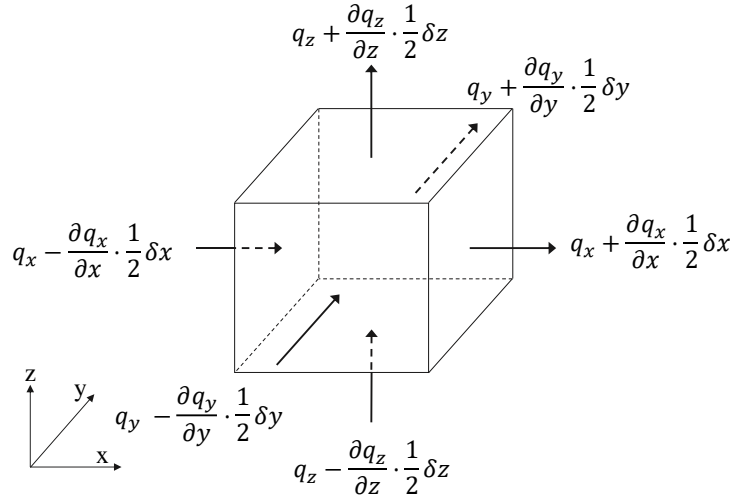


Figure 5. 3 Heat flux at a tiny fluid element.

The heat transfer added to the tiny fluid element by the heat flux in each direction can be described as Equation 10.

$$\begin{aligned}
 W_{h_x} &= \left\{ \left( q_x - \frac{\partial q_x}{\partial x} \frac{1}{2} \delta x \right) - \left( q_x + \frac{\partial q_x}{\partial x} \frac{1}{2} \delta x \right) \right\} \delta y \delta z = -\frac{\partial q_x}{\partial x} \delta x \delta y \delta z \\
 W_{h_y} &= \left\{ \left( q_y - \frac{\partial q_y}{\partial y} \frac{1}{2} \delta y \right) - \left( q_y + \frac{\partial q_y}{\partial y} \frac{1}{2} \delta y \right) \right\} \delta x \delta z = -\frac{\partial q_y}{\partial y} \delta x \delta y \delta z \\
 W_{h_z} &= \left\{ \left( q_z - \frac{\partial q_z}{\partial z} \frac{1}{2} \delta z \right) - \left( q_z + \frac{\partial q_z}{\partial z} \frac{1}{2} \delta z \right) \right\} \delta x \delta y = -\frac{\partial q_z}{\partial z} \delta x \delta y \delta z
 \end{aligned} \tag{10}$$

The total heat transfer per unit volume can be expressed as in Equation 11 below.

$$-\frac{\partial q_x}{\partial x} - \frac{\partial q_y}{\partial y} - \frac{\partial q_z}{\partial z} = -\text{div } q \tag{11}$$

According to Fourier's law, the heat transfer coefficient is related to the thermal conductivity  $k$  and

the temperature gradient, so  $q$  is expressed as follows.

$$q = -k \frac{\partial T}{\partial x} - k \frac{\partial T}{\partial y} - k \frac{\partial T}{\partial z} = -k \text{ grad } T \quad (12)$$

Also, Equation 11 can be written as Equation 13 below.

$$-\text{div } q = \text{div}(k \text{ grad } T) \quad (13)$$

Since the work acting on the surface of the fluid element is equal to the product of the force and the velocity in the direction of the force, the work acting on the fluid element can be calculated by the following equation (14).

$$\begin{aligned} W_x &= \left( -\frac{\partial(up)}{\partial x} + \frac{\partial(u\tau_{xx})}{\partial x} + \frac{\partial(u\tau_{yx})}{\partial y} + \frac{\partial(u\tau_{zx})}{\partial z} \right) \delta x \delta y \delta z \\ W_y &= \left( -\frac{\partial(vp)}{\partial y} + \frac{\partial(v\tau_{xy})}{\partial x} + \frac{\partial(v\tau_{yy})}{\partial y} + \frac{\partial(v\tau_{zy})}{\partial z} \right) \delta x \delta y \delta z \\ W_z &= \left( -\frac{\partial(wp)}{\partial z} + \frac{\partial(w\tau_{xz})}{\partial x} + \frac{\partial(w\tau_{yz})}{\partial y} + \frac{\partial(w\tau_{zz})}{\partial z} \right) \delta x \delta y \delta z \end{aligned} \quad (14)$$

### ***Reynolds averaged model***

In this simulation, we used the realizable  $k-\varepsilon$  model. Therefore the principle of the Reynolds averaged model and the realizable  $k-\varepsilon$  model, which is one of the Reynolds averaged model, will be mainly described here.

The Reynolds-Averaged Navier-Stokes equation or Reynolds Averaged Numerical Simulation (RANS) is a general term for turbulent flow analysis methods that perform calculations based on the time-averaging of the Navier-Stokes equations and the continuity equation. Therefore, it is also called the “time averaging model” sometimes.

A model that uses the Reynolds averaging is called a Reynolds averaging model or RANS model.

There are two types of modeling, one for modeling the Reynolds stress of the RANS equation and the other for modeling the Reynolds stress transport equation. It is a kind of turbulence model.

Since the RANS model models large-scale turbulence, it is considered that the RANS model is also modeled, including the conditions of the analysis target referenced for modeling. Hence, it is difficult for it to be general-purpose.

Therefore, various models have been proposed according to the analysis target. Due to the nature of Reynolds averaging, steady calculation and two-dimensional calculations are possible, and it is generally used in the engineering field due to its ease of use. Still, it is not suitable for reproducing detailed unsteadiness of flow.

### ***Standard k-ε model***

The standard *k-ε* model developed by Launder and Spalding is one of the most widely applied models due to its simple form, robust performance, and broad validation[10].

$$v_t = C_\mu \frac{k^2}{\varepsilon} \quad (15)$$

Here,  $C_\mu$  is a constant. The transport equation of  $k$  is expressed by the following equation 16. The transport equation of  $\varepsilon$  is represented by the following equation 17.

$$\frac{\partial(\rho k)}{\partial t} + \frac{\partial(\rho k u_i)}{\partial x_i} = \frac{\partial}{\partial x_j} \left[ \left( \mu + \frac{\mu_t}{\sigma_k} \right) \frac{\partial k}{\partial x_j} \right] + G_k + G_b - \rho \varepsilon - Y_M + S_k \quad (16)$$

$$\begin{aligned} \frac{\partial(\rho \varepsilon)}{\partial t} + \frac{\partial(\rho \varepsilon u_i)}{\partial x_i} \\ = \frac{\partial}{\partial x_j} \left[ \left( \mu + \frac{\mu_t}{\sigma_\varepsilon} \right) \frac{\partial \varepsilon}{\partial x_j} \right] + C_{1\varepsilon} \frac{\varepsilon}{k} (G_k + G_{3\varepsilon} G_b) - C_{2\varepsilon} \rho \frac{\varepsilon^2}{k} + S_\varepsilon \end{aligned} \quad (17)$$

Here,

$G_k$ : Turbulent kinetic energy generation term due to mean velocity gradients

$G_b$ : Turbulent kinetic energy generation term due to the buoyancy effects

$Y_M$ : Contribution of expansion fluctuation to dissipation rate incompressible turbulence

$C_{1\varepsilon}$ ,  $C_{2\varepsilon}$ ,  $C_{3\varepsilon}$ : constants

$\sigma_k$ ,  $\sigma_\varepsilon$ : Turbulent Prandtl number of  $k$  and  $\varepsilon$

$S_k$ ,  $S_\varepsilon$ : Source term

Although the standard  $k$ - $\varepsilon$  model is applied to a wide range of engineering fields, it cannot be a general-purpose model because it is a RANS model. Hence, various improved models have been proposed based on the standard  $k$ - $\varepsilon$  model.

The standard  $k$ - $\varepsilon$  model is a relatively easy model to use in engineering because it does not require parameters such as length scale. It is necessary to specify the values of  $k$  and  $\varepsilon$  as initial values and inflow conditions, and it is essential to estimate some value. The turbulence intensity  $I$  is defined by the following equation, where  $U$  is the representative velocity of the average flow.

$$I = \frac{u'}{U} \quad (18)$$

This is the ratio of flow to average flow, which is a few percent for fully developed flows. The following equation estimates the  $k$ .

$$k = \frac{3}{2}(UI)^2 \quad (19)$$

The following equation is used to estimate  $\varepsilon$ .

$$\varepsilon = \frac{C_\mu^{3/4} k^{3/2}}{l_m} \quad (20)$$

It is necessary to give the mixing length  $l_m$ , which can be estimated by the following equation in a fully developed flow.

$$l_m = 0.07L \quad (21)$$

Here,  $L$  is a representative length. The hydraulic diameter is used as the representative length in the duct flow. If the hydraulic diameter is  $D$ , the cross-sectional area is  $A$ , and the cross-section perimeter is  $l$ , then  $D=4 A / l$ . In a circular cross-section,  $D$  is the diameter of the circle.

### **Realizable $k$ - $\varepsilon$ model**

The Realizable  $k$ - $\varepsilon$  model is a model in which physical realizability is considered so that  $k$  and the like do not take negative values. It is effective for flows with curvature and swirl[11].

The equation of the Realizable  $k$ - $\varepsilon$  model is as follows.

$$\frac{\partial k}{\partial t} + \frac{\partial k \bar{u}_j}{\partial x_j} = P_k - \varepsilon + D_k \quad (24)$$

$$\frac{\partial \varepsilon}{\partial t} + \frac{\partial \varepsilon \bar{u}_j}{\partial x_j} = \frac{\varepsilon}{k} C_{\varepsilon 1} P_k - C_{\varepsilon 2} \frac{\varepsilon^2}{k + \sqrt{\nu \varepsilon}} + D_\varepsilon \quad (25)$$

Here,

$$C_{\varepsilon 1} = \max \left( 0.43, \frac{\eta}{\eta + 5} \right) \quad (26)$$

$$\eta = \frac{k}{\varepsilon} \sqrt{2 \bar{D}_{ij} \bar{D}_{ij}} \quad (27)$$

The turbulent viscosity coefficient is modeled as in Equation 28.

$$\nu_t = C_\mu \frac{k}{\varepsilon} \quad (28)$$

$$C_\mu = \frac{1}{A_0 + A_s \frac{k U^*}{\varepsilon}} \quad (29)$$

$$U^* = \sqrt{\bar{D}_{ij} \bar{D}_{ij} + \bar{\Omega}_{ij} \bar{\Omega}_{ij}} \quad (30)$$

$$\bar{\Omega}_{ij} = \frac{1}{2} \left( \frac{\partial \bar{u}_i}{\partial x_j} - \frac{\bar{u}_j}{\partial x_i} \right) \quad (31)$$

$$A_s = \sqrt{6} \cos \varphi \quad (32)$$

$$\varphi = \frac{1}{3} \arccos(\sqrt{6}W) \quad (33)$$

$$W = \min \left[ \max \left( 2\sqrt{2} \frac{\bar{D}_{ij}\bar{D}_{jk}\bar{D}_{ik}}{(\bar{D}_{ij}\bar{D}_{ij})^{\frac{3}{2}}}, -\frac{1}{\sqrt{6}} \right), \frac{1}{\sqrt{6}} \right] \quad (34)$$

Each constant is as follows.

$$\sigma_k=1 \quad \sigma_\varepsilon=2 \quad C_{\varepsilon 2}=1.9 \quad A_0=4.0$$

## 5.3 Previous study of gauge pressure and pressure drop analysis in piping system based on CFD method

### 5.3.1 Simulation objectives and method

#### Simulation target

In the previous study[12], we used the CFD method to predict the pressure loss in an experimental hydronic apparatus(as described in the construction of the water loop system, chapter3). A three-dimensional computational model of the flow path was created based on the piping system used in the hydronic experiments; the scale of the computational model was generally similar to that of the real experimental conditions. The accuracy of the CFD analysis-based prediction of the piping system pressure was evaluated by comparing the experimental and CFD results.

Two cases were established to evaluate the accuracy of the CFD-predicted pressure in the hydronic system. Case A represents the centralized pumping system with constant pressure control, and Case

B represents the decentralized pumping system. The arrangement of the model in Cases A and B correspond to the flow path and conditions of experimental Cases 1 and 2.

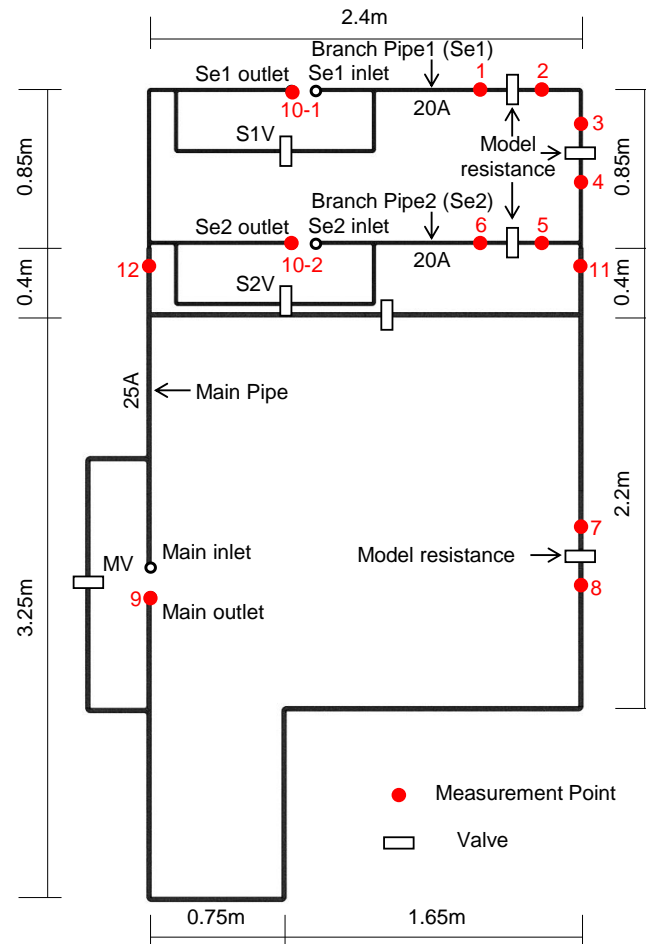


Figure 5. 4 Schematic of the computational model showing the target apparatus.

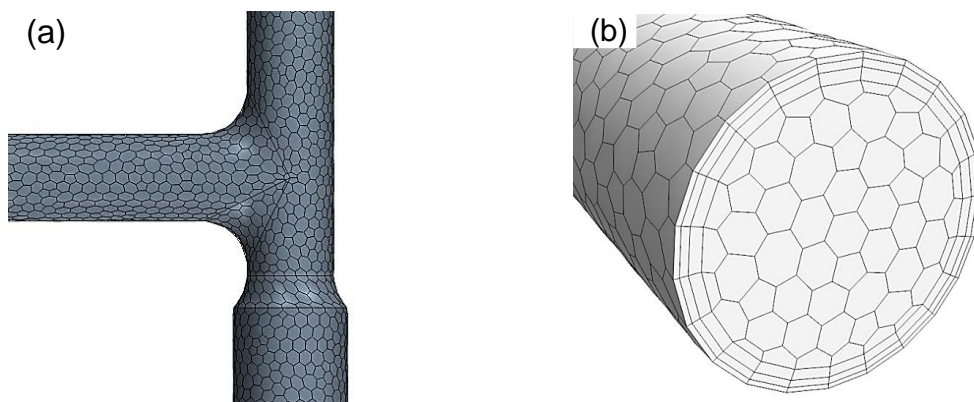


Figure 5. 5 Schematics of the computational model: (a) combination of concentric reducer and equal tee; (b) views of the computational grid (polyhedral mesh and prism layer mesh)

### Simulation conditions

The commercial software STAR-CCM+[13] was used. As mentioned above, the three-dimensional computational model of the flow path had to be consistent with the actual experimental conditions, so the diameter of the main pipe was set to 26.58 mm, and the diameter of the branch and bypass pipes was set to 20.22 mm to match the inner diameter of these pipes in the experiments. To improve the calculation speed without reducing accuracy, different mesh sizes were used in straight pipe sections and in special parts such as elbows and tee joints. The reference mesh size in straight pipe sections was 0.01 m and in elbow and tee joints was 0.003 m. Besides, as shown in Figure 5. 5, the combination of polyhedral mesh and prism layer mesh was used in this simulation.

Table 5. 1 Summary of boundary and initial conditions.

Type of flow		Incompressible flow (water)
Fluid density		998 kg/m <sup>3</sup>
Inlet boundary condition	Case A	Main inlet: 0.78 m/s (velocity inlet) Turbulence intensity: 0.05 Turbulence length scale: 0.001
	Case B	Se1 & Se2 branch inlets: 0.67 m/s (velocity inlet) Turbulence intensity: 0.05 Turbulence length scale: 0.001
Outlet boundary condition	Case A	Main outlet: 4.6 kPa (pressure outlet)
	Case B	Se1 outlet: 4 kPa (pressure outlet) Se2 outlet: 3.5 kPa (pressure outlet)
Wall boundary		Generalized logarithmic law Rough wall surface ( $k_s = 0.00005$ m)

### Case settings

Two CFD simulations were conducted: (1) a centralized system with constant pressure control, which was Case 1 in the experiments; and (2) a decentralized system with inverter control, which was Case B in the experiments. In both cases, the flow rate was set to 26 L/min in the main pipe and 13 L/min in each branch pipe, and the virtual resistances were set at the same values. The difference between these two cases is that they have different flow paths; the inlet velocity of the two cases is not the same because of the different inlet diameters. The detailed setting is shown in Table 5. 1.

### 5.3.2 Results and discussions

#### Gauge pressure at measuring point

As mentioned earlier, the scale of the computational model in this simulation was the same as in the real equipment; therefore, the results can be used to assess the validity of CFD in simulating the pressure of real hydronic systems.

Table 5. 2 shows the comparison between numerically simulated and experimentally measured gauge pressures in the flow path for Cases A and B. The numbers indicate the same locations shown in Figure 5. 4, and negative values indicate that the numerically simulated gauge pressure was less than the measured result. Table 5. 2 indicates that the results are generally in good agreement, with very small differences, all less than 10%.

In Case A, the maximum discrepancy between the CFD results and experimental results was 6.1% at Point 12, just before the reducing tee. In modeling the pipe tee, a variable diameter tee was replaced by a combination of a concentric reducer and equal tee. This structural change may have caused the relatively high discrepancy at this point. Therefore, the variable diameter tee should be studied in more detail. The other points exhibited a discrepancy of 5% or less. In Case B, the maximum discrepancy between the simulated and measured values was 7.2% at Point 7, which is before the virtual resistance arranged in the main return pipe. For other points, the CFD results and experimental results are in good agreement, with discrepancies of less than 5%.

Table 5. 2 Comparison of gauge pressure between CFD and experiment (discrepancy of CFD model against experimental results is given in parentheses)

Measurement point <sup>+</sup>	Case A		Case B	
	Experiment [kPa]	CFD [kPa]	Experiment [kPa]	CFD [kPa]
1	18.3	17.7 (-3.3%)	18.6	18.9 (+1.6%)
2	14.2	13.5 (-5.0%)	14.3	14.6 (+2.1%)
3	14.0	13.3 (-5.0%)	14.1	14.4 (+2.1%)
4	12.6	12.2 (-3.2%)	12.2	12.8 (+4.9%)
5	12.3	12.0 (-2.4%)	12.3	12.6 (+2.4%)

6		16.9	16.7 (-1.2%)	16.9	17.0 (+1.0%)
7		11.0	11.2 (+1.8%)	11.1	11.9 (+7.2%)
8		6.5	6.3(-3.0%)	6.8	7.1(+4.4%)
9		4.6	4.6* (0%)	N/A <sup>2</sup>	N/A <sup>2</sup>
10	10-1	N/A <sup>1</sup>	N/A <sup>1</sup>	4	4* (0%)
	10-2			3.5	3.5* (0%)
11		12	11.7(-2.5%)	12.1	12.3(+1.7%)
12		21.3	20(-6.1%)	3.7	3.6(-2.7%)

<sup>†</sup>Regarding measurement points, please refer to Figure 5. 4.

\*Measured value in experiment was used as the boundary condition in CFD.

<sup>1</sup>The bypass channels in two branches were used in Case A.

<sup>2</sup>The bypass channel in the main channel was used in Case B.

### **Total pressure drop in the whole system**

Table 5. 3 shows the comparison between numerically simulated and experimentally measured pressure losses in the flow path for Cases A and B. The pressure losses were calculated as the difference between the average pressure at each measuring point cross-section.

The numerically determined total pressure loss throughout the system was 15.7 kPa, which was slightly less than the experimental value of 16.8 kPa. The discrepancy between the simulated and measured values in Case A was a maximum of 21.4% between Points 3 and 4. At the other points, the CFD results and experimental results were in good agreement, with discrepancies of less than 10%. For  $\Delta R_{b1,2}$ , there was little difference between the absolute calculated and experimental values; the discrepancy did not exceed 0.9 kPa. In this CFD simulation, the absolute value of the pressure loss was small, and so even differences of 0.9 kPa or less resulted in large discrepancies of up to 21.4%.

In Case B, two decentralized pumps were used, and the total pressure loss of the system in each branch pipe was labelled  $\Delta P_{b1}$  and  $\Delta P_{b2}$ . The numerically determined values of  $\Delta R_{b1}$ ,  $\Delta R_{b2}$ ,  $\Delta R_{b1-b2}$ , and  $\Delta R_m$  were 4.3, 4.4, 1.6, and 4.8 kPa, respectively, which were not significantly

different from the experimental values. The total pressure losses  $\Delta P_{b1}$  and  $\Delta P_{b2}$  were 16.3 and 14.5 kPa, respectively. The simulated value of  $\Delta P_{b2}$  was almost the same as the experimental value, whereas  $\Delta P_{b1}$  was 9% higher than in the experiment. The maximum discrepancy in the prediction of the pressure losses in Case B was 15.8% between Points 3 and 4. As for Case A, excluding the virtual resistance part, the total pressure loss of piping system in Branch 1 and Branch 2 was 4.3 and 3.6 kPa, respectively, in the experiment and 5.4 and 3.7 kPa, respectively, in the simulation, resulting in a discrepancy of 20.4% and 2.7%, respectively.

Table 5. 3 Comparison of pressure loss between CFD and experiment [kPa] (discrepancy given in parentheses)

Pressure difference	Case A		Case B	
	Experiment	CFD	Experiment	CFD
$\Delta R_{b1}$	4.1	4.2 (+2.4%)	4.3	4.3 (0%)
$\Delta R_{b2}$	4.6	4.7 (+2.2%)	4.6	4.4 (-4.3%)
$\Delta R_{b1-b2}$	1.4	1.1 (-21.4%)	1.9	1.6 (-15.8%)
$\Delta R_m$	4.5	4.9 (+8.9%)	4.3	4.8 (+11.6%)
$\Delta P_m$	16.8	15.7 (-6.5%)	N/A <sup>2</sup>	N/A <sup>2</sup>
$\Delta P_{b1}$	N/A <sup>1</sup>	N/A <sup>1</sup>	14.8	16.1 (+9.0%)
$\Delta P_{b2}$	N/A <sup>1</sup>	N/A <sup>1</sup>	14.4	14.5 (+1.0%)

<sup>1</sup>The bypass channels in two branches were used in Case A.

<sup>2</sup>The bypass channel in the main channel was used in Case B.

Figure 5. 6 show the comparison of the pressure along the flow path in experiment apparatus shown in Figure 5. 4. The horizontal axis represents the flow path and the vertical axis represents the pipe gauge pressure. In both cases, although both methods have the same trend, it is clear that the CFD method (results represented by the dashed line) has a higher accuracy than equivalent method (results represented by the dotted line), which is more closer to the experimental value. The results also prove the CFD method could be used in studies and designs with an acceptable accuracy, and this is why we chose the CFD method later.

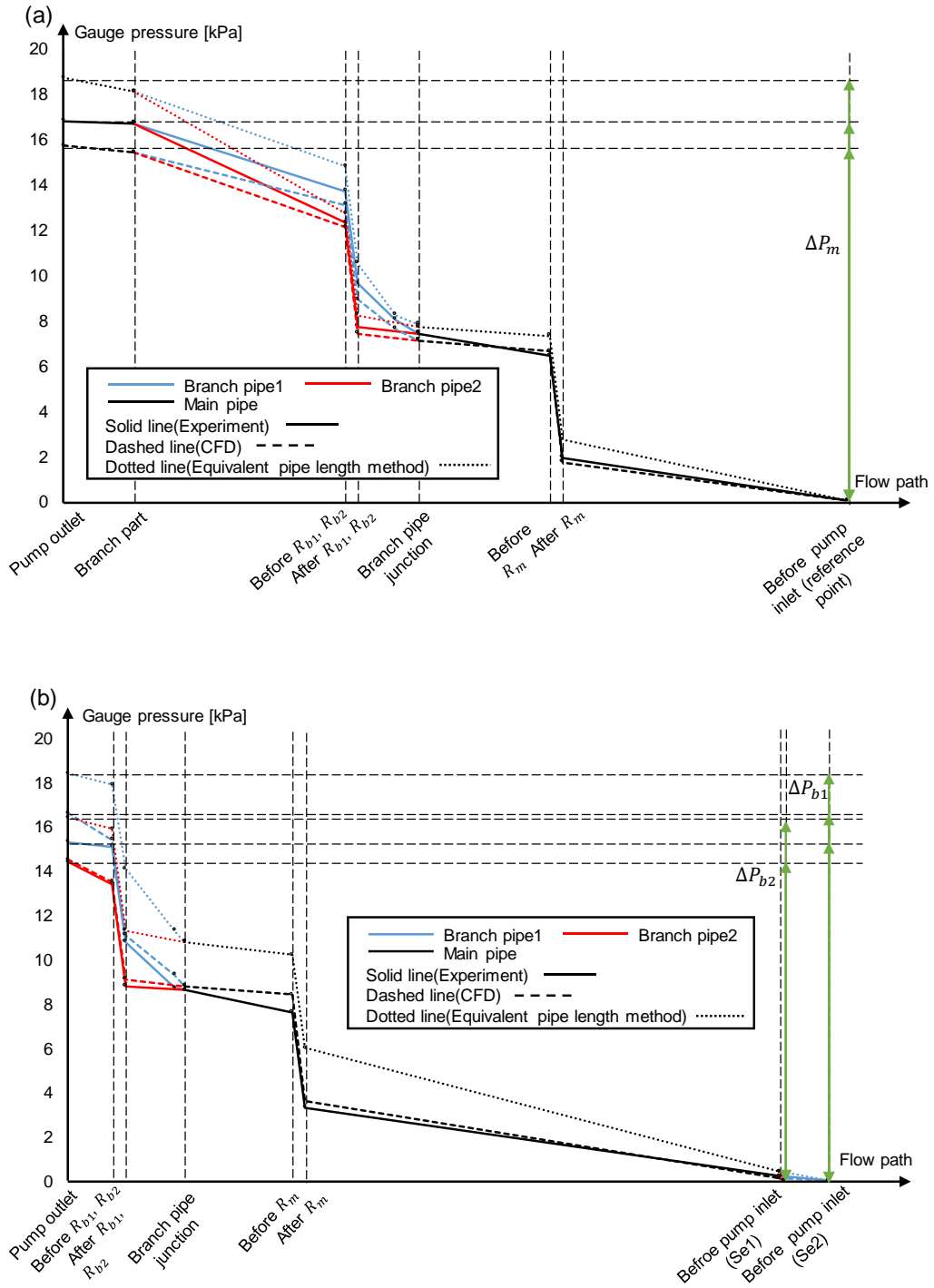


Figure 5. 6 Pipe internal water pressure distribution for system flow path: (a) centralized pumping system with CP Control; (b) decentralized pumping system

## 5.4 Pressure drop and temperature analysis in piping system based on CFD method

### 5.4.1 Simulation objectives and method

#### **Simulation target**

The prediction of pressure loss in the piping system using the CFD method is validated by comparing the numerical simulation results to the experimental results in the last section. The maximum discrepancy of the developed model for prediction of gauge pressure and system total pressure loss is 7.2% and 9%, respectively. The results prove this method is feasible for predicting the pressure in hydronic systems and could be useful in studies that have no access to a laboratory or full-scale facilities.

Therefore, in this section, the CFD method was used to predict the pressure and temperature in the piping system of the heat pump system in the RE house[14]. Based on the heat pump system used in the experimental house, a three-dimensional numerical model used to represent a real piping system with different operations was developed. Then several simulations such as heating and cooling operations were performed to verify the prediction accuracy by comparing with experimental data.

Figure 5. 7 shows the outline of the piping system of the RE house that was the subject of analysis. It is a system model similar to the experimental device described in chapter3 and connects the sky source heat pump (SSHP), and the double-helical underground heat exchanger (GHX) with a water loop to air conditioning, domestic hot water supply, and floor heating. The water source heat pump for heating exchanges heat with the circulating water in the water loop to offer cooling, heating, and hot water supply purposes. The circulating water temperature of the water loop is maintained near the ground temperature by the heat dissipation operation of the SSHP. Since the circulating water temperature of the water loop does not exceed 40 °C at the maximum, a resin pipe can be used for the piping system. Furthermore, considering the material construction cost, the PVC pipe was used to reduce the initial cost of the entire water piping system. Besides, in this system, the size of the main pipe is 40A, and the branch pipe is 25A in Japanese industrial standards.

Besides, a reverse return piping system was used between the GHX. For predicting the pressure and

temperature in the actual system, a piping system model of the same size as the actual one was created. The inner diameters of the main and branch pipes were set to 40 mm and 25 mm, respectively, which was the same as the inner diameter of the real piping system. As shown in Figure 5. 8, for the size of the created GHX, the inner diameter of the double helix is 36 mm, and the winding diameter, winding height, number of turns and pitch are 540 mm, 12 m, 75 and 160 mm, respectively. There are three GHXs in this system; the interval between two GHX is 2 meters. Figure 5. 9 and Figure 5. 10 shows the 3D model of the piping system used for simulation, which is the combination of pipe and GHX part. The connection with the heat pump unit(red and blue dot) is set as the inlet and outlet boundary.

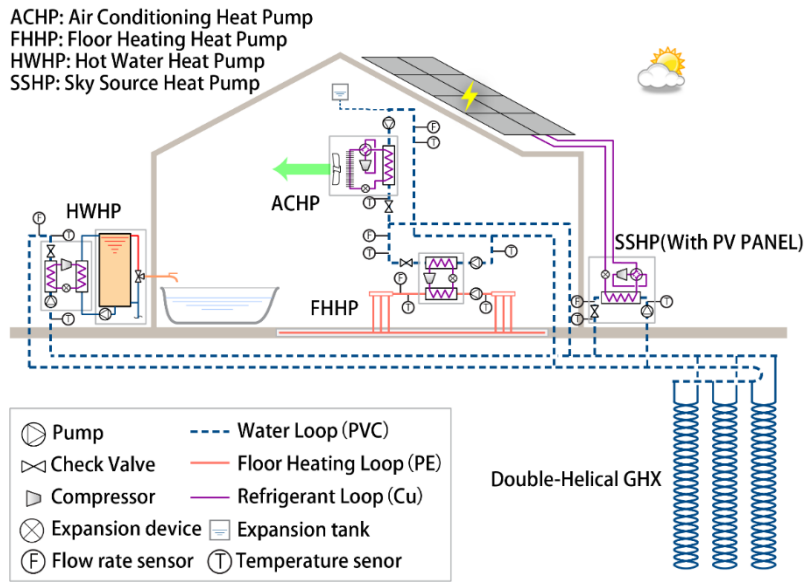


Figure 5. 7 Schematics of the RE house heat pump system.

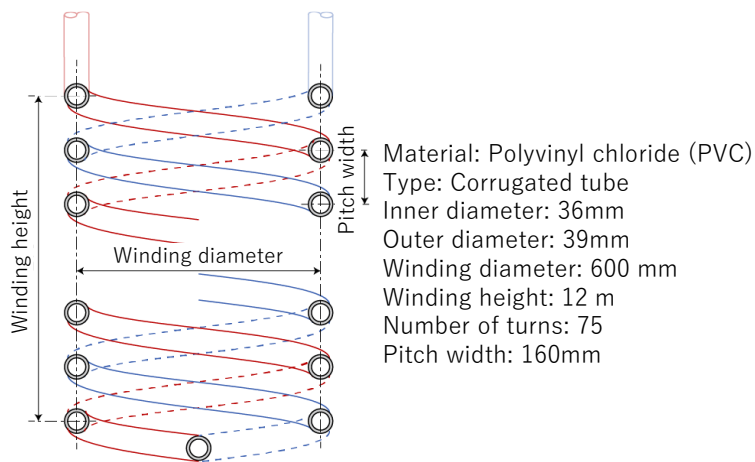


Figure 5. 8 Detailed parameters of GHX used in the piping system.

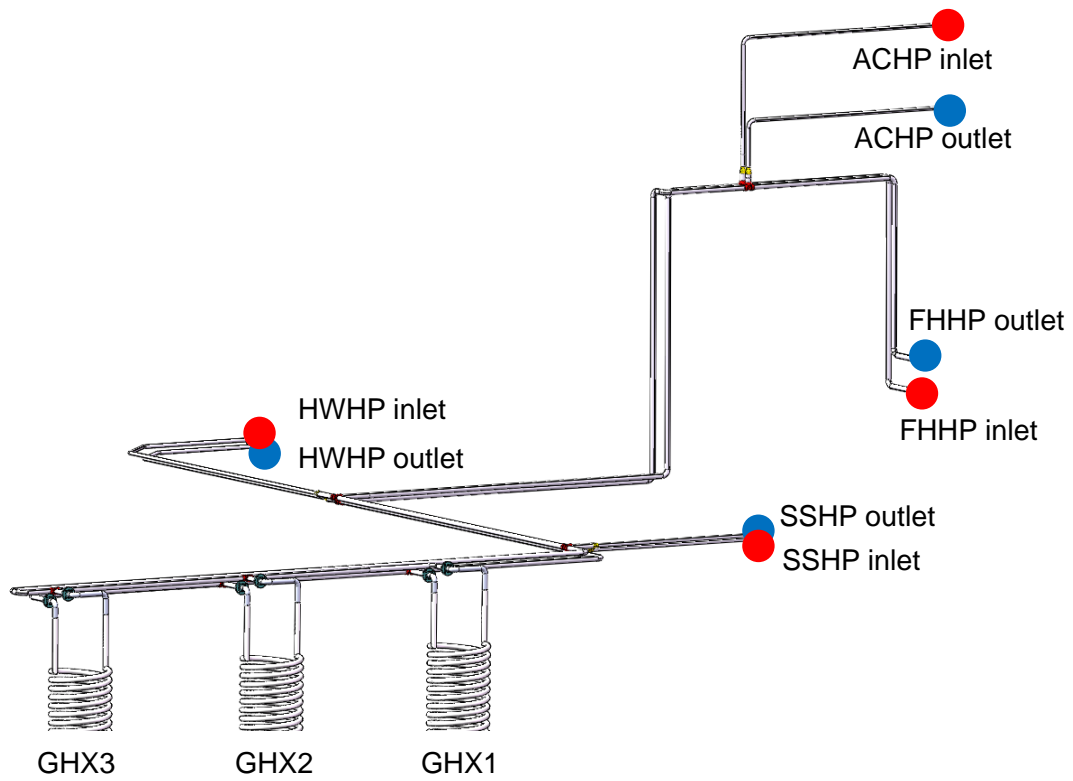


Figure 5. 9 Schematics of the piping system of the RE house.

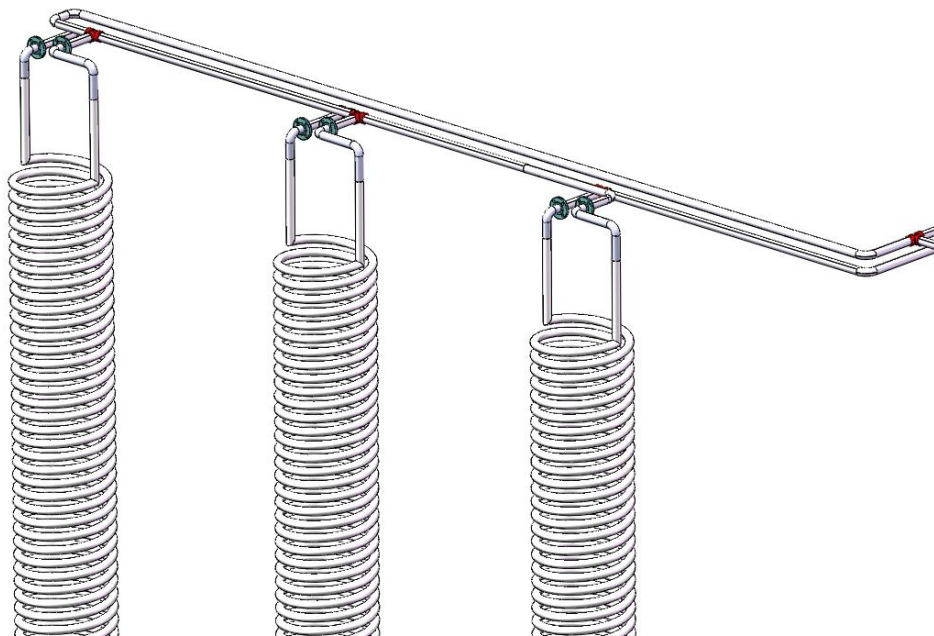


Figure 5. 10 Three dimensional model of GHX.

### **Simulation conditions**

For the CFD simulation, the commercial software STAR-CCM+ was used. The method of mesh division can have a significant influence on the accuracy of a CFD model. Compared with the tetrahedral mesh often used in machine analysis, the use of an appropriate polyhedral mesh has been found to improve the accuracy of the analysis and reduce the total calculation time. Peric conducted a fluid analysis of the water jacket of an engine using a polyhedral mesh, and found that only 1/6 of the number of cells and 1/10 of the calculation time were required to obtain the same accuracy as obtained with a tetrahedral mesh[15]. Fukuyo carried out CFD simulations of miter bends with a polyhedral mesh and found that an adequate polyhedral mesh gives accurate loss coefficients when the elbow angle is less than 90°[16]. In previous studies, we confirmed the accuracy of pressure analysis in the piping system using a combination of a polyhedral lattice and a prism layer[12]. In this simulation, the analysis grid uses a polyhedral grid in the center of the piping model, and a prism layer is created near the wall surface. As shown in Figure 5. 11, three prism layers were positioned along the inner walls and the mesh was refined in geometrically important areas. To improve the calculation speed without reducing accuracy, different mesh sizes were used in straight pipe sections and in special parts such as elbows and tee joints. The reference mesh size in straight pipe sections was 0.01 m and in elbow and tee joints was 0.003 m.

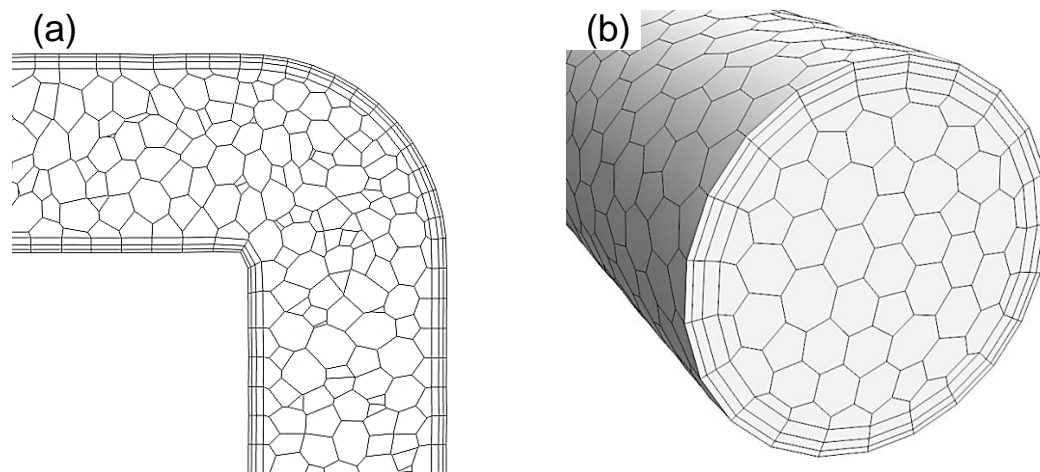


Figure 5. 11 Views of the computational grid (polyhedral mesh and prism layer mesh) on some of the domain surfaces: (a) elbow; (b) inlet & outlet.

For the flow rates in both the analyzed cases, the Reynolds number was approximately 20000, indicating fully developed turbulent flow. All simulations were conducted under isothermal conditions and the object fluid was assumed incompressible. Based on the result of the previous study described before, the turbulence model used in this simulation was the realizable  $k-\varepsilon$ [17]. Regarding the setting of the inlet and outlet boundaries, in this piping system model, the circulation pump and the heat pump unit were excluded from the analysis. The connection was used as the outflow boundary. In addition, the GHX part refers to the GHX that is actually used in the real system, creates a three-dimensional double-helix model of the same size, and connects it using the reverse return piping method.

For each boundary condition, the flow rate, pressure, and temperature obtained in the winter field testing were measured or calculated based on the measured values. A rough wall surface is assumed to consider the friction loss of the pipe part, excluding GHX. For the average roughness, refer to [18] and use the average roughness of hard vinyl chloride pipe of 0.03 mm. Since GHX uses a PVC corrugated tube, there is no average roughness information corresponding to this specification. Therefore, in this simulation, GHX was assumed to be a circular tube, and average roughness of 1 mm was used. Equivalent average roughness corresponding to PVC corrugated pipe will be estimated in the future.

Regarding the setting of temperature conditions, this time, we assume a steady-state and make the GHX pipe surface temperature the same as the underground temperature to avoid long calculation times. The distribution of underground temperature, according to the analysis case, is shown in Figure 5. 12.

It was assumed that the surface temperature of GHX in Case 1 was 12.1 °C, based on the average temperature in the vertical direction of the ground in Case 1 at 13:00 on March 25. As in Case 1, the temperature from the ground surface to 15 m below the ground fluctuated around 11.7 °C based on the continuous measurement results of the temperature sensor in the center of the GHX at 6 o'clock on March 25, 6th in Case 2. Therefore, the surface temperature of GHX was assumed to be 11.7 °C, which is the average vertical temperature. Since all underground pipes are adequately wrapped with a heat-insulating material, the heat loss from the pipes was ignored, and the pipes were set as the heat insulation boundary condition.

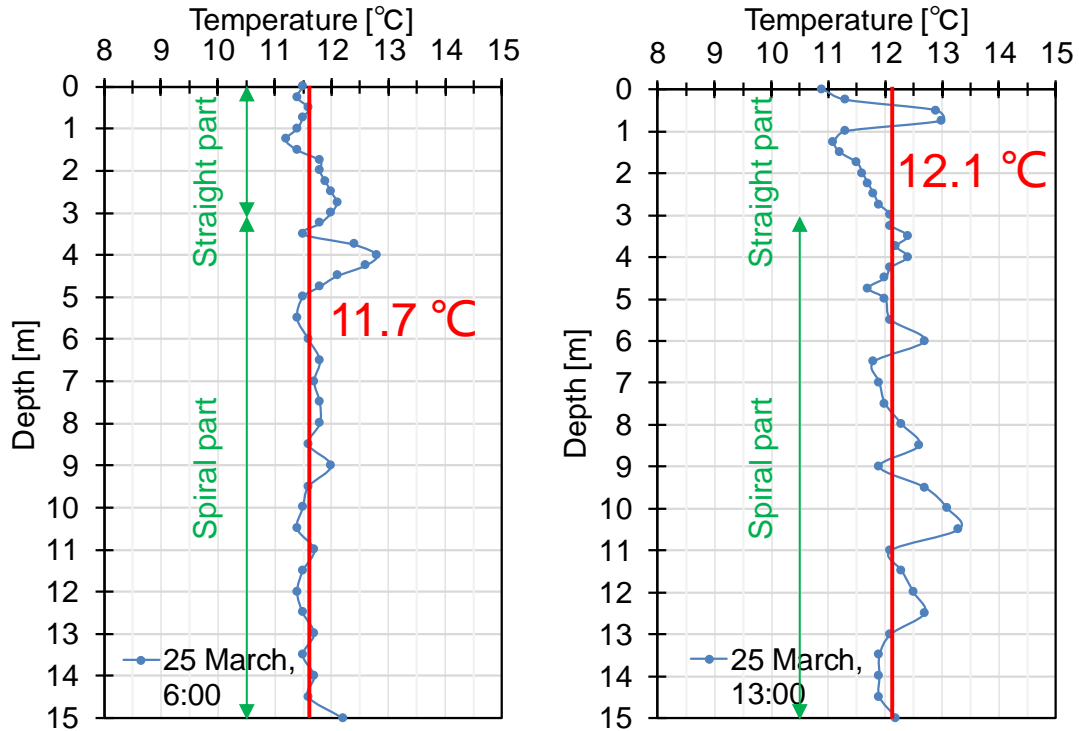


Figure 5. 12 Central GHX temperature distribution at 6:00 and 13:00 on March 25.

Table 5. 4 Summary of simulation conditions.

Type of flow		Incompressible flow (water)
Fluid density		998 kg/m <sup>3</sup>
Lattice type		Basic size: 0.01 m
		Case1&2: 19 million in total center(polyhedron); boundary layer(prism layer)
Inlet boundary condition	Case 1	SSHP inlet: 0.78 m/s (velocity inlet) Flow in temperature: 18.85 °C Turbulence intensity: 0.1 Turbulence length scale: 0.001
	Case 2	FHHP inlets: 0.82 m/s (velocity inlet) Flow in temperature: 10.25 °C Turbulence intensity: 0.1 Turbulence length scale: 0.001
Outlet boundary condition	Case 1	SSHP outlet: 42.8 kPa (pressure outlet)
	Case 2	FHHP outlet: 23.9 kPa (pressure outlet)
GHX		Case1: 12.1 °C(Surface temperature) Case2: 11.7 °C(Surface temperature)
Wall boundary		adiabatic; rough wall; average roughness = 0.03 mm (pipe); 1 mm(GHX)

## Case settings

As shown in Table 5. 4, in the simulation of this report, there are two cases of heating operation period set during the heating operation period of the RE house, Case 1: Heat collection operation period by the sky source heat pump (SSHP, the operating device is only SSHP) and Case 2: Heat pump for floor heating (FHHP, only operating equipment is FHHP). As shown in Figure 5. 9, in Case 1, the circulating water heated by SSHP enters the water loop from the SSHP inlet, flows through the three underground heat exchangers, stores heat in the ground, and then returns to the SSHP outlet. The flow rate of circulating water was 27.4 L / min. In Case 2, the circulating water that has transferred heat to the indoor floor heating enters the water loop from the FHHP inlet, flows through the underground heat exchanger, is heated, and then returns to the FHHP outlet to supply heat to the floor heating. The circulating water flow rate during the operation was 24 L / min as shown in Figure 5. 13 and Figure 5. 14.

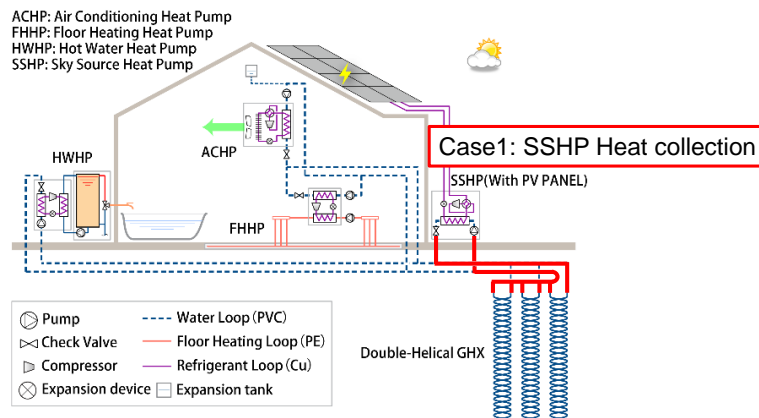


Figure 5. 13 Schematics of the system diagram to demonstrate case1.

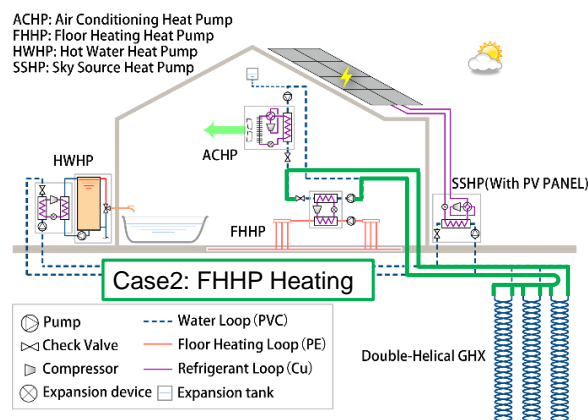


Figure 5. 14 Schematics of the system diagram to demonstrate case2.

## 5.4.2 Results and discussions

### **Total pressure drop in the whole system**

Table 5. 5 shows a comparison of gauge pressures at the inlet and outlet of the piping system by CFD simulation and experiment. Table 5. 6 shows a comparison of the whole system pressure loss. The positions of the measurement items in Table 5. 5 and Table 5. 6 are shown in Figure 5. 9. The pressure loss of the entire system is the difference in gauge pressure between the pipe inlet and the pipe outlet. Besides, the piping system inlet temperature SSHP inlet and FHHP inlet were installed as boundary conditions.

As shown in Table 5. 5, the gauge pressure prediction results were close to the experimental values in both cases. For the heat collection operation period by SSHP in Case 1, the outlet pressure of the heat pump unit (piping system inlet pressure) by CFD simulation was 45.1 kPa, which was smaller than the experimental value of 45.8 kPa. There were. In the heating operation period by FHHP in Case 2, the outlet pressure of the heat pump unit by CFD simulation was 30.8 kPa, which was not much different from the experimental value but was slightly smaller than the experimental value of 31.9 kPa.

Table 5. 6 shows a comparison between the pressure loss of the whole piping system calculated using gauge pressure and the experimental value. From Table 5. 6, the pressure loss of the whole piping system in Case 1 was estimated to be 2.3 kPa and calculated to be 3.0 kPa, and the error rate was  $-23.3\%$ . In Case 2, the calculated pressure loss of the entire piping system was 8.0 kPa, and the calculated value was 6.9 kPa, and the error rate was  $-13.8\%$ . Regarding the prediction of pressure loss in the entire piping system, the absolute error between the calculated value and the experimental value was small. Still, the relative error was relatively large, so it is necessary to improve the accuracy further. Regarding the cause of the difference, in this simulation, since there is no average roughness information corresponding to GHX using a PVC corrugated pipe, the calculation was performed using an average roughness of 1 mm assuming that GHX is a circular pipe. The corrugated tube has grooves in the pipe that cause strong turbulent motion in the flow in the pipe to improve the heat transfer characteristics significantly. The pressure loss is expected to increase due to the presence of this groove. Therefore, it is considered that one of the causes is the underestimation of the pressure loss in the GHX part. Since the two-way valve was not considered

this time, ignoring the pressure loss due to this part may be one of the causes. In the future, to improve the prediction accuracy, it is planned to estimate the equivalent mean roughness corresponding to PVC corrugated pipe and add a two-way valve model.

Table 5. 5 Comparison of gauge pressure between CFD and experiment [kPa].

Measuring point	Inlet of piping system	Outlet of piping system
Case1 (experiment)	42.8	45.8
Case1 (simulation)	42.8*	45.1
Case2 (experiment)	23.9	31.9
Case2 (simulation)	23.9*	30.8

\*boundary condition

Table 5. 6 Comparison of pressure loss between CFD and experiment [kPa] (discrepancy given in parentheses).

Measuring point	Pressure loss of whole piping system Difference in cage pressure between pipe inlet and pipe outlet
Case1 (experiment)	3.0
Case1 (simulation)	2.3(23.3%)
Case2 (experiment)	8.0
Case2 (simulation)	6.9(13.8%)

### **Temperature at the measuring point**

Table 5. 7 shows a comparison of system inlet and outlet temperatures by CFD and experiment. As shown in Table 5. 7, the two cases were higher than the experimental values. The system outlet temperature by CFD was 13.9 °C, which was smaller than the experimental value of 15.9 °C, and the absolute error was -2 °C for the heat collection operation period by SSHP in Case 1. The system outlet temperature by CFD was 12.6 °C, which was higher than the experimental value of 11.9 °C

during the heating operation period by FHHP in Case 2. The absolute error was + 0.7 °C. The average temperature in the vertical direction used in the setting of the boundary condition in the GHX part is regarded as the cause of the difference. The temperature distribution different from the actual temperature distribution taken as the surface temperature of the GHX is considered to be the cause of the error. In the future, it is necessary to improve the prediction accuracy by using the actual vertical temperature distribution.

Table 5. 7 Comparison of temperature between CFD and experiment [°C].

Measuring point	Inlet of piping system	Outlet of piping system
Case1 (experiment)	18.9	15.9
Case1 (simulation)	18.9*	13.9
Case2 (experiment)	10.2	11.9
Case2 (simulation)	10.2*	12.6

\*boundary condition

## 5.5 Summary

In this chapter, we created a dimensional model of the target piping system and conduct simulation to predict the pressure loss and temperature, based on the experimental piping system of the RE house by CFD for two operating states. There are two case settings in the simulation, which is a heat collection operation period using the sky source heat pump and a heating operation period utilizing the heat pump for floor heating. By comparing with the experimental data, the prediction accuracy of pressure loss and temperature in this piping system model was confirmed based on the result. For the prediction of pressure loss, the maximum relative error is 23.3 %, with an absolute error of 0.7 kPa. Regarding the cause of the difference, in this simulation, since there is no average roughness information corresponding to GHX using a PVC corrugated pipe, the calculation was performed using an average roughness of 1 mm assuming that GHX is a circular pipe. In the future, it is necessary to estimate the equivalent mean roughness corresponding to PVC corrugated pipe. For

the prediction of temperature, the maximum absolute error of + 2 °C. The temperature distribution different from the actual temperature distribution taken as the surface temperature of the GHX is considered to be the cause of the error.

## 5.6 Reference

- [1] Harish VSKV, Kumar A. A review on modeling and simulation of building energy systems. *Renew Sustain Energy Rev* 2016. doi:10.1016/j.rser.2015.12.040.
- [2] Kusiak A, Li M, Tang F. Modeling and optimization of HVAC energy consumption. *Appl Energy* 2010. doi:10.1016/j.apenergy.2010.04.008.
- [3] Ma Z, Wang S. Supervisory and optimal control of central chiller plants using simplified adaptive models and genetic algorithm. *Appl Energy* 2011;88:198–211. doi:10.1016/j.apenergy.2010.07.036.
- [4] Yang L, Yan H, Lam JC. Thermal comfort and building energy consumption implications - A review. *Appl Energy* 2014. doi:10.1016/j.apenergy.2013.10.062.
- [5] Arun Shankar VK, Umashankar S, Paramasivam S, Hanigovszki N. A comprehensive review on energy efficiency enhancement initiatives in centrifugal pumping system. *Appl Energy* 2016. doi:10.1016/j.apenergy.2016.08.070.
- [6] Mast M, Leibundgut H. Introduction and analysis of a concept for decentralized heat pumping in hydronic networks. *Energy Build* 2012. doi:10.1016/j.enbuild.2012.06.021.
- [7] Aitken A, Tatam G, Woodford L. *Guide to Best Practice Maintenance & Operation of HVAC Systems for Energy Efficiency*. 2012.
- [8] Asfour OS, Gadi MB. A comparison between CFD and Network models for predicting wind-driven ventilation in buildings. *Build Environ* 2007;42:4079–85. doi:10.1016/j.buildenv.2006.11.021.
- [9] Martinez-Almansa JJ, Fernandez-Gutierrez A, Parras L, Del Pino C. Numerical and experimental study of a HVAC wall diffuser. *Build Environ* 2014;80:1–10. doi:10.1016/j.buildenv.2014.05.001.
- [10] Zhai ZJ, Zhang Z, Zhang W, Chen QY. Evaluation of various turbulence models in predicting airflow and turbulence in enclosed environments by cfd: Part 1—summary of prevalent turbulence models. *HVAC R Res* 2007. doi:10.1080/10789669.2007.10391459.
- [11] Shih TH, Liou WW, Shabbir A, Yang Z, Zhu J. A New K-epsilon Eddy Viscosity Model for High Reynolds Number Turbulent Flows: Model Development and Validation. *Comput & Fluids* 1995. doi:10.1016/0045-7930(94)00032-T.

- [12] Liu M, Ooka R, Choi W, Ikeda S. Experimental and numerical investigation of energy saving potential of centralized and decentralized pumping systems. *Appl Energy* 2019;251. doi:10.1016/j.apenergy.2019.113359.
- [13] STAR-CCM+ User guide, Version 11.06 2016.
- [14] Liu M, Ooka R, Wen K, Hino T, Lee D, Choi W, et al. 再生可能エネルギー利用のための水循環分散型ヒートポンプシステムの開発 (第17報) CFDによるREハウス配管システムの圧力と温度の解析 Development of distributed water source heat pump system for renewable energy ( Part17 ) Analysis of pressure and temperature in piping system of RE house based on CFD. 平成30年度空気調和・衛生工学会大会 (名古屋) 学術講演論文集, 2019.
- [15] Peric M. Flow simulation using control volumes of arbitrary polyhedral shape. vol. 62. 2004.
- [16] Fukuyo K. Practical accuracy of internal-flow simulations using polyhedral meshes. *Trans Soc Heating, Air-Conditioning Sanit Eng Japan* 2008;33:47–50. doi:10.18948/shase.33.136\_47.
- [17] Shih TH, Liou WW, Shabbir A, Yang Z, Zhu J. A new  $k-\epsilon$  eddy viscosity model for high reynolds number turbulent flows. *Comput Fluids* 1995. doi:10.1016/0045-7930(94)00032-T.
- [18] ASHRAE. 2013 ASHRAE Handbook - Fundamentals (SI Edition). 2013 ASHRAE Handbook—Fundamentals 2013.

# **Chapter 6: Modeling of distributed heat pump system using renewable energy with Modelica**

## 6.1 Introduction and objectives

In this study, a new heat pump system to supply heat to necessary places (the distributed heat pump system using multiple kinds of renewable energy) was developed and installed in the test building (after this referred to as RE house). In this heat pump system, various renewable energies such as geothermal heat, solar heat, and air used as heat sources (heat collection and heat dissipation) of heat pumps. The heating and cooling operation performance of this system were studied based on field testing of the test building in the previous chapters focus on the winter, summer, and interim period measurement. Based on the field testing, High performance of each heat pump and the whole system was confirmed.

However, for an advanced building energy system application, the control strategy plays an essential role in realizing the energy saving of the building. For the design and test of advanced control strategy such as the model predictive control, modeling and simulation method that can reproduce the flexible thermal interaction between system components is essential. In this research, the Modelica language, which has been attracting attention as an advanced and useful system modeling language in recent years, is used for the thermal analysis of the RE house and distributed heat pump system. To further optimize the control and use strategy, the purpose of this chapter is to conduct the modeling of this heat pump system that can express the system dynamics, and verify its effectiveness and accuracy by comparing it with experiment data. Based on the developed model, it is possible to optimize and test the control and use strategy by simulation.

## 6.2 Review of methods and tools for modeling and simulation of HVAC system

Research methods based on modeling and simulation have a wide range of applications in the field of building energy. Starting from the design stage of the energy system (such as prototype design and comparison of new systems/technologies), relevant issues in building energy system include the real-time operation prediction and diagnosis of the system (such as rapid simulation and diagnosis

based on building information models), and optimization and transformation of specific systems (such as the model development of model predictive control, the evaluation of transformation schemes), these problems cannot be solved without the use of simulation research methods. On the one hand, because the experimental approach will have a high cost, more importantly, it requires more execution time. Computer-based modeling and simulation can provide us with a fast and economical solution. Now, for different purposes and applications, in the field of building energy, there are many modeling and simulation software, such as EnergyPlus[1], TRNSYS[2], Modelica[3], Dalec[4], Simulink[5] with its relative libraries, and so on.

As one of the mainstream tools, EnergyPlus has been used in many studies, including such as phase change materials and envelope structures[6–20]. To understand how the simulation accurately predicted actual energy use, Rhodes et al. [7] determined the accuracy of the model by considering the houses in 54 smart grid demonstration projects in Austin, Texas. They collect data about the house through an energy audit and then use BEopt, which is a residential building-centric graphical user interface front end developed by NREL for EnergyPlus, to convert it into an energy model. The actual meter reading (kWh) in the four cases was compared with the simulation results. The results show that the model can reasonably predict the usage of houses with average usage, but the model is difficult to predict the usage of houses with low or high consumption. Royapoor et al. [13] deployed a set of two calibrated environmental sensors together with a weather station in a 5-story office building to check the accuracy of the EnergyPlus virtual building model. The model was calibrated using the ASHRAE Guide 14 indicators. Langevin et al. introduced the Human-Building Interaction Toolkit to simulate the thermal adaptation behavior, energy use, and thermal comfort of office building occupants as part of the overall building performance simulation. The toolkit uses the Building Controls Virtual Test Bench to jointly simulate the seat-based comfort and behavior models in MATLAB, and the entire building energy consumption simulation and evaluation in EnergyPlus[15]. Pang et al. proposed a simulation-based overall building performance monitoring tool that can compare the actual and expected performance of a building in real-time. The tool continuously obtains relevant building model input variables from existing energy management and control systems. Then, they report the expected energy consumption simulated with EnergyPlus and gives a proof of concept.

Besides EnergyPlus, TRNSYS is also a usable and popular tool for simulation of the HVAC system

that can offer a system dynamic fluctuation. Antoniadis et al. [21] used TRNSYS modeling software to optimize building-integrated solar thermal systems with seasonal storage capabilities to evaluate different integration options for solar collector arrays. The model calculates the space heating demand during heating and the annual household hot water demand. Parametric analysis of the effects of various solar collector areas and types, building integration types, and seasonal storage tank capacity is also proposed to optimize system design. Asadi et al. [22] adopted a simulation-based multi-objective optimization scheme (combining TRNSYS, GenOpt, and Tchebycheff optimization techniques) to optimize the renovation cost, energy-saving, and thermal comfort of residential buildings. Optimization parameters include alternative materials for exterior wall insulation, roof insulation, different window types, and installation of solar collectors in existing buildings. They used actual case studies for the proposed method, and verified the practicability of the method and analyzed possible problems. Chargui et al. [23] modeled and simulated the heat pump on TRNSYS to study the thermodynamic phenomena of the heat pump system. They used HVAC technology to describe the heat pump on the TRNSYS model mathematically and gave the simulation results (such as COP, power consumption, and output power) of the geothermal heat pump. Kuznik et al. developed a new TRNSYS type (called Type 260) to model the thermal behavior of exterior walls using PCM. They detailed the model and verified it using experimental data from the literature[24].

However, conventional simulation tools such as EnergyPlus and TRNSYS still have some problems in modeling, simulation and optimization of air conditioning and heat source systems. Large and complex system models are often used to model building air conditioning and heat source systems. Such systems include differential-algebraic equations describe different physical systems (heat, electricity, etc.) with different time scales of dynamic properties. Usually, when a simulation is performed, numerical expressions are numerically solved to calculate and evaluate the performance of the system. Conventional tools have difficulty in dynamic simulation of multi-domain physical systems, including electrical, thermal, and control.

Most state-of-the-art building simulation programs such as EnergyPlus implement models in an imperative programming language. In such programs, developers write sequences of computer instructions that assign values to variables in a predetermined order of execution. Generally, such programs mix codes describing physical processes with codes used for data management and

numerical solutions[25]. The imperative programming language assigns values to functions, declares the execution order of these functions, and changes the state of the program, as in MATLAB/Simulink. These programs were developed for use cases of building energy performance evaluation. However, the use of models to support operations such as control design and verification, and multi-physics dynamic analysis that combine building, HVAC, electrical, and control models are rarely considered or not even considered[25]. Among most of them, the reuse rate of the model is meager. In other words, whenever a new system model needs to be constructed, it is inevitable to rewrite the same model as before. Another critical point is to evaluate the dynamic characteristics of the building, which means how the HVAC system that includes heat storage, electricity storage, renewable energy power generation and the grid affect each other internally. In these tools, the close integration of numerical solutions with model equations and input/output routines makes it difficult for users to understand how component models interact with other parts of the system model, and cannot effectively judge simulation results and problem solutions. Because of the need to use different numerical methods, such as control design and verification, coupled modeling of thermoelectric systems and model use during operation, it is difficult to use these tools to complete experiments[26]. Also, the nested solvers in the program can lead to numerical noise in the simulation results that can make the use of optimization programs difficult[27].

For example, a coupling simulation of feedback control with a time constant of a few seconds to a building energy model with a time constant of a few hours leads to a rigid ordinary differential equation. In this case, an implicit method is generally required. But in EnergyPlus and many TRNSYS components, HVAC equipment and controllers are usually approximated using steady-state models to derive algebraic equations. In this case, the results can be obtained by the explicit method, but the approximation causes a deviation from the actual control, and the dynamic characteristics of the system cannot be correctly reflected and evaluated. For example, for EnergyPlus, we employ ideal control to reduce the computation time, and the proportional-integral (PI) control loop is assumed to be ideal, and there is no overshoot. Also, control based on the flow rate is simplified in many device models, and the flow rate distribution is ideally distributed in the system rather than the result of the flow rate distribution based on friction loss. Due to such a limit, it is difficult to verify the actual control logic. Although a dynamic control model has been introduced in TRNSYS, the adoption of certain time steps poses a numerical problem.

The Modelica language can overcome problems such as dynamic characteristics and control simplified by conventional modeling and simulation tools. For example, using the State Graph package of Modelica Standard Library[3], it is possible to execute the discrete control considering the dead zone or the delay time. Simulation of multi-domain systems with thermal and electrical components does not require the data synchronizer for co-simulation, which is essential for traditional tools like TRNSYS and can be realized in one environment. Besides, libraries for different air conditioning and building energy systems are in development, and their models are extended to develop and evaluate optimal control techniques, fault detection and diagnostics for the whole building energy system, and air conditioning system. Moreover, due to its object-oriented modeling characteristics, the model developed based on Modelica can be used to achieve an optimal design and operation even when conditions change. For example, the environmental co-simulation that contains room airflow is possible based on the building library[28]. Because it is suitable for hybrid modeling in multiple physical fields, including electrical and thermal, as well as more realistic control system modeling, Modelica has been widely used for modeling building energy systems in recent years[9,25,26,28–34]. Therefore, for further optimization and control method design, the modeling of innovative systems like the proposed distributed heat pump system in the study is constructed based on Modelica.

## 6.3 Fundamentals of Modelica and its application in HVAC and building field

Modelica is an object-oriented multi-domain modeling language[3]. It is most suitable for modeling complex multi-domain physical systems (e.g., including mechanical, electrical, thermal, control) across many fields, and is usually used for modeling physical phenomena. Dr. Hilding Elmqvist invented the concept and design of Modelica in 1996, and Modelica ver1.0 was released next year. The main difference from imperative programming languages is that equation-based languages do not need to specify the computer assignment order required by the simulation model.

Equation-based languages (such as Modelica) can solve the problem of modeling multi-domain

physical systems in traditional modeling tools. Specifically, it can effectively help the hybrid modeling of building energy systems and control systems. In the Modelica modeling process, the physical equations and numerical solvers are separated as much as possible. In simple terms, an equation-based language does not require model developers to specify the computer calculation sequence needed by the simulation model. And the design of the solution method will have mathematics researchers to study more efficient and optimized algorithms[25].

Modelica is a declarative language used to describe the mathematical properties of things. It can easily describe the working characteristics of different types of engineering components (such as pipes, resistors, pumps, etc.). Also, these components can be easily combined into subsystems, systems, and even architectural models. The important thing I think it that the Modelica language supports the simultaneous description of continuous and discrete characteristics in mixed differential-algebraic equations. The Modelica language supports the use of both causals (usually used in control system design) and non-causal (usually used to create a principle-oriented physical model design) modeling methods in the same model. Therefore, I can use Modelica to support the physical model design and control model design more realistically.

Here I will use the examples in the textbook[35] to briefly explain the basic grammar of Modelica language. For Newton's law of cooling, the mathematical formulation of Newton's law can be expressed as follows:

$$m c_p \frac{dT}{dt} = h \times A \times (T_{env} - T)$$

Where  $m$  is the mass of thermal capacitance,  $c_p$  is the specific heat,  $T$  is the temperature of thermal capacitance,  $h$  is the heat transfer coefficient,  $A$  is the heat transfer surface area,  $T_{env}$  is the temperature of the environment.

In Modelica language, the above formula can be expressed as follows:

$$m * c_p * \text{der}(T) = h * A * (T_{env} - T)$$

The operator `der()` represents the time derivative in Modelica. If the types of variables, constants,

and initial conditions are added, the model of Newton's cooling formula can be expressed as follows:

#### **model Newtonscooling**

```
type Temperature=Real(unit="K", min=0);  
type HeatTransferCoefficient=Real(unit="W/(m2.K)", min=0);  
type Area=Real(unit="m2", min=0);  
type Mass=Real(unit="kg", min=0);  
type SpecificHeat=Real(unit="J/(K.kg)", min=0);  
parameter Temperature T_env=288.15;  
parameter Temperature T0=363.15;  
parameter HeatTransferCoefficient h=0.7;  
parameter Area A=1.0;  
parameter Mass m=0.1;  
parameter SpecificHeat c_p=1.2;  
  
Temperature T;
```

#### **initial equation**

```
T = T0;
```

#### **equation**

```
m*c_p*der(T) = h*A*(T_env-T);
```

#### **end Newtonscooling;**

In this modeling description, the **parameter** indicates a variable that must provide an assignment.

The **initial equation** section specifies how the variables are initialized. At the same time, a physical type **Temperature** is defined in the model, which can be used to declare multiple variables such as  $T_{env}$  and  $T_0$ . Because many physical variables have been predefined in the Modelica standard library, they can be directly declared without pre-definition when called.

Based on the conditions described before, the simulation result is shown as follows:

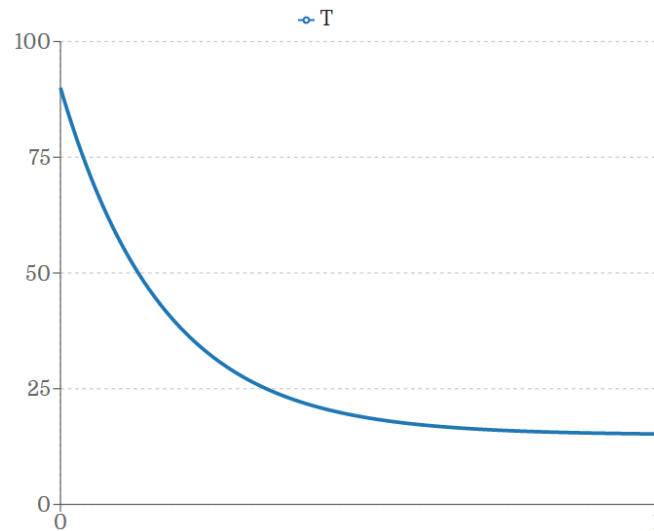


Figure 6. 1 Simulation result of Newtonscooling.

As mentioned in the last section, object-orientation is one of the main points of Modelica language, and the behavior of physical phenomenon is described as the interaction between objects based on the physical principle. The reusability of the model is high accordingly. For example, a heat pump has a compressor, a condenser, etc. The compressor is composed of a primary heat exchanger and a refrigerant. We can create essential elements such as compressor and build different types of heat pumps to meet our purposes. Other than this, Modelica also has commercial and free libraries from universities and industries. For example, a series of libraries for building and district energy simulation based on the Annex60 project[36]. It is also possible to model large-scale energy systems such as city scale.

## 6.4 Modeling description of distributed water source heat pump system using renewable energy

### 6.4.1 Modeling objectives and method

#### Overview of modeling

The purpose of this research is to build a model that can express the thermal behavior of the RE

house and heat pump system using Modelica language. By using this model, make it possible to develop an optimal control method based on simulation. As content, we will compare the outline of the model and the simulation results with the winter operation test results, and report the effectiveness and accuracy of this model.

In the construction of the model, it includes a detailed building model of the RE house, including three interconnected rooms, two of which are equipped with a floor heating system, so they are directly thermally coupled with the heat pump system. Another independent room (facility room) has no floor heating system, so during the winter experiment, it directly exchanged heat with the other two rooms. For the distributed heat pump system, this system model concludes the water source heat pump for floor heating, an equivalent sky source heat pump, and the ground heat exchanger. Therefore, we evaluated the validity and accuracy of the model based on the comparison with the experimental results of March 21 and March 25 during the winter experiment.

### ***Modeling of RE house***

As mentioned in chapter3, we carry out the development research of the improved equipment and import it to a full-scale test building for verification, and confirm the system performance based on field testing. As shown in Figure 6. 2, the basic configuration of this system is introduced in detail. This figure is the distributed heat pump system designed to use these multiple kinds of renewable energy complementarily. Renewable energy, such as geothermal heat is utilized through the ground heat exchanger(GHX). A sky source heat pump(SSHP) uses renewable energy from the sky, such as solar radiation and air heat from the atmosphere. A water circulation loop integrates both renewable energy sources from earth and sky. The HVAC system for heating, cooling, and domestic hot water supply purposes are constructed by using several water source heat pumps.

The configuration of the RE house is shown in Figure 6. 3 and Figure 6. 4. As mentioned before, the RE house includes three interconnected rooms, two of which are equipped with a floor heating system, so they are directly thermally coupled with the heat pump system. Another independent room (facility room) has no floor heating system, so during the winter experiment, it directly exchanged heat with the other two rooms.

The setting of the floor heating system is shown in Figure 6. 5. According to machines such as floor heating heat pumps, the heat pump models heating and cooling used in this model can achieve

acceptable accuracy, and the performance of the heat pumps actually used in the heat pump system is about the same. Therefore, only the floor heating heat pump is modeled this time, and the air conditioning and hot water heat pump can be obtained by modifying the parameters using the heat pump for the floor heating model. The size of the building is the same as the actual one. Based on the actual configuration of materials used in the construction, the detailed settings used in the modeling are shown in Table 6. 1 according to the actual materials used in the building.

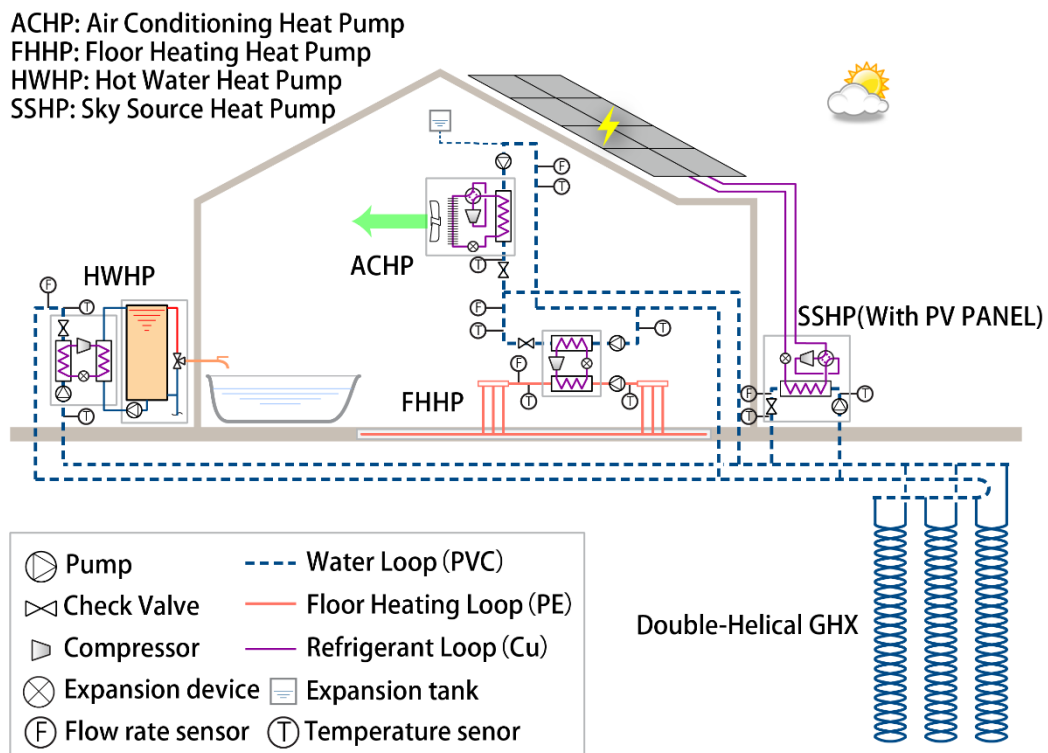


Figure 6. 2 schematics of RE house and heat pump system.

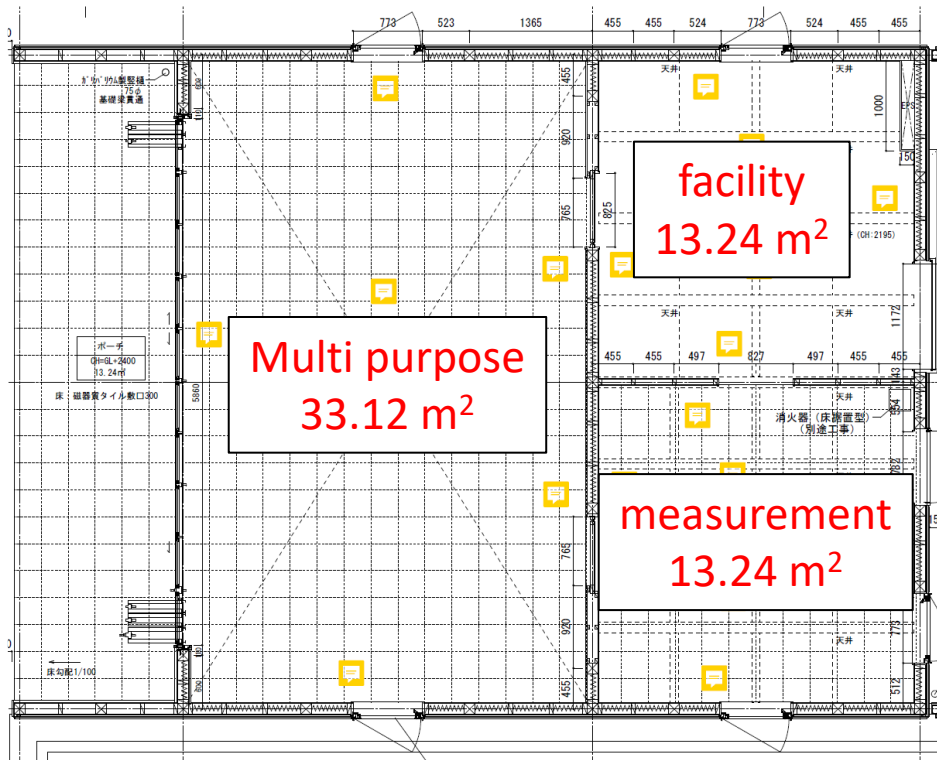


Figure 6. 3 Building plan of RE house.

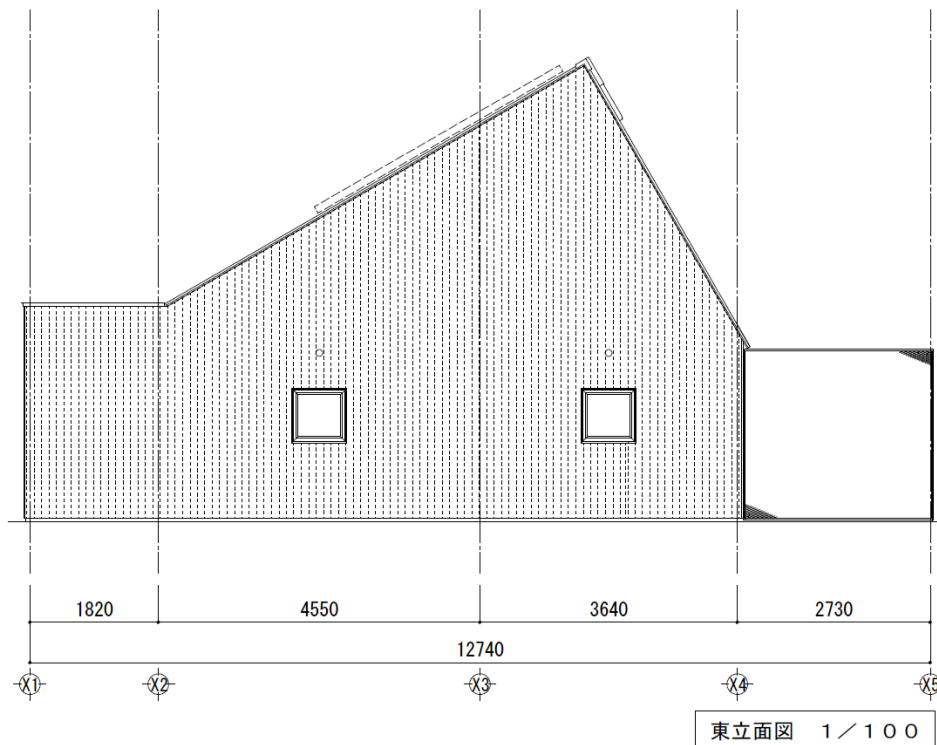
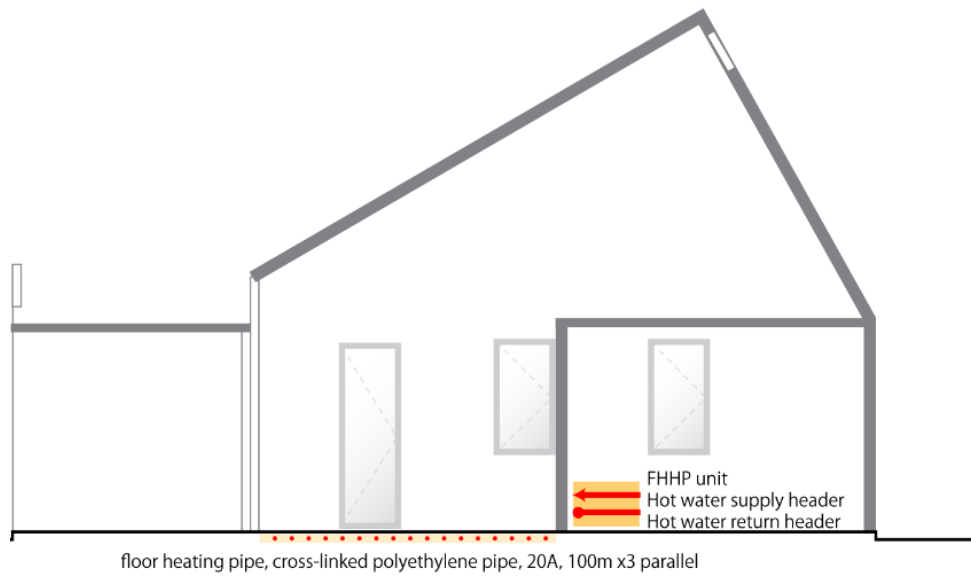
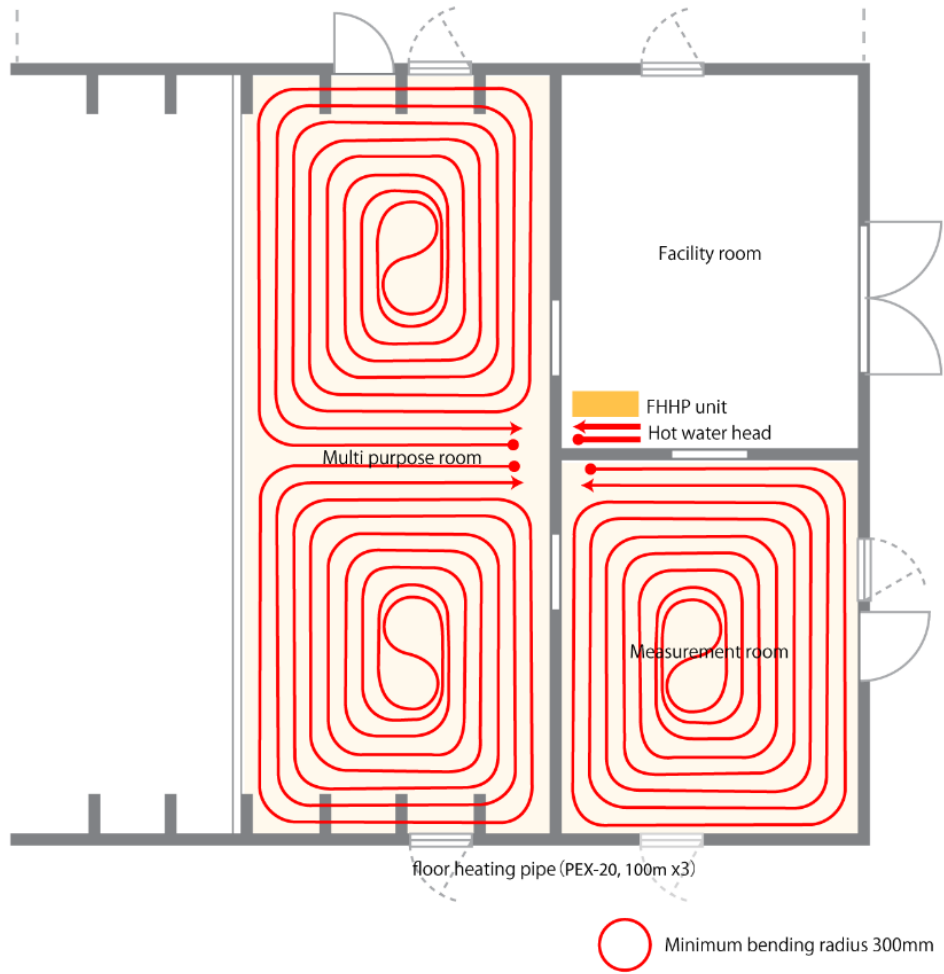


Figure 6. 4 Building elevation of RE house.



### RE house floor heating system

Figure 6. 5 Configuration of RE house floor heating system.

Table 6. 1 configuration and materials of RE house

Floor configuration of multi purpose and measurement room					
The floor heating piping system: 100m*3 in parallel; pipe size: PEX-20					
k value(Thermal conductivity); c value(Specific heat capacity); d value(Mass density); x value(Material thickness)					
Floor layer (from indoor to outdoor)		k (W/(m*k))	c (J/(kg*k))	d (kg/m3)	x (m)
first	Porcelain tile (t=10mm)	1.3	840	2400	0.01
second	mortar (t=30mm)	1.5	800	2000	0.03
third	mortar (t=80mm)	1.5	800	2000	0.08
fourth	concrete (t=150mm)	1.6	840	2400	0.15
Floor configuration of facility room					
k value(Thermal conductivity); c value(Specific heat capacity); d value(Mass density); x value(Material thickness)					
Floor layer (from indoor to outdoor)		k (W/(m*k))	c (J/(kg*k))	d (kg/m3)	x (m)
first	concrete (t=120mm)	1.6	840	2400	0.12
second	concrete (t=150mm)	1.6	840	2400	0.15
Exterior wall configuration					
Exterior wall (from indoor to outdoor)		k (W/(m*k))	c (J/(kg*k))	d (kg/m3)	x (m)
first	Gypsum board (t=12.5mm, multi purpose)extWall1	0.22	1100	750	0.0125
	Larch plywood (t=9mm, facility/measurement)extWall2	0.16	1300	550	0.009
second	Insulation glass wool 14K	0.038	840	14	0.1

d	(t=100mm)				
third	Structural plywood (t=9mm)	0.16	1300	550	0.009
Roof configuration					
Roof (from indoor to outdoor)		k (W/(m*k))	c (J/(kg*k))	d (kg/m3)	x (m)
first	Structural plywood (t=24mm)	0.16	1300	550	0.024
second	Insulation material Styrofoam (t=45mm)	0.033	1500	29	0.045
third	Structural plywood (Keical board, t=12mm)	0.2	920	1100	0.012
Partial wall (equipment/measurement room)					
	Partial wall	k (W/(m*k))	c (J/(kg*k))	d (kg/m3)	x (m)
first	Larch plywood (t=9mm)	0.16	1300	550	0.009
second	Larch plywood (t=9mm)	0.16	1300	550	0.009
Partial wall (among three rooms)					
	Interior wall (from others to multi purpose)	k (W/(m*k))	c (J/(kg*k))	d (kg/m3)	x (m)
first	Larch plywood (t=9mm, measurement/facility)	0.16	1300	550	0.009
second	Insulation material glass wool 14K (t=10mm)	0.038	840	14	0.01
third	plasterboard (t=12.5mm, multi purpose)	0.22	1100	750	0.0125
Exterior doors					
	Exterior doors	k (W/(m*k))	c (J/(kg*k))	d (kg/m3)	x (m)
first	Insulation material glass wool	0.038	840	14	0.025

	14K (t=50-1.6*2mm)				
second	Insulation material glass wool	0.038	840	14	0.025
d	14K (t=50-1.6*2mm)				
	Partial doors				
	Partial doors	k (W/(m*k))	c (J/(kg*k))	d (kg/m3)	x (m)
first	Basswood plywood	0.16	1300	550	0.025
second	Basswood plywood	0.16	1300	550	0.025
d					
	Exterior windows, U value: heat transmission coefficient				
	Exterior windows	U (W/(m2*k))	absorption rate		
first	Double glazing (t=6mm)	3.3	0.74		
	French windows, U value: heat transmission coefficient				
	French windows	U (W/(m2*k))	absorption rate		
first	Double glazing (t=6mm)	3.3	0.74		

### **Heat pump system component modeling**

The modeling of the system is focusing on the component such as heat pump and GHX, and the whole system model is constructed by partially adopting the Modelica open-source library Building library[33] and AixLib library[37]. The description of the main models is as follows:

#### **Detailed room model**

The model of each room adopts a detailed room model developed by Zuo et al.[28]. The room model is assumed to be a completely mixed air room model. The room can have any number of structures and surfaces. Based on different structures and surfaces, there could be convection, conduction, infrared radiation, and solar radiation that participate in the heat exchanger. The critical points in

this model are 1) transient or steady-state heat conduction through an opaque surface; 2) heat transfer through the glass system takes into account solar radiation, infrared radiation, heat conduction, and heat convection, and can be set up to adjust Solar radiation; 3) For convective heat transfer between the outside air and the outer surface, the heat transfer coefficient is related to wind speed, wind direction, and temperature, and can also be set to a constant value; 4) The pairing between indoor air and the surface of the opaque structure The flow heat transfer coefficient can be selected to be temperature-dependent or constant. 5) Assume that all solar radiation will hit the floor first, and then be partially absorbed and partially reflected by the floor.

Besides, internal heat sources and instantaneous simulated substance concentrations can be set, but they are not within the scope of this model.

### Heat pump for floor heating model

For the heat pump for floor heating, the coefficient of performance (COP) of the heat pump will change with the temperature, which is the same as the Carnot efficiency changes. At the same time, the speed of the compressor (the control parameters) can be controlled to achieve a variable speed operation. The Carnot effectiveness can be calculated as:

$$\eta_{Carnot,n} = \frac{COP_n}{\left(\frac{T_{con,n}}{T_{con,n} - T_{eva,n}}\right)}$$

And the COP of the heat pump can be calculated as:

$$COP = \eta_{Carnot,n} \times COP_{Carnot} \times \eta_P$$

Where,  $\eta_{Carnot,n}$  is the Carnot effectiveness,  $COP_n$  is the COP at the nominal condition,  $T_{con,n}$   $T_{eva,n}$  is the condensing and evaporating temperature (K) at the nominal condition, respectively.  $\eta_P$  is a function of the part load ratio used to take into account the influence on COP at part load conditions. The realization of the heat pump model in Modelica is shown in Figure 6. 6, there is a condenser component(con in the figure) and an evaporator component(eva in the figure). By inputting the compressor speed signal, the temperature change can be determined.

Moreover, we need to specify the proper performance parameters under nominal conditions to have good accuracy. Based on performance verification experiments conducted at the factory, we use performance parameters under normal operating conditions. The data represented by the solid green line shown in Figure 6. 7 is used at nominal condition data in modeling, which is seen as the normal operation.

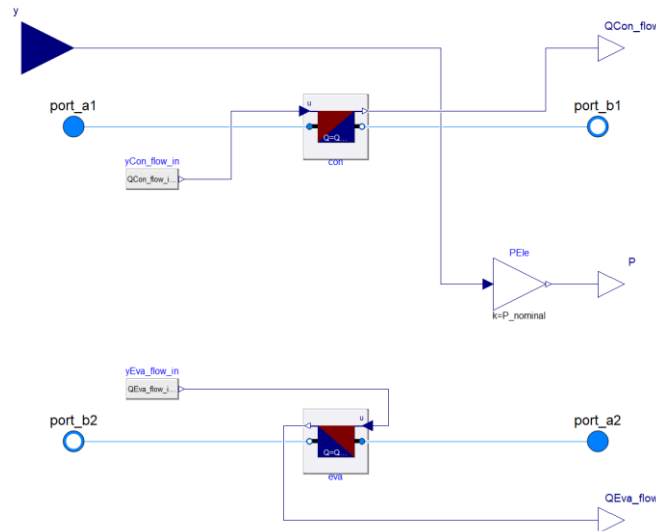


Figure 6. 6 The model of heat pump for floor heating used in modeling.

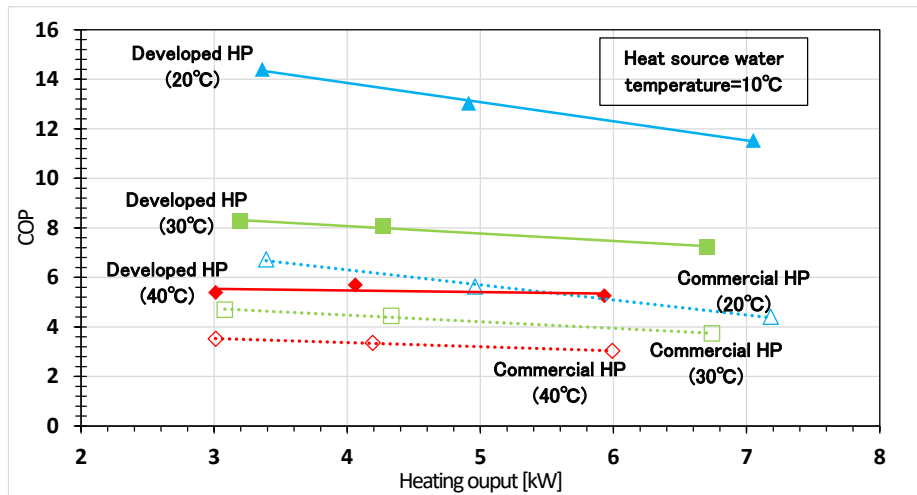


Figure 6. 7 FHHP performance data at nominal condition(solid green line).

### Floor heating system model

For the floor heating system, the radiant slab model developed in the Building Library by Wetter et

al.[33] was used as the main part of the floor heating system. As shown in Figure 6. 8, in this model,  $con\_a$  calculates the transient heat conduction between the upper surface and the structural layer containing the pipeline, and  $con\_b$  is between the plane containing the pipeline and the lower surface. The virtual resistance  $R_{Fic}$  is used to calculate the temperature of the structural layer containing the pipe. Besides, considering the thermal resistance of the tube wall, the convective heat transfer coefficient between the fluid and the inner wall of the tube is a function of the mass flow rate. The material layer can be set according to the actual installation. Based on the resistance network model

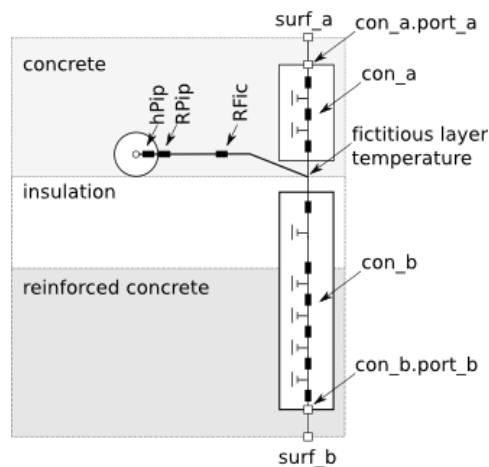


Figure 6. 8 Thermal resistance network of floor heating system model[33].

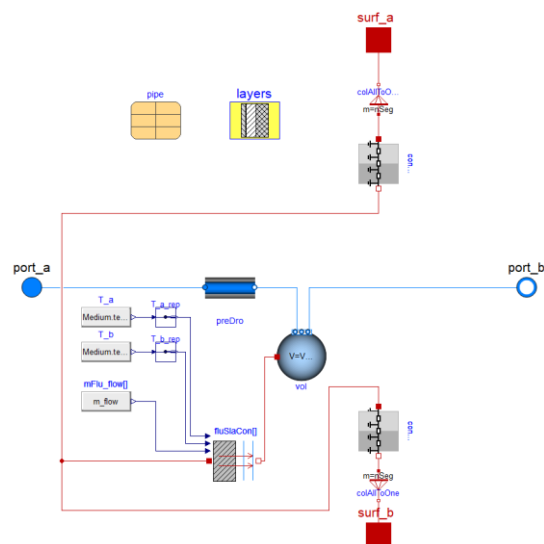


Figure 6. 9 Modeling of single circuit slab as the floor heating system[34].

described before, the realization of the floor heating system model in Modelica is shown in Figure 6. 9. The fluid component  $vol$  exchange heat with  $surf\_a$  and  $surf\_b$ , according to the resistance

network, to realize the heat transfer within the floor heating system. In this modeling, the same configuration as the actual material layer of the RE house is used. The piping system is a single circuit type; there is no insulation layer under the floor heating pipeline. The specific arrangement is shown in Table 6. 1.

### **Ground heat exchanger**

Because there is no available model for double helical ground heat exchangers, U-tube ground heat exchangers are used instead in the system modeling. Compared with the U-tube heat exchanger, the heat exchange area per unit depth of the spiral heat exchanger is higher. Therefore, while keeping other structural parameters unchanged, the U-tube ground heat exchangers of the same length are used instead. The combination of the GHX is constructed by using a hybrid model for the borefield heat exchanger, which is developed and realized in Modelica by Picard et al. [38]. The model uses a combination of a short-term response model and a long-term response model to calculate the step response that takes into account the heat transfer fluid, grouting, and transient heat transfer in the immediate ground with both short and long-term accuracy. The specific case can be simulated by setting 1) the thermal characteristics of the hole filling material; 2) including the thermal characteristics of the surrounding soil; 3) the parameters of the borehole configuration.

Each borehole is discretized in the vertical direction and has a common wall temperature, and only radial effects are considered. The thermal effects of circulating fluids, pipe, and filling materials are also taken into account. As shown in Figure 6. 10, by using a resistance-capacitance network to model the thermal behavior between the pipe and borehole wall, and the grouting capacitance can be distributed according to the number of pipes. Besides, the ground heat transfer has the same thermal boundary condition as the boreholes at the wall. It is modeled as an integral convolution model between the heat flux at the borehole wall and the thermal response factor of the borefield[38]. The realization of the borehole model with a single U-tube configuration in Modelica is shown in Figure 6. 11[33]. The circulating fluids (vol1 and vol2 in the figure) exchange heat with the borehole wall based on the resistance network model shown in Figure 6. 11.

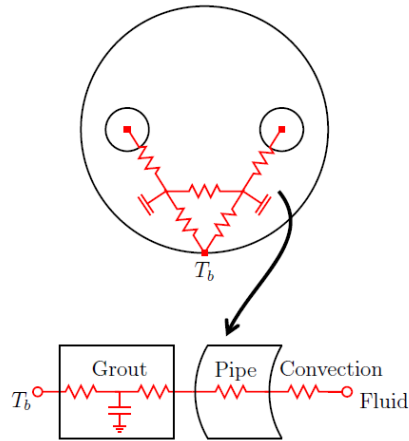


Figure 6.10 Resistance-capacitance network for a single U-tube borehole configuration[37].

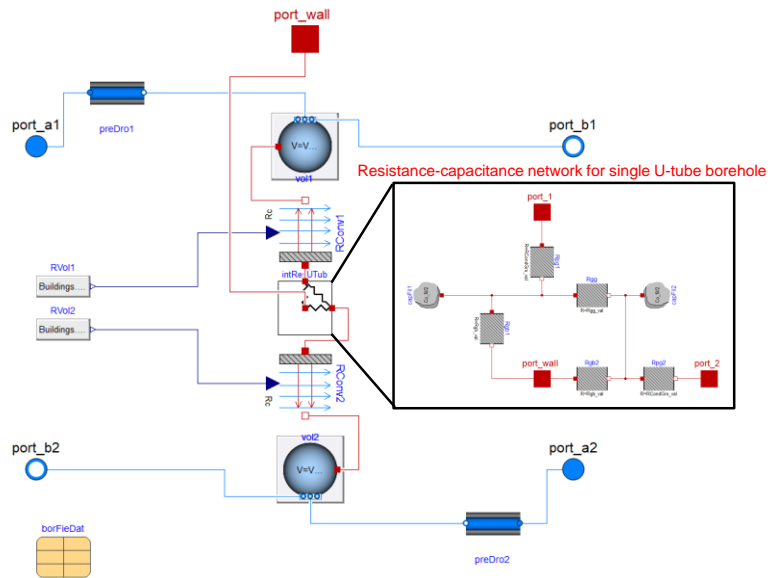


Figure 6.11 Heat transfer model between circulating fluid and filling of a single U-tube[33].

### Sky source heat pump

Because there is no direct expansion type heat pump model suitable for sky source heat pumps(SSHP, can collect heat during the day time and dissipate heat during the night time) at present, this system uses the solar-assisted heat pump form model as shown in Figure 6.13 instead[39]. Because there is an approximate principle, the same utilization solar radiation, and the ambient air by a solar collector, so there are similar performance changes that related to solar radiation and outdoor temperature.

Based on the actual measured performance data of the SSHP from field testing and the actual specifications of the solar collector, a solar-assisted heat pump system with the same performance

characteristics can be constructed. The nominal parameters can be determined according to the experiment, and modify the model of FHHP to obtain other parts except the collector. The solar collector model uses the model of the test method in the American standard ANSI/ASHRAE STANDARD 93-2010 Methods of Testing to Determine the Thermal Performance of Solar Collectors[40], to calculate the solar gain and heat loss in the model. The realization of the solar collector in Modelica is shown in Figure 6. 12. The fluid vol is heated or cooled(heat loss to air) based on global radiation, and dry bulb temperature read from weather data(weaBus in the figure). For the other components of the heat pump, the same model as FHHP was used here for the modeling of SSHP. As mentioned before, The Carnot effectiveness of heat pump can be calculated as:

$$\eta_{Carnot,0} = \frac{COP_0}{\left(\frac{T_{con,0}}{T_{con,0} - T_{eva,0}}\right)}$$

And the COP of the heat pump can be calculated as:

$$COP = \eta_{Carnot,0} \times COP_{Carnot} \times \eta_P$$

The meaning of each symbol is the same as previously stated. As with FHHP, specific values are determined by experimental and factory test results.

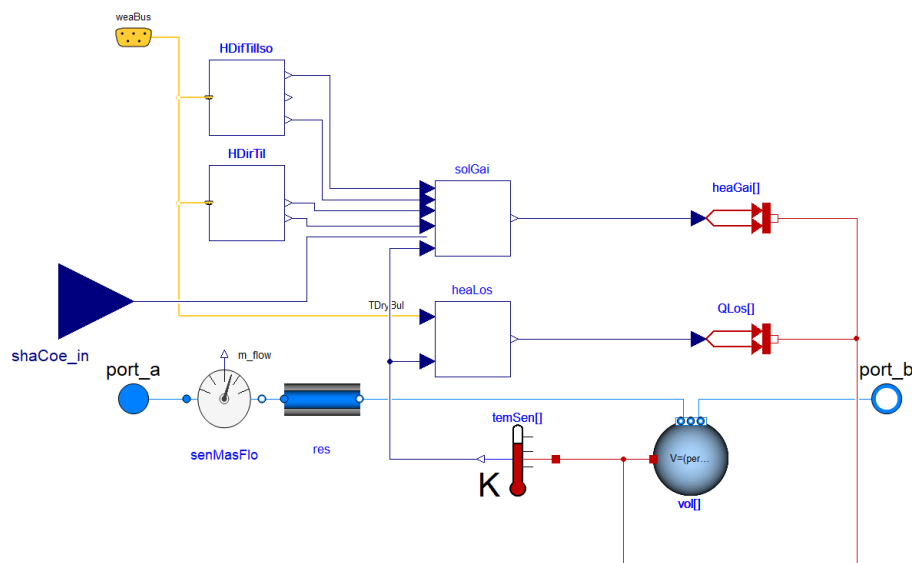


Figure 6. 12 Model of solar collector for ASHRAE STANDARD 93-2010 in Modelica[36].

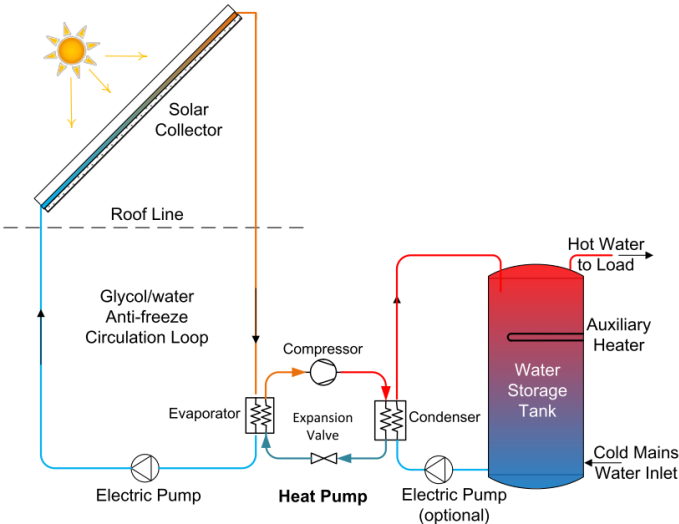


Figure 6. 13 indirect configuration of solar assisted heat pump.

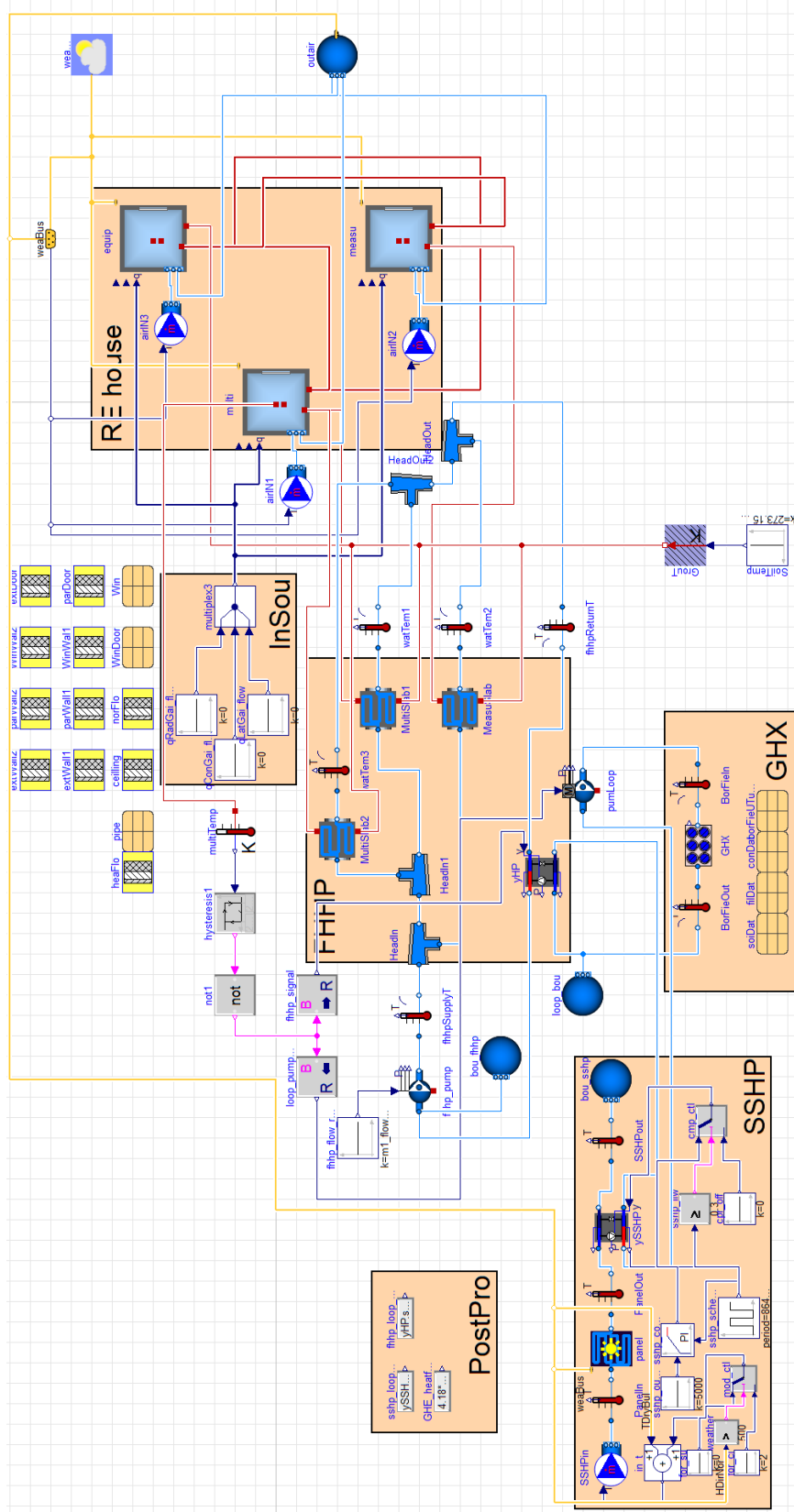


Figure 6. 14 Model of combination of RE house and heat pump system.

The model of the whole system that contains RE house and heat pump system is shown in Figure 6.14. In addition to the main heat pump and other components, the weather data is using TMY3 weather data[41]. Because Modelica's pump model sometimes has numerical problems, the pump model uses the fan pump model developed by Wetter to ensure that there is a unique solution for most situations[42].

As shown in InSou part in the system model, this is a preset internal heat source assembly. It can be used to model the internal heat sources such as radiation and convection. However, this was not used in this simulation because there was no internal heat source during the experiment. Also, each room has mechanical ventilation; the value is set according to the actual situation.

### **Modeling conditions**

The nominal conditions of each machine are set based on the results of experiments and factory tests. The specifications of the house structure, heat pump system, and water loop pipe network are also the same as the actual system. The specific setting parameters are shown in the following tables.

#### **RE house**

The parameter used for setting the structure of all three rooms in RE house are shown in Table 6.2. The material and schematics information are shown in section 6.4.1.

Table 6.2 Parameters of RE house setting.

	Multi-purpose	Measurement	Facility
Room area (m <sup>2</sup> )	33.12	13.24	13.24
Hight (m)	3.05 – 6.555	2.4	2.4
Ventilation frequency(times/h)	0.6	0.6	0.6
Floor heating area (m <sup>2</sup> )	33.12	13.24	0

#### **Heat pump for floor heating**

As mentioned before, the factory test result was used as the nominal condition for setting the performance data of FHHP. Besides, the data represented by the solid green line in Figure 6.7 is used at nominal condition data in modeling, the Carnot effectiveness was set to 0.65 according to the test result.

### Floor heating system

Besides the detailed information mentioned in 6.4.1, other settings used in modeling are given in Table 6. 3 below.

Table 6. 3 Parameters of the floor heating system.

Connection of piping system	Parallel
Length of pipe in the multi-purpose room (m)	200
Length of pipe in the measurement room (m)	100
Pipe distance (m)	0.1656
Circulating medium	Water

### Ground heat exchanger

Because it is necessary to ensure the same heat exchange area of the GHX, besides the length, other parameters used for modeling are the same as the double-helical ground heat exchanger and are given in the Table 6. 4 below.

Table 6. 4 Parameters of the GHX

Borehole configuration	Single u-tube
Height of the borehole (m)	75
Radius of the borehole (m)	0.35
Borehole buried depth (m)	3
Number of boreholes	3
Outer radius of the ground heat exchanger (m)	0.039
Thermal conductivity of the pipe (W/(m·k))	0.42
Thickness of pipe (m)	0.0015
Shank spacing (m)	0.15

Table 6. 5 Physical property values used for GHX modeling.

	Thermal conductivity [W/m·k]	Density [kg/m <sup>3</sup> ]	Specific heat capacity [J/kg·k]
soil	1.5	1800	1650
Silica sand	2	2050	1320

### Sky source heat pump

Based on the actual measured performance data of the SSHP from the winter field testing and the actual specifications of the solar collector[43], the parameters used for modeling a solar-assisted heat pump system are shown in Table 6. 6 below.

Table 6. 6 Parameters of SSHP, including outdoor panel and performance of heat pump.

Panel type	Glazed flat plate
Panel orientation and angle	Facing south, 30 degrees
Panel area (m <sup>2</sup> )	8
Circulating medium	Propylene glycol water
Carnot effectiveness	0.65

## 6.4.2 Simulation and validation

### Case setting and simulation condition

To verify the validity and accuracy of the model, we chose to compare the actual measurements on March 21 and March 25 as the typical days in the continuous operation experiment in winter to evaluate the accuracy of the model. As shown in Table 6. 7, there are 4 cases set in the simulation. We conducted the comparison under the same conditions, which means the weather data obtained by the actual measurement is used as weather input of simulation.

Firstly, we verify the effectiveness of the house and FHHP model by comparing the operation of the floor heating system on March 21 and March 25 and the changes in the thermal environment in the

RE house. Afterward, the effectiveness and accuracy of the system model after adding the SSHP model were verified by comparing the performance changes of the SSHP during the two-day SSHP heat collector operation. The detailed case setting is shown in Table 6. 7. Regarding the control method, the FHHP is set to be an ON/OFF control that keeps the room temperature between 20–25 °C, which corresponds to the winter experiment.

Table 6. 7 Case setting for verification of the system model.

Case1	21 March (cloudy day), space heating operation by FHHP
Case2	25 March (sunny day), space heating operation by FHHP
Case3	21 March (cloudy day), heat collecting operation by SSHP
Case4	25 March (sunny day), heat collecting operation by SSHP

## **Results and discussion**

### **Case1: Space heating operation by FHHP on 21 March**

Figure 6. 15 to Figure 6. 23 show the experimental and simulation result of space heating operation by FHHP on 21 March. Figure 6. 16 and Figure 6. 17 shows the experiment and simulation result of indoor environment changes in the multi-purpose room, respectively. As shown in the figure, under the same weather conditions and underfloor heating pump operating conditions, the experimental value and the simulated value directly affected by the indoor ground temperature are almost the same, and the temperature difference is less than 1 degree. However, for the indoor air temperature, the simulation result has a temperature difference of about 1 degree from the experimental value. For the reason of the error, we think it is because the house model used assumes that the indoor air is completely mixed. Therefore, the temperature stratification in the room is not taken into account, so this difference is generated.

Figure 6. 18 and Figure 6. 19 show the simulation result of changes in the floor heating system in the multi-purpose and measurement room, respectively. According to the measured values, the ground temperature under the floor of the room was set to 23 degrees in the simulation. As shown in Figure 6. 18, because the FHHP runs continuously throughout the day, the indoor floor temperature does not change much, as the same with experimental results. The simulation results

also show that the indoor floor temperature in two different rooms is slightly different. We believe that the indoor ground temperature of the multi-purpose room drops faster because the enclosing structure area of the room is larger, and the insulation performance is average, so it is more susceptible to external temperature changes.

In addition, because in the RE house floor heating system, there is no insulation layer under the hot water loop system. Therefore, it can be expected that this will cause some heat loss. According to the simulation results, we found that about 1/3 of the heat flowed into the ground when the supply and return water temperature, flow rate, and indoor state were the same as the experimental value. The area of the multi-purpose room is larger, so there is more heat loss than the measurement room. Figure 6. 20, Figure 6. 21, Figure 6. 22, and Figure 6. 23 shows the experiment and simulation result of changes in the water loop side of FHHP and changes in the performance of FHHP, respectively. Comparing Figure 6. 20 and Figure 6. 21, the difference between the simulation result and the experimental value is minimal, showing good accuracy. However, the simulation result does not show the change in flow rate and water temperature caused by the operation of SSHP. Because SSHP was not added in this case, there were no fluctuations due to SSHP. The verification, including the SSHP, will be shown in case3. Figure 6. 22and Figure 6. 23 show the FHHP performance changes. The results show acceptable accuracy, the simulation results reproduce the FHHP performance (COP) well, and the thermal output and power consumption are not much different from the experimental values. For the same reason, the performance of FHHP did not fluctuate due to the operation of SSHP in the simulation

The simulation results of case 1 show that under cloudy conditions, the constructed system model has good accuracy and can reflect the performance changes of the indoor and FHHP. The verification under sunny conditions will be explained in case2.

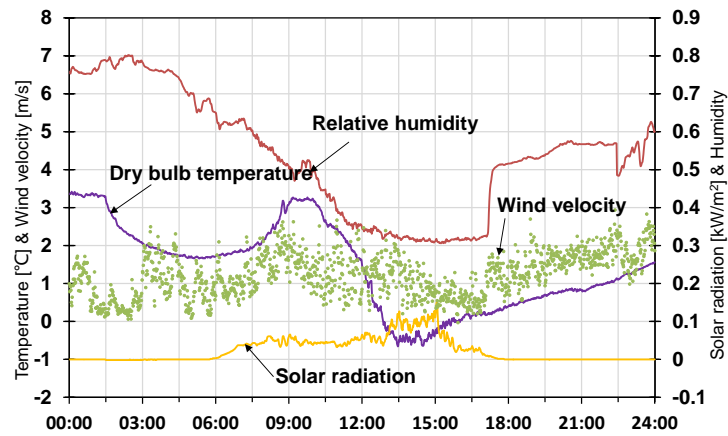


Figure 6. 15 Weather condition on 21 March.

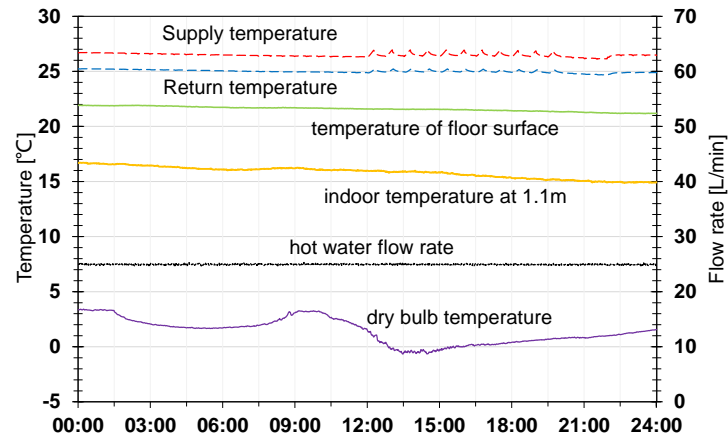


Figure 6. 16 Indoor environment changes in the multi-purpose room(experiment).

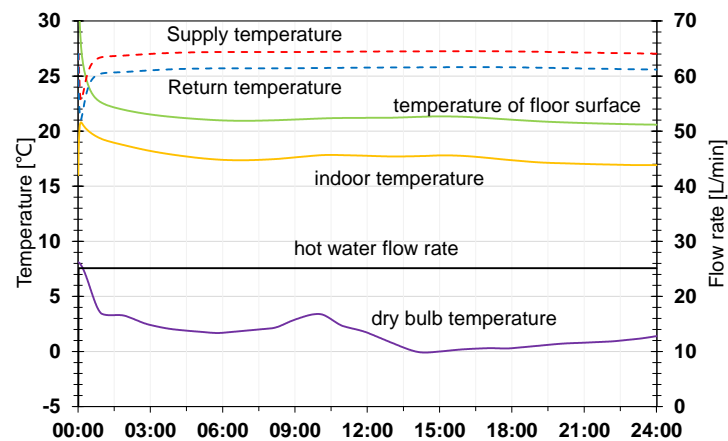


Figure 6. 17 Indoor environment changes in the multi-purpose room(simulation).

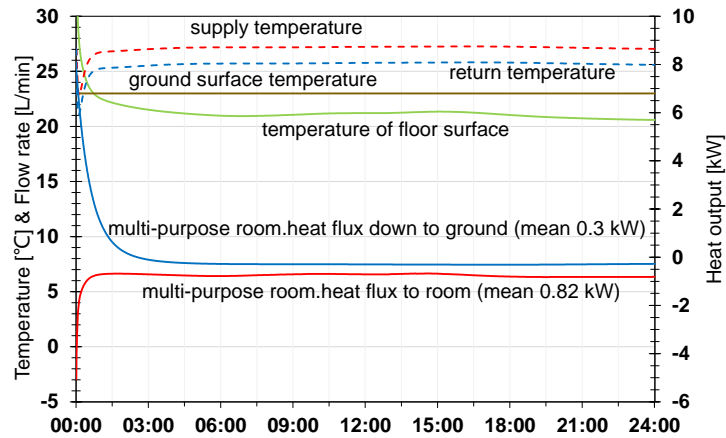


Figure 6. 18 Changes of floor heating system in the multi-purpose room(simulation).

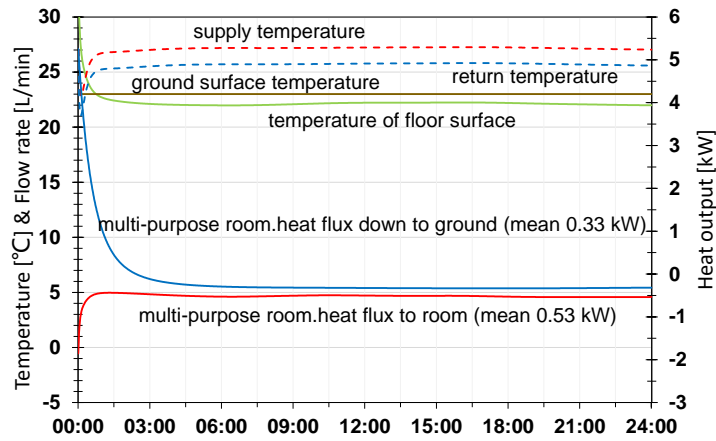


Figure 6. 19 Changes of floor heating system in the measurement room(simulation).

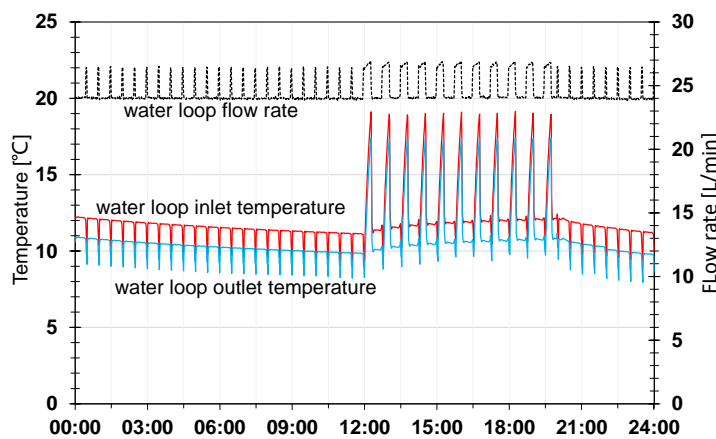


Figure 6. 20 Changes in the water loop side of FHHP(experiment).

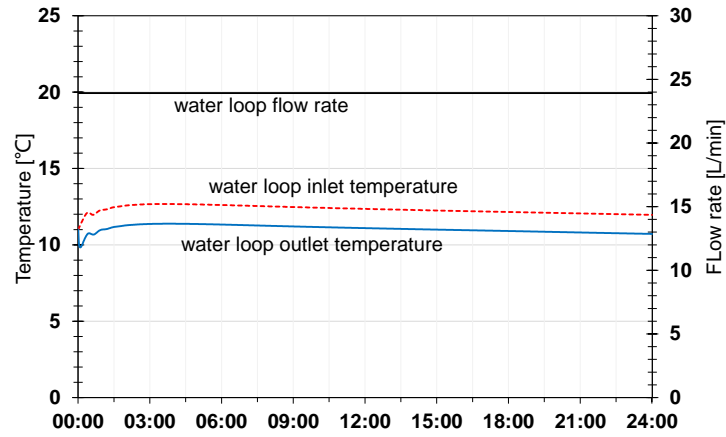


Figure 6. 21 Changes in the water loop side of FHHP(simulation).

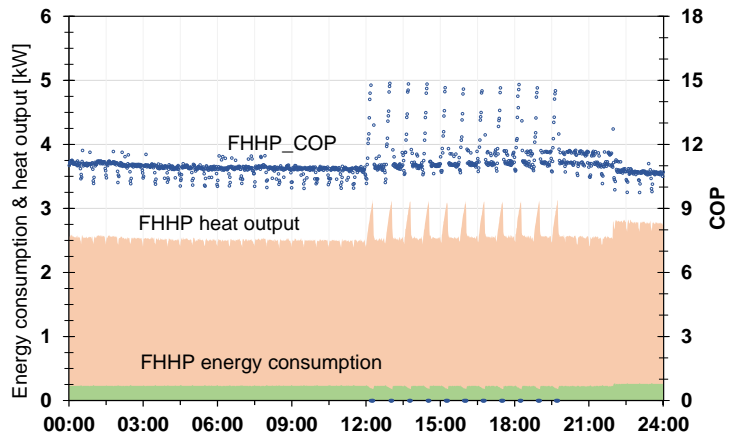


Figure 6. 22 Changes in the performance of FHHP(experiment).

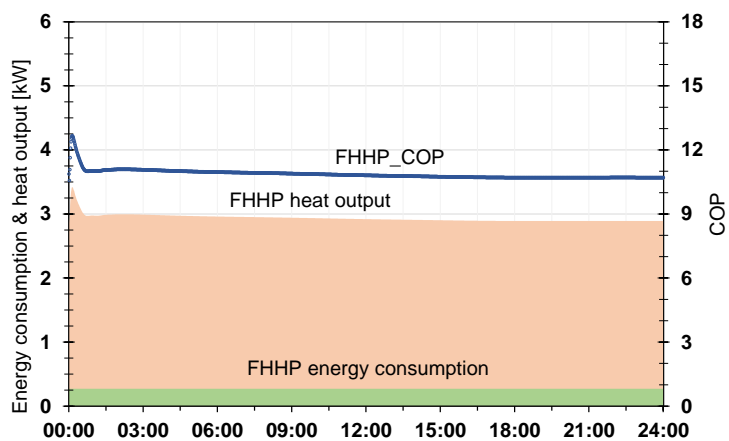


Figure 6. 23 Changes in the performance of FHHP(simulation).

**Case2: Space heating operation by FHHP on 25 March**

Figure 6. 24 to Figure 6. 32 show the experimental and simulation result of space heating operation

by FHHP on 25 March, which was a sunny day. Figure 6. 24 shows the weather conditions of the day because it was sunny, there was sufficient solar radiation during the day, and the dry bulb temperature also kept a higher temperature. Figure 6. 25 and Figure 6. 26 shows the experiment and simulation result of indoor environment changes in the multi-purpose room, respectively. As shown in Figure 6. 25 and Figure 6. 26, around 10:30, because the indoor temperature reached the upper limit of the set value, the FHHP stopped running. The simulation results also showed the same running conditions, and the FHHP stopped running at almost the same time. However, it can be seen by comparison that the simulation values of indoor air temperature and floor surface temperature are higher than the experimental values. As for a reason, as mentioned above, one of the reasons is that the house model adopted assumes that the indoor air is completely mixed. Hence, the result is average indoor air temperature, not the air temperature at the experimental value of 1.1 meters. Besides, this comparison is based on the results of the multi-purpose room. There is a large floor-to-ceiling window facing south in this room, so there will be plenty of solar radiation entering the room during the day. In the room model, it is assumed that the sunlight is first irradiated on the floor and then reflected other surfaces of the room, so a higher floor temperature appears in the simulation results. We also think that this may also cause the indoor temperature to be higher than the experimental value.

Figure 6. 27 and Figure 6. 28 show the simulation result of changes in the floor heating system in the multi-purpose and measurement room, respectively. Figure 6. 27 shows the simulation results of the multi-purpose room. As with the experimental results, after the FHHP stopped operating, due to sufficient solar radiation, the indoor temperature and the floor surface temperature increased. At the same time, the simulation results show that after about 10 o'clock, the indoor floor surface temperature is higher than the circulating water temperature of the floor heating system. At this time, the heat flow direction starts to change from indoor to the underground. The measurement room in Figure 6. 28 also shows the same result, but because the window area is small, the size of the heat flow is not so apparent. As the outside air temperature changes, the indoor floor surface temperature became lower than the temperature of the floor heating circulating water, and the heat flow direction returns to its original state.

Figure 6. 29 to Figure 6. 32 shows the FHHP performance changes for 25 March. Since there was also no SSHP operation, there were no changes in temperature and flow rate caused by SSHP in the

simulation results. For the heating performance of FHHP, as shown in Figure 6. 31 and Figure 6. 32, compared with the experimental results, it can be found that the simulation results reproduce the FHHP performance under the same conditions well. The simulation results reflecting the COP of the heat pump differ from the experimental values by less than 1.

Therefore, based on the result, it can be judged that this system model can reproduce the running condition of the distributed heat pump system in both sunny and cloudy conditions, and has good accuracy.

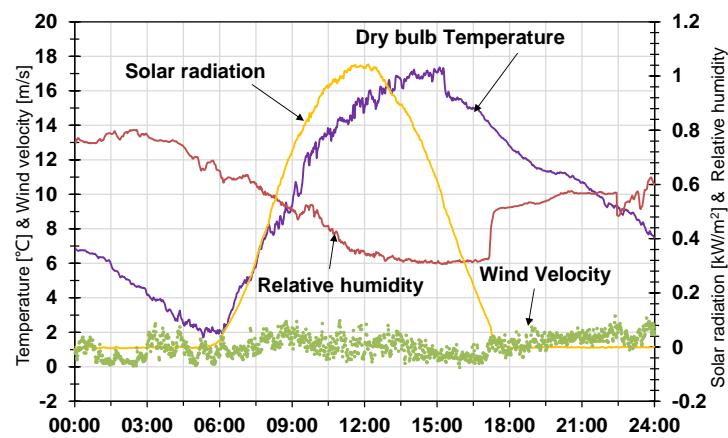


Figure 6. 24 Weather condition on 25 March.

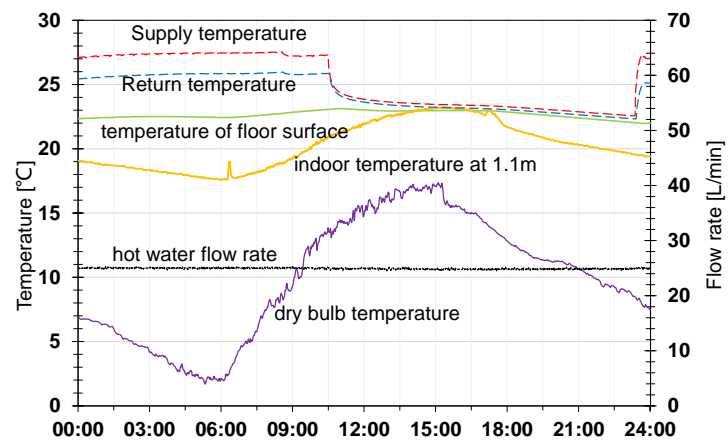


Figure 6. 25 Indoor environment changes in the multi-purpose room(experiment).

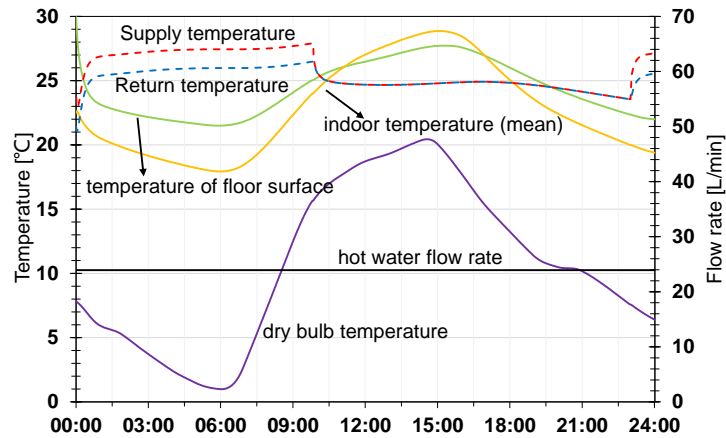


Figure 6. 26 Indoor environment changes in the multi-purpose room(simulation).

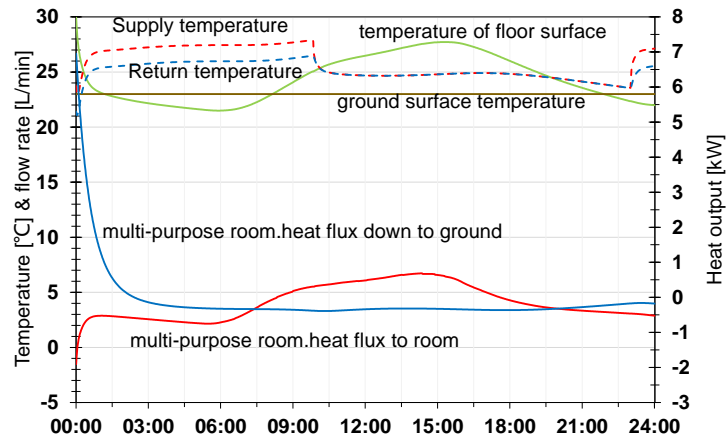


Figure 6. 27 Changes of floor heating system in the multi-purpose room(simulation).

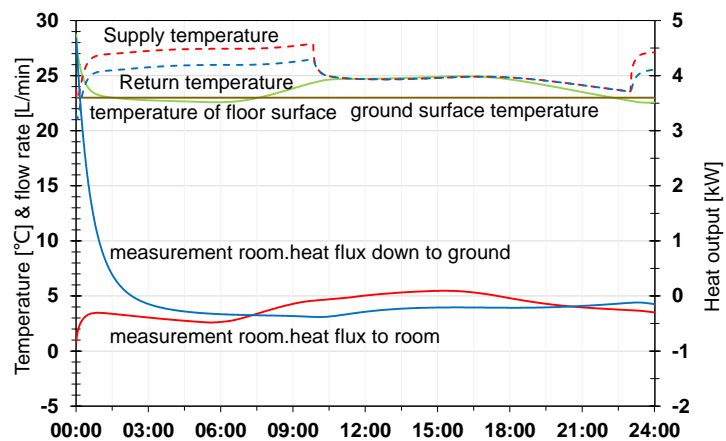


Figure 6. 28 Changes of floor heating system in the measurement room(simulation).

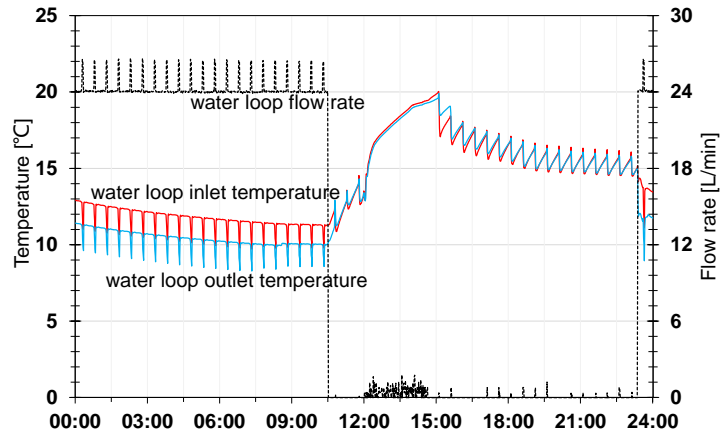


Figure 6. 29 Changes in the water loop side of FHHP(experiment).

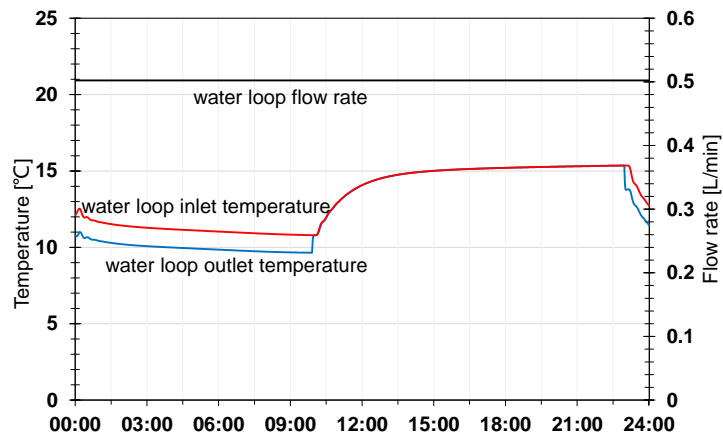


Figure 6. 30 Changes in the water loop side of FHHP(simulation).

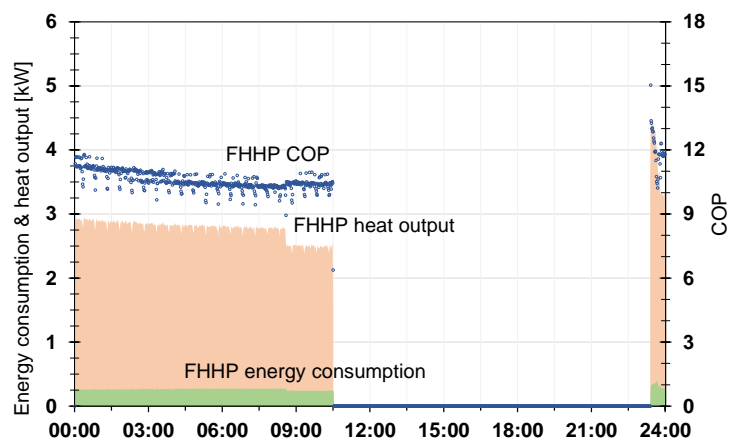


Figure 6. 31 Changes in the performance of FHHP(experiment).

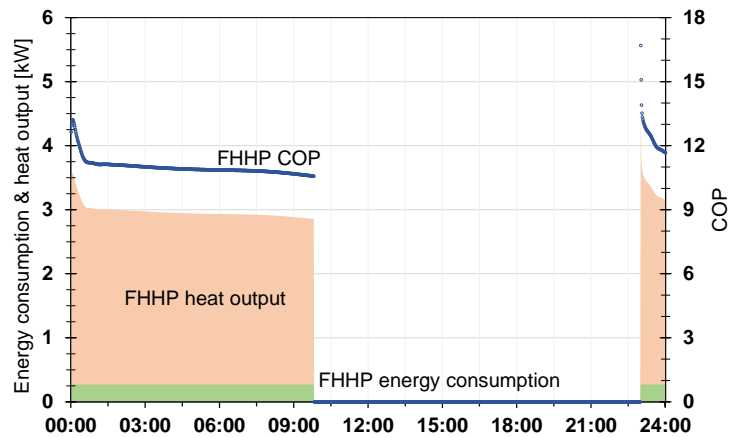


Figure 6. 32 Changes in the performance of FHHP(simulation).

### Case3: Heat collecting operation by SSHP on 21 March

Figure 6. 33 to Figure 6. 36 show the experiment and simulation results of the SSHP heating operation on a cloudy day, March 21. Figure 6. 33 and Figure 6. 34 show the experimental and simulation results of the performance change of SSHP, respectively. It can be seen from the comparison that the difference between the experimental value and the simulation value is minimal, indicating that the simulation results in Figure 6. 34 reproduces the performance of the SSHP well. In the case of ensuring the heat output of FHHP, the simulation value of the average COP during operation is about one degree higher than the experimental value; we think it is an acceptable accuracy.

Figure 6. 35 and Figure 6. 36 shows the temperature and flow changes on the water loop side when the SSHP is running. The changes in the experimental results in Figure 6. 35 are due to the changes in FHHP and SSHP running simultaneously. Because the water loop circulating water temperature is lower than the set value, the SSHP started and began to heat the circulating water. The simulation results in Figure 6. 36 also show the same results. The irregular changes in the inlet and outlet temperatures in Figure 6. 35 are considered to be caused by the reversal of the circulating water flow in the experiment. By setting the pump reasonably to change the direction of circulating water flow direction, this did not appear in the simulation.

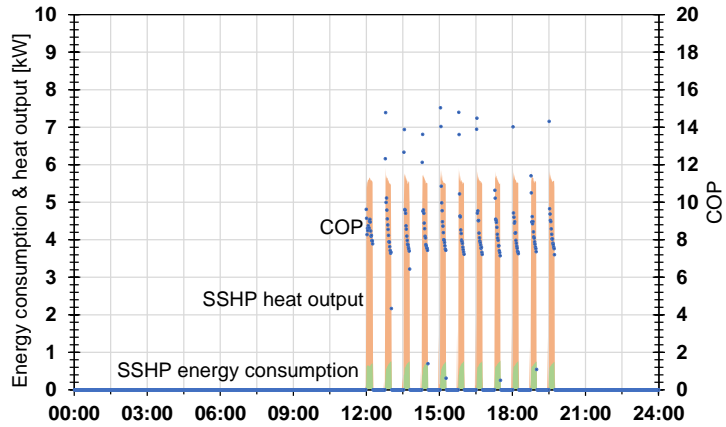


Figure 6. 33 Changes in the performance of SSHP(experiment).

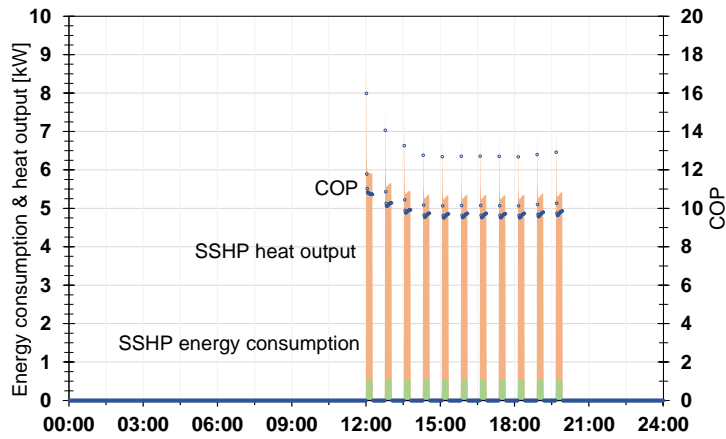


Figure 6. 34 Changes in the performance of SSHP(simulation).

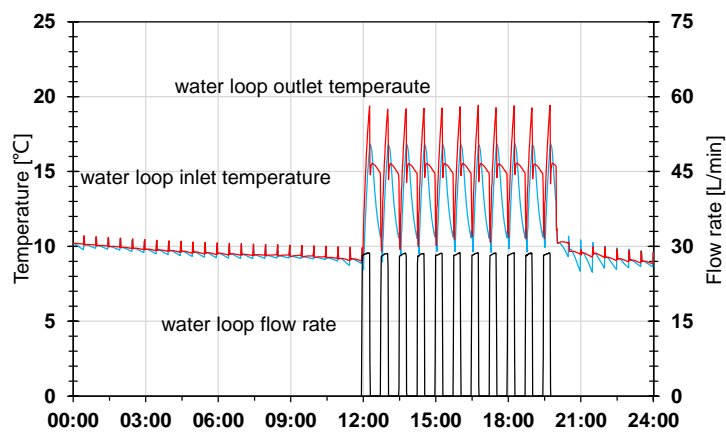


Figure 6. 35 Changes in the water loop side of SSHP(experiment).

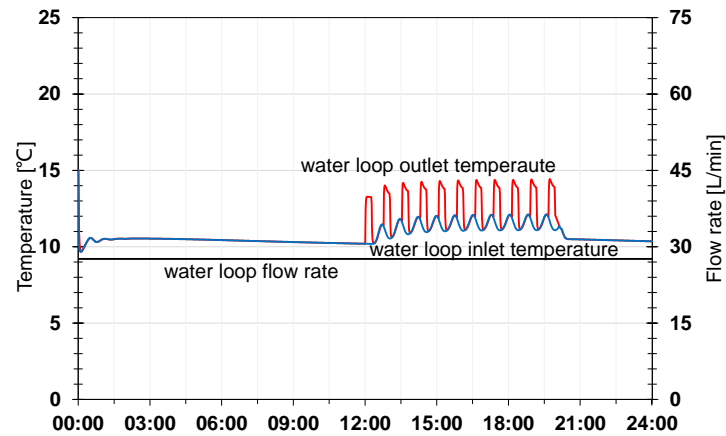


Figure 6. 36 Changes in the water loop side of SSHP(simulation).

#### Case4: Heat collecting operation by SSHP on 25 March

Figure 6. 37 to Figure 6. 41 show the experiment and simulation results of the SSHP heating operation on a sunny day, March 25. Figure 6. 37 and Figure 6. 38 show the experimental and simulation results of the performance change of SSHP, respectively. Similar to the cloudy day, it can be seen from the comparison that the difference between the experimental value and the simulation value is not apparent, indicating that the simulation results reproduce the performance of the SSHP well. However, although the difference between the experimental results of the COP and the simulation results gradually decreased, at the beginning of the heat pump operation, the simulation value did not appear to rise as the experimental value. With the increase of solar radiation and dry bulb temperature after reaching the highest point, the simulation value of COP showed a downward trend as the experimental value.

Figure 6. 39 and Figure 6. 40 show the temperature and flow rate changes on the water loop side when the SSHP is running. The change in the experiment results in Figure 6. 39 is due to the change in the operation of SSHP. In the simulation, the forced pump operation was not set to detect the circulating water temperature, and there was no change in the water temperature and flow rate outside the operating period of the SSHP. It can be seen from Figure 6. 39 and Figure 6. 40 that during the running time of FHHP and SSHP, the model reproduces the water temperature changes in the water loop well. Figure 6. 41 shows the difference between the inlet temperature and the outlet temperature when the SSHP is running. With the operation, the difference between the experimental value and the simulation value is gradually reduced.

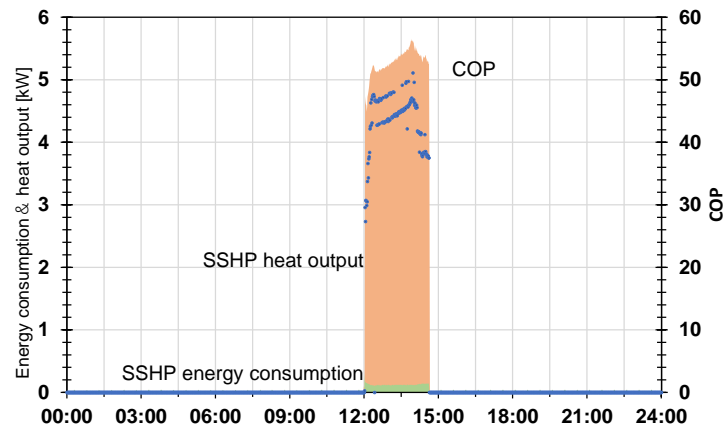


Figure 6. 37 Changes in the performance of SSHP(experiment).

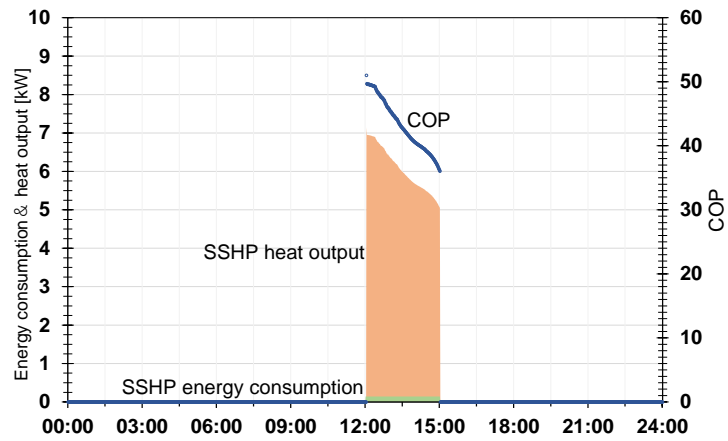


Figure 6. 38 Changes in the performance of SSHP(simulation).

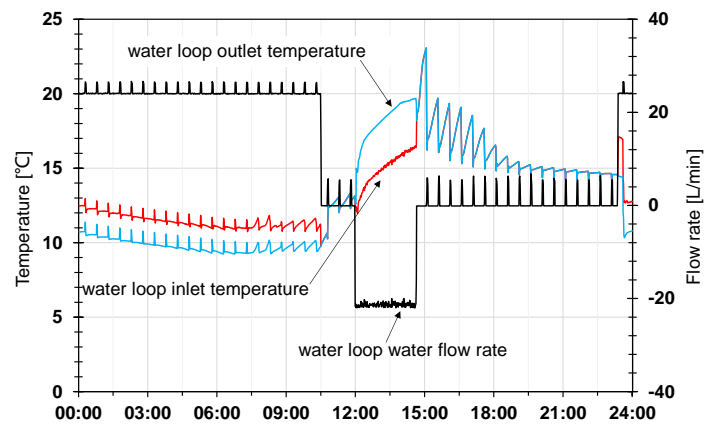


Figure 6. 39 Changes in the water loop side of SSHP(experiment).

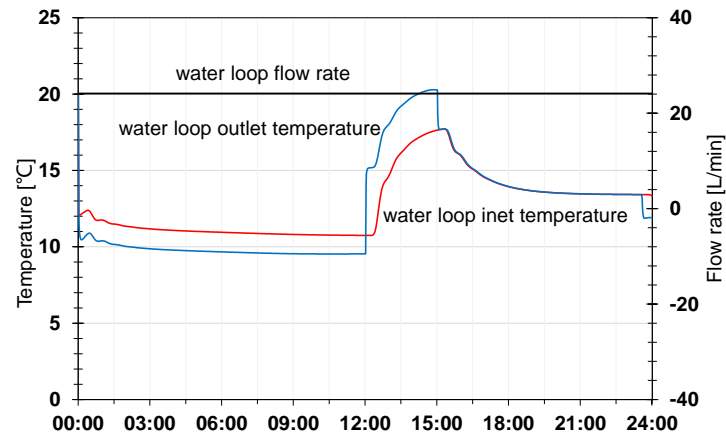


Figure 6. 40 Changes in the water loop side of SSHP(experiment).

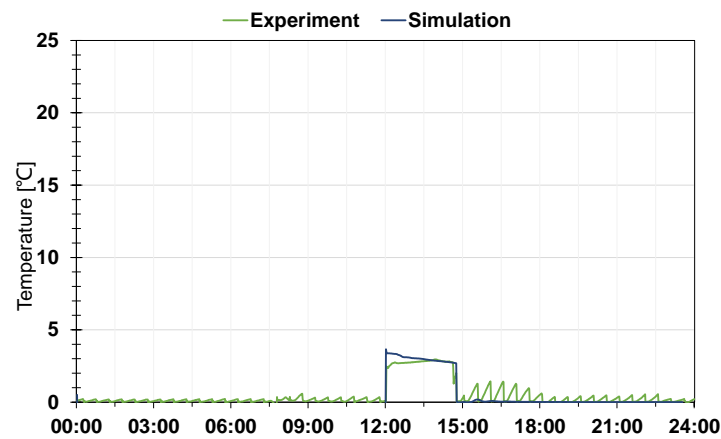


Figure 6. 41 Change of temperature difference between SSHP inlet and outlet(simulation).

## 6.5 Summary

In this chapter, we first analyze the characteristics and advantages and disadvantages of the tools and methods used in modeling and simulation of building energy systems and review the relevant research literature in recent years. According to the research needs and goals, it explains why Modelica was chosen as a modeling tool. We briefly introduce the Modelica language and its application in the field of architecture. Next, we introduced the modeling of the distributed heat pump system proposed earlier, including the description of each model and the whole system description.

The validity and accuracy of the model are verified by comparing the experiment results, including

a sunny day and a cloudy day in winter. In the comparison, we compared the changes in the water loop (such as temperature and flow rate), and the performance (mainly COP) of the floor heating heat pump and sky source heat pump. According to the comparison with the experiment results, the validity of the system model built by Modelica is proved. Also, the constructed system model has acceptable accuracy and can well reproduce the performance changes and dynamic characteristics of the system.

Moreover, in addition to reflecting the performance and thermal characteristics changes of the heat pump system well, modeling and simulation using Modelica also clarified the phenomena that did not obtain through this experiment. For example, there was no insulation installed under the floor in test building, experiment results did not reveal how much heat escaped from floor heating system to the ground. A detailed model of the floor heating system contained in the test building was constructed, and the floor heat flow rate in all rooms was qualitatively and quantitatively determined by simulation in different operating conditions.

As a model of the distributed heat pump system built using Modelica, various control methods can be developed and verified based on this model, as well as verification of further system design and optimization.

## 6.6 Reference

- [1] Crawley DB, Lawrie LK, Winkelmann FC, Buhl WF, Huang YJ, Pedersen CO, et al. EnergyPlus: Creating a new-generation building energy simulation program. *Energy Build* 2001. doi:10.1016/S0378-7788(00)00114-6.
- [2] Daum A, Wolf DM. TRANSYS - A multidisciplinary software system for preliminary design, analysis, and evaluation of space transportation systems. 5th Symp. Multidiscip. Anal. Optim. 1994, 1994. doi:10.2514/6.1994-4342.
- [3] Hilding Elmqvist. Modelica — A unified object-oriented language for physical systems modeling. *Simul Pract Theory* 1997. doi:10.1016/s0928-4869(97)84257-7.
- [4] Steinau S, Marrella A, Andrews K, Leotta F, Mecella M, Reichert M. DALEC: a framework for the systematic evaluation of data-centric approaches to process management software. *Softw Syst Model* 2019. doi:10.1007/s10270-018-0695-0.
- [5] Perelroyzen E, Evgeni P. Simulink®: Dynamic System Simulation for MATLAB®. *Digit. Integr. Circuits*, 2018. doi:10.1201/9781315222110-1.
- [6] Yi H, Srinivasan RS, Braham WW. An integrated energy-emergy approach to building form optimization: Use of EnergyPlus, emergy analysis and Taguchi-regression method. *Build Environ* 2015;84:89–104. doi:10.1016/j.buildenv.2014.10.013.
- [7] Rhodes JD, Gorman WH, Upshaw CR, Webber ME. Using BEopt (EnergyPlus) with energy audits and surveys to predict actual residential energy usage. *Energy Build* 2015;86:808–16. doi:10.1016/j.enbuild.2014.10.076.
- [8] Pang X, Bhattacharya P, Neill ZO, Haves P, Wetter M, Bailey T. REAL-TIME BUILDING ENERGY SIMULATION USING ENERGYPLUS AND THE BUILDING CONTROLS VIRTUAL TEST BED Lawrence Berkeley National Laboratory , Berkeley , CA , USA United Technologies Research Center , East Hartford , CT , USA. *Proc Build Simul 2011* 2011:2890–6.
- [9] Wetter M. Co-simulation of building energy and control systems with the building controls virtual test bed. *J Build Perform Simul* 2011;4:185–203. doi:10.1080/19401493.2010.518631.
- [10] Fumo N, Mago P, Luck R. Methodology to estimate building energy consumption using EnergyPlus Benchmark Models. *Energy Build* 2010;42:2331–7.

- doi:10.1016/j.enbuild.2010.07.027.
- [11] Kämpf JH, Wetter M, Robinson D. A comparison of global optimization algorithms with standard benchmark functions and real-world applications using EnergyPlus. *J Build Perform Simul* 2010;3:103–20. doi:10.1080/19401490903494597.
- [12] Winkelmann F, Buhl F, Pedersen C, Fisher D, Liesen R, Taylor R, et al. LINKING THE COMIS MULTI-ZONE AIRFLOW MODEL WITH THE ENERGYPLUS BUILDING ENERGY SIMULATION PROGRAM 1999;2:1065–70.
- [13] Royapoor M, Roskilly T. Building model calibration using energy and environmental data. *Energy Build* 2015;94:109–20. doi:10.1016/j.enbuild.2015.02.050.
- [14] Zhao J, Lam KP, Ydstie BE, Karaguzel OT. EnergyPlus model-based predictive control within design–build–operate energy information modelling infrastructure. *J Build Perform Simul* 2015;8:121–34. doi:10.1080/19401493.2014.891656.
- [15] Langevin J, Wen J, Gurian PL. Including occupants in building performance simulation: Integration of an agent-based occupant behavior algorithm with energyplus. 2014 ASHRAE/IBPSA-USA Build Simul Conf 2014:417–24.
- [16] Lam KP, Zhao J, Ydstie EB, Wirick J, Qi M, Park J. An energyplus whole building energy model calibration method for office buildings using occupant behavior data mining and empirical data. 2014 ASHRAE/IBPSA-USA Build Simul Conf 2014:160–7.
- [17] Chuah JW, Raghunathan A, Jha NK. ROBESim: A retrofit-oriented building energy simulator based on EnergyPlus. *Energy Build* 2013;66:88–103. doi:10.1016/j.enbuild.2013.07.020.
- [18] Zhu D, Hong T, Yan D, Wang C. A detailed loads comparison of three building energy modeling programs: EnergyPlus, DeST and DOE-2.1E. *Build Simul* 2013;6:323–35. doi:10.1007/s12273-013-0126-7.
- [19] Tabares-Velasco PC, Christensen C, Bianchi M. Verification and validation of EnergyPlus phase change material model for opaque wall assemblies. *Build Environ* 2012;54:186–96. doi:10.1016/j.buildenv.2012.02.019.
- [20] Eisenhower B, O’Neill Z, Fonoberov VA, Mezić I. Uncertainty and sensitivity decomposition of building energy models. *J Build Perform Simul* 2012;5:171–84. doi:10.1080/19401493.2010.549964.
- [21] Antoniadis CN, Martinopoulos G. Optimization of a building integrated solar thermal system

- with seasonal storage using TRNSYS. *Renew Energy* 2019;137:56–66.  
doi:10.1016/j.renene.2018.03.074.
- [22] Asadi E, da Silva MG, Antunes CH, Dias L. A multi-objective optimization model for building retrofit strategies using TRNSYS simulations, GenOpt and MATLAB. *Build Environ* 2012;56:370–8. doi:10.1016/j.buildenv.2012.04.005.
- [23] Chargui R, Sammouda H, Farhat A. Geothermal heat pump in heating mode: Modeling and simulation on TRNSYS. *Int J Refrig* 2012;35:1824–32. doi:10.1016/j.ijrefrig.2012.06.002.
- [24] Kuznik F, Virgone J, Johannes K. Development and validation of a new TRNSYS type for the simulation of external building walls containing PCM. *Energy Build* 2010;42:1004–9. doi:10.1016/j.enbuild.2010.01.012.
- [25] Wetter M, Bonvini M, Nouidui TS. Equation-based languages - A new paradigm for building energy modeling, simulation and optimization. *Energy Build* 2016;117:290–300. doi:10.1016/j.enbuild.2015.10.017.
- [26] Wetter M, Treeck C Van, Hensen J. New generation computational tools for building and community energy systems. *IEA EBC Annex 60* 2013:1–11.
- [27] Wetter M, Wright J. A comparison of deterministic and probabilistic optimization algorithms for nonsmooth simulation-based optimization. *Build. Environ.*, 2004. doi:10.1016/j.buildenv.2004.01.022.
- [28] Zuo W, Wetter M, Tian W, Li D, Jin M, Chen Q. Coupling indoor airflow, HVAC, control and building envelope heat transfer in the Modelica Buildings library. *J Build Perform Simul* 2016;9:366–81. doi:10.1080/19401493.2015.1062557.
- [29] Fu Y, Zuo W, Wetter M, VanGilder JW, Yang P. Equation-based object-oriented modeling and simulation of data center cooling systems. *Energy Build* 2019;198:503–19. doi:10.1016/j.enbuild.2019.06.037.
- [30] Fu Y, Zuo W, Wetter M, VanGilder JW, Han X, Plamondon D. Equation-Based object-oriented modeling and simulation for data center Cooling: A case study. *Energy Build* 2019;186:108–25. doi:10.1016/j.enbuild.2019.01.018.
- [31] Wetter M. Multizone building model for thermal building simulation in modelica. *Submitt to Model Conf* 2006 2006:517–26. doi:10.1016/j.ijthermalsci.2007.10.011.
- [32] Wetter M. Modelica-based modelling and simulation to support research and development in

- building energy and control systems. *J Build Perform Simul* 2009;2:143–61.  
doi:10.1080/19401490902818259.
- [33] Wetter M, Zuo W, Nouidui TS, Pang X. Modelica Buildings library. *J Build Perform Simul* 2014. doi:10.1080/19401493.2013.765506.
- [34] Wetter M, Zuo W, Nouidui TS. Recent Developments of the Modelica “Buildings” Library for Building Energy and Control Systems. *Proc from 8th Int Model Conf Tech Univeristy, Dresden, Ger 2011*;63:266–75. doi:10.3384/ecp11063266.
- [35] Tiller M. *Modelica by Example*. n.d.
- [36] Wetter M, Treeck C van. *IEA EBC Annex 60: New Generation Computing Tools for Building and Community Energy Systems*. 2017.
- [37] Müller D, Lauster M, Constantin A, Fuchs M, Remmen P. AIXLIB – AN OPEN-SOURCE MODELICA LIBRARY WITHIN THE IEA-EBC ANNEX 60 FRAMEWORK RWTH Aachen University , E.ON Energy Research Center , Institute for Energy Efficient Buildings and Indoor Climate , Germany INTEGRATION WITH ANNEX 60 2016:3–9.
- [38] Picard D, Helsen L. Advanced Hybrid Model for Borefield Heat Exchanger Performance Evaluation , an Implementation in Modelica 2014. doi:10.3384/ECP14096857.
- [39] Harrison S. The Potential and Challenges of Solar Boosted Heat Pumps for Domestic Hot Water Heating. *12th IEA Heat Pump Conf*. 2017, n.d., p. 1–14.
- [40] ASHRAE. *ANSI/ASHRAE STANDARD 93-2010 Methods of Testing to Determine the Thermal Performance of Solar Collectors*. 2010.
- [41] Wilcox S, Marion W. *Users Manual for TMY3 Data Sets* 2008.
- [42] Wetter M. FAN AND PUMP MODEL THAT HAS A UNIQUE SOLUTION FOR ANY PRESSURE BOUNDARY CONDITION AND CONTROL SIGNAL Michael Wetter Lawrence Berkeley National Laboratory Environmental Energy Technologies Division Building Technology and Urban Systems Department Simulatio n.d.:3505–12.
- [43] Liu M, Toshiyuki H, Ryoza O, Ke W, Wonjun C, Doyun L, et al. 再生可能エネルギーを利用する分散型マルチソース・マルチユース ヒートポンプシステムの開発 試験建屋の構築及び実測による冷暖房性能評価. *日本建築学会環境系論文集* 2020;85:361–70.  
doi:<https://doi.org/10.3130/aije.85.361>.

# Chapter 7: Conclusions and future work

## 7.1 Conclusions

This thesis focused on the development of a novel distributed water source heat pump system using multiple kinds of renewable energy.

Chapter 1 demonstrated the research background, research objectives, originality of this research, and the overall structure of this thesis. In this thesis, this study proposed a heat pump system designed to utilize multiple renewable energy sources, providing an idea and possibility for the next generation building or district energy or heat supply systems. Our purpose is to verify the feasibility and performance of this system through field testing and to build a suitable system model, which can optimize the system composition and control strategy for further explore the performance under different conditions. This thesis reports the detailed system development process and field testing based verification, as well as the modeling of the heat pump system.

Chapter 2 reviewed different heat pump systems widely used in the building/industries and analyzed their characteristics based on the review of previous research. In the field of building heating and cooling, heat pump technology has significant advantages over traditional heating and cooling systems. On the other hand, with the proposal and development plan of the fifth generation heat supply network, the realization of low heating temperature and the integration of renewable energy have become the future trend. These trends require the use of systems that can cope with such low-temperature heat sources, and heat pumps are the best choice that can meet the requirements. However, as mentioned above, each renewable energy has its advantages and disadvantages. The energy supply system that relies on a single heat source cannot efficiently and stably meet the heat demand of buildings that may change at any time. Therefore, this research is also from this aspect; the goal is to build a heat pump system that can utilize a variety of renewable energy, can provide a stable and high-efficiency building heat supply.

In chapter 3, we started with the basics and explained the concept and composition of this system. These include the development of sky source heat pumps, floor heating heat pumps, air conditioning heat pumps and hot water heat pumps. The concept, structure, and performance test of each machine are also explained in detail. The development and improvement of each device are to cooperate with the design and operation concept of the system, that is, the integrated use of multiple renewable energy sources, including solar radiation, air heat, and geothermal heat. Also, the soil is used as a heat storage body to achieve peak shaving operation.

Through the factory performance test, the performance of each heat pump was confirmed. In the next chapter, we will introduce experiments which are the field testing, and test each machine and the overall performance of the system through experiments.

In chapter 4, we verified and evaluated the performance of the proposed system. To evaluate the system performance of each heat pump and the entire system for heating or cooling supply, a test building (RE house) was constructed for the field testing of the proposed heat pump system. The heating and cooling operation performance evaluations obtained by the field testing are summarized below.

It was confirmed by the field testing that the performance of the heat collection operation of the sky source heat pump significantly changed, mainly depending on the amount of solar radiation and the ambient temperature. a COP of about 23.2 was achieved on a clear winter day and a COP of about 7.4 on a cloudy day in winter. Although COP was 4.5 for heat dissipation operation at night in summer, it is considered that there is room for performance improvement by adopting an electronic subcooling degree control expansion valve. The average COP of the heat collection operation was 12 on a cloudy day in the interim period because the outside temperature was higher than that of winter.

Besides, it was confirmed by a long-term continuous operation test that the daily cycle operation method combined with ground heat exchanger and sky source heat pump could help eliminates the temporal disagreement between the cold heat demand and the hot heat demand and the non-equilibrium of the heat quantity. It can expect a stable and efficient long-term system operation based on this system.

After satisfying the thermal comfort range, a stable COP of about 11 of the floor heating heat pump

was obtained during the space heating operation in Chiba for one month in March. In a space cooling experiment conducted in summer, the COP of the air conditioning heat pump was stable and achieved a value of 12.5. In a space heating experiment conducted on 13 November under an average temperature of 12 °C and no solar radiation, the COP of the air conditioning heat pump achieved a value of 6.5.

The performance of the heat pump for hot water supply was evaluated based on field testing in summer. The result shows an average COP of around 4 due to the limitation of the basic EcoCute machine. Based on the previous studies (an average COP of about 8 for instant hot water supply type), we think it is possible to get a higher COP, such as by using an instant hot water supply heat pump.

In chapter 5, we created a dimensional model of the target piping system and conduct simulation to predict the pressure loss and temperature, based on the experimental piping system of the RE house by CFD for two operating states. There are two case settings in the simulation, which is a heat collection operation period using the sky source heat pump and a heating operation period utilizing the heat pump for floor heating. By comparing with the experimental data, the prediction accuracy of pressure loss and temperature in this piping system model was confirmed based on the result. For the prediction of pressure loss, the maximum relative error is 23.3%, with an absolute error of 0.7 kPa. Regarding the cause of the difference, in this simulation, since there is no average roughness information corresponding to ground heat exchanger using a PVC corrugated pipe, the calculation was performed using an average roughness of 1 mm assuming that ground heat exchanger is a circular pipe. In the future, it is necessary to estimate the equivalent mean roughness corresponding to PVC corrugated pipe. For the prediction of temperature, the maximum relative error is 14.3%, with an absolute error of 2 °C. The temperature distribution different from the actual temperature distribution taken as the surface temperature of the ground heat exchanger is considered to be the cause of the error.

In chapter 6, we first analyzed the characteristics and advantages and disadvantages of the tools and methods used in modeling and simulation of building energy systems by reviewing the relevant research. Then, we briefly introduced the Modelica language and its application in the field of

architecture. Next, we introduced the modeling of the distributed heat pump system proposed earlier, including the description of each model and the whole system description.

The validity and accuracy of the model are verified by comparing the experiment results, including a sunny day and a cloudy day in winter. In the comparison, we compared the changes in the water loop (such as temperature and flow rate), and the performance (mainly COP) of the floor heating heat pump and sky source heat pump. According to the comparison with the experiment results, the validity of the system model built by Modelica is proved. Also, the constructed system model has acceptable accuracy and can well reproduce the performance changes and dynamic characteristics of the system.

## 7.2 Recommendations for future work

The distributed water source heat pump using multiple kinds of renewable energy is still in its infancy in the world. This principle helps to achieve the fifth generation of district heating, and cooling network is intimately connected, so it is very promising to become a mainstream solution. Therefore, we built an actual system based on this principle and verified and evaluated its performance through experiments. However, there are still some parts that need to be improved:

We found that the refrigerant evaporating temperature fluctuated during the heat dissipation operation. It is conceivable that the liquid and gas refrigerant separated during the process, causing hunting of the refrigerant flow rate due to sudden opening and closing of the drainer, that is, unstable operation occurred. Therefore, the development of a suitable electronic control expansion valve will be necessary for a stable operation of SSHP.

Also, it was determined through experiments that the sky source heat pump generated enough power (higher than the overall power consumption in winter), so it is necessary to introduce energy storage equipment to improve the system. In addition, the system in the experiment adopted a constant flow rate operation. However, according to different situations, it is necessary to find the most economical operation plan (select constant/variable flow rate operation and water loop temperature range).

This advanced heat pump system is also accompanied by such as a higher risk of occurring fault, which means a relatively higher cost in operating than conventional systems. Hence the cost reduction of whole system is critical for expanding the application of this system in the future. For example, the cost reduction of maintenance is important due to the direct expansion SSHP (mostly physical damage) and thermal/water loop configuration (mostly heat loss and maintenance). Also, to reduce the operating cost, it is necessary to determine the most efficient operation strategy, such as switching the constant flow rate operation or variable flow rate operation accordingly.

Moreover, it may be difficult to implement a complete system for all purposes which may contain several heat pumps for all heating and cooling utilization. In addition, the extreme weather and heat load variation will affect the system's operating performance; the integrated use of this system with traditional systems also has the potential to improve overall efficiency. Therefore, determining what kind of combination and how much performance and economy can be achieved under different conditions such as regions will be a critical task to expand this system.

Finally, this novel heat pump system using renewable energy requires a more complicated/advanced operation strategy to achieve its best efficiency. Various control methods can be developed and verified based on developed Modelica model; therefore, operation optimization and design optimization will be the critical work in the future. Moreover, the sky source heat pump model in this system is replaced by non-direct expansion solar assisted heat pump. To better reflect its characteristics, further detailed model of direct expansion solar assisted heat pump is needed.

# Publications

## 1. Peer-reviewed journals

- 1) 劉明哲, 日野俊之, 大岡龍三, 文可, 崔元準, 李度胤, 池田伸太郎, 再生可能エネルギーを利用する分散型マルチソース・マルチユースヒートポンプシステムの開発 試験建屋の構築及び実測による冷暖房性能評価, 日本建築学会環境系論文集, 第85巻, 第771号, 361–370頁, DOI: <https://doi.org/10.3130/aije.85.361>
- 2) Mingzhe Liu, Ryoza Ooka, Wonjun Choi, Shintaro Ikeda, Experimental and numerical investigation of energy saving potential of centralized and decentralized pumping systems, Applied Energy, Volume 251, 113359, DOI: <https://doi.org/10.1016/j.apenergy.2019.113359>

## 2. Conference proceedings (International)

- 1) Mingzhe Liu, Ryoza Ooka, Toshiyuki Hino, Ke Wen, Wonjun Choi, Doyun Lee, Shintaro Ikeda and Djafar Reza Palasz, Experimental performance analysis of a multiple-source and multiple-use heat pump system: winter field experiment and heating operation performance evaluation, E3S Web of Conferences, Volume 111, 01076, CLIMA 2019 Congress, DOI: <https://doi.org/10.1051/e3sconf/201911101076>
- 2) Ke Wen, Ryoza Ooka, Toshiyuki Hino, Mingzhe Liu, Wonjun Choi, Doyun Lee, Shintaro Ikeda and Djafar Reza Palasz, Experimental performance analysis of a multiple-source and multiple-use heat pump system: a predictive ANN model of sky-source heat pump, E3S Web of Conferences, Volume 111, 01076, CLIMA 2019 Congress, DOI: <https://doi.org/10.1051/e3sconf/201911105018>
- 3) Mingzhe Liu, Ryoza Ooka, Toshiyuki Hino, Ke Wen, Wonjun Choi, Doyun Lee, Shintaro Ikeda, Analysis of pressure and temperature in piping system of RE house based on CFD, Seminar of Sustainable Building in China, Japan and Korea 2019, 19–20 December, 2019, Seoul, Korea.
- 4) Ke Wen, Ryoza Ooka, Toshiyuki Hino, Mingzhe Liu, Wonjun Choi, Doyun Lee, Shintaro Ikeda, Study on prediction of thermal performance of RE house in winter based on neural network models, Seminar of Sustainable Building in China, Japan and Korea 2019, 19–20 December, 2019, Seoul, Korea.

- 5) Mingzhe Liu, Ryoza Ooka, Toshiyuki Hino, Ke Wen, Wonjun Choi, Doyun Lee, Shintaro Ikeda, Experimental performance analysis of a multiple-source and multiple-use heat pump (MMHP) system, Sustainable Built Environment Conference 2019, 6–7 August, Tokyo, Japan.
- 6) Ke Wen, Ryoza Ooka, Toshiyuki Hino, Mingzhe Liu, Wonjun Choi, Doyun Lee, Shintaro Ikeda, Experimental performance analysis of a multiple-source and multiple-use heat pump system: a predictive ANN model of sky-source heat pump, Sustainable Built Environment Conference 2019, 6–7 August, Tokyo, Japan.
- 7) Ke Wen, Ryoza Ooka, Toshiyuki Hino, Mingzhe Liu, Wonjun Choi, Doyun Lee, Shintaro Ikeda and Djafar Reza Palasz, A study of predicting sample size required for regression performance using learning curves, The Joint Seminar on Sustainable Built Environment in East Asia, Tokyo, Japan, November 2018.
- 8) Mingzhe Liu, Ryoza Ooka, Toshiyuki Hino, Ke Wen, Wonjun Choi, Doyun Lee, Shintaro Ikeda and Djafar Reza Palasz, Experimental performance evaluation of heating performance of a multiple source and multiple use heat pump (MMHP) system utilizing renewable energy, The Joint Seminar on Sustainable Built Environment in East Asia, Tokyo, Japan, November 2018.

### 3. Conference proceedings (Domestic)

- 1) 文可, 大岡龍三, 日野俊之, 劉明哲, 崔元準, 李度胤, 池田伸太郎, 再生可能エネルギー利用のための水循環・分散型ヒートポンプシステムの開発 その9 システム概要及び天空熱源ヒートポンプの冬期集熱運転特性, 日本建築学会大会学術講演梗概集, 2018.09.
- 2) 劉明哲, 大岡龍三, 日野俊之, 文可, 崔元準, 李度胤, 池田伸太郎, 再生可能エネルギー利用のための水循環・分散型ヒートポンプシステムの開発 その8 冬期運転試験及び暖房運転性能の実測, 日本建築学会大会学術講演梗概集, 2018.09.
- 3) 文可, 大岡龍三, 日野俊之, 劉明哲, 李度胤, 崔元準, 池田伸太郎, Djafar Reza Palasz, 再生可能エネルギー利用のための水循環・分散型ヒートポンプシステムの開発 (第11報) ANNによる天空熱源ヒートポンプの冬期集熱運転性能の予測, 空気調和・衛生工学会大会学術講演論文集, 2018.09.
- 4) 劉明哲, 大岡龍三, 文可, 日野俊之, 李度胤, 崔元準, 池田伸太郎, Djafar Reza Palasz, 再生可能エネルギー利用のための水循環・分散型ヒートポンプシステムの開発 (第10

報) 冬期運転試験及び実測による暖房運転性能評価, 空気調和・衛生工学会大会学術講演論文集, 2018.09.

- 5) 劉明哲, 大岡龍三, 日野俊之, 文可, 崔元準, 李度胤, 池田伸太郎, 再生可能エネルギー利用のための水循環・分散型ヒートポンプシステムの開発 その 14 夏期運転試験及び運転性能実測, 日本建築学会大会学術講演梗概集, 2019.09.
- 6) 文可, 大岡龍三, 日野俊之, 劉明哲, 崔元準, 池田伸太郎, 李度胤, 再生可能エネルギー利用のための水循環・分散型ヒートポンプシステムの開発, その 15 天空熱源ヒートポンプの回帰モデルの予測性能に必要な学習データ数に関する検討, 日本建築学会大会学術講演梗概集, 2019.09.
- 7) 劉明哲, 大岡龍三, 日野俊之, 文可, 崔元準, 李度胤, 池田伸太郎, 再生可能エネルギー利用のための水循環分散型ヒートポンプシステムの開発, (第 17 報) CFD による RE ハウス配管システムの圧力と温度の解析, 空気調和・衛生工学会大会学術講演論文集, 2019.09.
- 8) 文可, 大岡龍三, 劉明哲, 日野俊之, 崔元準, 李度胤, 池田伸太郎, 再生可能エネルギー利用のための水循環・分散型ヒートポンプシステムの開発, (第 16 報) ANN と RNN による RE ハウスの冬期集熱運転消費電力の予測性能の比較, 空気調和・衛生工学会大会学術講演論文集, 2019.09.
- 9) 劉明哲, 大岡龍三, 崔元準, 文可, 再生可能エネルギー利用のための水循環・分散型ヒートポンプシステムの開発, その 20 Modelica によるシステムのモデリングとシミュレーション, 日本建築学会大会学術講演梗概集, 2020.(投稿中)

# Acknowledgement

First and foremost, I sincerely thank Professor. Ryozo Ooka as my supervisor for five years from my master course to doctoral course. I always appreciate your kind suggestions and continuous support for my study and research. The most important thing is that, thank you so much for taking me as your student and helped me realize my dream at Todai. With so many years of research experience and the platform you provided, I have benefited a lot these years. I will continue to improve myself in the future and look forward to working with you again.

I also thank Professor. Shinsuke Kato. Although there are not many opportunities to discuss research with you, I can still receive your teachings and useful suggestions at every weekly meeting. Your experience makes me understand the mastering the solid fundamental knowledge is a must to become an excellent researcher. Thanks again for your recommendation for my future work.

I really thank to Associate Professor Hideki Kikumoto. Thank you for your continuous help and very constructive comments on my research. It was you during my master's course that made me find the problem in my study and want to stick to it. From your talking, I learned how to think about issues, which can help me a lot in my future work.

Professor Toshiyuki Hino, I thank you for your advice on my research and life. You can always offer me beneficial suggestions for my study and living in Japan. Besides, you have taught me so many things about how to work properly. I hope to have the opportunity to continue to communicate with you in the future.

I extend my appreciation to my advising committee members, Prof. Takashi Akimoto, Prof. Yasunori Akashi, and Prof. Shinichi Sakamoto for giving their time and providing excellent comments and suggestions.

Prof. Takashi Akimoto, you are an authoritative expert in the field of building facilities and air environment. You are so enthusiastic and are providing valuable suggestions on my research in both practical and theoretical aspects, which helps to make my research more complete and perfect.

Prof. Yasunori Akashi, you are a leading scientist in the fields of building energy system. It is really my honor to receive your detailed comment on my thesis and I really appreciated your valuable suggestion.

Prof. Shinichi Sakamoto, I really thank you for providing me with priceless advice on how to improve the completeness of my thesis and gave me a further thinking on the originality of a study. Your comments made my research more realistic and valuable.

Extraordinary appreciation goes to Qi Zhou, who taught and helped me a lot in my life. It's my honor and luck to know you because I think it is not easy to meet a friend who has the same idea and can maintain the relationship at the age. I appreciate the precious time you discussed any problems with me. I think we can continue and cooperate in the future.

Assistant Professor Wonjun Choi and Shintaro Ikeda, I thank you for your advice on my research and life in Japan. You can always offer me beneficial suggestions for my research and how to live well in Tokyo. Besides, you have taught me so many things about how to conduct research and write an academic paper. The experience in California with you is also enjoyable for me. I hope to continue to communicate with you in the future.

Dr. Mengtao Han, thank you for your advice and help in my life and career planning. It is interesting to talk with about many things, not just research, but also current affairs. Your experience helped me consider differently about career planning. I hope there will be an opportunity to discuss and cooperate with you in the future.

Mr. Ke Wen, thank you for your help not only in the research but also in life. It is my pleasure to know you and cooperate with you; your perseverance in knowledge impressed me so much. I am looking forward to your excellent performance from now on; I hope I can work with you again in the future.

Dr. Li Wang, I appreciate your help and advice in my life. The time spent with you is beneficial and gave me an unforgettable memory in my life. You made me know what I should do in my student life and what I should plan for my future, which help me cultivate the habit of making plans that will benefit me forever. I hope to cooperate with you again in the future.

Mr. Takeo Takahashi, thank you as a kindly elder who always given us support and help, making me feel at home here. Dr. Keigo Nakajima, thank you for the time to help with my problem in life. I so appreciate to know you here, to discuss with one that has an interesting talking style. I hope to have the opportunity to continue Niku-kai again in the future.

I am also very grateful to the people who have helped me in my student life: Associate Professor Weirong Zhang at Beijing University of Technology, Dr. Hang Yin, Dr. Kan Lin, Ms. Qiuyue Wang,

Dr. Wonseok Oh, Mr. Shintaro Kobayashi, Ms. Shan Gao, Ms. Doyun Lee, Mr. Bingchao Zhang, Mr. Hongyuan Jia, Mr. Chao Lin, Mr. Haoran Li at Norwegian University of Science and Technology, and so many people that helped me and supported me always.

Special thanks to my dear girlfriend Weian (Vivian) Chen, who always support me during my whole doctoral life. It is you who always encourage me when I encounter difficulties and made me never give up. You are the treasure that I seek, and I will cherish my whole life with you.

Finally, I express my honest appreciation to my parents(My father Yan Liu, My mother Xiying Yang) and family(My grandfather Wenxian Liu and Shiqi Yang, My grandmother Xianzhi Su and Xiuju Geng), who always supported me and allowed me to do what I wanted to do. Thanks to your support and encouragement, I could entirely focus on my study. I will return the favor to all my family and girlfriend.

May 2020

刘明哲

Mingzhe Liu